A DEEP SEISMIC ANALYSIS OF THE FLEMISH CAP CONTINENTAL MARGIN OFF NEWFOUNDLAND, CANADA

by

Joanna Gerlings

Submitted in partial fulfillment of the
requirements for the degree of
Doctor of Philosophy

at

Dalhousie University
Halifax, Nova Scotia
January 2013

DALHOUSIE UNIVERSITY

DEPARTMENT OF EARTH SCIENCES

The undersigned hereby certify that they have read and recommend to the Faculty of Graduate Studies for acceptance a thesis entitled "A DEEP SEISMIC ANALYSIS OF THE FLEMISH CAP CONTINENTAL MARGIN OFF NEWFOUNDLAND, CANADA" by Joanna Gerlings in partial fulfillment of the requirements for the degree of Doctor of Philosophy.

Dated: January 28, 2013

External Examiner: _____

Research Supervisor: _____

Examining Committee: _____

_____

_____

Departmental Representative: _____

DALHOUSIE UNIVERSITY

DATE: January 28, 2013

AUTHOR: Joanna Gerlings

TITLE: A DEEP SEISMIC ANALYSIS OF THE FLEMISH CAP CONTINENTAL MARGIN OFF NEWFOUNDLAND, CANADA

DEPARTMENT OR SCHOOL: Department of Earth Sciences

DEGREE: Ph.D. CONVOCATION: May YEAR: 2013

Signature of Author

Table of Contents

List of Tables

List of Figures

Abstract

The crustal structure of the NE Flemish Cap margin off Newfoundland, Canada has been determined along a 460-km-long wide-angle reflection seismic transect (FLAME Line). The westward section crossing Flemish Cap displays an up to 32-km-thick continental crust. The thick crust thins to a 6-km-thick crust over a distance of only 40 km, which then continues seaward for an additional 100 km. S-wave velocities favor a thin crust of continental composition. Beneath the thin crust velocities infer that the upper mantle is partially serpentinized. The seaward-most end of the model displays velocities and thicknesses typical of oceanic crust. The raw multichannel seismic (MCS) reflection data of Line 85-3, coincident with the FLAME Line, were reprocessed. Results were combined with the velocity model and then compared with similar results across the conjugate Goban Spur margin (NE Europe). Previous studies had suggested a model of symmetric pure shear extension followed by asymmetric breakup. The new results indicate that asymmetric structures are formed during all stages of rifting, breakup, and transition to oceanic spreading. The differing nature of the two transition zones is particularly striking. For Flemish Cap, the reprocessed image of the MCS profile shows tilted fault blocks beneath syn-rift sediment packages, consistent with a wide region of highly thinned continental crust suggested by P- and S-wave velocities. In contrast, the Goban Spur transition zone consists primarily of exhumed serpentinized mantle. To define potential variations along-strike of the margin, the raw MCS data of Line 87-4 to the north of Flemish Cap were reprocessed. Interpretation of the image indicates a different crustal structure along the profile in comparison to Line 85-3. Fault blocks with a roughly NW-SE rift direction are indicated in the landward region of Line 87-4, followed seaward by a block indicating complex 3D rifting. The basement morphology farther seaward indicates crust of an oceanic affinity. In light of the results of the reprocessed images, Erable lines (E43, E44, E46-E52) situated between Lines 87-4 and 85-3 were re-interpreted. The results together with gravity data indicate along-strike variations both in rifting as well as mantle serpentinization on the NE Flemish Cap margin.

List of Abbreviations Used

AGC	Atlantic Geoscience Centre
BTJ	Biscay Triple Junction
CCGS	Canadian Coast Guard Ship
CDP	common-depth-point
COB	Continent-ocean boundary
DS	Davis Strait
DSDP	Deep Sea Drilling Project
FC	Flemish Cap
FLAME	Flemish Cap Margin Transect
FZ	Fracture zone
GA	Galicia Bank
GB	Galicia Bank
GS	Goban Spur
GSA	Geological Society of America
GSC	Geological Survey of Canada
GSI	Geophysical Servise Incorporated
IAP	Iberian Abyssal Plain
IB	Iberia
Ifremer	Institut Français de Recherche pour l'Exploitation de la Mer

Lab	Labrador
LIFT	Leading edge InFormation Technology
MCS	Multichannel seismic
NB	Newfoundland Basin
NS	Nova Scotia
NSERC	Natural Sciences and Engineering Research Council of Canada
OB	Orphan Basin
OBS	Ocean-bottom seismometer
OCT	Ocean-continent transition
ODP	Ocean Drilling Program
OK	Orphan Knoll
PB	Porcupine Basin
R/WAR	Refraction/wide-angle reflection
RK90	Reid and Keen (1990) wide-angle profile
rms	root-mean-squares
S/N	signal-to-noise
SCREECH	Study of Continental Rifting and Extension of the Eastern Canadian Shelf
SRME	Surface Related Multiple Elimination
TWT	Two-way traveltime
WAM	Western Approaches Margin

Acknowledgements

First and foremost I would like to thank Keith Louden for supervising my PhD project, for always having the door open and being ready to discuss and tackle problems, and for welcoming me to Halifax, NS.

I would also like to thank my committee members Ruth Jackson and Mladen Nedimović for always being ready to discuss my work and encourage me. Ruth, thank you for including me in your many out-door adventures. It has made life in Halifax fun and enjoyable. Mladen, thank you for making a great work space for the students and taking an active part in our fun.

Thank you to everyone in the Dalhousie Geophysics Group (aka Mladen's Lab). Louise Watremez, I will miss our walks to the library for "fancy" coffee. Omid Aghaei, no more fighting over "the nodes". John Thibodeau, for assisting with the technical. All the rest of you, it was a pleasure to share the Lab with you.

I would like to thank the faculty and especially the other graduate students and Post Docs at the Department of Earth Sciences at Dalhousie University. This place seems to be a magnet for great, interesting and accepting people. Alan Hidy, thank you for always making me laugh with a dirty remark.

I would like to thank all the people I got to know in Halifax outside university life. A special thanks to Sarah Wakely for becoming my family.

I would also like to thank people at the Geophysics Department at the Geological Survey of Denmark and Greenland (GEUS), especially Jens Jørgen Møller, for their patience, understanding and support in the final stage of my thesis. I would also like to extend this thanks to Fi Prowe, Sofie Gradmann and Louise Watremez.

Finally, a big thank you to my parents for making sure I got a hot meal in the final write-up stage.

Chapter 1

Introduction

Passive margins have been intensely studied over the past two to three decades and insight into the complex mechanisms of continental rifting and its evolution to seafloor spreading has been gained as a result. There exist two end-members of continental margins: a magma-rich margin (volcanic; Fig. 1.1a) and a magma-poor margin (non-volcanic; Fig. 1.1b). Magma-rich margins form when large volumes of mantle melt occur prior to and during rifting (*White et al.*, 1987). Rifting is followed by continental breakup and the formation of oceanic crust. Initial oceanic crust may be several times thicker than normal oceanic crust, which has an average thickness of about 7 km (*White et al.*, 1992). An ocean-continent transition zone (OCT) is formed during rifting prior to breakup. The OCT is characterized as a region, whose affinity lies between unequivocal continental and oceanic crust. In the OCT of magma-rich margins, basalt flows imaged as seaward dipping reflections (SDR) in the upper crust and magmatic underplating modelled as high-velocity (7.2-7.6 km s^{-1}) bodies in the lower crust (*White and McKenzie*, 1989) (Fig. 1.1a) are often observed. In contrast, magma-poor margins are associated with little or no melting of the mantle. The OCT is most often associated with broad regions of exposed mantle (Fig. 1.1b). Continental breakup on magma-poor margins does not necessary lead directly to the formation of oceanic crust as on volcanic margins. The exhumed mantle material is serpentinized by reaction with seawater, which reduces the mantle velocity (8.0 km s^{-1}), as well as density and rheological strength. Hence, we commonly observe velocities increasing with depth from about 5.0 to 8.0 km s^{-1} in these regions.

The crustal structures and compositions across passive margins are studied on these magma-poor margins, where the extensional fabric has not been modified by large volumes of syn-rift and post-rift volcanism. To study these margins, a P-wave velocity models are developed from wide-angle data. The crustal characteristics are reflected in the velocity structure of the models, e.g. the velocity gradient in the

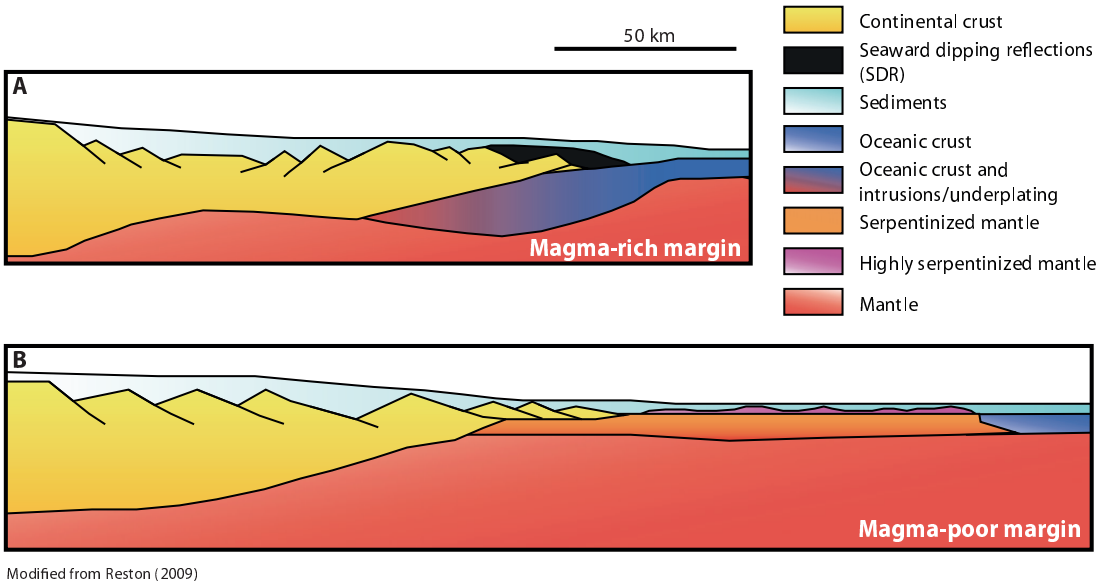

Figure 1.1: Schematic of a) magma-rich and b) magma-poor margins. See legend and text for details. Modified from *Reston* (2009).

upper crustal layer is often higher in oceanic crust than in continental crust (*White et al.*, 1992). S-wave velocities provide an additional constraint on the lithology of the crustal material. For instance, Poisson's ratio helps distinguish serpentinized mantle from oceanic or continental crust, and in some cases also helps distinguish between the two crustal types (e.g., *Christensen*, 1996). Poisson's ratio i the ratio of radial to axial strain when a uniaxial stress is applied (See. e.g. *Lay and Wallace* (1995) for further details). The Poisson's ratio can discribed with the Lamé constants, λ and μ: $\lambda = (2(\lambda + \mu))$ or P- and S-wave velocities, α and β, respectively: $(\alpha^2 - 2\beta^2)/(2(\alpha^2 - \beta^2))$.

Multi-channel seismic (MCS) imaging is a highly-complementary tool in wide-angle studies of passive margins. The geometry of the sedimentary and crustal structures that are imaged at high resolution using reflection seismology provide information on the crustal nature. For example, a basement morphology of rotated normal faulted blocks often indicates a continental affinity, exhumed mantle often displays a more subdued basement, and slow-spreading oceanic crust is characterized by a normal faulted high-relief basement morphology (e.g. *Small*, 1994). Magnetic and gravity data can sometimes be helpful and provide additional constraints on the composition

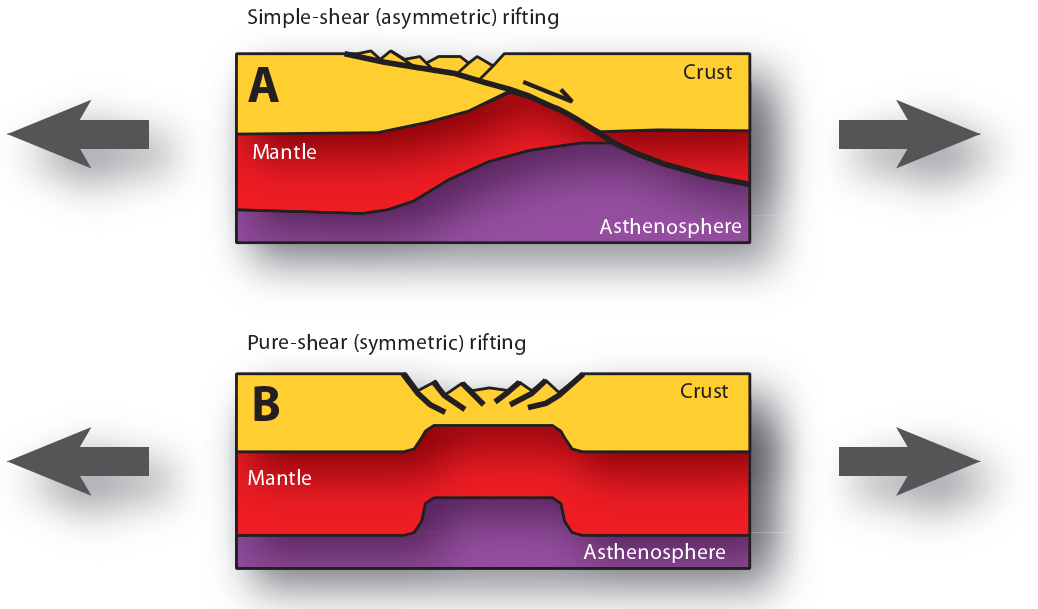

Figure 1.2: Models of a) simple-shear asymmetric rifting (*Wernicke*, 1981) and b) pure-shear symmetric rifting (*McKenzie*, 1978).

of the crust. Strong magnetic anomalies along a margin are present in the oceanic domain and are formed during seafloor spreading. Weaker magnetic anomalies may be present in the OCT if mantle exhumed (e.g. *Sibuet et al.*, 2007a). Magnetic and gravity data can also help us constrain the extent of a crustal domain between profiles along-strike of the margin.

Based on the observations above, geodynamic models were developed to understand the rift evolution of a margin and its conjugate. In early models, the rifting style of a margin pair was classified as either pure-shear symmetric (*McKenzie*, 1978) or simple-shear asymmetric (*Wernicke*, 1981) rifting (Fig. 1.2). These two lithospheric stretching models describe large-scale two-dimensional rifting to first order. In the pure shear uniform rifting model, the thinning of the crust occurs by ductile shear in the lower crust and upper mantle, and as normal faulting in the brittle upper crust. In the simple shear rifting model, a low-angle detachment fault or shear zone penetrates into the upper mantle creating asymmetric rifting between the two margins.

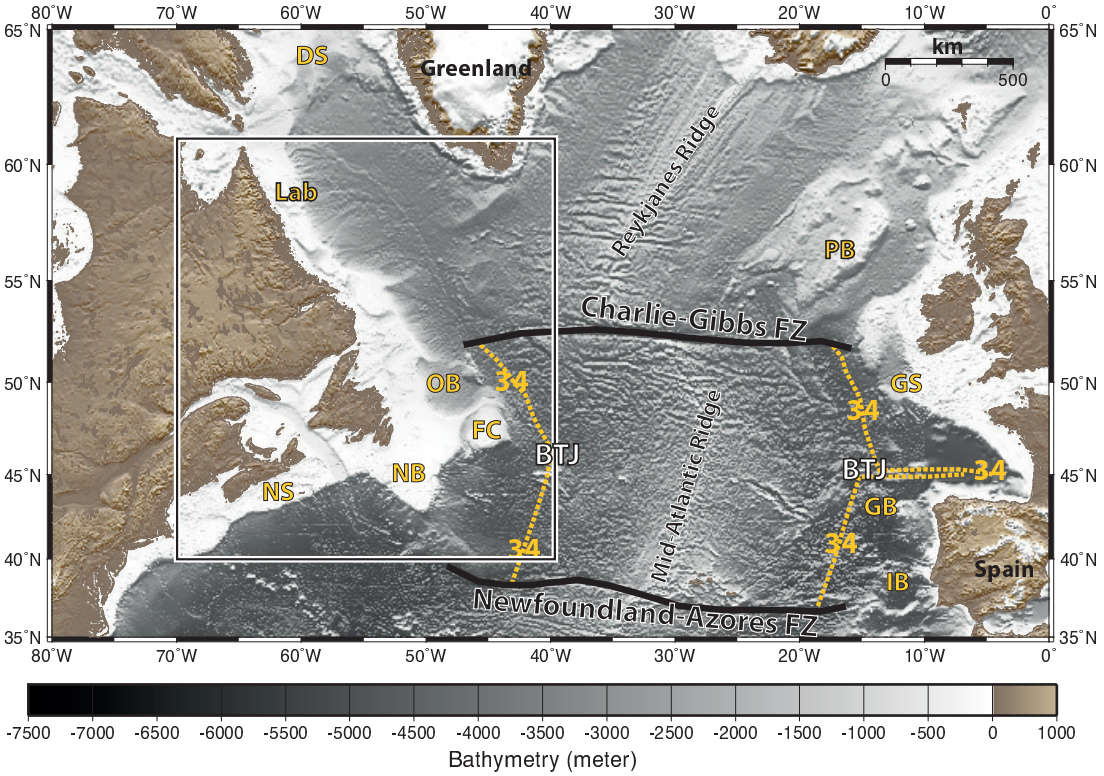

Figure 1.3: Map of the North Atlantic. Abbreviations, NS: Nova Scotia; NB: Newfoundland Basin; FC: Flemish Cap; Lab: Labrador; DS: Davis Strait; PB: Porcupine Basin: GS: Goban Spur; GB: Galicia Bank; IB: Iberia; BTJ: Biscay Triple Junction; FZ: Fracture zones. Magnetic anomaly 34 is indicated by dashed yellow lines. Black solid lines represent the Charlie-Gibbs and Newfoundland-Azores fracture zones. Close-up (black box) of the eastern Canadian coast with locations of seismic profiles are shown in Fig. 1.4

The eastern Canadian margins, from the Labrador margin in the north to the Nova Scotia margin in the south, and their conjugates, are primarily considered magma-poor margins (Fig. 1.3-1.4) (*Louden and Chian*, 1999). Some examples from the Newfoundland and Nova Scotia margins are shown in Fig. 1.5. These margins display a number of common features, but some variability can also be observed:

1. On magma-poor margins spanning from central Nova Scotia to the Labrador Sea and their conjugates, thinning of continental crust spans a distance of roughly 100 km (Fig. 1.5) (e.g. *Chian et al.*, 1995a,b; *Chian and Louden*, 1994; *Funck et al.*, 2003; *Van Avendonk et al.*, 2006; *Shillington et al.*, 2006; *Lau et al.*, 2006a,b; *Funck et al.*, 2004; *Wu et al.*, 2006; *Bullock and Minshull*, 2005; *Dean*

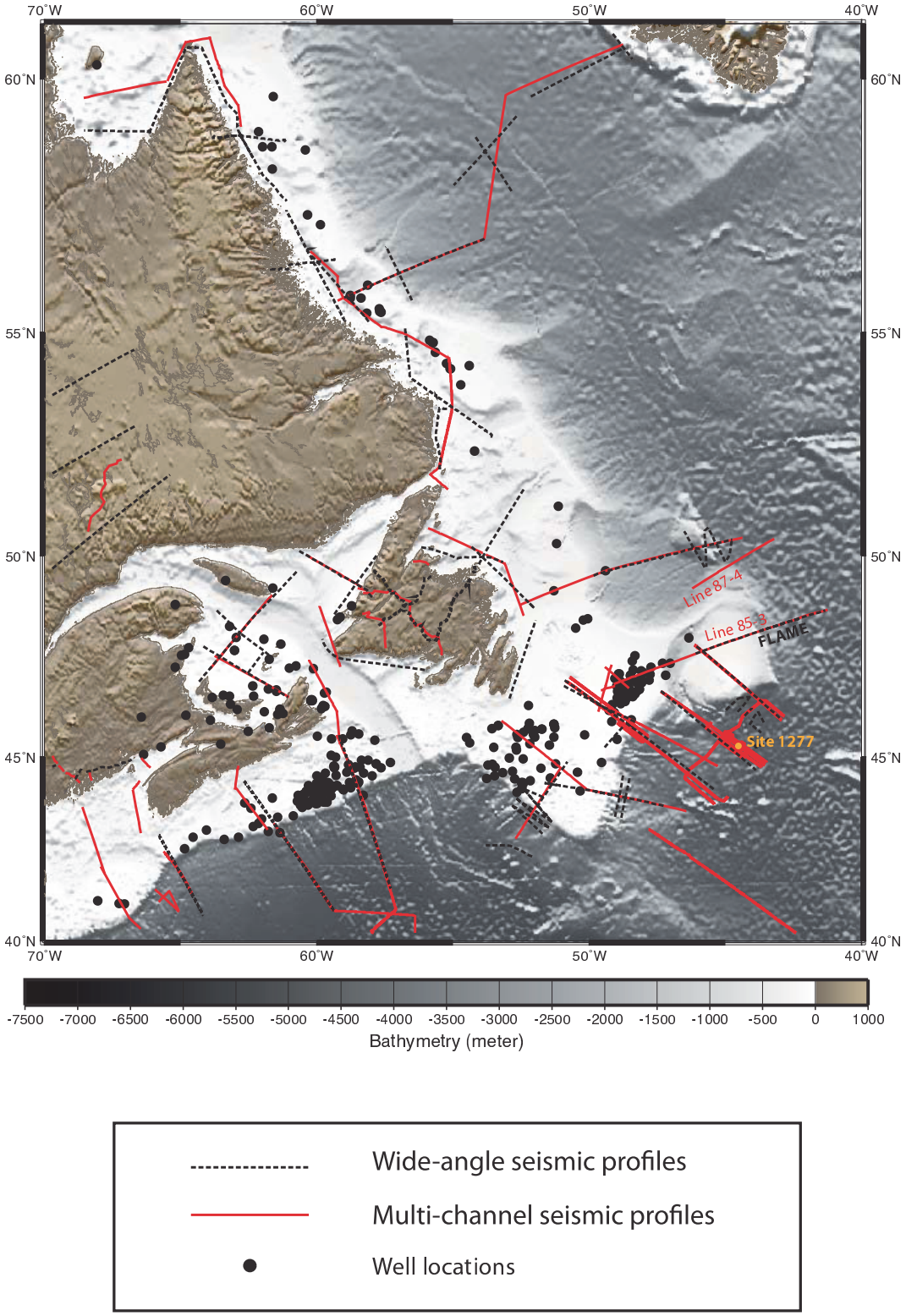

Figure 1.4: Map of the East Canadian coast with locations of seismic profiles.

et al., 2000; *Maillard et al.*, 2006). This distance continues from the edge of unstretched continental crust (∼30 km thick) to almost zero km thick crust. In this zone of crustal thinning, faulted blocks are often imaged. Geodynamic models suggest that thinning of the crust initially is symmetric (Figs. 1.6a and 1.7a) (.e.g. *Huismans and Beaumont*, 2011; *Reston*, 2009).

2. The thin continental crust is commonly interpret to be undercrusted by partially serpentinized mantle (e.g. *Chian et al.*, 1995a,b; *Chian and Louden*, 1994; *Funck et al.*, 2003; *Lau et al.*, 2006a; *Funck et al.*, 2004; *Wu et al.*, 2006; *Bullock and Minshull*, 2005; *Dean et al.*, 2000). This inter pretation is based on modelled P-wave velocities that are too low to be interpreted as mantle velocities (¡8.0 km s^{-1}) and too high to interpreted as crustal velocities (<7.2 km s^{-1}). When extension of the crust reaches a factor of 4 (roughly <8-10 km), the entire crust can become brittle, and faults and fractures form that may provide conduits for water down into the mantle, which then will serpentinize the mantle (Figs. 1.5 and 1.7b) (*Pérez-Gussinyé and Reston*, 2001). The SCREECH Line 2 profile on the Newfoundland margin (*Van Avendonk et al.*, 2006) and the velocity profile situated along the SIS04 MCS line on the Moroccan margins (*Maillard et al.*, 2006) appear to be exceptions. On SCREECH Line 2, there appears to be no modelled velocities indicating an undercrusted layer of partially serpentinized mantle under thin continental crust and on SIS04, a high-velocity layer is interpreted as underplating. The stage of rifting to continental breakup, where thin crust is underlain by partially serpentinized mantle, was shown to be asymmetric (Fig. 1.6b and 1.7c) (*Huismans and Beaumont*, 2011; *Reston*, 2009), and often after breakup a tongue of thin continental crust is left on one side of a conjugate margin (*Reston*, 2009). While the magma-poor margins in this part of the North Atlantic commonly appear asymmetric, pure-shear rifted margins may be encountered elsewhere, e.g in the Black Sea (*Shillington et al.*, 2008).

3. Geodynamic models (Figs. 1.6c and 1.7d) show that continental breakup is

followed by the emplacement of a wide region of mantle exhumation (*Huismans and Beaumont*, 2011; *Reston*, 2009; *Lavier and Manatschal*, 2006). This is according to interpretations from results of the presently most researched magma-poor margin, the Iberia margin. This margin's OCT is characterized by a wide region (>100 km) of exhumed mantle (e.g. *Dean et al.*, 2000) that was first discovered and investigated in the 1980's and 1990's (*Boillot et al.*, 1988; *Pickup et al.*, 1996). Similar broad regions of exhumed mantle are encountered on the northeastern Nova Scotia (*Funck et al.*, 2004), southern Newfoundland (*Lau et al.*, 2006a) and Labrador-SW Greenland margins (*Chian et al.*, 1995a,b; *Chian and Louden*, 1994). Although not common on all margins, a ridge feature was observed on the Newfoundland, Iberia and perhaps on the SW Greenland margins (*Boillot et al.*, 1988; *Pickup et al.*, 1996; *Dean et al.*, 2000; *Shillington et al.*, 2006; *Deemer et al.*, 2009). This ridge feature is located in the OCT and interpreted as a serpentinized ridge.

Seismic data and ODP drilling results show that the along-strike characteristics of the crust in the OCT vary significantly. A narrower region of exhumed mantle (*Van Avendonk et al.*, 2006; *Shillington et al.*, 2006) to possibly no mantle exhumation (*Funck et al.*, 2003; *Hopper et al.*, 2004; *Wu et al.*, 2006) is encountered on the SE Flemish Cap and central Nova Scotia margins (Figs. 1.3-1.5). Velocities in the thin crust of the OCT on SE Flemish Cap are interpreted to be of an oceanic affinity formed by ultra-slow spreading (e.g. *Funck et al.*, 2003). This oceanic crust is unusually thin (1-3 km thick) and underlain by partially serpentinized mantle. The region of exhumed mantle along the eastern Canadian margin (Fig. 1.5) narrows and pinches-out both to the south on the central Nova Scotian margin (*Wu et al.*, 2006) and to the north at SE Flemish Cap (*Funck et al.*, 2003; *Van Avendonk et al.*, 2006; *Lau*, 2005).

Numerical and conceptual models may explain some of the more complex features we observe on passive rifted margins. These models however, have not yet focused on along-strike variations in the OCT because modelling in 3D is challenging and computationally expensive. So far, modelling is primary focused on reproducing the rift

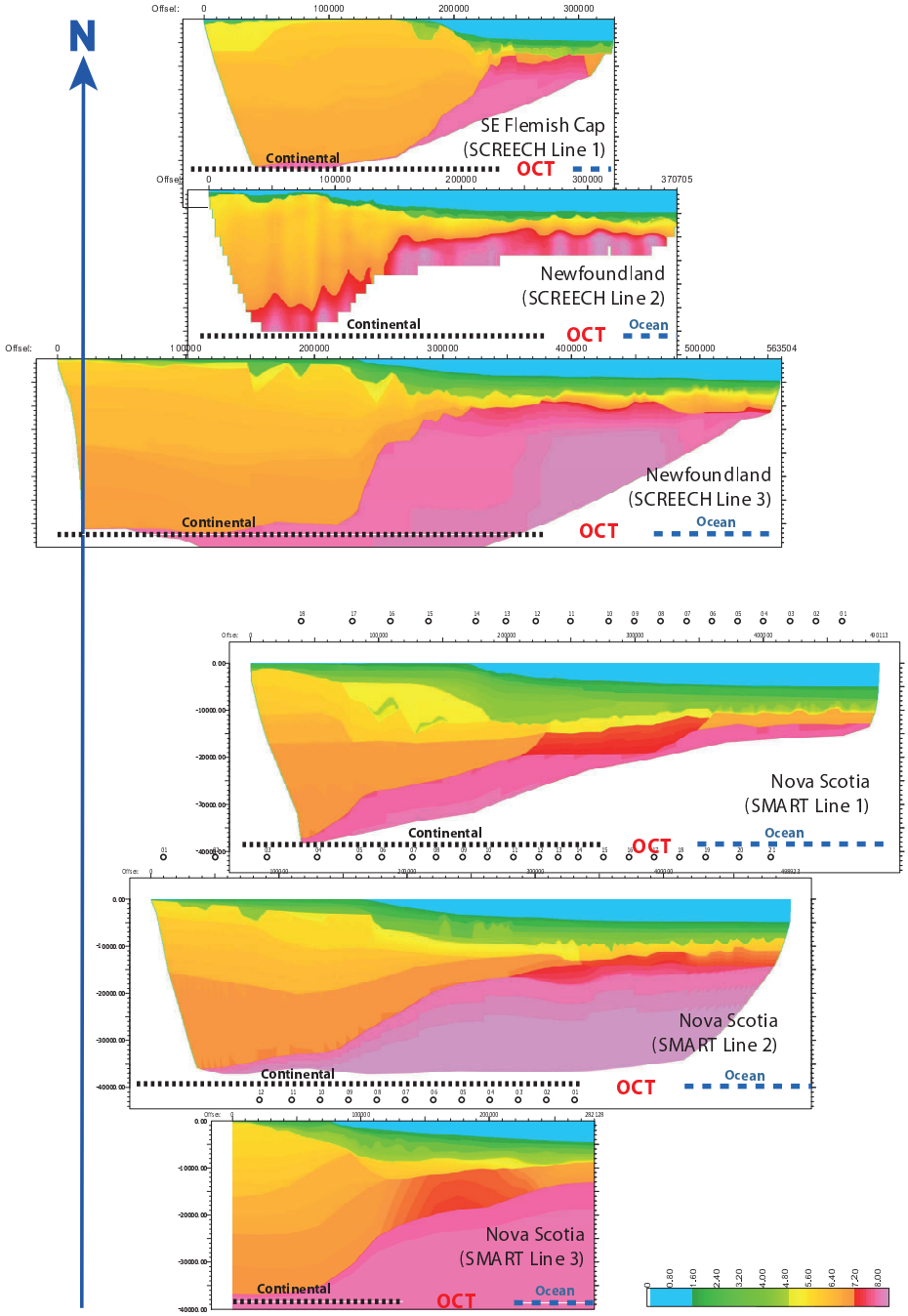

Figure 1.5: Examples of P-wave velocity models from the Nova Scotia and Newfoundland margins, eastern Canada (*Funck et al.*, 2003; *Van Avendonk et al.*, 2006; *Lau et al.*, 2006a; *Funck et al.*, 2004; *Wu et al.*, 2006; *Dehler et al.*, 2004). All of the velocity models were developed using the program RAYINVER (*Zelt and Smith*, 1992; *Zelt and Forsyth*, 1994) and FAST (*Zelt and Barton*, 1998) except SCREECH line 2, which used tomography (*Van Avendonk et al.*, 2006). Dotted black line indicate crust with sesimic properties of typical continental crust. The blue dashed line indicates crust with an oceanic composition. OCT: ocean-continent transition. The horizontal colored bar (bottom right) indicates P-wave velocities in km s^{-1}.

evolution of the Newfoundland-Iberia conjugate margins (e.g *Huismans and Beaumont*, 2011; *Lavier and Manatschal*, 2006; *Reston*, 2009) to explain how wide regions of mantle are exhumed. These models suggest slightly different modes of thinning of the continental crust (Figs. 1.6 and 1.7), but they all reproduce many of the features observed on the Iberia margin. The models do not take three-dimensionallity into account; however. The northern part of these margins, the SE Flemish Cap-Galicia Bank margin pair, was subjected to 3D rifting (e.g. *Sibuet*, 2004; *Sibuet et al.*, 2007b). While the Newfoundland and Iberia margins were experiencing extension, Flemish Cap and Galicia Bank were attached to each other. This resulted in roughly N-S rifting of Flemish Cap from Orphan Knoll, or possibly rotation of Flemish Cap (e.g. *Sibuet et al.*, 2007b). Detailed 3D modelling will be needed to better understand the tectonic processes in these complex rift areas.

During the final stage of rifting, the lithosphere completely will rupture and oceanic crust are to form. The structures formed during this process have not been thoroughly investigated using seismic data, since coincident MCS and wide-angle profiles that cross unambiguous seafloor spreading magnetic anomalies, and hence sample unambiguous oceanic crust, are still not common at most margins. The three SCREECH Lines 1, 2 and 3 cross magnetic anomaly M3, the oldest recognized anomaly on the Newfoundland margin, and Lines 1 and 2 cross magnetic anomaly M0. It is disputed whether anomaly M3 represents a magnetic anomaly formed by seafloor spreading, since anomaly M3 is situated on crust interpreted as continental on Line 1 and landward of drilled serpentinized mantle on Line 2 (*Funck et al.*, 2003; *Van Avendonk et al.*, 2006; *Shillington et al.*, 2006). Both lines display a region of unusual oceanic crust. Line 1 displays a 2-3 km thick layer of oceanic crust on top of partially serpentinized mantle, whereas Line 2 displays a more gradual transition into formation of only <4-km-thick oceanic crust, with intermixed regions of volcanic and mantle material (*Jagoutz et al.*, 2007).

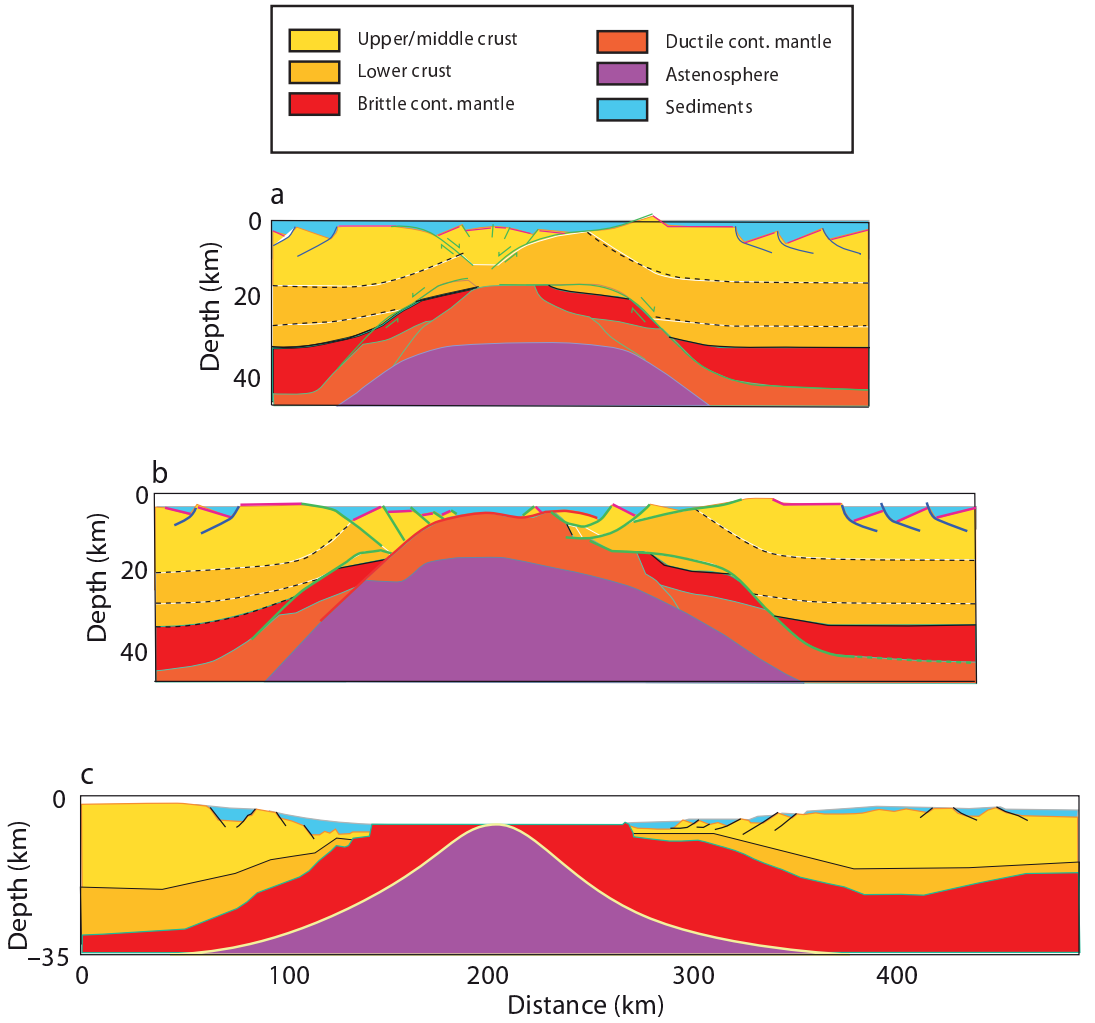

Figure 1.6: Conceptual rifting model of *Péron-Pinvidic and Manatschal* (2008). This model suggests that extension is depth-dependent in which the crust and mantle lithosphere is strong and strongly bonded. The upper lithosphere undergoes brittle deformation and the lower lithosphere by ductile deformation. Rifting is divided into three phases: a) Subsidence of a symmetric crustal block bounded by conjugate brittle faulting and shearing in the upper layer underlain by ductile necking of the lower lithosphere. b) This phase is followed by asymmetric simple shear extension. c) Finally, breakup of continental crust followed by extension, necking and mantle exhumation. For more details see e.g. *Péron-Pinvidic and Manatschal* (2008); *Huismans and Beaumont* (2011).

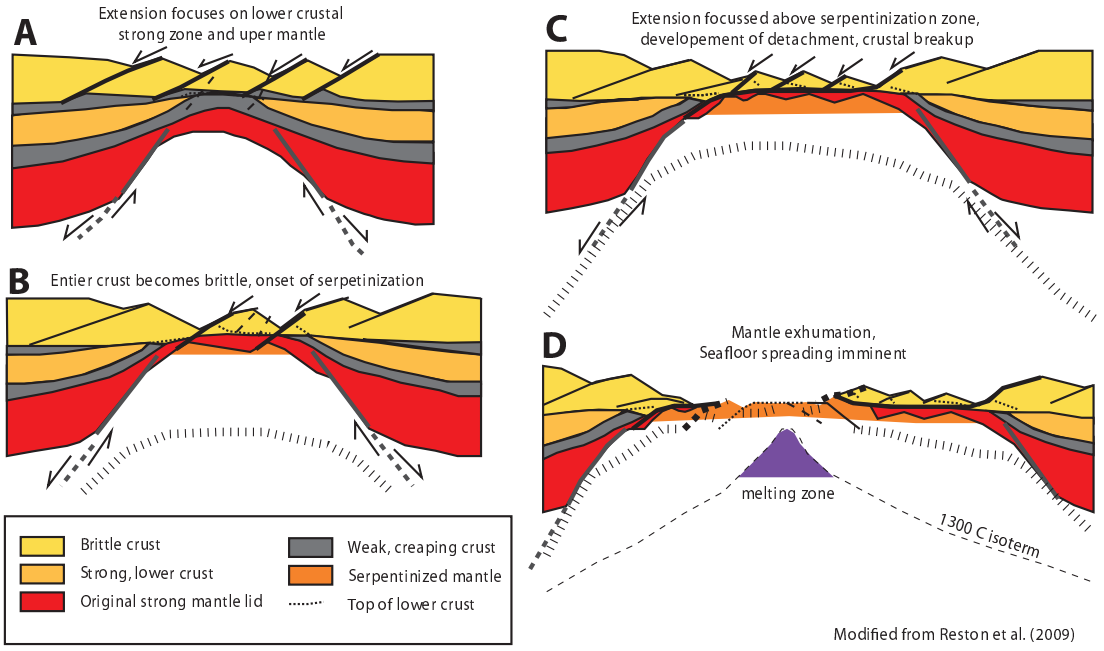

Figure 1.7: Conceptual rifting model of *Reston* (2009). This conceptual model suggests that no depth-dependent stretching occurs. Instead polyphase extension occurs, which may obscure older faulting. As a result, it may be difficult to quantify extension. He proposes a model in which: A) Rifting is initially symmetric until the entire crust becomes brittle. B) Onset of mantle serpentinization when the entire crust becomes brittle. C) Coupling of crust and mantle leads to the development of single large faults and shear zones, which may leave the highly thinned crust on one side producing a late-state asymmetric rifted margin. D) Continental breakup is followed by mantle exhumation. For more details see *Reston* (2009).

1.1 Flemish Cap: Backgound and Motivation for Study

The rifting style of the Flemish Cap-Goban Spur conjugate margin pair was studied in the 1980's (*Keen et al.*, 1989). This is the first place where deep seismic reflection data were used to interpret the rifting style of a passive conjugate margin pair. Seismic reflection profiles from the Flemish Cap-Goban Spur margins (Fig. 1.3) were used to support a symmetric pure shear model of extension, followed by an asymmetric breakup with a sharp continent-ocean-boundary (COB; Fig. 1.8). A more recent wide-angle seismic study of Goban Spur (*Bullock and Minshull*, 2005) situated along the Western Approaches Margin (WAM) multichannel seismic (MCS) profile (*Peddy et al.*, 1989) indicates that extension was more complex on the Flemish Cap-Goban Spur conjugate margins than initially proposed. The P-wave velocity model of Goban Spur includes a wide transition zone interpreted as serpentinized mantle similar to the wide regions of exhumed mantle interpreted on the Iberia margin. This and an OCT with a muted basement morphology on the NE Flemish Cap margin, prompted the suggestion that a similar wide region of exhumed mantle may exist on the Canadian side (*Louden and Chian*, 1999; *Bullock and Minshull*, 2005). A high-velocity body (7.4 km s^{-1}) was previously modelled along a small 50-km-long segment in the OCT of NE Flemish Cap (*Reid and Keen*, 1990). Due to the interpretation of this region as oceanic (*Keen and de Voogd*, 1988), the high-velocity body was assumed to be underplated igneous material. In light of the interpretation of exhumed mantle on Goban Spur (*Bullock and Minshull*, 2005) and the subdued basement morphology (*Louden and Chian*, 1999), this body could potentially consist of exhumed partially serpentinized mantle. Still, the rifting style of this margin pair appears simpler than the rifting style of the SE Flesmish Cap-Galicia Bank conjugate margin pair.

In order to determine a complete conjugate section, the Flemish Cap margin including results from a 460-km-long seismic refraction profile (*Gerlings et al.*, 2011) situated along the original deep MCS reflection profile (Lithoprobe Line 85-3, *Keen and de Voogd*, 1988) was re-examined. As with the MCS profiles the wide-angle seismic lines cross magnetic anomaly 34 well into oceanic crust, which makes this margin pair ideal for studying the transition from rifting to the formation of initial oceanic crust. Line 85-3 was reprocessed and prestack Kirchhoff depth migrated using the raw field tapes. Furthermore, Line 87-4 situated between Line 85-3 and Orphan

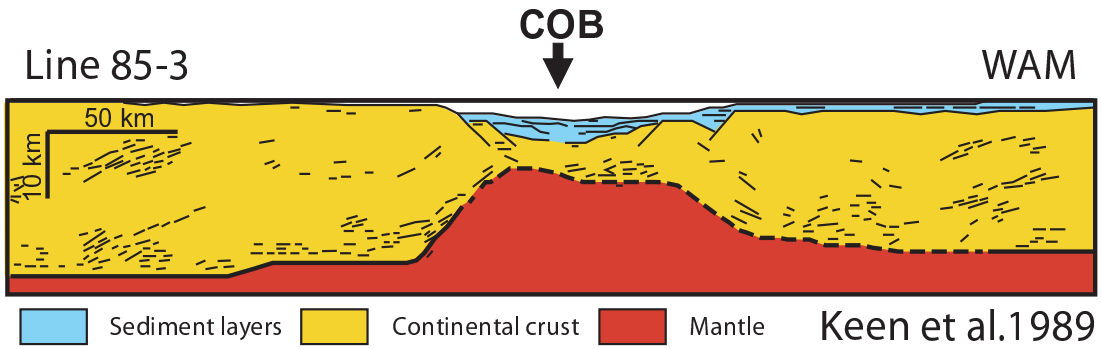

Figure 1.8: Examples of P-wave velocity models from the Nova Scotia and Newfoundland margins, eastern Canada (*Funck et al.*, 2003; *Van Avendonk et al.*, 2006; *Lau et al.*, 2006a; *Funck et al.*, 2004; *Wu et al.*, 2006; *Dehler et al.*, 2004).

Knoll (Fig. 1.3), was reprocessed and prestack Kirchhoff time migrated in order to study the along-strike variation of the NE Flemish Cap margin.

1.2 Tectonic Setting

Flemish Cap, located 475 km east of Newfoundland, is an approximately circular block of Appalacian continental crust (*King et al.*, 1985) some 30 km thick (*Funck et al.*, 2003; *Gerlings et al.*, 2011); the most easterly continental crust of North America (Figs. 1.3 and 1.4). The basement consists of Hadrynian (751-833 Ma) granodiorite and minor granite, dacite and volcanic siltstone, with an onlapping sequence of undisturbed to disturbed Mesozoic-Cenozoic sediments (*King et al.*, 1985). Flemish Cap is separated from the Grand Banks by Flemish Pass, a bathymetric saddle over 1000 m deep. Previous seismic refraction measurements in Flemish Pass indicate a Moho depth of 20-22 km, sediment fill over 5-km-thick, and continental crust about 15-17 km thick (*Keen and Barrett*, 1981). A triple junction divides SE and NE Flemish Cap into two different margin segments. Flemish Cap is part of the North American plate with SE Flemish Cap and Newfoundland margins conjugate to Galicia Bank and the Iberia margins, which are part of the Eurasia Plate. NE Flemish Cap is conjugate to Goban Spur, which is part of the Eurasia (Porcupine) Plate. In this thesis focus is mainly on the NE Flemish Cap margin (Figs. 1.3 and 1.4).

Seafloor spreading progressed from south to north in the North Atlantic (*Srivastava et al.*, 2000). While regions in the south were spreading, the regions north of

them were undergoing extension (Fig. 1.9). Thus, as seafloor spreading progressed to the north with Flemish Cap remaining attached to Galicia Bank, a large portion of the Grand Banks off Newfoundland (including Flemish Cap) underwent extension from Late Triassic to Late Cretaceous (*Sibuet et al.*, 2007b).

Orphan Knoll (Fig. 1.4) is a fragment of thick continental crust, which was part of Flemish Cap before rifting left it behind (*Sibuet et al.*, 2007b). Extension was initially accommodated in Orphan Basin and Flemish Pass (*Sibuet et al.*, 2007b). Rifting in Flemish Pass did not lead to continental breakup, but separation instead took place seaward of Flemish Cap. *Sibuet et al.* (2007b) have suggested that Flemish Cap was rotated clockwise relative to Newfoundland during rifting in the Late Jurassic to Early Aptian.

The dating of syn-rift sedimentary sequences from boreholes (DSDP Sites 549, 550, 551) on the Goban Spur margin indicates that extension of the Flemish Cap-Goban Spur conjugate margin pairs started in the early Barremian (126-128 Ma) (*de Graciansky et al.*, 1985) with final breakup leading to formation of oceanic crust in the Albian (∼110 Ma). Time-scales are taken from *Ogg and Smith* (2004). Magnetic chron 34 (∼84 Ma) is the oldest magnetic anomaly identified on the Flemish Cap-Goban Spur margins and is located close to the continental margin (Figs. 1.3).

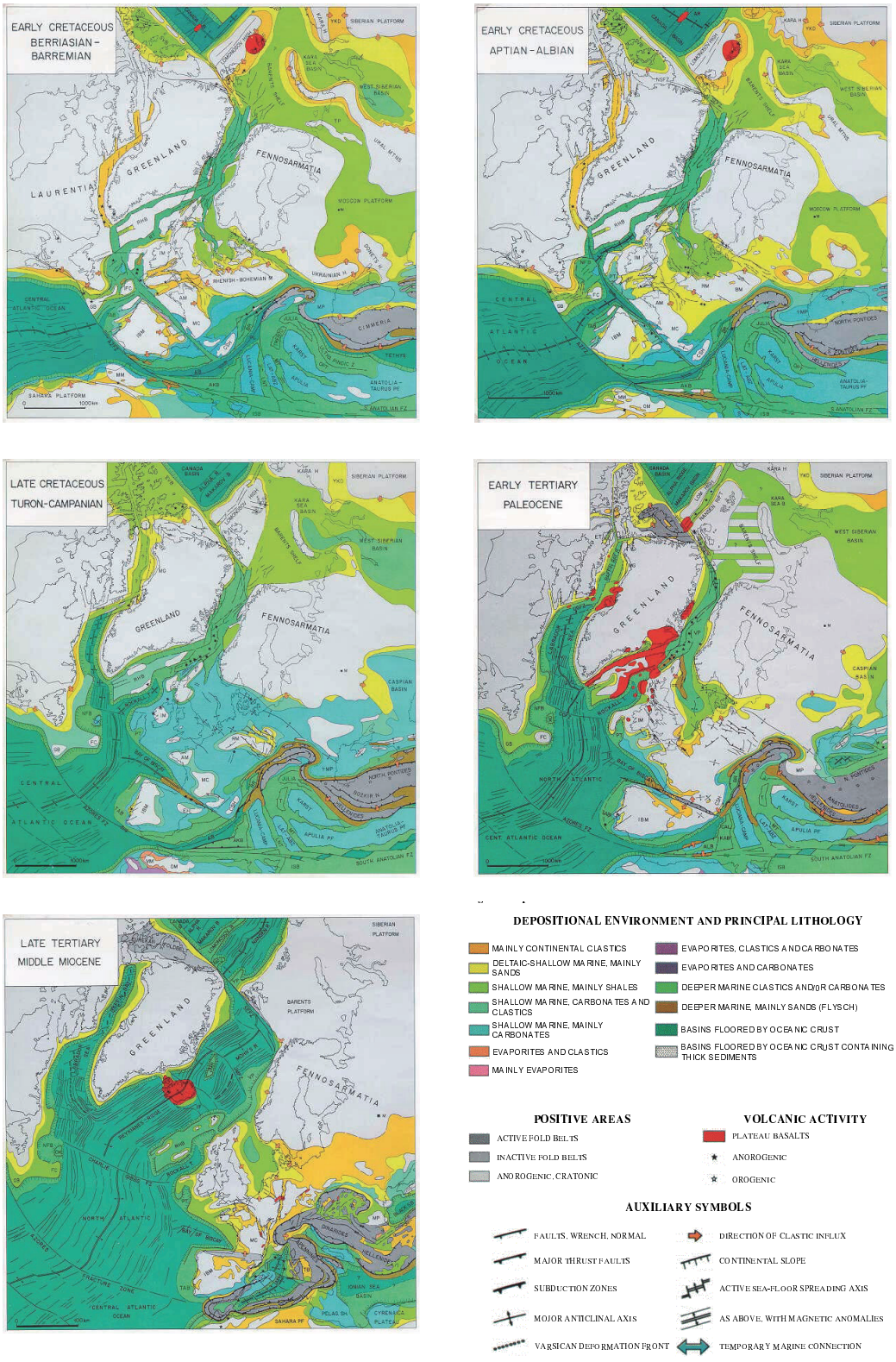

Figure 1.9: Tectonic reconstruction of the North Atlantic Ocean. From *Ziegler* (1988)

1.3 Objectives

The combined wide-angle and MCS datasets have allowed for the following objectives to be pursued with regards to the NE Flemish Cap margin:

1. Determine the thickness, structure and nature of the crust and upper mantle across the NE Flemish Cap margin.
2. Determine the rifting style of the Flemish Cap-Goban Spur conjugate margin pair.
3. Determine the nature and transition into formation of initial oceanic crust.
4. Determine the nature of the along-strike variation of the NE Flemish Cap margin (NE Flemish Cap to Orphan Knoll).

These results may help answer the following questions:

1. What is the nature of the OCT? Is it exhumed serpentinized mantle, as suggested by *Louden and Chian* (1999), perhaps continental, or is there no transition but a sharp boundary and the region is oceanic, as initially suggested by *Keen and de Voogd* (1988)?
2. Is partially serpentinized mantle present within the OCT?
3. What is the nature of the ridge feature observed on Line 85-3?
4. Is the rifting style symmetric or asymmetric? Is it purely two-dimensional or is there a three-dimentional component?
5. Does the transition into formation of oceanic crust appear abrupt or does it take place over a finite distance? Is this transition similar on both sides of the conjugate margins?
6. Is the rifting style similar or does it vary along the margin as on the Newfoundland-Iberia and SE Flemish Cap-Galicia Bank conjugate margins?

7. Did Flemish Cap rotate?

1.4 Chapter Overview

In the following chapters the objectives and questions of section 1.3 are adressed:

Chapter 2:
In this chapter, the P- and S-wave velocity results from the FLAME wide-angle seismic profile across the NE Flemish Cap margin (*Gerlings et al.*, 2011) is presented. The velocity models allowed to determine the thickness, structure and nature of the crust and upper mantle. I processed the raw data and developed the velocity model.

Chapter 3 section 3.1:
The rifting style of the Flemish Cap-Goban Spur conjugate margin pair (*Gerlings et al.*, 2012) will be discussed in this section. Seismic profiles from both margins cross from unextended continental crust across the magnetic anomaly 34, the most landward undisputed anomaly (*Srivastava et al.*, 1988) and hence into unambiguous oceanic crust. This allowed me to interpret the full rift evolution, from stretching to rifting to continental breakup and initial formation of oceanic crust. The addition of wide-angle data to MCS data changed a previous interpretation of the rifting style of the conjugate margin pair from pure shear symmetric (*Keen et al.*, 1989) to simple shear asymmetric rifting (*Gerlings et al.*, 2012). Results from *Gerlings et al.* (2011) and *Bullock and Minshull* (2005) were used to derive the rifiting style, with the addition of a seismic image of the poststack time migrated Line 85-3.

Chapter 3 section 3.2:
The results of the reprocessed poststack time migrated and prestack depth migrated Line 85-3 coincident with the FLAME Line will be discussed in this section. The reprocessing of the MCS data of Line 85-3 has significantly improved the seismic image. The depth migration allowed to observe the true geometry of the crustal structures and more crustal details are visible in the improved image. Hence, further constraints on the nature and structure of the crust and upper mantle are possible (e.g. normal faults seem to cut the entire thin continental crust). A ridge feature on the profile

also gives some indications of its complex nature. I performed the processing and interpretation of Line 85-3 from raw data.

Chapter 4:

In this chapter, the reprocessed result of Line 87-4 located north of Line 85-3 are presented. The two lines show very different crustal structures and hence indicate a change in the rifting style along-strike the margin. For this reason, the nature and extent of crustal domains on the Erable lines, originally interpreted by *Welford et al.* (2010a), situated between Line 85-3 and Line 87-4 are reinterpreted. The combined results show three-dimensional complexity of the crustal domains and a poly-phase rifting style along the margin. This work provides insight into what could be the most profitable areas for understanding the development of rifted magma-poor margins, and that is the three-dimensionality to this process.

Chapter 5:

In this final chapter I summarize the conclusions made in the previous chapters.

References

Boillot, G., J. Girardeau, J. Kornprobst, et al. (1988), Rifting of the Galicia margin: crustal thinning and emplacement of mantle rocks on the seafloor, in *Proceedings of the Ocean Drilling Program, Scientific Results*, vol. 103, pp. 741–756.

Bullock, A. D., and T. A. Minshull (2005), From continental extension to seafloor spreading: crustal structure of the Goban Spur rifted margin, southwest of the UK, *Geophysical Journal International*, *163*(2), 527–546, doi: 10.1111/j.1365-246X.2005.02726.x.

Chian, D., and K. Louden (1994), The continent-ocean crustal transition across the southwest Greenland margin, *Journal of geophysical research*, *99*(B5), 9117–9135.

Chian, D., K. Louden, and I. Reid (1995a), Crustal structure of the Labrador Sea conjugate margin and implications for the formation of nonvolcanic continental margins, *Journal of Geophysical Research*, *100*(B12), 24,239–24.

Chian, D., C. Keen, I. Reid, and K. Louden (1995b), Evolution of nonvolcanic rifted margins: New results from the conjugate margins of the Labrador Sea, *Geology*, *23*(7), 589–592.

Christensen, N. I. (1996), Poisson's ratio and crustal seismology, *Journal of Geophysical Research*, *101*(B2), 3139, doi: 10.1029/95JB03446.

de Graciansky, P., C. Poag, R. Cinningham, P. Loubere, D. Masson, J. Mazzullo, L. Montadert, C. Müller, K. Otsuka, L. Reynolds, et al. (1985), The Goban Spur transect: Geologic evolution of a sediment-starved passive continental margin, *Geological Society of America Bulletin*, *96*(1), 58–76.

Dean, S., T. Minshull, R. Whitmarsh, and K. Louden (2000), Deep structure of the ocean-continent transition in the southern Iberia Abyssal Plain from seismic refraction profiles: The IAM-9 transect at 40°20'N, *Journal of Geophysical Research*, *105*(B3), 5859–5885.

Deemer, S., J. Hall, K. Solvason, K. H. Lau, K. Louden, S. Srivastava, and J.-C. Sibuet (2009), Structure and development of the southeast Newfoundland continental passive margin: derived from SCREECH Transect 3, *Geophysical Journal International*, *178*(2), 1004–1020, doi: 10.1111/j.1365-246X.2009.04162.x.

Dehler, S., C. Keen, T. Funck, H. Jackson, and K. Louden (2004), The limit of volcanic rifting: A structural model across the volcanic to non-volcanic transition off Nova Scotia, in *AGU Spring Meeting Abstracts*, vol. 1, p. 04.

Funck, T., J. Hopper, H. Larsen, K. Louden, B. Tucholke, and W. Holbrook (2003), Crustal structure of the ocean-continent transition at Flemish Cap: Seismic refraction results, *Journal of Geophysical Research*, *108*(B11), 2531.

Funck, T., H. Jackson, K. Louden, S. Dehler, and Y. Wu (2004), Crustal structure of the northern Nova Scotia rifted continental margin (eastern Canada), *Journal of Geophysical Research*, *109*(B9), B09,102.

Gerlings, J., K. E. Louden, and H. R. Jackson (2011), Crustal structure of the Flemish Cap Continental Margin (eastern Canada): an analysis of a seismic refraction profile, *Geophysical Journal International*, *185*(1), 30–48, doi: 10.1111/j.1365-246X.2011.04931.x.

Gerlings, J., K. E. Louden, T. A. Minshull, and M. R. Nedimović (2012), Flemish Cap-Goban Spur conjugate margins: New evidence of asymmetry, *Geology*, *40*(12), 1107–1110, doi: 10.1130/G33263.1.

Hopper, J. R., T. Funck, B. E. Tucholke, H. Christian Larsen, W. S. Holbrook, K. E. Louden, D. Shillington, and H. Lau (2004), Continental breakup and the onset of ultraslow seafloor spreading off Flemish Cap on the Newfoundland rifted margin, *Geology*, *32*(1), 93, doi: 10.1130/G19694.1.

Huismans, R., and C. Beaumont (2011), Depth-dependent extension, two-stage breakup and cratonic underplating at rifted margins, *Nature*, *473*(7345), 74–8, doi: 10.1038/nature09988.

Jagoutz, O., O. Müntener, G. Manatschal, D. Rubatto, G. Péron-Pinvidic, B. D. Turrin, and I. M. Villa (2007), The rift-to-drift transition in the North Atlantic: A stuttering start of the MORB machine?, *Geology*, *35*(12), 1087, doi: 10.1130/G23613A.1.

Keen, C., and B. de Voogd (1988), The continent-ocean boundary at the rifted margin off eastern Canada: new results from deep seismic reflection studies, *Tectonics*, *7*(1), 107–124.

Keen, C., C. Peddy, B. de Voogd, and D. Matthews (1989), Conjugate margins of canada and europe: Results from deep reflection profiling, *Geology*, *17*(2), 173–176.

Keen, C. E., and D. L. Barrett (1981), Thinned and subsided continental crust on the rifted margin of Eastern Canada: crustal structure, thermal evolution and subsidence history, *Geophysical Journal International*, *65*(2), 443–465, doi: 10.1111/j.1365-246X.1981.tb02721.x.

King, L. H., G. B. Fader, W. H. Poole, and R. K. Wanless (1985), Geological setting and age of the Flemish Cap granodiorite, east of the Grand Banks of Newfoundland, *Canadian Journal of Earth Sciences*, *22*(9), 1286–1298, doi: 10.1139/e85-133.

Lau, K. (2005), Structure of the Eastern Grand Banks/Newfoundland basin rifted margin, Ph.D. thesis, Dalhousie University, Halifax, Nova Scotia.

Lau, K. W. H., K. E. Louden, T. Funck, B. E. Tucholke, W. S. Holbrook, J. R. Hopper, and H. Christian Larsen (2006a), Crustal structure across the Grand Banks-Newfoundland Basin Continental Margin - I. Results from a seismic refraction profile, *Geophysical Journal International*, *167*(1), 127–156, doi: 10.1111/j.1365-246X.2006.02988.x.

Lau, K. W. H., K. E. Louden, S. Deemer, J. Hall, J. R. Hopper, B. E. Tucholke, W. S. Holbrook, and H. Christian Larsen (2006b), Crustal structure across the Grand Banks-Newfoundland Basin Continental Margin - II. Results from a seismic reflection profile, *Geophysical Journal International*, *167*(1), 157–170, doi: 10.1111/j.1365-246X.2006.02989.x.

Lavier, L. L., and G. Manatschal (2006), A mechanism to thin the continental lithosphere at magma-poor margins., *Nature*, *440*(7082), 324–8, doi: 10.1038/nature04608.

Lay, T., and C. Wallace (1995), *Modern global seismology*, Academic Press.

Louden, K., and D. Chian (1999), The deep structure of non–volcanic rifted continental margins, *Philosophical Transactions A*, *357*(1753), 767.

Maillard, A., J. Malod, E. Thiébot, F. Klingelhoefer, and J.-P. Réhault (2006), Imaging a lithospheric detachment at the continentocean crustal transition off Morocco, *Earth and Planetary Science Letters*, *241*(3-4), 686–698, doi: 10.1016/j.epsl.2005.11.013.

McKenzie, D. (1978), Some remarks on the development of sedimentary basins, *Earth and Planetary Science Letters*, *40*(1), 25–32.

Ogg, J., and A. Smith (2004), The geomagnetic polarity time scale, in *A Geologic Time Scale 2004*, edited by O. J. Gradstein, F.M. and A. Smith, pp. 63–86, Cambridge University Press.

Peddy, C., B. Pinet, D. Masson, R. Scrutton, J. Sibuet, M. Warner, J. Lefort, I. Shroeder, et al. (1989), Crustal structure of the Goban Spur continental margin, Northeast Atlantic, from deep seismic reflection profiling, *Journal of the Geological Society*, *146*(3), 427–437.

Pérez-Gussinyé, M., and T. Reston (2001), Rheological evolution during extension at nonvolcanic rifted margins-onset of serpentinization and development of detachments leading to continental breakup, *Journal of Geophysical Research*, *106*(B3), 3961–3975.

Péron-Pinvidic, G., and G. Manatschal (2008), The final rifting evolution at deep magma-poor passive margins from Iberia-Newfoundland: anew point of view, *International Journal of Earth Sciences*, *98*(7), 1581–1597, doi: 10.1007/s00531-008-0337-9.

Pickup, S., R. Whitmarsh, C. Fowler, and T. Reston (1996), Insight into the nature of the ocean-continent transition off West Iberia from a deep multichannel seismic reflection profile, *Geology*, *24*(12), 1079–1082.

Reid, I., and C. Keen (1990), High seismic velocities associated with reflections from within the lower oceanic crust near the continental margin of Eastern Canada, *Earth and Planetary Science Letters*, *99*(1), 118–126.

Reston, T. (2009), The structure, evolution and symmetry of the magma-poor rifted margins of the North and Central Atlantic: A synthesis, *Tectonophysics*, *468*(1-4), 6–27, doi: 10.1016/j.tecto.2008.09.002.

Shillington, D., N. White, T. Minshull, G. Edwards, S. Jones, R. Edwards, and C. Scott (2008), Cenozoic evolution of the eastern Black Sea: A test of depth-dependent stretching models, *Earth and Planetary Science Letters*, *265*(3), 360–378.

Shillington, D. J., W. S. Holbrook, H. J. a. Van Avendonk, B. E. Tucholke, J. R. Hopper, K. E. Louden, H. C. Larsen, and G. T. Nunes (2006), Evidence for asymmetric nonvolcanic rifting and slow incipient oceanic accretion from seismic reflection data on the Newfoundland margin, *Journal of Geophysical Research*, *111*(B9), B09,402, doi: 10.1029/2005JB003981.

Sibuet, J.-C. (2004), Pyrenean orogeny and plate kinematics, *Journal of Geophysical Research*, *109*(B8), B08,104, doi: 10.1029/2003JB002514.

Sibuet, J.-C., S. Srivastava, and G. Manatschal (2007a), Exhumed mantle-forming transitional crust in the Newfoundland-Iberia rift and associated magnetic anomalies, *Journal of Geophysical Research*, *112*(B6), B06,105, doi: 10.1029/2005JB003856.

Sibuet, J.-C., S. P. Srivastava, M. Enachescu, and G. D. Karner (2007b), Early Cretaceous motion of Flemish Cap with respect to North America: implications on the formation of Orphan Basin and SE Flemish Cap Galicia Bank conjugate margins, *Geological Society, London, Special Publications*, *282*(1), 63–76, doi: 10.1144/SP282.4.

Small, C. (1994), A global analysis of mid-ocean ridge axial topography, *Geophysical Journal International*, *116*(1), 64–84.

Srivastava, S., J. Verhoef, and R. Macnab (1988), Results from a detailed aeromagnetic survey across the northeast Newfoundland margin, Part I: spreading anomalies and relationship between magnetic anomalies and the ocean-continent boundary, *Marine and petroleum geology*, *5*(4), 306–323.

Srivastava, S., J. Sibuet, S. Cande, W. Roest, and I. Reid (2000), Magnetic evidence for slow seafloor spreading during the formation of the Newfoundland and Iberian margins, *Earth and Planetary Science Letters*, *182*(1), 61–76.

Van Avendonk, H. J. A., W. S. Holbrook, G. T. Nunes, D. J. Shillington, B. E. Tucholke, K. E. Louden, H. C. Larsen, and J. R. Hopper (2006), Seismic velocity structure of the rifted margin of the eastern Grand Banks of Newfoundland, Canada, *Journal of Geophysical Research*, *111*(B11), B11,404, doi: 10.1029/2005JB004156.

Welford, J. K., J. Hall, J.-C. Sibuet, and S. P. Srivastava (2010), Structure across the northeastern margin of Flemish Cap, offshore Newfoundland from Erable multichannel seismic reflection profiles: evidence for a transtensional rifting environment, *Geophysical Journal International*, *183*(2), 572–586, doi: 10.1111/j.1365-246X.2010.04779.x.

Wernicke, B. (1981), Low-angle normal faults in the basin and Range Province: nappe tectonics in an extending orogen, *Nature*, *291*, 645–648.

White, R., and D. McKenzie (1989), Magmatism at rift zones: the generation of volcanic continental margins and flood basalts, *Journal of Geophysical Research*, *94*(B6), 7685–7729.

White, R., G. Spence, S. Fowler, D. McKenzie, G. Westbrook, and A. Bowen (1987), Magmatism at rifted continental margins, *Nature*, *330*(6147), 439–444.

White, R., D. McKenzie, and R. O'Nions (1992), Oceanic crustal thickness from seismic measurements and rare earth element inversions, *J. geophys. Res*, *97*(19), 683–19.

Wu, Y., K. E. Louden, T. Funck, H. R. Jackson, and S. A. Dehler (2006), Crustal structure of the central Nova Scotia margin off Eastern Canada, *Geophysical Journal International*, *166*(2), 878–906, doi: 10.1111/j.1365-246X.2006.02991.x.

Zelt, C., and P. Barton (1998), Three-dimensional seismic refraction tomography: A comparison of two methods applied to data from the Faeroe Basin, *Journal of Geophysical Research*, *103*(84), 7187–7210.

Zelt, C., and D. Forsyth (1994), Modeling wide-angle seismic data for crustal structure: Southeastern Grenville Province, *Journal of Geophysical Research*, *99*(B6), 11,687–11.

Zelt, C. A., and R. B. Smith (1992), Seismic traveltime inversion for 2-D crustal velocity structure, *Geophys. J. Int.*, *108*, 16–34.

Ziegler, P. (1988), Evolution of the arctic-north atlantic and the western tethys–a visual presentation of a series of paleogeographic-paleotectonic maps, *Mem.-Am. Assoc. Pet. Geol*, *43*, 164–196.

Chapter 2

Crustal Structure of the Flemish Cap Continental Margin (Eastern Canada): An Analysis of a Seismic Refraction Profile

This chapter is published as "*Gerlings, J., Louden, K.E., and Jackson, H.R. (2011), Crustal structure of the Flemish Cap Continental Margin (eastern Canada): an analysis of a seismic refraction profile, Geophys. J. Int., 185(1), 30-48.*" Minor editorial corrections were applied.

2.0 Summary

The crustal structure of the NE Flemish Cap margin was determined along a 460-km-long refraction/wide-angle reflection seismic transect (FLAME Line) to define the thickness, structure and composition of the crust and uppermost mantle along the line. A P-wave velocity model was developed from forward and inverse modelling of dense airgun shots recorded by 19 ocean bottom seismometers. A coincident multichannel seismic profile was used to guide the modelling as reflections could be identified down to Moho. The model displays a sediment cover of up to 3.6-km-thick, subdivided into three layers with velocities of 1.8-1.9 km s^{-1}, 2.8-3.1 km s^{-1} and 4.7-4.8 km s^{-1}. For the western part of the FLAME Line over Flemish Cap, the P-wave velocity modelindicate that the continental crust is up to 32-km-thick, and has a three layers. The continental crust has velocities of 5.8-6.1 km s^{-1}, 6.3-6.45 km s^{-1} and 6.65-6.85 km s^{-1} and thicknesses of about 5 km, 7 km and 20 km in the upper, middle and lower layers, respectively. The thick continental crust thins to a two-layer, 6-km-thick crust (upper layer is 5.55-6.0 km s^{-1} and the layer below is 6.65-6.8 km s^{-1}) over a distance of 45 km. S-wave velocities are determined in the upper layer of the thick continental crust over Flemish Cap and the transition zone by assigning Poisson's ratios in the P-wave velocity model. Comparison of calculated to observed arrival

times gives a Poisson's ratio of 0.27 in the upper layer and 0.28 in the layer below, which suggests that the composition of the crust is primarily continental in both the thick crust and the thin crust of the transition zone. The thin continental crust is stretched over a width of 80 km and is underlain by a layer with velocities of 7.5-7.9 km s^{-1}. We interpret this layer as partially serpentinized mantle, which is consistent with observations from the Newfoundland margin to the south. The serpentinized mantle terminates 30 km seaward of the thick continental crust. At the seaward-most end of the thin continental crust, a prominent ridge feature is observed. The seismic refraction and multichannel seismic data results indicate a mixed character between serpentinized mantle with volcanic extrusions or continental crust. The reflection seismic data show a high relief basement from the ridge feature and seaward. The FLAME Line crosses magnetic anomaly 34 and extends another ∼50 km seaward well into oceanic crust. The ridge is flanked seaward by a two-layer oceanic crust. The upper layer (Layer 2) has velocities of 4.8-5.0 km s^{-1} for the landward-most 35 km of oceanic crust and 4.8-6.2 km s^{-1} for the seaward 60 km. The average thickness of Layer 2 is ∼2 km. The lower layer (Layer 3) has velocities of 6.7-7.2 km s^{-1} and a thickness of ∼3.5 km. The velocity model is consistent with a sharp onset of seafloor spreading seaward of the ridge feature.

2.1 Introduction

Passive rifted continental margins were intensely studied over the last couple of decades. One focus weres on non-volcanic margins, which represent the majority of the eastern Canadian margins and their conjugates in Greenland or northern Europe (*Louden and Chian*, 1999). These non-volcanic margins are associated with little or no melting of the mantle in contrast to volcanic margins, which form where large volumes of magma are emplaced prior to and during rifting (*White et al.*, 1987). The crustal structures and compositions across passive margins are studied best on non-volcanic margins where the extensional fabric were not modified by large volumes of syn-rift and post-rift volcanism.

Studies from the last couple of decades give some insight into the complex mechanisms of continental rifting and its evolution to seafloor spreading. The results led to

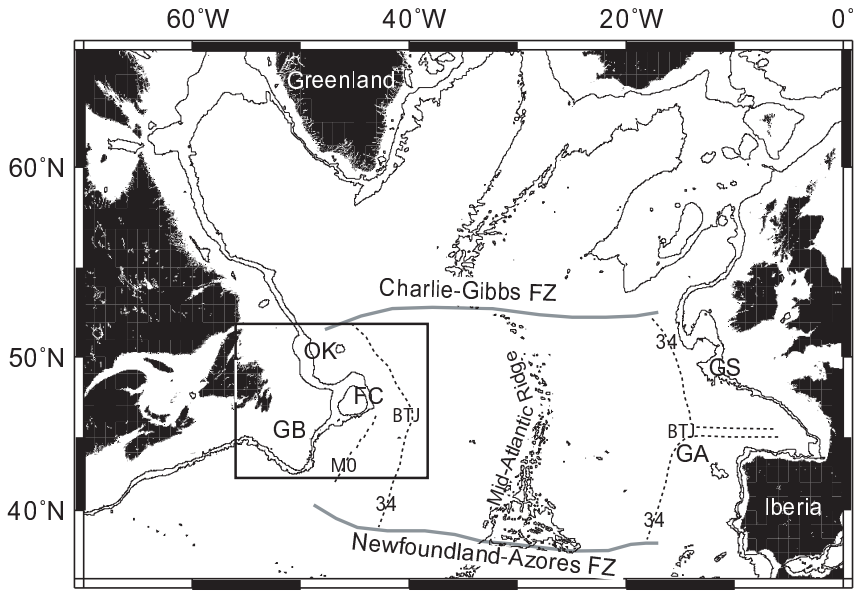

Figure 2.1: Regional map of the Atlantic. Black dashed lines indicate magnetic anomaly M0 and 34 taken from *Srivastava et al.* (2000). Grey solid lines indicate the two fracture zones: Charlie-Gibbs and Newfoundland-Azores. BTJ, Biscay Triple Junction; FC, Flemish Cap; GA, Galicia Bank; GB, Grand Banks; GS, Goban Spur; OK, Orphan Knoll. Black box indicates location map in Fig. 2.2.

discovery of an ocean-continent transition (OCT) zone, which exists between undisputed oceanic crust and extended continental crust. Offshore seismic data and ODP drilling results from the eastern Canadian non-volcanic margins show that the crust in the transition zone can have characteristics of either exhumed serpentinized mantle, thin continental crust or unusual ocean crust formed by ultra-slow spreading (*Srivastava and Roest*, 1999; *Funck et al.*, 2003, 2004; *Lau et al.*, 2006a; *Van Avendonk et al.*, 2006; *Party*, 2004). Underlying this crust is often a layer of partially serpentinized mantle (*Louden and Chian*, 1999).

These OCTs vary not only in their crustal composition, but also in width. We encounter wide zones of exhumed mantle over distances of 100 km on the northern Nova Scotian (*Funck et al.*, 2004) and southern Newfoundland (*Lau et al.*, 2006a) margins as well as its conjugate Iberian margin (*Dean et al.*, 2000). However, the transition zones narrow and pinch-out both to the south on the central Nova Scotian margin (*Wu et al.*, 2006) and to the north at SE Flemish Cap (*Funck et al.*, 2003; *Lau*, 2005; *Van Avendonk et al.*, 2006). In this paper, we focus on the OCT farther

north on the NE Flemish Cap margin (Figs. 2.1 and 2.2).

The FLAME (Flemish Cap Margin Transect; Figs. 2.1 and 2.2) refraction/wide-angle reflection seismic (R/WAR) experiment was carried out in 2002 (*Jackson et al.*, 2002) and is situated along the Lithoprobe Line 85-3, a deep multichannel reflection seismic (MCS) profile (*Keen and de Voogd*, 1988). The aim was to gain new insight into the transition from rifting to the onset of seafloor spreading. The FLAME Line offers a particular opportunity to detail the transition from rifting to formation of oceanic crust, given that it crosses magnetic anomaly 34 and extends another $\sim$50 km over ocean crust (Fig. 2.2). In this paper, we further concentrate on the nature of the crust in the transition zone and a comparison of the results with recent results from the Newfoundland margin to the south.

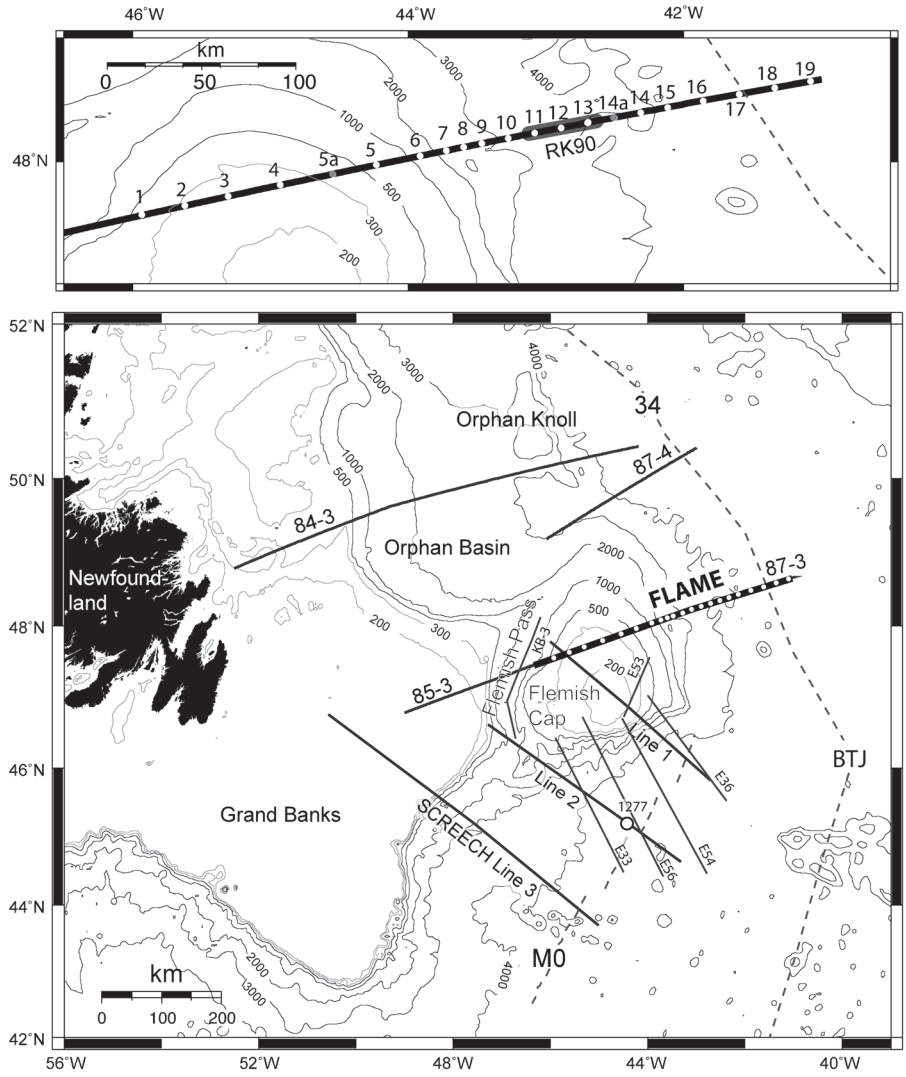

Figure 2.2: (Bottom) Bathymetry map of the study area showing the FLAME Line (thick black line), together with relevant lines to this study: SCREECH Line 1, 2 and 3, the Lithoprobe Line 84-3 and 87-4, and the Lithprobe Line 85-3 and 87-3 (thin grey lines). Line 85-3 and Line 87-3 are coincident with FLAME Line 1. Black circle indicate ODP drill site 1277 (*Party*, 2004). Magnetic anomalies M0 and 34 (grey dashed lines) are taken from *Srivastava et al.* (2000). Depth contours are shown as indicated. (Top) Locations of the OBSs on the FLAME Line. OBSs 5a and 14a (grey circles) contained no data. The remaining OBSs (white circles) are identified as OBSs 1 to 19. Thick grey line indicates the location of the (*Reid and Keen*, 1990) velocity profile (RK90) coincident with the FLAME Line.

2.2 Geological Setting

Flemish Cap is located 475 km east of Newfoundland and is an approximately circular block of Appalacian continental crust (*King et al.*, 1985), the most easterly continental crust of North America (Fig. 2.2). The basement consists of Hadrynian (751-833 Ma) granodiorite and minor granite, dacite and volcanic siltstone, with an onlapping sequence of undisturbed to disturbed Mesozoic-Cenozoic sediments (*King et al.*, 1985). Flemish Cap is separated from the Grand Banks by Flemish Pass, a bathymetric saddle over 1000 m deep. Previous seismic refraction measurements in Flemish Pass indicate Moho depth at 20-22 km, sediment fill over 5-km-thick and continental crust about 15-17 km thick (*Keen and Barrett*, 1981).

Seafloor spreading progressed from south to north in the North Atlantic (*Srivastava et al.*, 2000). While regions in the south were spreading, the regions north of them were undergoing extension. Thus as seafloor spreading progressed to the north, with Flemish Cap remaining attached to Galicia Bank, a large portion of the Grand Banks of Newfoundland, including Flemish Cap, underwent extension from Late Triassic to Late Cretaceous, thereby rotating Flemish Cap clockwise relative to Newfoundland (*Sibuet et al.*, 2007b). Orphan Knoll (Figs. 2.1 and 2.2) is a fragment of thick continental crust, which was part of Flemish Cap before the rotation but was left behind (*Sibuet et al.*, 2007b). Extension was initially accommodated in the Orphan Basin and Flemish Pass (*Sibuet et al.*, 2007b). However, rifting in Flemish Pass did not lead to continental breakup, but separation instead took place seaward of Flemish Cap. SE Flemish Cap was separated from Galicia Bank in Barremian close to M3 time (∼127 Ma, *Srivastava et al.*, 2000, timescales are taken from *Ogg and Smith* 2004) and with rifting progressing northward, NE Flemish Cap separated from Goban Spur in the Albian (∼110 Ma, *de Graciansky et al.*, 1985).

Flemish Cap is part of the North American Plate whereas the conjugate Goban Spur is part of the Eurasian (Porcupine) Plate (Fig. 2.1). South of the Eurasian Plate, Galicia Bank is the northern part of the Iberian Plate. The three plates form the Biscay Triple Junction (BTJ) at magnetic anomaly 34 (Fig. 2.1). The BTJ is located just south of the FLAME Line (Fig. 2.2). This is consistent with magnetic anomaly M0 (∼125 Ma), which is observed southeast of Flemish Cap in Newfoundland Basin but not northeast of Flemish Cap where the oldest magnetic anomaly is

magnetic anomaly 34 (∼84 Ma; Figs. 2.1 and 2.2).

At magnetic anomaly 34, the plates changed opening direction from a roughly east-west direction to a northeast-southwest direction.

2.3 Wide-angle Seismic Experiment

2.3.1 Data Acquisition and Processing

The FLAME Line is a 460-km-long transect across and westward of Flemish Cap (Figs. 2.1 and 2.2). The R/WAR FLAME Line is situated along Lithoprobe Line 85-3, a deep MCS profile (*Keen and de Voogd*, 1988) oriented in a roughly W-E direction. A total of 21 ocean bottom seismometers (OBS) were deployed along the line with a minimum spacing of 9.8 km and a maximum spacing of 30.1 km. The closest OBS spacing was in the middle of the profile seaward of the shelf break (Fig. 2.2). The energy source used in this survey was a tuned airgun array that consisted of 12 guns (2.0-16.4 L) with a total volume of 104 L. The average shot spacing was 165 m. The global positioning system was used for navigation and timing. Two of the OBSs (5a and 14a, see Fig. 2.2) failed to record data leaving 19 OBSs for developing a velocity model.

The OBS raw data were converted to SEGY format, debiased and corrected for the drift of the OBS clock. Positions of the OBS at the seafloor were determined from traveltime picks of the direct wave. For the record sections shown in this paper (Figs. 2.3-2.6), a 5 to 10 Hz bandpass filter was used, which contains the main seismic energy. Deconvolution was applied to the record sections to sharpen the wavelet. Trace amplitudes in the seismograms were weighted by their distance to the OBS to increase amplitudes with increasing offset. Water depths along the FLAME Line were obtained from shipboard soundings.

2.3.2 Methodology

The instrument positions were located on a great circle arc, which was the baseline for the 2-D velocity modelling. The P-wave velocity model for the crust and upper mantle was developed using the programs RAYINVR (*Zelt and Smith*, 1992; *Zelt and Forsyth*, 1994) and FAST (*Zelt and Barton*, 1998). Generally, the hydrophones had

a better signal-to-noise ratio and were used for modelling, except for OBSs 3 and 4 where the vertical geophones were used instead. FAST was used to produce a starting model, then a forward model was developed using RAYINVR from top to bottom by fitting the observed traveltimes. Velocities within the individual layer boundaries were further optimized by inversion. The coincident MCS data were used to define layers with low ray coverage such as sediment layers and basement. Synthetic seismograms were use to check and adjust velocity gradients in the individual layers and gravity data were then used for a final adjustment of the velocity model, particularly regarding the Moho depth.

2.3.3 Wide-angle Seismic Data

The nature of the seismograms changes significantly along the line. Some of the key features of the seismic phases are illustrated in Figs. 2.3-2.6 for OBSs 4, 12, 15 and 18. These sections represent various characteristic aspects of the data. Phase names of refractions and reflections are summarized in Table 2.1.

OBSs 1 to 7 are located on Flemish Cap and constrain both the structure of the thick continental crust and the onset of crustal thinning; OBSs 3-7 have an especially high signal-to-noise ratio. An example of these data is shown for OBS 4 (Fig. 2.3). The energy on the vertical geophone of OBS 4 can be traced up to 170 km away from the receiver. A sediment refraction, P_{S3}, with apparent velocities of 4.8 km s^{-1} west of the OBS and 4.9 km s^{-1} east of the OBS is observed both east and west of the OBS between offsets of 0 to10 km. The P_{S3} phase was modelled with a velocity of 4.8 km s^{-1}. Continental crustal refractions, P_{C1} and P_{C2}, were observed on both sides of the OBS. They were modelled with velocities of 6.0-6.3 km s^{-1}, respectively. The P_{C1} refraction has an apparent velocity of 6.0 km s^{-1} west and until 80 km east of the OBS where the P_{C2} refraction appears and starts interfering with the P_{C1} refraction. The apparent velocity of the P_{C1} phase decreases to $\sim$4.5 km s^{-1} at 80 km. P_{C2} has an apparent velocity of 6.2 km s^{-1} west of the OBS and an apparent velocity of 5.5-6.0 km s^{-1} east of the OBS. Crustal reflections, $P_{C1}P$ and $P_{C2}P$, and the Moho reflection, $P_{m1}P$, are also observed. Use of different reduction velocities, filters and gains help to identity these reflections, although we do not have as good a control of these mid-crustal reflections as the Moho reflection. The mantle refraction, P_n, has

Table 2.1: Identification of layers in the P-wave velocity model, the name of the seismic phases and record sections on which they were identified.

Layer	Phase	OBS records for observed phases
Refractions in:		
Sediment layer 1	P_{S1}	2, 9, 11, 16
Sediment layer 2	P_{S2}	9, 18, 19
Sediment layer 3	P_{S3}	1-4, 8-11
Upper continental crust	P_{C1}	1-15
Middle continental crust	P_{C2}	2-14
Lower continental crust	P_{C3}	
Oceanic layer 2	P_{L2}	15-19
Oceanic layer 3	P_{L3}	15-19
Partially serpentinized mantel	P_Z	11, 12, 14, 15
Mantle	P_n	4-15, 17-19
Reflections at:		
Base of sediment layer 1	$P_{S1}P$	14, 15
Base of sediment layer 2	$P_{S2}P$	8-13, 15
Base of sediment layer 3	$P_{S3}P$	1-3, 8
Base of upper continental crust	$P_{C1}P$	3-7, 9
Base of middle continental crust	$P_{C2}P$	1-8
Base lower continental crust	$P_{m1}P$	1, 3-8
Base of cont. crust in trans. zone	$P_{m2}P$	7-13
Base of oceanic layer 3	$P_{m3}P$	16, 18, 19
Base of serpentinized mantle	P_ZP	11, 12, 14

an apparent velocity of 8.1 km s^{-1} and was modelled with a velocity of 8.0 km s^{-1}. The mantle refraction is observed east of the OBS.

OBSs 8-15 represent the initial thinning of the continental crust where the refractions have rapidly changing character. One example is shown for OBS 12 (Fig. 2.4). The energy is traced up to 120 km away from the OBS. On this section a new high-velocity phase, P_Z, is introduced with modelled velocity of 7.7 km s^{-1}. This phase has an apparent velocity of 7.8 km s^{-1}. Furthermore, the crustal refractions, P_{C1} and P_{C2} , and the mantle refraction, P_n , are also observed with modelled velocities of 5.55 km s^{-1}, 6.65 km s^{-1} and 8.0 km s^{-1} , respectively. The P_{C1} phase has an apparent velocity of 5.5 km s^{-1} west of the OBS and 5.6 km s^{-1} east of the OBS. The P_{C2} phase has an apparent velocity of 6.7 km s^{-1}. The ray tracing of the mantle refraction shows the initial thinning of the continental crust (Fig. 2.4). The P_n phase has an apparent velocity of 7.0 km s^{-1} between 160 and 200 km, 10.0 km

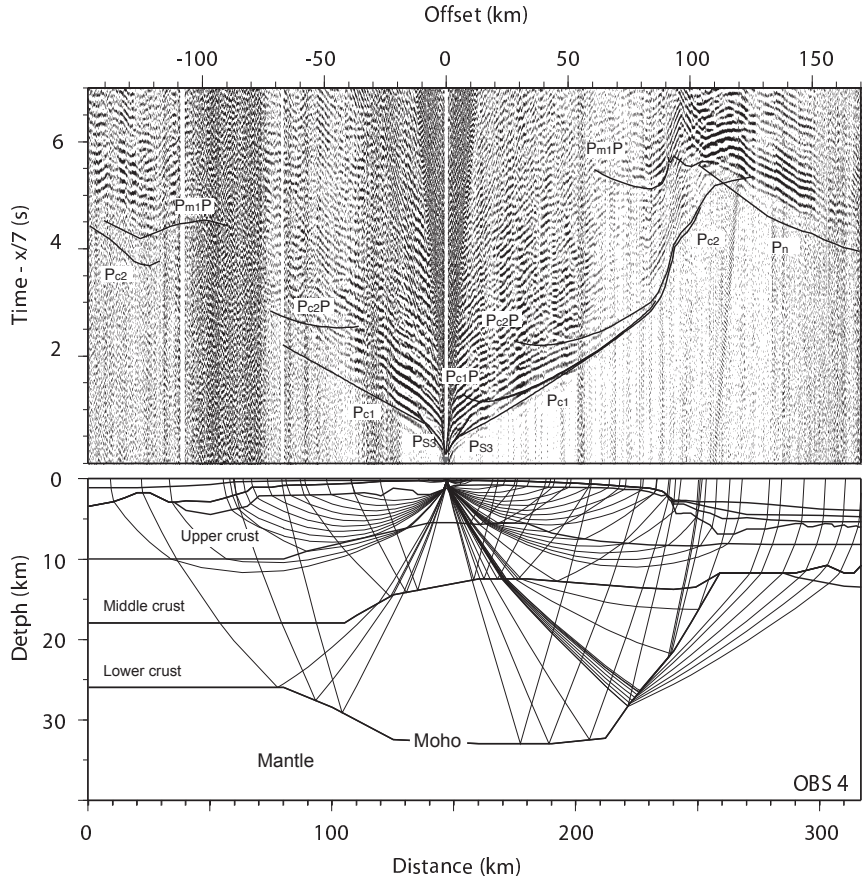

Figure 2.3: Record section (top) with computed traveltimes and ray path diagram (bottom) for the vertical geophone of OBS 4. The vertical scale for the record section is traveltime (s) using a reduction velocity of 7.0 km s^{-1}, and the horizontal scale is shot-receiver distance (offset in km). The horizontal scale in the ray path diagram is distance (km) along the velocity model. Layers are labelled as interpreted in the P-wave velocity model of Fig. 2.7. The phases are described in the text.

s^{-1} between 240 and 250 km and 8.3 km s^{-1} between 255 and 270 km west of the OBS. The sediment reflection, $P_{S2}P$, is clear but the Moho reflection, $P_{m2}P$, is just notable on either side of the OBS. Furthermore, a reflection, P_ZP, is observed below the Moho reflection.

OBSs 14 and 15 represent the transition to oceanic crust located on either side of the continent-ocean boundary (COB). OBS 14 (Fig. 2.5, left) is located on a ridge feature (see MCS data in Fig. 2.12 at 360 km distance). The apparent velocities of the upper crustal phase, P_{C1}, appear to differ on either side of the OBS (5.2 km s^{-1} west; 3.8 km s^{-1} east), as the upper crustal layer thins and pinches out just east

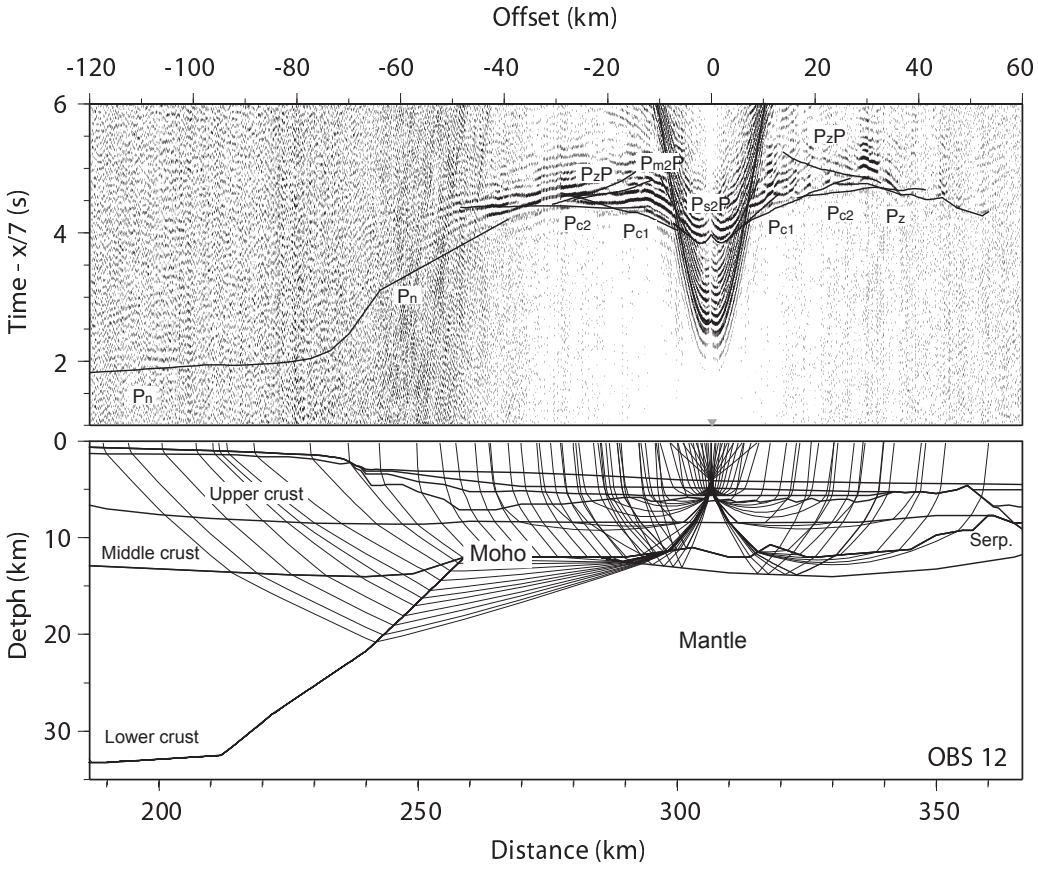

Figure 2.4: Record section (top) with computed traveltimes and ray path diagram (bottom) for the hydrophone of OBS 12. The vertical scale for the record section is traveltime (s) using a reduction velocity of 7.0 km s^{-1}, and the horizontal scale is shot-receiver distance (offset in km). The horizontal scale in the ray path diagram is distance (km) along the velocity model. Layers are labelled as interpreted in the P-wave velocity model of Fig. 2.7. The phases are described in the text.

of the OBS. The crustal refractions P_{C2} and P_Z are observed as well as the mantle refraction, P_n, whichare observed up to 85 km away from the OBS with apparent velocities of 6.5 km s^{-1}, 7.8 km s^{-1} and 8.0 km s^{-1}, respectively. The reflection, P_ZP, is also observed.

Energy is traced out to about 40 km of either side of OBS 15 (Fig. 2.5, right). West of the OBS, we observe the refractions P_{C1} and P_Z with apparent velocities of 5.0 km s^{-1} and 7.4 km s^{-1}, respectively. The reflections $P_{S1}P$ and $P_{S2}P$ sre observed. East of the OBS 15, two new refractions, P_{L2} and P_{L3} are interpreted with modelled velocities of 4.8 km s^{-1} and 6.7 km s^{-1}, respectively. The apparent velocities

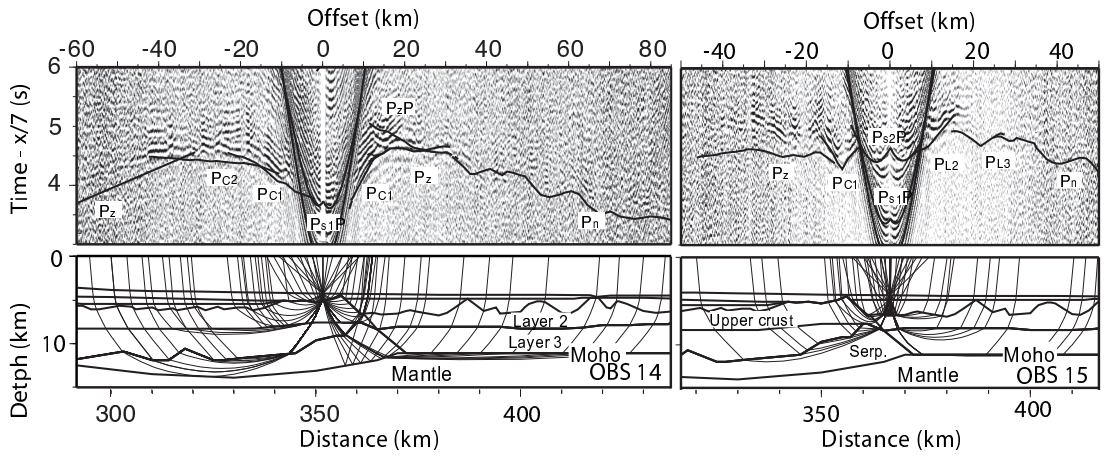

Figure 2.5: Record section (top) with computed traveltimes and ray path diagram (bottom) for the hydrophone of OBSs 14 and 15. The vertical scale for the record section is traveltime (s) using a reduction velocity of 7.0 km s^{-1}, and the horizontal scale is shot-receiver distance (offset in km). The horizontal scale in the ray path diagram is distance (km) along the velocity model. Layers are labelled as interpreted in the P-wave velocity model of Fig. 2.7. The phases are described in the text.

of these refractions are 4.7 km s^{-1} and 7.1 km s^{-1}, respectively. OBS 15 is located just seaward of the ridge feature. The energy starts to diminish abruptly at about 380 km (Fig. 2.5, right) as observed on OBSs 10 to 15. OBSs 16 and 17 have a low signal-to-noise ratio and only a weak P_{L3} phase that can be traced only up to 30 km away from the OBS. The signal-to-noise ratio increases again on OBSs 18 and 19.

OBS 18 (hydrophone, Fig. 2.6) is located seaward of magnetic anomaly 34 and hence we consider the crust to be of oceanic composition. On this record, energy is traced about 90 km west of the OBS and the shots terminate about 25 km east of the OBS. Sediment refraction P_{S2} and crustal refractions, P_{L2} and P_{L3} with modelled velocities of 4.7 km s^{-1} and 6.7 km s^{-1}, respectively, are observed. The apparent velocity of the P_{L2} refraction varies to the west of the OBS due to the high relief basement with velocities of 4.0 km s^{-1} west of 415 km and 8.5 km s^{-1} east of 415 km. East of the OBS the phase (P_{L2}) has an apparent velocity of 4.5 km s^{-1}. The P_{L3} refraction appears disrupted, consistent with a faulted basement. The phase has an average apparent velocity of 7.0 km s^{-1}. The P_n refraction arrives at 3.3 s reduced traveltime between distance 335-360 km with an apparent velocity of 7.0 km s^{-1} and at 4.2 s between distance 365-385 km with an apparent velocity of 8.0 km s^{-1}. Rays traced through the transition zone thus arrive 0.9 s earlier than those traced through

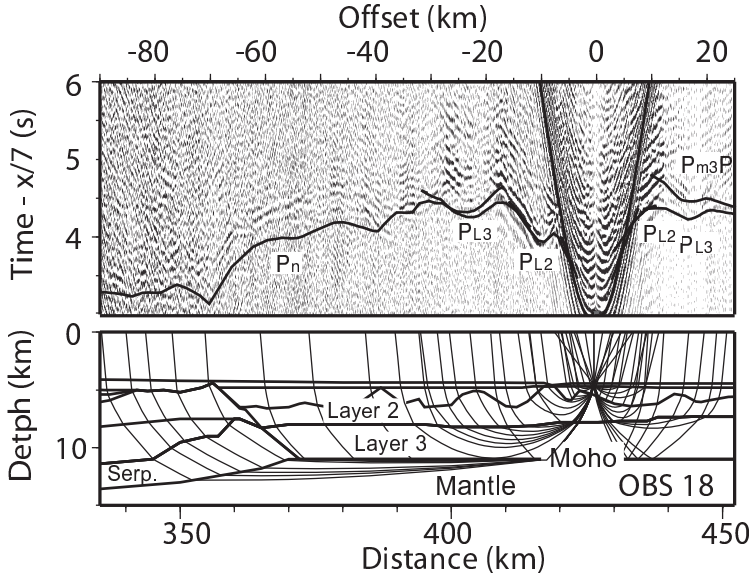

Figure 2.6: Record section (top) with computed traveltimes and ray path diagram (bottom) for the hydrophone of OBS 18. The vertical scale for the record section is traveltime (s) using a reduction velocity of 7.0 km s^{-1}, and the horizontal scale is shot-receiver distance (offset in km). The horizontal scale in the ray path diagram is distance (km) along the velocity model. Layers are labelled as interpreted in the P-wave velocity model of Fig. 2.7. The phases are described in the text.

oceanic crust (Fig. 2.6). The mantle phase has an apparent velocity of 8.5 km s^{-1} east of 385 km. The Moho reflection, $P_{m3}P$, is observed to the east.

2.4 Results

2.4.1 P-Wave Velocity Model

The P-wave velocity model is shown in Fig. 2.7. The landward end of the model from 0 to 210 km is characterized by a up to 32-km-thick three layer crust with velocities of 5.8-6.1 km s^{-1}, 6.3-6.45 km s^{-1} and 6.65-6.85 km s^{-1} and thicknesses of about 5 km, 7 km and 20 km in the upper, middle and lower layers, respectively. Between 0 and 130 km, a sediment layer with velocities of 2.9-3.1 km s^{-1} is encountered, pinching out at about 130 km. Below this layer is another sedimentary layer with velocities of 4.7-4.9 km s^{-1} that extends from 35 to 235 km. This layer is 2-km-thick at 50 km and thins to less than 1 km on the central part of Flemish Cap.

At 210 km, about 30 km before the shelf break, the continental crust thins rapidly over a distance of 45 km to a thickness of 6 km at 255 km. The crust between

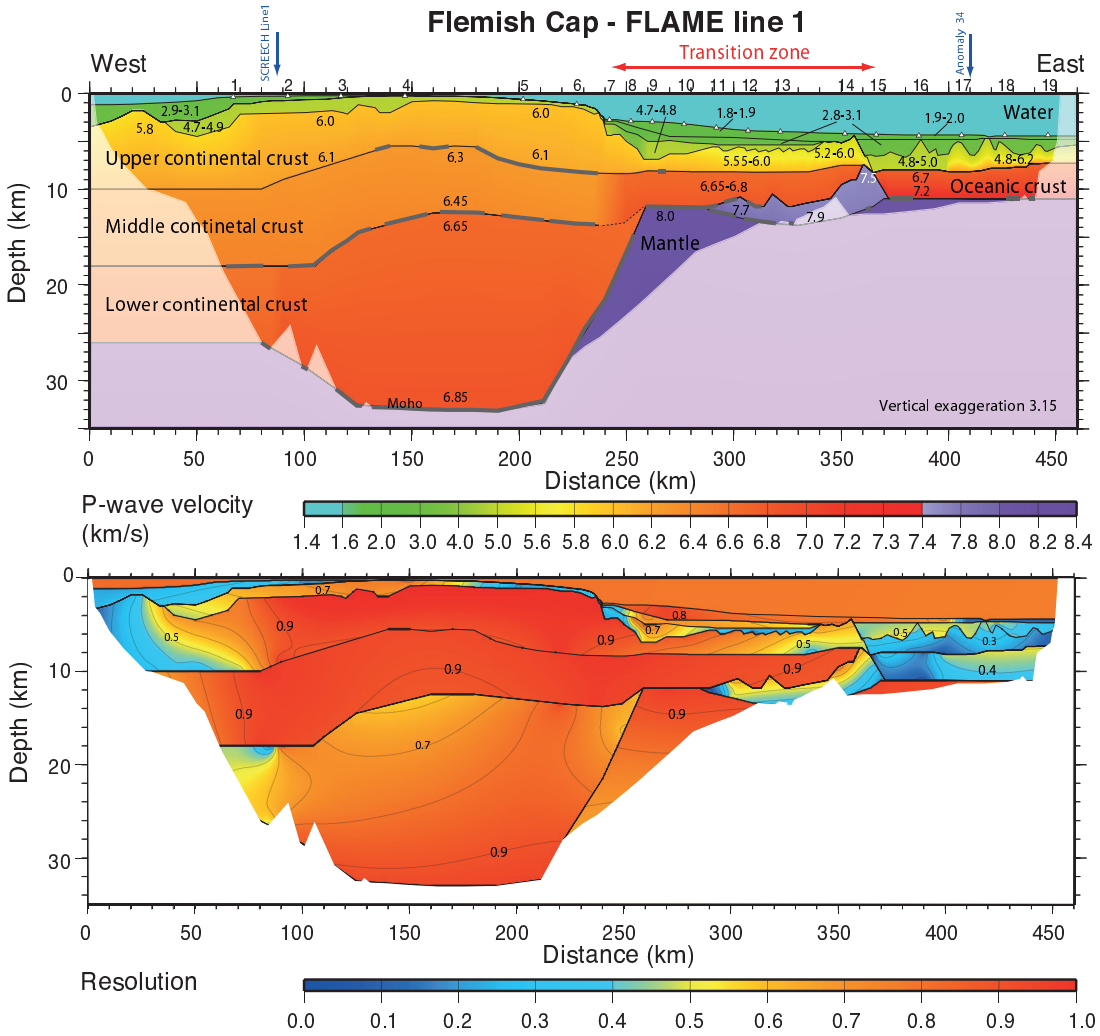

Figure 2.7: P-wave velocity model (top) along the FLAME Line. Numbers indicate velocity in km s^{-1}. Triangles mark the location of the OBS used for the modelling. Wide-angle reflection interfaces are marked with bold grey lines. The vertical blue arrows near OBSs 2 and 17 show the position of the cross point with SCREECH Line 1 and magnetic anomaly 34, respectively. Areas with no ray coverage in the P-wave velocity model have light shading. Diagonal values of the resolution matrix of the P-wave velocity model (bottom). The values for the velocity nodes have been contoured. Values >0.5 indicate a good resolution.

210 and 360 km is overlain by sediment layers up to 3.6-km-thick with velocities of 1.8-1.9 km s^{-1}, 2.8-3.1 km s^{-1} and 4.7-4.8 km s^{-1}. The crust between 210 and 360 km can be divided into two layers with velocities of 5.55-6.0 km s^{-1} and 6.65-6.8 km s^{-1} and with thicknesses of about 2.5 km and 3.5 km, respectively. Moho is defined by the $P_{m2}P$ reflections with a depth of ∼11 km between 255 to 340 km. Between 290 km and 360 km an up to 5-km-thick high velocity layer (7.5-7.9 km s^{-1}) is modelled below the two crustal layers. We refer to this section of the model as transitional crust and will discuss its characteristics and origin in further detail in Section 5.2.

At 360 km, we encounter a significant change in the velocity structure of the crust. At this point the transitional crust has almost zero thickness (< 1 km). Further seaward the crust thickens abruptly (∼5 km thick) and can be divided into two layers. The upper layer has a thickness that varies between 2 and 3 km with velocities of 4.8-6.0 km s^{-1} between distance 360 and 410 km and 4.8-6.2 km s^{-1} from distance 410 km and seaward. The 4-km-thick lower layer has velocities of 6.7-7.2 km s^{-1}. These layers are interpreted as oceanic crust layer 2 and 3 (see Section 5.3 later). Moho depth is at 11 km.

2.4.2 P-Wave Velocity Model Uncertainty and Resolution

The assigned pick uncertainty, the root-mean-square (rms) traveltime residual, the number of observations for individual P-phases and the normalized χ^2 are summarized in Table 2.2. A comparison of observed and calculated traveltimes for OBSs 1-19 is shown in Fig. 2.8 together with the corresponding ray paths. Pick uncertainties are indicated by the heights of the vertical bars. Our results show a good agreement between observed and calculated traveltimes. The traveltime residual is 109 ms and the normalized χ^2 is 0.921 for the P-phases. Fig. 2.7 shows the diagonal of the resolution matrix of the velocity model. Resolution matrix diagonals >0.5 are considered to be well-resolved model parameters (*Lutter et al.*, 1990; *Zelt*, 1999). The resolution matrix shows that the velocity model is well resolved in areas where there is good ray coverage (Fig. 2.7). There is, however, reduced resolution within the sedimentary layers, which is related to the lack of reversed observations in the thin sediment layers. The MCS data compensate partly for the lack of these reversed observations. Oceanic layers 2 and 3 (360-460 km) are also poorly resolved. No reverse

rays were traced in this part and the P_{L2} and P_{L3} refractions could only be traced a short distance from the OBS. Zones in the mantle that are sampled by rays show an acceptable resolution, although only mantle in the OCT zone and beneath the oceanic crust are sampled. Moho is well resolved (Fig. 2.7) on most parts of the model, except between 0 and 70 km (see Section 4.4 for further discussion) and at the initial thinning of the continental crust, where Moho is steep and hence rays are difficult to trace.

To determine the uncertainty of the velocity and layer boundaries, selected nodes

Phase	n	t_{ass} (ms)	t_{rms} (ms)	χ^2
Direct	822	85	90	1.011
P_{S1}	92	92	82	0.992
$P_{S1}P$	35	115	117	1.038
P_{S2}	54	85	91	1.325
$P_{S2}P$	223	110	97	0.736
P_{S3}	451	80	73	0.822
$P_{S3}P$	101	75	78	0.763
P_{C1}	3682	100	93	0.928
$P_{C1}P$	878	100	91	0.850
P_{C2}	2375	110	106	0.893
$P_{C2}P$	1698	105	99	0.804
$P_{m1}P$	2157	150	151	1.139
$P_{m2}P$	368	105	112	0.947
P_{L2}	128	120	124	1.074
P_{L3}	277	120	91	0.769
$P_{m3}P$	103	120	123	0.954
P_Z	438	105	100	0.787
P_ZP	181	120	135	1.357
P_n	2177	120	115	0.844
Total	16240	110	109	0.921

Table 2.2: The number of observations (n), the assigned average pick uncertainty (t_{ass}), the root-mean-squares (rms) traveltime residual (t_{rms}) and the normalized χ^2 for individual P-phases.

in the model were perturbed to check for the sensitivity of the traveltimes to these changes. The velocity uncertainty in the crust is generally ± 0.1 km s^{-1}, although it was somewhat higher (± 0.2 km s^{-1}) in the seaward end of the model. The depth uncertainty of the layer boundaries is up to ± 1 km for well-sampled boundaries.

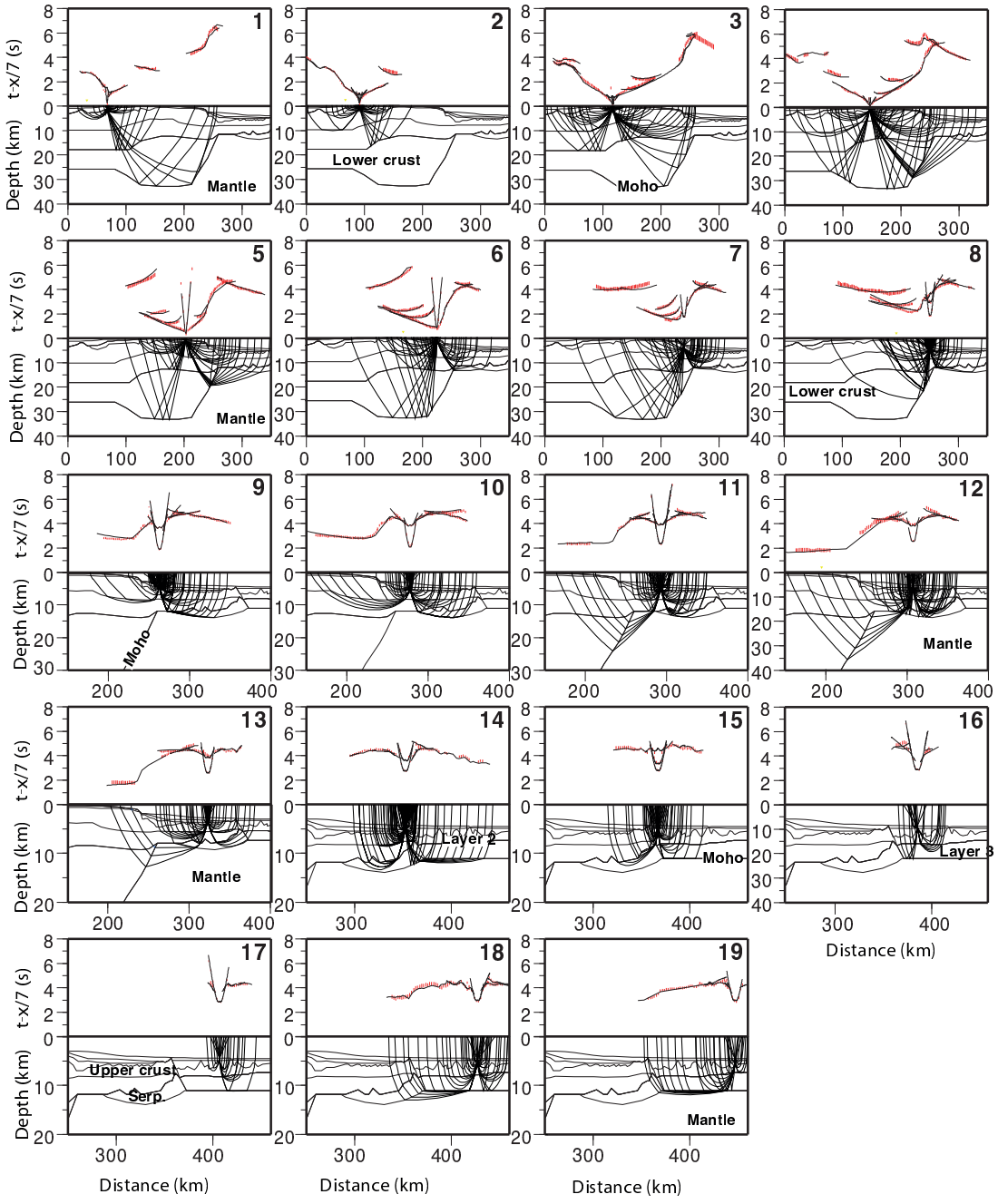

Figure 2.8: Comparison of observed (red bars) and calculated (lines) traveltimes for OBSs 1-19 shown together with the corresponding ray paths and model layers. Traveltimes are displayed with a reduction velocity of 7.0 km s^{-1}. Pick uncertainties of the observed traveltimes are indicated by the heights of the vertical red bars. Horizontal scale is distance (in km) for the velocity model of Fig. 2.7.

2.4.3 S-Wave Velocity Model

S-waves were observed on the horizontal geophones of OBSs 2, 5, 6 and 8-13 in the continental and transitional parts of the velocity model. No S-waves were observed in the oceanic part. OBSs 2, 5 and 6 sample the upper crust and OBSs 8 to 13 the middle crustal layer in the transition zone. We used the horizontal geophone with the highest signal-to-noise ratio regardless of orientation in modelling the arrival times of the S-wave. Furthermore, we calculated S-wave velocities from the P-wave velocity model by assigning Poisson's ratios to the different layers of sediment and crust in the model. Calculated arrival times were then compared to the observed arrival times. The P-to-S phase conversion occurs at the basement beneath the shot and from there the rays continue as S-waves to the OBS (with no conversion back to P waves), except for the deepest part of the sediment basin between distance 245 and 290 km. In the latter region, the P-to-S conversion occurs at the top of an extra high velocity sediment layer with velocities of 4.7-4.8 km s^{-1}. The boundary for the P-to-S phase conversion is marked with a red line in Fig. 2.9. Conversions at other boundaries or other phases (e.g. P-to-S phase conversion occurring at the basement and converting again back to P-waves at the basement, or a P-to-S conversion at the seafloor) would not fit the observed arrivals for reasonable velocities.

We obtained a good fit between observed and calculated arrival times using Poisson's ratios of 0.27 for the upper crustal layer and 0.28 for the middle layer in the transition zone (Fig. 2.9). An example of modelled traveltimes in comparison with observed traveltimes is shown in Fig. 2.9 (left) for the horizontal geophone of OBS 11. The assigned pick uncertainty, the rms traveltime residual, the number of observations for individual S-phases and the normalized χ^2 are summarized in Table 2.3. For all the S-phases we obtained a total rms traveltime residual of 109 ms and a total normalized χ^2 of 0.956 for 1635 observations on the nine OBSs.

It has previously been suggested that the transition zone on NE Flemish Cap may be composed entirely of serpentinized mantle (e.g. *Louden and Chian*, 1999; *Bullock and Minshull*, 2005). Hence, we also tested a model using Poisson's ratio representing serpentinized mantle with decreasing serpentinization with depth. Following *Christensen* (1996), we assigned Poisson's ratios of 0.36, 0.33 and 0.30 to the upper, middle and lower crust in the transition zone, respectively. The assigned pick uncertainty,

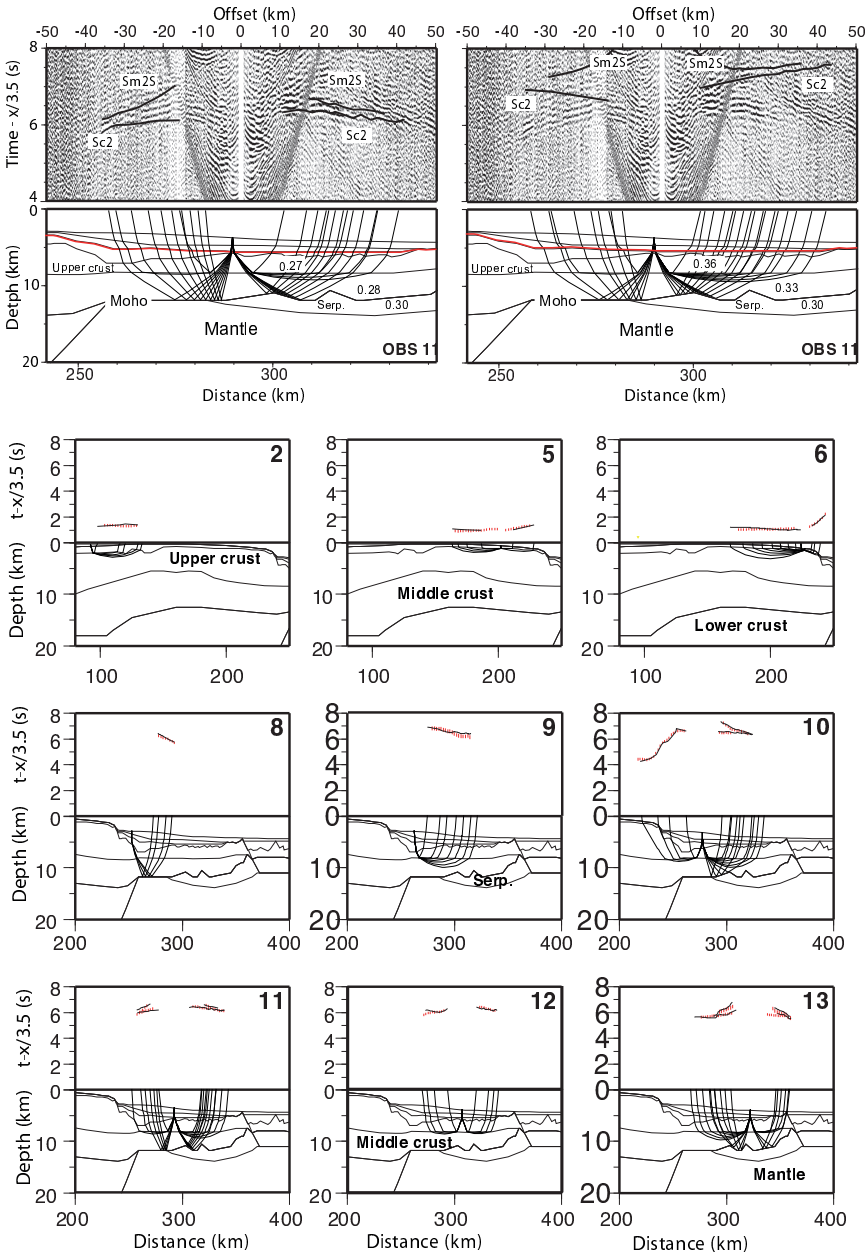

Figure 2.9: Record section (top) with computed traveltimes of S-wave and ray path diagram below for the horizontal geophone of OBS 11 for values of Poisson's ratio associated with either serpentinized mantle (right) or thin continental crust underlain by serpentinized mantle (left). Numbers in the layers indicate the assigned Poisson's ratio. The vertical scale of the record section is the traveltime (s) using a reduction velocity of 3.5 km s^{-1}, and the horizontal scale is shot-receiver distance (offset in km). The P-to-S phase conversion is indicated by a red thin line in the ray path diagram. (Bottom) Comparison of observed (red bars) and calculated (lines) traveltimes for OBSs 2, 5, 6, 8-13 shown together with the corresponding ray paths and model layers. Traveltimes are displayed with a reduction velocity of 3.5 km s^{-1}. Pick uncertainties of the observed traveltimes are indicated by the heights of the vertical red bars. Horizontal scale is distance (in km) for the velocity model of Fig. 2.7.

Phase	n	t_{ass} (ms)	t_{rms} (ms)	χ^2
Continent. crust				
S_{C1}	579	100	95	0.898
S_{C2}	736	110	116	1.149
$S_{m2}S$	320	120	100	0.623
Total	1635	110	109	0.956
Serpent. mantle				
S_{C1}	579	100	95	0.898
S_{C2}	616	110	913	91.370
$S_{m2}S$	314	120	1060	69.892
Total	1509	110	760	47.831

Table 2.3: The number of observations (n), the assigned average pick uncertainty (t_{ass}), the root-mean-squares (rms) traveltime residual (t_{rms}) and the normalized χ^2 for individual S-phases.

the rms traveltime residual, the number of observations for individual S-phases and the normalized χ^2 for the case of a transition zone consistent of serpentinized mantle are summarized also in Table 2.3. In this case, we obtained for a total rms traveltime residual of 760 ms and a total normalized χ^2 of 43.813. Fig. 2.9 (right-hand side) shows an example of calculated arrival times for a transition zone where the whole zone is partially serpentinized mantle. On this section, the misfit between calculated and observed arrival times is ∼600 ms or greater.

2.4.4 The Gravity Model

To check the velocity model for consistency with the gravity data, 2-D gravity modelling was carried out using the Talwani algorithm (*Talwani et al.*, 1959). Free-air gravity data were extracted from satellite altimetry of *Sandwell and Smith* (2009). The gravity model was obtained from conversion of P-wave velocities to density using the empirical relationship of *Ludwig et al.* (1970), which is given by

$$\rho = -0.00283v^4 + 0.0704v^3 - 0.598v^2 + 2.23v - 0.7, \tag{2.1}$$

where v is P-wave velocity in km s^{-1} and ρ is density in kilogram per cubic metre. The mantle under the continental crust was modelled with a density of 3330 kg m^{-3} and mantle under transitional and oceanic crust was modelled with a density of 3270 kg m^{-3}. The theoretical gravity profile computed from the P-wave velocity model is

shown in Fig. 2.10. The model was extended 300 km in each direction to minimize edge effects.

The calculated and observed gravity display a generally good fit. The density model is approximately isostatically balanced at its base (65 km), where the lithostatic pressure is 1966 MPa with variations of up to 25 MPa (Fig. 2.10). The maximum difference between calculated and observed gravity is 15.2 mGal and the rms misfit is 4.46 mGal. Some misfits can be attributed to deviations from the two dimensionality of the model. Within 10 km of either side of the model plane, the gravity varies by up to 15 mGal, except in the most westward part of the model (0-70 km) where it varies by up to 30 mGal. In this latter region of Flemish Cap Basin and at the edge of Flemish Pass, we have raised Moho depth to 26 km to fit the gravity. Previous seismic refraction results (Line KB-3) indicate that Moho depth decreases to about 22 km in Flemish Pass (Fig. 2.2, *Keen and Barrett*, 1981).

The most complex area to model due to the abrupt lateral velocity changes are found to be in the centre of the model at the shelf break where the continental crust thins rapidly and the water depth increases from a few 100 m to almost 4 km. Fig. 2.10 shows the best gravity fit we have obtained without compromising the fit of the R/WAR data.

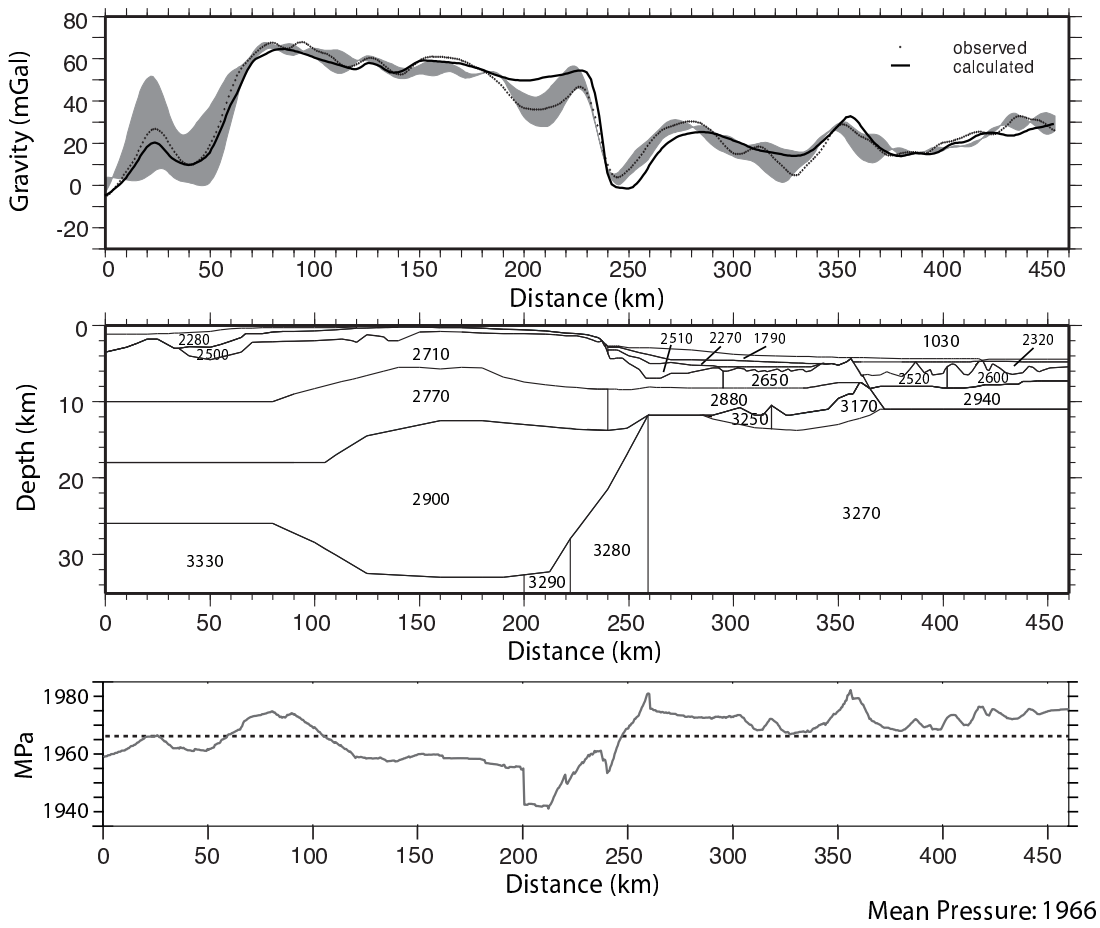

Figure 2.10: Gravity model for the FLAME Line. A comparison (top) of the calculated (solid line) and observed satellite gravity (dashed line). Grey shaded area indicates the gravity 10 km of either side of the model plane. The P-wave velocity model (Fig. 2.7) was converted to density (middle) using the velocity-density relationship of *Ludwig et al.* (1970). The densities in the polygons are given in kilogram per cubic metre. (Bottom) The lithostatic pressure at the base of the model (depth of 65 km) is shown as solid line. Dashed line is the mean pressure, 1966 MPa.

2.5 Discussion

The velocity model (Fig. 2.7) displays three main features. Continental crust, with a maximum thickness of 32 km, thins rapidly to a 6-km-thick, 110-km-wide transition zone beyond which up to 6-km-thick oceanic crust is encountered. In the following sections, we will discuss in relation to other seismic profiles: (1) the unextended continental crust and the rapid thinning of the continental crust; (2) the nature of the transitional crust; and (3) the transition to and nature of the oceanic crust.

2.5.1 Continental Crust

The crust under Flemish Cap was already examined with R/WAR data by *Funck et al.* (2003, SCREECH (Study of Continental Rifting and Extension of the Eastern Canadian Shelf) Line 1) . SCREECH Line 1 crosses the FLAME Line near OBS 2 (see Figs. 2.2 and 2.7). Flemish Cap was also drilled down to shallow basement, which was determined to consist mainly of granodiorite and minor granite (Hadrynian; 751-833 Ma *King et al.*, 1985). Granodiorite has a Poisson's ratio of 0.27 ± 0.02 and an upper crustal P-wave velocity of 6.08 ± 0.35 km s^{-1} (*Holbrook et al.*, 1992). Modelled S-wave arrivals (Poisson's ratio of 0.27) and P-wave velocity (6.0 km s^{-1}) of the upper crustal layer on the FLAME Line under Flemish Cap support this crustal composition.

The westward part of the FLAME velocity model displays a typical unextended three-layer continental crust similar to what was observed on SCREECH Line 1 (*Funck et al.*, 2003).

A comparison of 1-D velocity-depth curves of the continental crust at the crossing point is shown in Fig. 2.11 together with the velocity-depth curve of SCREECH Line 3 (*Lau et al.*, 2006a), which represents the continental crust beneath the outer Grand Banks. The overall average thickness of the thick continental crust on Flemish Cap in the models of the FLAME Line and SCREECH Line 1 is similar ($\sim 30 - 31$ km) (*Funck et al.*, 2003). The average thickness of the unextended continental crust of SCREECH Line 3 located on Grand Banks is a few kilometres thicker, ∼35 km (*Lau et al.*, 2006a). SCREECH Line 3 and the FLAME Line have a similar velocity profile at the top of the crust with an upper crustal velocity of 6.0 km s^{-1}. SCREECH Line

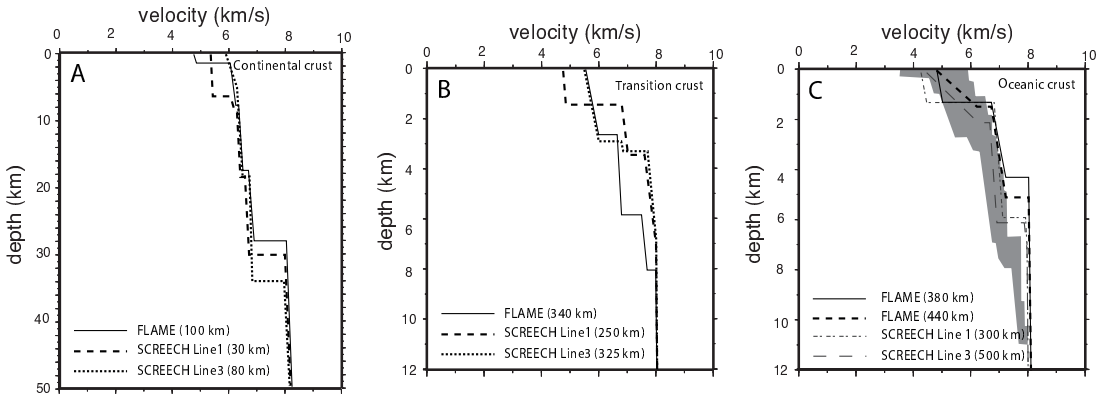

Figure 2.11: Velocity-depth curves from of the FLAME Line together with SCREECH Line 1 and 3. Vertical scale represents depth from basement to upper mantle. (A) Velocity-depth curves from Flemish Cap the thick continental part of the FLAME Line together with velocity-depth curves from unextended continental crust from SCREECH Line 1 and 3. (B) Velocity-depth curves from the transition zones of the FLAME Line and SCREECH Line 1 and 3. (C) Thick dashed black lines represent velocity-depth curves from the oceanic part of the FLAME model, the thin solid line represent the transition zone in the FLAME model and the grey shaded area stacked velocity-depth curves for 59-127 Myr old oceanic crust in the Atlantic Ocean (*White et al.*, 1992). Thin dashed lines represent velocity-depth curves from the oceanic part of SCREECH Lines 1 and 3.

1 has a 6-km-thick layer at the top with a lower velocity (5.4 km s^{-1}) than that of the two other lines. This layer was interpreted to consist of either pre-rift sedimentary rocks, mixed sedimentary/igneous rocks, or basement (*Funck et al.*, 2003). The FLAME Line contains a layer on top of the basement with slightly lower velocities (4.7-4.9 km s^{-1}; Figs. 2.7 and 2.11) than that of SCREECH Line 1. The base of the 4.7 km s^{-1} layer has a depth of 2 km at the crosspoint with SCREECH Line 1 (Fig. 2.11) but deepens to $\sim$5 km at distance 50 km (Fig. 2.7) compared to a depth of 6.9 km on SCREECH Line 1. However, the FLAME model is poorly resolved in this area (Fig. 2.7) and we are not able to give further constraints on the characteristics of this layer.

Clear Moho reflections are observed on Line 85-3 at 180-230 km distance beneath Flemish Cap at two-way time (TWT) 10-10.5 s (depths of 31-33 km, *Keen and de Voogd*, 1988), which fits well with our modelled Moho depth of 32-33 km. Moho is, however, more difficult to observe farther seaward. A major tilted fault block is observed on the profile at 240-245 km distance (Fig. 2.12). The resolution of the

R/WAR data was not high enough to model this major fault block and hence the MCS profile was used. The fault block is underlain by a clear, slightly landward dipping reflection (R1; at 250 km distance and 6.5 s), which was suggested to be a mid-crustal reflection by *Louden and Chian* (1999). In our model, the reflection coincides with the boundary between the upper and middle continental crust of the velocity model.

At the shelf break, the continental crust thins abruptly from 32 km to 6 km over a distance of ∼45 km. This abrupt thinning is consistent with results of the SCREECH Lines from the Newfoundland margin to the south where recent R/WAR seismic results (*Funck et al.*, 2003; *Lau et al.*, 2006a; *Van Avendonk et al.*, 2006) show a transition from unextended continental crust to thin crust (>10 km) over a distance of 50-70 km (Fig. 2.13). This abrupt thinning contrasts with the Nova Scotia, Iberia, and Labrador margins where the reduction in crustal thickness occurs over a range of 100-200 km (*Chian et al.*, 1995a; *Dean et al.*, 2000; *Funck et al.*, 2004; *Wu et al.*, 2006). There may be a relationship between the fault block (Fig. 2.12) located at the shelf break in the basement and the abrupt necking. The fault block may relate to the H-block described by *Lavier and Manatschal* (2006). The H-block is formed during stretching and thinning of the crust in their numerical model for rifting of magma-poor margins.

2.5.2 Transition Zone

Upper Crust

Offshore seismic data and ODP drilling results from the Newfoundland margin show that the transition zone may exhibit characteristics of either exhumed serpentinized mantle, thin continental crust or thin ocean crust formed by ultra-slow spreading (e.g. *Funck et al.*, 2003; *Hopper et al.*, 2004; *Lau et al.*, 2006a; *Shillington et al.*, 2006; *Van Avendonk et al.*, 2006; *Party*, 2004). Underlying the thin continental or oceanic crust there is a partially serpentinized layer. *Welford et al.* (2010b) subdivide the transition zone into two zones (T1 and T2). T1 has a deeper basement with either thin continental crust on top or partially serpentinized mantle, where the thin continental crust may be isolated blocks in the zone of exhumed mantle (*Deemer et al.*, 2009). T2 has a shallower basement where oceanic layer 2 overlies partially serpentinized

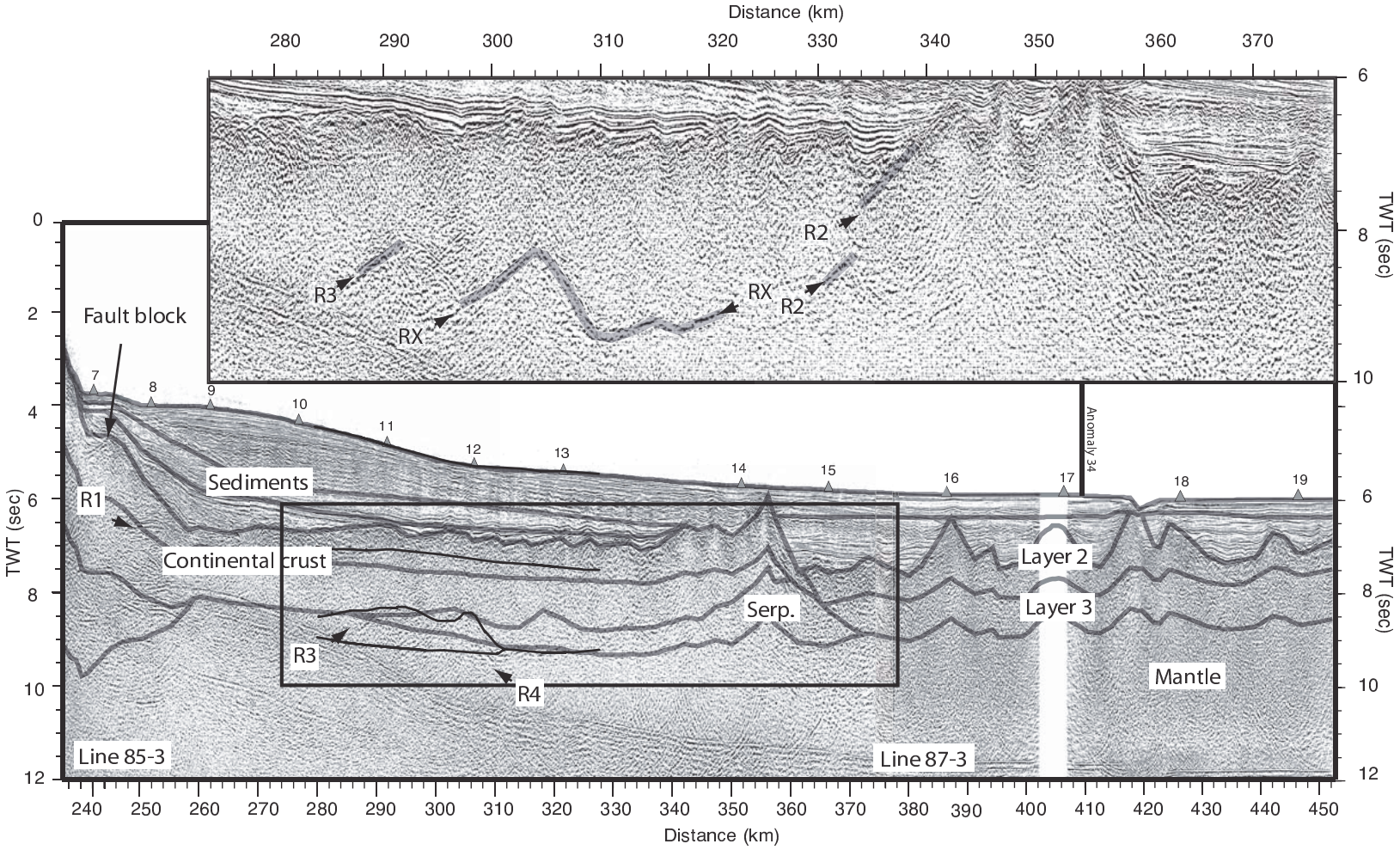

Figure 2.12: Finite difference time migrated MCS data on Line 85-3 and Line 87-3 superimposed on part of the P-wave velocity model (thick grey lines) converted to TWT. For the time migration, a simplified version of the velocity model was used. Triangles indicate OBS locations. R1-R4 and RX reflections are described in the text. Thin black lines indicate the boundaries of *Reid and Keen*'s (1990) velocity model.

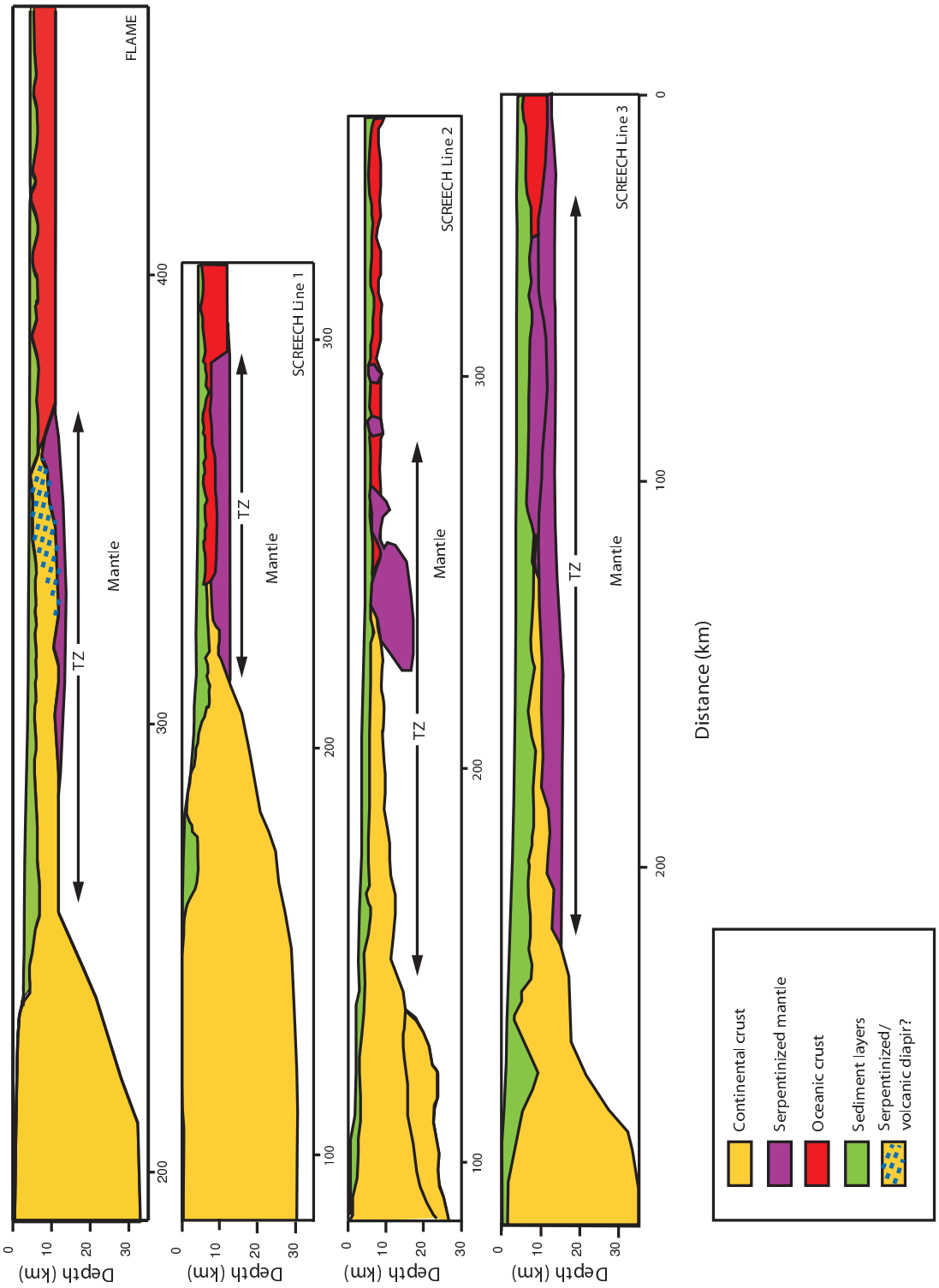

Figure 2.13: Crustal cross-sections of the FLAME Line and the SCREECH Lines 1, 2 and 3 with no vertical exaggeration (*Funck et al.*, 2003; *Lau et al.*, 2006a; *Van Avendonk et al.*, 2006).

mantle. In this zone, basalt begins to intrude the serpentinized mantle.

All these kinds of transition zones are observed on the SCREECH Lines. Just to the south, SCREECH Line 1 is interpreted todisplay thin oceanic crust formed by ultra-slow spreading on top of partially serpentinized mantle (Fig. 2.13, *Funck et al.*, 2003; *Hopper et al.*, 2004). South of SCREECH Line 1, SCREECH Lines 2 and 3 are interpreted to display a tongue of thin continental crust in the transition zone (Fig. 2.13, *Lau et al.*, 2006a; *Van Avendonk et al.*, 2006). A zone of exhumed mantle is observed on SCREECH Line 2 and 3 (*Van Avendonk et al.*, 2006; *Lau et al.*, 2006a).

For the FLAME Line, there is a transition zone between the thick continental crust that forms Flemish Cap and the thin oceanic crust associated with magnetic anomalies 34 and younger. It was suggested previously (e.g. *Louden and Chian*, 1999; *Bullock and Minshull*, 2005), based on the MCS data Line 85-3 and an earlier 50-km-long R/WAR profile along a small segment by *Reid and Keen* (1990) that the transition zone at NE Flemish Cap may consist of serpentinized mantle. However, modelled S-wave arrivals from the middle layer (P-wave velocity of 6.65- 6.8 km s^{-1}) give a good fit with Poisson's ratios of 0.27 for the upper layer and 0.28 for the layer below (Fig. 2.9). These Poisson's ratios are not characteristic of serpentinized mantle but could correspond to rocks of either continental or oceanic composition (*Holbrook et al.*, 1992). Where the basement is deepest (∼250-300 km) the basement morphology is subdued (Fig. 2.12). Between distances 300-340 km, the basement has characteristics of a series of small-rotated fault blocks. The velocities of the two upper layers are similar to the velocities of the upper and lower layers of the thick continental crust beneath Flemish Cap. Velocity-depth curves from the transition zone of the FLAME Line and of SCREECH Line 1, where thin oceanic crust is observed, display different velocities and velocity gradients (Fig. 2.11) for the upper and middle layer. The character of the two layers of the FLAME Line appears more similar to the part of SCREECH Line 3, where thin continental crust is observed, although the thickness of the lower continental crust is different (Fig. 2.11). The upper layer is assigned a Poisson's ratio of 0.27, which fits well with a granodioritic crust and is comparable to the upper crust of Flemish Cap. A Poisson's ratio of 0.28 may be a little high for a granodioritic crust (Poisson's ratios of 0.27, *Holbrook et al.*, 1992). However, we only have S-wave arrivals from the lower part of the crust in the transition zone (Fig. 2.9)

and the mafic content in the lower continental crust tends to increase (*Holbrook et al.*, 1992). Gabbro has a Poisson's ratio of 0.29 ± 0.02 (*Holbrook et al.*, 1992). Hence, a Poisson's ratio of 0.28 is reasonable for lower continental crust. This part of the transition zone (∼250-340 km) is similar to the T1-type zone described by *Welford et al.* (2010b).

A ridge feature is apperent at 340-365 km distance (Fig. 2.12). The velocity model for this feature is composed of three layers with velocities of 5.2-6.0 km s^{-1}, 6.65-6.8 km s^{-1} and 7.5-7.9 km s^{-1}. This ridge feature is the most seaward extension of the thin continental crust on the velocity model. Similar ridges are interpreted as serpentinized mantle on several other seismic profiles (e.g. *Pickup et al.*, 1996; *Dean et al.*, 2000; *Shillington et al.*, 2006; *Van Avendonk et al.*, 2006; *Deemer et al.*, 2009). In the MCS profile, the morphology changes from a muted to a higher relief basement and the reflectivity is more disrupted around the ridge, which could be either an extrusion of volcanic rock and/or serpentinized mantle. There are two landward dipping reflections (R2) at distance 330-335 km (Fig. 2.12) and the upper reflection terminates at the landward edge of the ridge feature. These R2-reflections may indicate a boundary between the thin continental crust and the ridge feature. The shallower and higher relief basement indicates a T2-type zone, as described by *Welford et al.* (2010b).

Fully (100 %) serpentinized mantle has a P-wave velocitiy of ∼5.0 km s^{-1} (*Holbrook et al.*, 1992; *Christensen*, 1996). A small lateral change from 5.55-6.0 km s^{-1} to 5.2-6.0 km s^{-1} occurs in the velocity structure of the upper crustal layer in the transition zone from the thin continental crust to the ridge feature (Fig. 2.7). If the ridge is exhumed, serpentinized mantle, it would be fully serpentinized at the basement with decreasing serpentinization with depth. An argument against this type of transitional crust is that it is not consistent with a three-layer crust. However, we observe no reflections in either the R/WAR or MCS data. There are a few S-waves that sample the ridge feature (Fig. 2.9) observed on OBS 13. The OBS is located ∼20 km landward of the ridge feature and samples the middle crustal layer (P-wave velocities of 6.65-6.8 km s^{-1}). The Poisson's ratio of 0.28 indicates that the ridge is of continental or oceanic composition. With the diapiric nature of the ridge feature, the velocities and Poisson's ratio, we favour an interpretation of the ridge as a combination of serpentinized mantle and volcanic rock.

Mantle Serpentinization

Under the thin continental crust, the FLAME velocity model shows a layer with velocities of 7.5-7.9 km s^{-1}, which we interpret as partially serpentinized mantle. The velocities are too high to be continental or oceanic crust but too low to be unaltered mantle. The layer follows the same velocity trend as the layer below the thin crust on SCREECH Lines 1 and 3 (Fig. 2.11), which also was interpreted as partially serpentinized mantle (*Funck et al.*, 2003; *Lau et al.*, 2006a). Furthermore, serpentinized mantle was drilled on ODP Site 1277 on SCREECH Line 2 ∼300 km south of the FLAME Line (Fig. 2.2, *Party*, 2004). The P- and S-wave velocities modelled on the FLAME Line suggest about 10 % serpentinization of the mantle in this layer (*Christensen*, 1996).

Reid and Keen (1990) identified a low-velocity mantle layer of velocity 7.4 km s^{-1} on their velocity profile (Fig. 2.12), which they interpreted to be mafic material underplating the thin crust. Their model layer approximately coincides with the layer of partially serpentinized mantle on the FLAME model (Fig. 2.12). The landward ends of the two-modelled layers coincide, but in the FLAME model the serpentinized mantle stretches about 60 km farther seaward. The thin crust above was previously interpreted as oceanic (*Keen and de Voogd*, 1988) with a sharp COB typical of a volcanic margin. Underplated bodies usually have P-wave velocities ranging from 7.0 to 7.6 km s^{-1} (*Coffin and Eldholm*, 1994). This velocity range fits well with the modelled velocities of *Reid and Keen* (1990). However, only on the topmost part of this layer at distance ∼350 km have we modelled a velocity of 7.5 km s^{-1}. Most of the velocities are greater than 7.6 km s^{-1} and beyond the velocity range of typical underplated bodies.

Some prominent reflections are identified on the MCS profile (Fig. 2.12) that appear to be associated with the partially serpentinized lower layer of the transition zone. A landward (R3) and a seaward (R4) dipping reflection are observed at distance 285 km and 310 km, respectively, and at about 9-9.5 s (12-13 km depth). The landward reflection (R3) was previously discussed as representing the COB (*Keen and de Voogd*, 1988) but this interpretation is not consistent with the FLAME velocity model. An alternative interpretation is that the (R3) reflection represents the landward limit of the lower layer of the transition zone (*Reid and Keen*, 1990; *Louden*

and Chian, 1999), which is consistent with the FLAME velocity model where the layer of partially serpentinized mantle terminates at the location of reflection (R3). Previously, the (R4) reflection was suggested to represent the seaward limit of the mafic layer modelled by *Reid and Keen* (1990, Fig 2.12). *de Voogd and Keen* (1987) and *Keen and de Voogd* (1988) observed an unusual pattern of reflections (RX), including the R4 reflection, at the base of the transitional crust (distance 290-340 km) on MCS profile Line 85-3 (Fig. 2.12). They described the reflections as a broken and tilted horizon with topography of about 1 s (2-3 km) appearing at typical Moho depths. The reflections are located in what *de Voogd and Keen* (1987) interpreted as the oceanic domain and hence were interpreted as oceanic Moho. In our new interpretation, these reflections (RX and R4) coincide with the lower boundary of serpeninized mantle, or cut through the layer of partially serpentinized mantle. The RX reflections may represent Moho or may be related to the serpentinization of the mantle, but further processing of the reflection data is required.

We observe only partially serpentinized mantle beneath part of the thin continental crust on the FLAME Line. The layer terminates ∼30 km seaward of the thick continental crust (Figs. 2.7 and 2.13). In contrast, serpentinized mantle is observed beneath the entire section of thin crust on SCREECH Lines 1 and 3 on the Newfoundland margin (*Funck et al.*, 2003; *Lau et al.*, 2006a), as well as beneath the Labrador-SW Greenland margin pair and Galicia Bank (*Chian and Louden*, 1994; *Chian et al.*, 1995a; *Whitmarsh et al.*, 1996). Observations from those margins agree with the model of *Pérez-Gussinyé and Reston* (2001) for mantle serpentinization, which suggests that when the crust thins to about 6-10 km it becomes brittle and faults and fractures form, which will channel water down to serpentinize the lithospheric mantle. However, this model does not agree with observations from the FLAME Line. To our knowledge there is only one other line, SCREECH Line 2, where serpentinized mantle is not observed beneath the landward-most section of highly thinned continental crust. On this line serpentinized mantle is only observed seaward of the thin continental crust.

The distribution of serpentinized mantle and width of the transition zone vary along-strike on the Newfoundland and Flemish Cap margins. If we look at the lateral extent of exhumed serpentinized mantle and partially serpentinized mantle from the

southern Newfoundland margin to the NE Flemish Cap margin, we can observe significant variations in width (Fig. 2.13). SCREECH Line 3 displays a broad zone of exhumed serpentinized mantle, which narrows northward on SCREECH Line 2 and disappears completely on SCREECH Line 1. North of the BTJ on NE Flemish Cap, the exhumed mantle reappears where we interpret a serpentinized ridge. The zone of partially serpentinized mantle also narrows northward and broadens again at NE Flemish Cap. The zone is widest roughly at the location of SCREECH Line 3 and narrows southward of SCREECH Line 3 (*Welford et al.*, 2010b).

2.5.3 Oceanic Crust

The FLAME Line crosses magnetic anomaly 34 at ∼410 km near OBS 17 (Figs. 2.2, 2.7 and 2.12), and thus the most seaward end of the profile is located in crust that is definitely oceanic. According to *Srivastava et al.* (1988), the half-spreading rate at this magnetic anomaly is 10.2 mm yr^{-1}. This spreading rate is comparable to that of the slow-spreading Newfoundland and Iberian margins, which have initial spreading rates of 8 mm yr^{-1} and 10 mm yr^{-1}, respectively (*Srivastava et al.*, 2000).

In Fig. 2.11 two 1-D velocity-depth curves are displayed, together with typical velocities for 59-127 Ma oceanic crust in the North Atlantic (*White et al.*, 1992). The two profiles are located on either side of magnetic anomaly 34 at distance 380-440 km. The velocities and velocity gradients of these two profiles fit into the range of typical values for oceanic Layer 2 and 3, although the velocity gradient of Layer 2 at 380 km is a factor of 10 smaller than typical oceanic crust but comparable to Layer 2 of SCREECH Line 1 (Fig. 2.11). The velocities of Layer 3 do not change across magnetic anomaly 34. The lower boundary of Layer 3 (Fig. 2.7) is constrained by $P_{m3}P$ reflections from OBSs 16, 18 and 19 (Fig. 2.8). Although, the signal-to-noise ratio is high on OBS 16, the $P_{m3}P$ reflections indicate that the Moho depth is the same on either side of magnetic anomaly 34 in this zone. We do not have many rays from OBSs 16 and 17 sampling the two crustal layers between distances 365 and 410 km (Fig. 2.8). However, rays from the mantle phase, P_n, from other OBSs (e.g. OBSs 15, 18 and 19) do travel through these two layers and their arrival times are consistent with velocities and thicknesses of the model. The oceanic crust (4.5-6.5 km) is somewhat thinner than typical oceanic crust (∼7 km, *White et al.*, 1992), but

comparable to that observed on the three SCREECH Lines on the Newfoundland margin.

The zone between the ridge feature and magnetic anomaly 34 (∼365-400 km) may be: (1) thin oceanic crust formed by ultraslow spreading on top of partially serpentinized mantle; (2) highly serpentinized mantle on top of partially serpentinized mantle; or (3) oceanic crust formed by slow spreading. The type of material will result in different styles for the onset of seafloor spreading. The first scenarios can be observed on SCREECH Line 1 (Fig. 2.13, *Funck et al.*, 2003; *Hopper et al.*, 2004). After continental breakup and mantle exhumation, the SE Flemish Cap margin experienced a stage of magma-starved seafloor spreading, creating thin oceanic crust (3-4 km thick) followed by a stage of mantle exhumation and then a stage of magmatic event that create a 1.5-km-thick oceanic Layer 2 on top of partially serpentinized mantle (*Hopper et al.*, 2004). The onset of seafloor spreading in this case is transitional. On the coincident MCS profile of SCREECH Line 1, strong primary reflections is observed, which indicate a boundary between oceanic crust and serpentinized mantle. No such reflections can be identified on Line 85-3 and Line 87-3 coincident with the FLAME Line (Fig. 2.12).

The second scenario is observed on SCREECH Line 3 (Fig. 2.13). Seaward of a serpentinized ridge, a zone of exhumed and serpentinized mantle (*Lau et al.*, 2006a) was interpreted. In this case, onset of seafloor spreading would be a sharp transition just landward of magnetic anomaly 34. On the coincident MCS profile to SCREECH Line 3, the basement morphology is muted in the zone of exhumed mantle. This contrasts with the high relief basement observed on Line 85-3 and Line 87-3 (Fig. 2.12).

The last scenario would indicate a sharp transition to the formation of oceanic crust after emplacing a ridge. We favour this interpretation because the velocities fit into the range of oceanic crust and the velocities of Layer 3 are consistent with the velocities seaward of magnetic anomaly 34. Furthermore, a high-relief basement as well as no primary reflections are observed in the MCS data in this zone. The ridge feature with a combination of serpentinized mantle and volcanics may be the first indication of melt. Seaward of the ridge feature our results are consistent with normal oceanic crust. This is similar to SCREECH Line 3, which also displays a

sharp boundary between exhumed and serpentinzed mantle and formation of typical oceanic crust (*Lau et al.*, 2006a).

There have been various other approaches to define the onset of seafloor spreading. *Tucholke et al.* (2007) define the onset of seafloor spreading by a breakup unconformity. *Cannat et al.* (2009) define the onset of seafloor spreading as the time of active thermal equilibrium, where crustal thinning occurs up until spreading begins with mantle exhumation overlapping the end of the thinning phase and the beginning of the spreading phase. *Jagoutz et al.* (2007) show that multiple magmatic events indicate a gradual transition calling this crust embryonic oceanic crust. *Péron-Pinvidic et al.* (2007) favour a gradual transition for the Newfoundland-Iberia margin pair. *Welford et al.* (2010b) also suggest a gradual transition to formation of undisputed oceanic with increasing volumes of melt in the transition zone seaward (*Whitmarsh et al.*, 2001) and call this zone thin oceanic crust. A zone of thin oceanic crust with increasing melt is not compatible with the results from the FLAME Line. The velocity model together with the coincident MCS profiles indicate a sharp transition from rifting to seafloor spreading, where a serpentinized ridge feature with extruded volcanic separates thin continental crust from oceanic crust. However, we need more detailed surveys (e.g. seismic R/WAR data with denser OBS spacing or MCS data with longer streamers) and expand the number of profiles that extend into oceanic crust to improve our understanding of the transition from rifting to formation of oceanic crust.

2.6 Conclusions

The results of the P-wave velocity model developed from R/WAR data across the NE Flemish Cap margin together with MCS data from a coincident line lead us to the following conclusions:

1. The continental crust beneath Flemish Cap is a 31-km-thick 3-layer crust, which is consistent with previous results.

2. The thick continental crust thins rapidly to 6-km-thick crust over a distance of only 45 km. The rapid thinning of the NE Flemish Cap margin is consistent

with the Newfoundland margin just south of NE Flemish Cap margin, which also displays rapid thinning of the continental crust.

3. S-waves were found on several horizontal geophones, which show that the thin crust in the transition zone is predominantly of a continental nature. The thin continental crust is underlain by partially serpentinized mantle. This partially serpentinized layer appears to terminate 30 km seaward of the thick continental crust. Furthermore, the partially serpentinized layer can be associated with reflections in the MCS data Line 85-3. The landward extension of the serpentinized mantle coincides with a landward dipping reflector previously interpreted as the COB. Furthermore, an unusual pattern of reflections in the MCS profile of broken and tilted horizons coincides with the partially serpentinized mantle interpreted from the P-wave velocity model.

4. A ridge feature is present the seaward extension of the transition zone. The velocity model and the MCS profile indicate a mixed character between continental crust or a combination of serpentinized mantle and volcanics.

5. Oceanic crust occurs seaward of the ridge feature. Only the ridge feature separates thin continental crust from oceanic crust and hence the onset of seafloor appears sharp.

2.7 Acknowledgments

We would like to thank all personnel onboard CCGS Hudson who helped to collect the seismic data. We also thank the Geological Survey of Canada Atlantic for providing digital copies of the coincident multichannel reflection profiles and Patrick Potter for arranging for its transfer to Dalhousie University. We thank Thomas Funck and John Hopper for helpful reviews, which have helped make significant improvements. We also thank NSERC (Natural Sciences and Engineering Research Council of Canada) and GSC (Geological Survey of Canada) for joint program funding of the MARIPROBE program.

References

Bullock, A. D., and T. A. Minshull (2005), From continental extension to seafloor spreading: crustal structure of the Goban Spur rifted margin, southwest of the UK, *Geophysical Journal International*, *163*(2), 527–546, doi: 10.1111/j.1365-246X.2005.02726.x.

Cannat, M., G. Manatschal, D. Sauter, and G. Péron-Pinvidic (2009), Assessing the conditions of continental breakup at magma-poor rifted margins: What can we learn from slow spreading mid-ocean ridges?, *Comptes Rendus Geoscience*, *341*(5), 406–427, doi: 10.1016/j.crte.2009.01.005.

Chian, D., and K. Louden (1994), The continent-ocean crustal transition across the southwest Greenland margin, *Journal of geophysical research*, *99*(B5), 9117–9135.

Chian, D., K. Louden, and I. Reid (1995), Crustal structure of the Labrador Sea conjugate margin and implications for the formation of nonvolcanic continental margins, *Journal of Geophysical Research*, *100*(B12), 24,239–24.

Christensen, N. I. (1996), Poisson's ratio and crustal seismology, *Journal of Geophysical Research*, *101*(B2), 3139, doi: 10.1029/95JB03446.

Coffin, M., and O. Eldholm (1994), Large igneous provinces: crustal structure, dimensions, and external consequences, *Reviews of Geophysics*, *32*(1), 1–36.

de Graciansky, P., C. Poag, R. Cinningham, P. Loubere, D. Masson, J. Mazzullo, L. Montadert, C. Müller, K. Otsuka, L. Reynolds, et al. (1985), The Goban Spur transect: Geologic evolution of a sediment-starved passive continental margin, *Geological Society of America Bulletin*, *96*(1), 58–76.

de Voogd, B., and C. Keen (1987), Lithoprobe east: results from reflection profiling of the continental margin: Grand banks region., *Geophysical Journal of the Royal Astronomical Society*, *89*(1), 195–200.

Dean, S., T. Minshull, R. Whitmarsh, and K. Louden (2000), Deep structure of the ocean-continent transition in the southern Iberia Abyssal Plain from seismic refraction profiles: The IAM-9 transect at 40°20'N, *Journal of Geophysical Research*, *105*(B3), 5859–5885.

Deemer, S., J. Hall, K. Solvason, K. H. Lau, K. Louden, S. Srivastava, and J.-C. Sibuet (2009), Structure and development of the southeast Newfoundland continental passive margin: derived from SCREECH Transect 3, *Geophysical Journal International*, *178*(2), 1004–1020, doi: 10.1111/j.1365-246X.2009.04162.x.

Funck, T., J. Hopper, H. Larsen, K. Louden, B. Tucholke, and W. Holbrook (2003), Crustal structure of the ocean-continent transition at Flemish Cap: Seismic refraction results, *Journal of Geophysical Research*, *108*(B11), 2531.

Funck, T., H. Jackson, K. Louden, S. Dehler, and Y. Wu (2004), Crustal structure of the northern Nova Scotia rifted continental margin (eastern Canada), *Journal of Geophysical Research*, *109*(B9), B09,102.

Holbrook, W., W. Mooney, and N. Christensen (1992), The seismic velocity structure of the deep continental crust, in *Continental lower crust*, edited by A. R. . K. R. Fountain, D.M., pp. 1–43, Elsevier Sci, New York.

Hopper, J. R., T. Funck, B. E. Tucholke, H. Christian Larsen, W. S. Holbrook, K. E. Louden, D. Shillington, and H. Lau (2004), Continental breakup and the onset of ultraslow seafloor spreading off Flemish Cap on the Newfoundland rifted margin, *Geology*, *32*(1), 93, doi: 10.1130/G19694.1.

Jackson, R., K. Asprey, B. Chapman, S. Goold, P. Girouard, L. Johnston, and K. Louden (2002), Cruise report Hudson 2002011, Flemish Cap Margin Transect, *Tech. rep.*, Geological Survey of Canada, Dartmouth, Nova Scotia, Canada. Open File Rep. 1234, pp. 40.

Jagoutz, O., O. Müntener, G. Manatschal, D. Rubatto, G. Péron-Pinvidic, B. D. Turrin, and I. M. Villa (2007), The rift-to-drift transition in the North Atlantic: A stuttering start of the MORB machine?, *Geology*, *35*(12), 1087, doi: 10.1130/G23613A.1.

Keen, C., and B. de Voogd (1988), The continent-ocean boundary at the rifted margin off eastern Canada: new results from deep seismic reflection studies, *Tectonics*, *7*(1), 107–124.

Keen, C. E., and D. L. Barrett (1981), Thinned and subsided continental crust on the rifted margin of Eastern Canada: crustal structure, thermal evolution and subsidence history, *Geophysical Journal International*, *65*(2), 443–465, doi: 10.1111/j.1365-246X.1981.tb02721.x.

King, L. H., G. B. Fader, W. H. Poole, and R. K. Wanless (1985), Geological setting and age of the Flemish Cap granodiorite, east of the Grand Banks of Newfoundland, *Canadian Journal of Earth Sciences*, *22*(9), 1286–1298, doi: 10.1139/e85-133.

Lau, K. (2005), Structure of the Eastern Grand Banks/Newfoundland basin rifted margin, Ph.D. thesis, Dalhousie University, Halifax, Nova Scotia.

Lau, K. W. H., K. E. Louden, T. Funck, B. E. Tucholke, W. S. Holbrook, J. R. Hopper, and H. Christian Larsen (2006), Crustal structure across the Grand Banks-Newfoundland Basin Continental Margin - I. Results from a seismic refraction profile, *Geophysical Journal International*, *167*(1), 127–156, doi: 10.1111/j.1365-246X.2006.02988.x.

Lavier, L. L., and G. Manatschal (2006), A mechanism to thin the continental lithosphere at magma-poor margins., *Nature*, *440*(7082), 324–8, doi: 10.1038/nature04608.

Louden, K., and D. Chian (1999), The deep structure of non–volcanic rifted continental margins, *Philosophical Transactions A*, *357*(1753), 767.

Ludwig, W., J. Nafe, and C. Drake (1970), Seismic refraction, in *The Sea*, edited by A. Maxwell, pp. 53–84, Wiley-Interscience, New York.

Lutter, W., R. Nowack, and L. Braile (1990), Inversion for crustal structure using reflections from the PASSCAL Ouachita experiment, *Journal of Geophysical Research*, *95*(B4), 4623–4646.

Ogg, J., and A. Smith (2004), The geomagnetic polarity time scale, in *A Geologic Time Scale 2004*, edited by O. J. Gradstein, F.M. and A. Smith, pp. 63–86, Cambridge University Press.

Party, S. S. (2004), Leg 210 summary, in *Proceedings of the Ocean Drilling Program, Initial Reports*, vol. 210, pp. 1–78.

Pérez-Gussinyé, M., and T. Reston (2001), Rheological evolution during extension at nonvolcanic rifted margins-onset of serpentinization and development of detachments leading to continental breakup, *Journal of Geophysical Research*, *106*(B3), 3961–3975.

Péron-Pinvidic, G., G. Manatschal, T. a. Minshull, and D. S. Sawyer (2007), Tectonosedimentary evolution of the deep Iberia-Newfoundland margins: Evidence for a complex breakup history, *Tectonics*, *26*(2), 1–19, doi: 10.1029/2006TC001970.

Pickup, S., R. Whitmarsh, C. Fowler, and T. Reston (1996), Insight into the nature of the ocean-continent transition off West Iberia from a deep multichannel seismic reflection profile, *Geology*, *24*(12), 1079–1082.

Reid, I., and C. Keen (1990), High seismic velocities associated with reflections from within the lower oceanic crust near the continental margin of Eastern Canada, *Earth and Planetary Science Letters*, *99*(1), 118–126.

Sandwell, D., and W. Smith (2009), Global marine gravity from retracked geosat and ERS-1 altimetry: Ridge segmentation versus spreading rate, *Journal of geophysical Research*, *114*(B01411), B01,411.

Shillington, D. J., W. S. Holbrook, H. J. a. Van Avendonk, B. E. Tucholke, J. R. Hopper, K. E. Louden, H. C. Larsen, and G. T. Nunes (2006), Evidence for asymmetric nonvolcanic rifting and slow incipient oceanic accretion from seismic reflection data on the Newfoundland margin, *Journal of Geophysical Research*, *111*(B9), B09,402, doi: 10.1029/2005JB003981.

Sibuet, J.-C., S. P. Srivastava, M. Enachescu, and G. D. Karner (2007), Early Cretaceous motion of Flemish Cap with respect to North America: implications on the formation of Orphan Basin and SE Flemish Cap Galicia Bank conjugate margins, *Geological Society, London, Special Publications*, *282*(1), 63–76, doi: 10.1144/SP282.4.

Srivastava, S., and W. Roest (1999), Extent of oceanic crust in the Labrador Sea, *Marine and Petroleum Geology*, *16*(1), 65–84.

Srivastava, S., J. Verhoef, and R. Macnab (1988), Results from a detailed aeromagnetic survey across the northeast Newfoundland margin, Part I: spreading anomalies and relationship between magnetic anomalies and the ocean-continent boundary, *Marine and petroleum geology*, *5*(4), 306–323.

Srivastava, S., J. Sibuet, S. Cande, W. Roest, and I. Reid (2000), Magnetic evidence for slow seafloor spreading during the formation of the Newfoundland and Iberian margins, *Earth and Planetary Science Letters*, *182*(1), 61–76.

Talwani, M., J. Worzel, and M. Landisman (1959), Rapid gravity computations for two-dimensional bodies with application to the Mendocino submarine fracture zone, *Journal of Geophysical Research*, *64*(1), 49–59.

Tucholke, B. E., D. S. Sawyer, and J.-C. Sibuet (2007), Breakup of the Newfoundland Iberia rift, *Geological Society, London, Special Publications*, *282*(1), 9–46, doi: 10.1144/SP282.2.

Van Avendonk, H. J. A., W. S. Holbrook, G. T. Nunes, D. J. Shillington, B. E. Tucholke, K. E. Louden, H. C. Larsen, and J. R. Hopper (2006), Seismic velocity structure of the rifted margin of the eastern Grand Banks of Newfoundland, Canada, *Journal of Geophysical Research*, *111*(B11), B11,404, doi: 10.1029/2005JB004156.

Welford, J. K., J. A. Smith, J. Hall, S. Deemer, S. P. Srivastava, and J.-C. Sibuet (2010), Structure and rifting evolution of the northern Newfoundland Basin from Erable multichannel seismic reflection profiles across the southeastern margin of Flemish Cap, *Geophysical Journal International*, *180*(3), 976–998, doi: 10.1111/j.1365-246X.2009.04477.x.

White, R., G. Spence, S. Fowler, D. McKenzie, G. Westbrook, and A. Bowen (1987), Magmatism at rifted continental margins, *Nature*, *330*(6147), 439–444.

White, R., D. McKenzie, and R. O'Nions (1992), Oceanic crustal thickness from seismic measurements and rare earth element inversions, *J. geophys. Res*, *97*(19), 683–19.

Whitmarsh, R., R. White, S. Horsefield, J. Sibuet, M. Recq, and V. Louvel (1996), The ocean-continent boundary off the western continental margin of Iberia: Crustal structure west of Galicia Bank, *Journal of Geophysical Research*, *101*(B12), 28,291–28.

Whitmarsh, R. B., G. Manatschal, and T. a. Minshull (2001), Evolution of magma-poor continental margins from rifting to seafloor spreading., *Nature*, *413*(6852), 150–4, doi: 10.1038/35093085.

Wu, Y., K. E. Louden, T. Funck, H. R. Jackson, and S. A. Dehler (2006), Crustal structure of the central Nova Scotia margin off Eastern Canada, *Geophysical Journal International*, *166*(2), 878–906, doi: 10.1111/j.1365-246X.2006.02991.x.

Zelt, C., and P. Barton (1998), Three-dimensional seismic refraction tomography: A comparison of two methods applied to data from the Faeroe Basin, *Journal of Geophysical Research*, *103*(84), 7187–7210.

Zelt, C., and D. Forsyth (1994), Modeling wide-angle seismic data for crustal structure: Southeastern Grenville Province, *Journal of Geophysical Research*, *99*(B6), 11,687–11.

Zelt, C. A. (1999), Modelling strategies and model assessment for wide-angle seismic traveltime data, *Geophys. J. Int.*, *139*, 183–204.

Zelt, C. A., and R. B. Smith (1992), Seismic traveltime inversion for 2-D crustal velocity structure, *Geophys. J. Int.*, *108*, 16–34.

Chapter 3

Flemish Cap-Gobans Spur Conjugate Margins

In this chapter, I first present the paper that is published as "*Gerlings, J., Louden, K.E., Minshull, T.A. and Nedimović, M.R. (2012), The Flemish Cap - Goban Spur conjugate margins: New evidence of asymmetry, Geology., 40(12), 1107-1110*" (Section 3.1). This paper describes the most recent discoveries regarding the rifting style between the Flemish Cap-Goban Spur conjugate margin pair. In Section 3.2, I will present the LIFT methodology (noise attenuation), a comparison of the reprocessed Line 85-3 with a previous processing (*Keen and de Voogd*, 1988) of the line, and the result from a prestack Kirchhoff depth migration of Line 85-3, none of which were included in *Gerlings et al.* (2012).

3.1 The Flemish Cap - Goban Spur Conjugate Margins: New Evidence of Asymmetry

3.1.0 Abstract

We present the combined results of deep multichannel reflection and refraction seismic surveys across the Flemish Cap-Goban Spur conjugate margin pair (North Atlantic), which we use to infer rifting style and breakup. Profiles on both margins cross magnetic anomaly 34 and extend into oceanic crust, making it possible to observe the complete history from continental rifting through to the formation of initial oceanic crust. The deep multichannel seismic (MCS) reflection data have previously been used to support a model of symmetric pure shear extension followed by asymmetric breakup and a sharp continent-ocean boundary. Using both types of seismic data, our results indicate instead that asymmetric structures are formed during all stages of rifting, breakup, and complex transition to oceanic spreading. The differing nature of the two ocean-continent transition zones is particularly striking. For Flemish Cap, our reprocessed image of the MCS profile clearly shows tilted fault blocks beneath

back-tilted sediment packages, consistent with a wide region of highly thinned continental crust inferred from wide-angle seismic data. In contrast, normal incidence and wide-angle seismic data for the Goban Spur transition zone indicate the presence of exhumed serpentinized mantle.

3.1.1 Introduction

Deep seismic reflection data were used for the first time in the 1980s to derive the rifting style of a passive conjugate margin pair (*Keen et al.*, 1989). Seismic reflection profiles from the Flemish Cap-Goban Spur margins (Fig. 3.1) were used to support a symmetric pure shear model of extension followed by an asymmetric breakup and a sharp continent-ocean boundary (COB; Fig. 3.2). A more recent wide-angle seismic study across Goban Spur (*Bullock and Minshull*, 2005) coincident with the Western Approaches Margin multichannel seismic (MCS) profile (*Peddy et al.*, 1989) indicates that extension is more complex on the Flemish Cap-Goban Spur conjugate margins than initially proposed. The *Bullock and Minshull* (2005) velocity model of the Goban Spur margin includes a wide ocean-continent transition zone with a serpentinized mantle composition. In order to determine a complete conjugate section, the Flemish Cap margin has been reexamined, including results from a 460-km-long refraction seismic profile (*Gerlings et al.*, 2011) situated along the original deep MCS reflection profile (Lithoprobe Line 85-3, *Keen and de Voogd*, 1988). The MCS profile has been reprocessed and Kirchhoff time migrated (see the GSA Data Repository[1] for details).

The dating of synrift sedimentary sequences from boreholes (Deep Sea Drilling Project (DSDP) Sites 549, 550, and 551) on the Goban Spur margin indicates that extension of the Flemish Cap-Goban Spur conjugate margin pairs started in the early Barremian (126-128 Ma, *de Graciansky et al.*, 1985). Early and latest Albian postrift sediments indicate final breakup ca. 100 Ma (using the time scales of *Ogg and Smith* (2004)) leading to formation of oceanic crust. Magnetic chron 34 (ca. 84 Ma, *Srivastava et al.*, 1988) is the oldest undisputed magnetic anomaly identified on the Flemish Cap-Goban Spur margins, and is located close to the continental margin (Fig. 3.1). Unlike many other margins without clear seafloor spreading anomalies,

[1]GSA Data Repository item 2012320, seismic reflection profiles, is available online at www.geosociety.org/pubs/ft2012.htm, or on request from editing@geosociety.org or Documents Secretary, GSA, P.O. Box 9140, Boulder, CO 80301, USA.

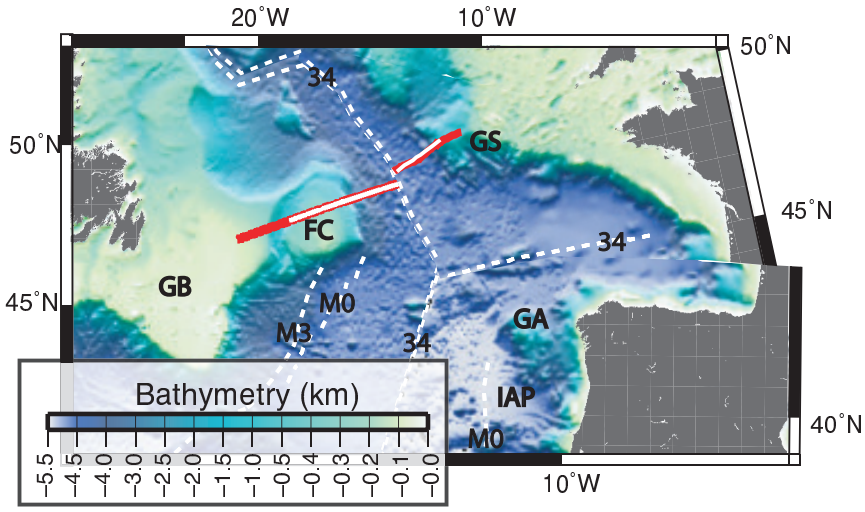

Figure 3.1: Plate reconstruction of North Atlantic Ocean at magnetic chron 34. Red lines indicate multichannel seismic profiles 85-3 and 87-3 (Flemish Cap) and Western Approaches Margin line (Goban Spur); solid white lines indicate refraction profiles. White dashed lines indicate magnetic anomalies M3, M0, and 34 from *Srivastava et al.* (1988). Abbreviations: FC: Flemish Cap; GB: Grand Banks; GS: Goban Spur; GA: Galicia Bank; IAP: Iberia Abyssal Plain.

both of the conjugate MCS and wide-angle profiles cross magnetic anomaly 34 and extend onto unambiguous oceanic crust.

3.1.2 The Flemish Cap-Goban Spur Conjugate Profiles

The crustal structure across Goban Spur was determined along a 640-km-long MCS profile, the Western Approaches Margin (WAM; Figs. 3.1 and 3.3) (*Peddy et al.*, 1989). Previous studies of the Goban Spur margin (*Peddy et al.*, 1989; *Horsefield et al.*, 1994) identified three large fault blocks beneath which Moho depths decrease from 28 km to 12 km over a distance of 80 km. Tholeiitic basalt was recovered from DSDP Sites 551 and 550 (*de Graciansky et al.*, 1985) and was interpreted as evidence for a sharp continent-ocean boundary located at the foot of the continental slope (Figs. 3.2 and 3.3). Major element compositions of these basalts are consistent with synrift melting of normal-temperature mantle (*Dean et al.*, 2000). Although dating of the basalt was not possible, the earliest overlying sediments are late Cenomanian postrift chalks (*de Graciansky et al.*, 1985). Seaward of the inferred continent-ocean boundary (120 km distance in Fig. 3.3), the basement is initially smooth (60-120 km), but increases in relief farther seaward (0-60 km). There is no clear Moho reflection in

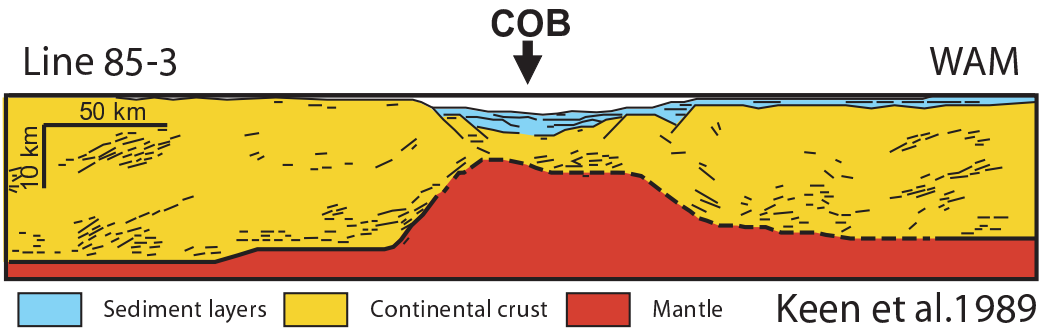

Figure 3.2: Line drawing of previous reconstruction of Flemish Cap-Goban Spur (FC-GS) conjugate margin pairs using Lithoprobe 85-3 and Western Approaches Margin (WAM) multichannel seismic profiles. COB-continent-ocean boundary. Modified from *Keen et al.* (1989).

the region of subdued basement relief, but several weak dipping reflections (G1 and G2) are observed at 10-12 km depth. The Moho reflection (M3) appears just seaward of magnetic anomaly 34. Poisson's ratio in this zone is constrained by traveltime delays for S-wave converted at the top of the basement, resulting in values of 0.34-0.36 in the upper 1 km of the crust (*Bullock and Minshull*, 2005). These values are too high for typical continental crustal lithologies and are more consistant with exhumed serpentinized mantle. The composition of the zone of higher relief is less well constrained, consisting of a basaltic layer on top of either partially serpentinized mantle or gabbro (Figs. 3.3 and 3.4).

The Lithoprobe MCS Lines 85-3 and 87-3 (*Keen and de Voogd*, 1988, Fig. 3.3) cross Flemish Cap and extend well into oceanic crust beyond anomaly 34. Only one prominent fault block is observed at the foot of the continental slope (B1), underlain by a landward-dipping reflection (R1). Seaward of this fault block, the basement relief is subdued over a distance of 40 km (245-285 km distance in Fig. 3.3), similar to Goban Spur. Our reprocessed image Fig. 3.3 clearly shows several minor faults over a distance of 50 km overlain by back-tilted (synrift?) sediment packages.

Poisson's ratio is constrained in the subdued basement region, but values of 0.27 in the upper and 0.28 in the lower crust are obtained (*Gerlings et al.*, 2011), indicating a crust of a continental composition. The thin continental crust is underlain by partially serpentinized mantle. Some landward- and seaward-dipping reflections (RX in Fig. 3.3; distance 290-320 km) are observed within and just beneath this layer. The basement abruptly changes character at a distance of ~290 km. Between distances

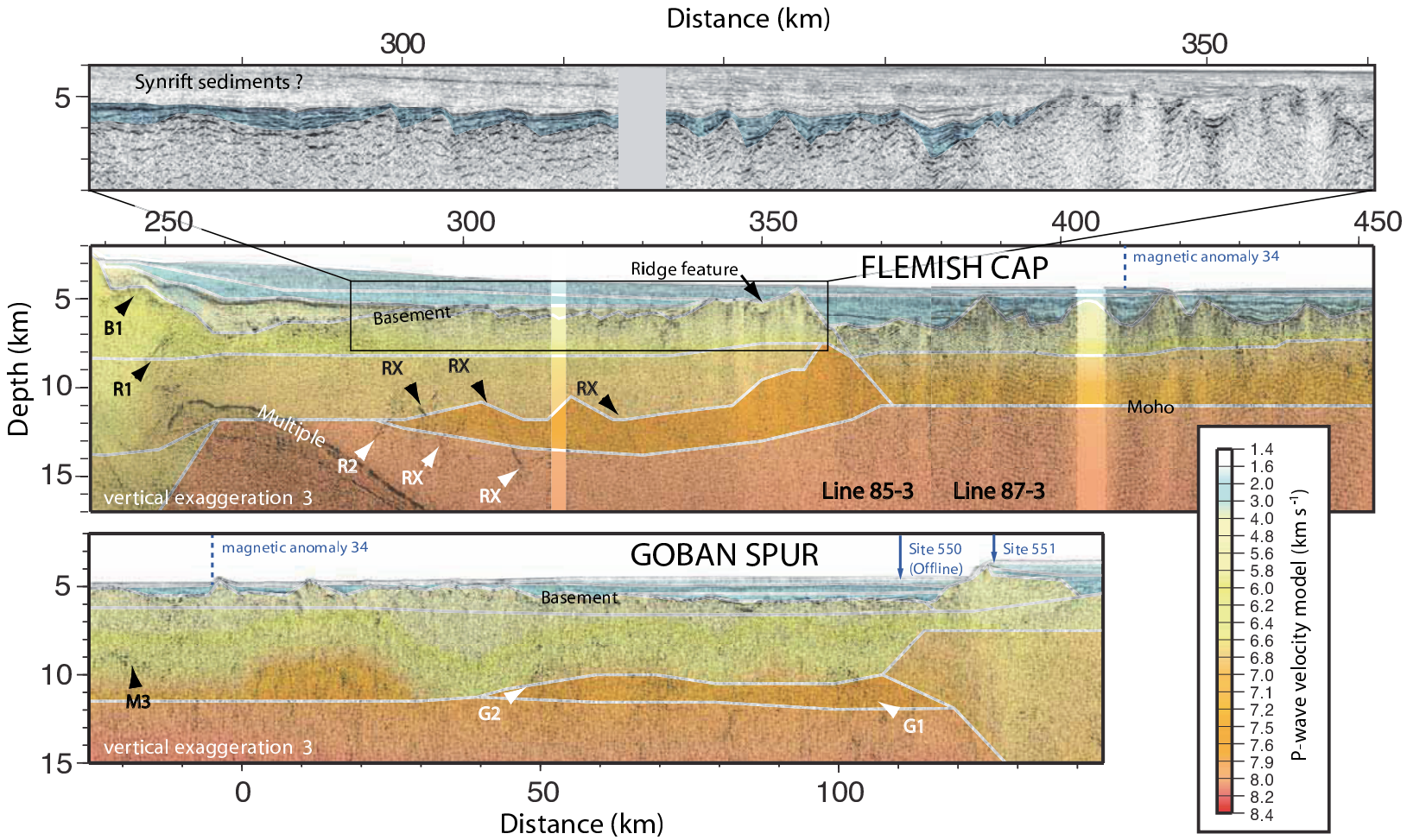

Figure 3.3: Deep water sections of poststack time migrated and time-to-depth converted MCS profiles across Flemish Cap (top, Lines 85-3 and 87-3) and MCS profile across Goban Spur (bottom, WAM line) superimposed on P-wave velocity models (*Bullock and Minshull*, 2005; *Gerlings et al.*, 2011). Layer boundaries of the velocity model are indicated by white lines. The velocity model of *Bullock and Minshull* (2005), which deviates by up to 8 km from the WAM profile (Figure 3.1), has been modified to better fit the seabed, basement and sedimentary layer boundaries. Top section is a close-up of the basement morphology in the ocean-continent transition zone of Flemish Cap. Light blue indicates a (syn-rift?) sediment package above the tilted fault blocks. B1: prominent fault block; G1: landward-dipping reflection; G2: seaward-dipping reflection; M3: Moho reflection; R1, R2: landward-dipping reflections; RX: landward- and seaward-dipping reflections.

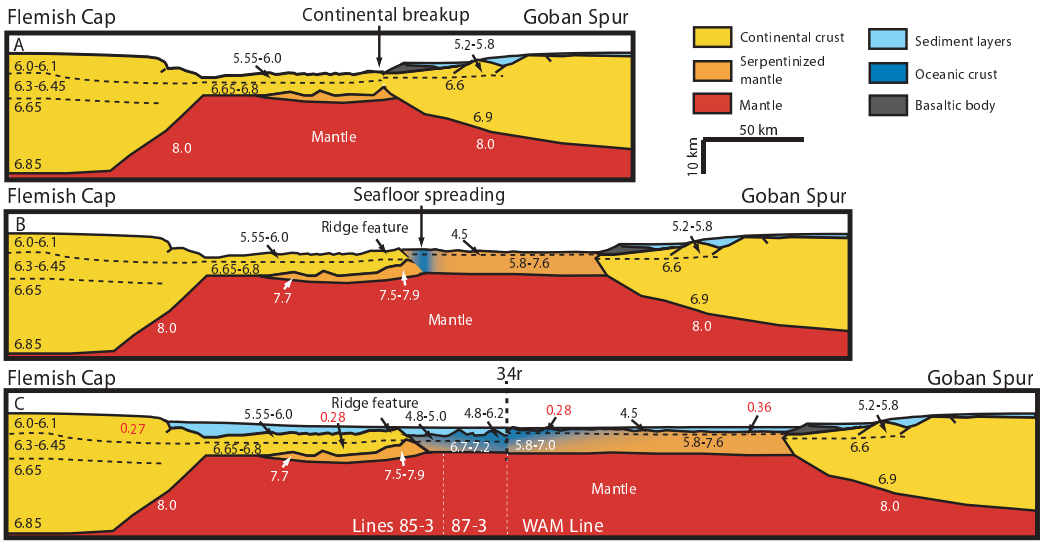

Figure 3.4: Reconstruction of Flemish Cap-Goban Spur (FC-GS) conjugate margin pairs. A: Under extension. B: Mantle exhumation. C: At magnetic chron 34, with seafloor spreading. Dashed horizontal black lines indicate layer boundaries. Numbers are P-wave velocities (black and white, in km s^{-1}) and Poisson's ratios (red). Poisson's ratio of 0.28 and P-wave velocity of 6.7 km s^{-1} indicate continental composition (*Christensen*, 1996), whereas Poisson's ratio of 0.28 and P-wave velocity of 4.5 km s^{-1} indicate basaltic composition. Poisson's ratio of 0.36 and P-wave velocities of 5.8-7.6 km s^{-1} indicate serpentinized mantle.

340 and 360 km a basement high is observed with velocities consistent with the presence of either continental crust or a combination of serpentinized mantle and incipient melt. Farther seaward, over distances of 365-460 km, is a region of rugged basement with crustal velocities consistant with slow-spreading oceanic crust.

3.1.3 Discussion

A combined interpretation using both the MCS and wide-angle seismic data is presented in Figure 3.4. The crust at the Flemish Cap margin thins rapidly from 32 km to 6 km over a distance of only 40 km (*Gerlings et al.*, 2011). In comparison, the Goban Spur margin thins from 28 km to 6 km over a distance of ~80 km (*Horsefield et al.*, 1994; *Peddy et al.*, 1989). Thus the Flemish Cap margin displays a sharper necking profile than that of the Goban Spur margin, indicating asymmetry during rifting.

A prominent asymmetric feature of the two conjugate margins is the different

nature of the ocean-continent transition zone. The similarity in basement features (low relief) was previously inferred to indicate a similar composition of the crust. *Keen and de Voogd* (1988), *Horsefield et al.* (1994) and *Peddy et al.* (1989) initially interpreted the thin layer at the foot of the slope on both margins as oceanic with a sharp continent-ocean boundary. However, this interpretation is incompatible with S-wave velocities for the Goban Spur margin (*Bullock and Minshull*, 2005) that indicate the presence of serpentinized mantle. Across Flemish Cap, a landward-dipping reflection (R2 in Fig. 3.3) on Line 85-3 has previously been suggested to represent a sharp continent-ocean boundary (Fig. 3.3, *Keen et al.*, 1989). In light of the inferred presence of wide zones of exhumed serpentinized mantle with low relief on the west Iberia margin, *Louden and Chian* (1999) suggested that this layer consisted of exhumed serpentinized mantle. However, S-wave velocities now favor a zone with the composition of continental crust on the Flemish Cap margin (*Gerlings et al.*, 2011). Tilted (synrift?) sediment packages on the Flemish Cap margin (distances 285-340 km; Fig. 3.3) also support the presence of thin continental crust. The presence of a tongue of thin continental crust on the Flemish Cap margin and the absence of thin continental crust on the Goban Spur margin suggest that continental breakup was asymmetric toward the side of Goban Spur (Figs. 3.4A and 3.4B). This interpretation contrasts with the suggestion by *Keen et al.* (1989) of an asymmetric breakup toward the Flemish Cap margin.

In general, observations elsewhere (e.g. *Reston*, 2009) would predict the breakup to occur either within the thin continental crust or toward the Flemish Cap margin, which has the sharper necking profile. However, the basaltic body observed at the Goban Spur margin (Fig. 3.4) may represent a local weakness in the thin continental crust and explain why continental breakup occurred at this location. The basalt was emplaced in the late stage of rifting by decompression melting prior to mantle exhumation (*Bullock and Minshull*, 2005). Melting at this time apparently was not extensive enough to initiate seafloor spreading; instead, mantle exhumation followed the thinning stage (Fig. 3.4B). Prior to mantle exhumation, the thin crust became brittle and part of the mantle beneath was serpentinized, in agreement with the model of *Pérez-Gussinyé and Reston* (2001, Fig. 3.4A). This interpretation is also consistent with observations further south on the Newfoundland margin, where there is direct

evidence of partially serpentinized mantle (e.g. *Party*, 2004). The zone of exhumed mantle spans a width of ∼100 km, similar to the maximum observed width on the west Iberia margin (e.g. *Dean et al.*, 2000).

The few profiles that exist of conjugate margin pairs with wide zones of exhumed mantle show zones of mantle exhumation on both sides (e.g. *Reston*, 2009), indicating that often seafloor spreading begins somewhere within this zone. However, our observations suggest that at Flemish Cap-Goban Spur initial seafloor spreading began at the same location as continental breakup, i.e., the eastward end of the tongue of thin continental crust (Fig. 3.4B), leaving all the exhumed mantle on the Goban Spur margin. Similar asymmetry has been suggested elsewhere. A wide zone of exhumed mantle is interpreted on the Nova Scotia margin but is inferred to be absent on the conjugate Morocco margin (*Maillard et al.*, 2006). A wide zone of exhumed mantle is also interpreted on the northern margins of the Gulf of Aden, but this zone is narrow or absent on the southern margins (*Leroy et al.*, 2010).

Such significant asymmetry between these transition zones remains a feature that has not yet been explained by numerical models. A broad region of highly thinned continental crust is observed at some South Atlantic margins and may be explained in models by the presence of a weak layer in the lower continental crust (*Huismans and Beaumont*, 2011). However, such models do not predict mantle exhumation, which instead in the *Huismans and Beaumont* (2011) model requires a strong lower crust.

The formation of the first 50 km of oceanic crust just landward of chron 34 also appears different on the two margins (Figs. 3.4B and 3.4C). On the Flemish Cap margin, both the MCS and wide-angle seismic results indicate a sharp boundary immediately seaward of a ridge feature, where the basement morphology becomes typical of slow seafloor spreading crust. The velocity (6.7-7.2 km s^{-1}) of the lower crust is typical for gabbro (e.g., Miller and Christensen, 1997). Farther seaward toward chron 34, there are no significant changes in either reflectivity or velocity. The velocity model of the Goban Spur margin indicates a change from the zone of exhumed serpentinized mantle ∼50 km landward of chron 34. In this region of initial oceanic crust, the basement morphology is shallower and has a more subdued relief than that of Flemish Cap (Fig. 3.3). The velocity (5.8-7 km s^{-1}) of the lower crust is more ambiguous and could support either a gabbroic or serpentinized composition (e.g. *Miller*

and Christensen, 1997). Therefore, neither MCS nor wide-angle data clearly support the presence of normal oceanic crust, although S-wave velocities are consistent with a basaltic composition for the upper crust (*Bullock and Minshull*, 2005). Evidence from plutonic rocks sampled by drilling on the Newfoundland and west Iberia margins suggests that melt supply wass subdued during earliest seafloor spreading there; instead, mantle exhumation is interspersed with short periods of igneous accretion and off-axis volcanism (*Jagoutz et al.*, 2007). The initial oceanic crust of the Flemish Cap margin has the characteristics of slow-spreading crust (velocity, density, and basement morphology) formed primarily by igneous accretion. The initial oceanic crust of the Goban Spur margin has lower velocity and basement relief characteristic of both igneous crust and exhumed mantle. Thus we infer that the initial igneous accretion was more dominant on Flemish Cap than on its conjugate. Such asymmetry is also observed on the ultraslow-spreading Southwest Indian Ridge (*Cannat et al.*, 2006), where subdued seafloor relief on one flank is interpreted as exhumed mantle, while at the conjugate location, a volcanic ridge topography is typical of slow seafloor spreading.

3.1.4 Conclusions

We have shown the following:

1. The rifting style of the Flemish Cap-Goban Spur conjugate margin pair is asymmetric during all stages of formation, i.e., crustal thinning, continental breakup, mantle exhumation, and initial seafloor spreading.

2. Evidence from P- and S-wave velocities and a clearer MCS image of basement morphology documents the presence of transition zones of contrasting compositions for the Flemish Cap-Goban Spur margins. On Flemish Cap, both observations indicate the presence of thin continental crust throughout the transition zone.

3. Based on our results, when determining the nature of the ocean-continent transition zone, careful imaging of the basement morphology is necessary with additional constraint from P- and S-wave velocities. Other margins, where subdued

basement relief has been attributed to mantle exhumation, may need to be reevaluated.

4. The transition to initial seafloor spreading appears complex and varies between margins. To better understand these breakup processes, combined MCS and wide-angle seismic surveys need to be acquired on both margin conjugates and extend into oceanic crust unambiguously identified by seafloor spreading magnetic anomalies.

3.1.5 Acknowledgements

We thank the Geological Survey of Canada Atlantic for providing digital copies of the coincident multichannel reflection profiles, and Patrick Potter for arranging for their transfer to Dalhousie University. We also thank anonymous reviewers for constructive reviews that helped us make significant improvements. Wide-angle seismic data acquisition on the Flemish Cap was jointly funded by the Natural Sciences and Engineering Research Council of Canada (NSERC) and the Geological Survey of Canada (GCS). Wide-angle seismic data acquisition on Goban Spur was supported by the UK Natural Environment Research Council (grant GR3/12351) and the EU Large Scale Facility at IFM-Geomar.

3.2 Multi-Channel Seismic Section Line 85-3

3.2.1 Reprocessing and Interpretation of Line 85-3

In this section, I will first discuss the LIFT method, which is the most important part of the data preparation for the final poststack Kirchhoff time migration and prestack Kirchhoff depth migration of Line 85-3. Then I will compare the poststack time-migrated result with the poststack time-migrated section of *Keen and de Voogd* (1988) to show what improvements have been made. Further details of the processing can be found in the Appendix E (see also Table 3.1) or *Yilmaz and Doherty* (1987). I will then show the result of the prestack Kirchhoff depth migration of Line 85-3 and discuss the implications of the resulting image on the previous interpretations of the rifting style of the Flemish Cap margin, as well as the nature of the different zones of the margin.

LIFT - Reprocessing of Line 85-3

LIFT (Leading edge InFormation Technology) is a methodology first published by *Choo et al.* (2004). LIFT is not a new filter but rather a new algorithm to filter the data that combines well known filters. In other words, it is not a new module but it is a new algorithm. The concept is very simple but the actual processing flow can be complex. The goal is as always to get the highest signal-to-noise ratio (S/N) while preserving the most signal possible. Often we stop at just trying to separate input data (A) into noise (C) and a signal (B) e.g. by using a bandpass filter, FK-filter, or noise burst attenuation such as a median filter. However, these methods are not perfect and the signal (B) and noise (C) are not completely separated. There will still be some noise left in the resulting signal (B; Fig. 3.5a; S/N=90/5) and we also may eliminate part of the signal, which is included in the noise (C; Fig. 3.5a; S/N=10/95). To counteract these difficulties, we sometimes go a step further and add back a percentage (D) of the original input (A; Fig. 3.5a) or the noise (C; Fig. 3.5b) to the signal (B). The output is then B+D. In *Choo et al.*'s (2004) examples, they get a S/N of 140/55 relative to the original S/N when adding back 50% of the original input data (Fig. 3.5a) and a S/N of 95/52.5 when adding back 50% of the noise (Fig. 3.5b).

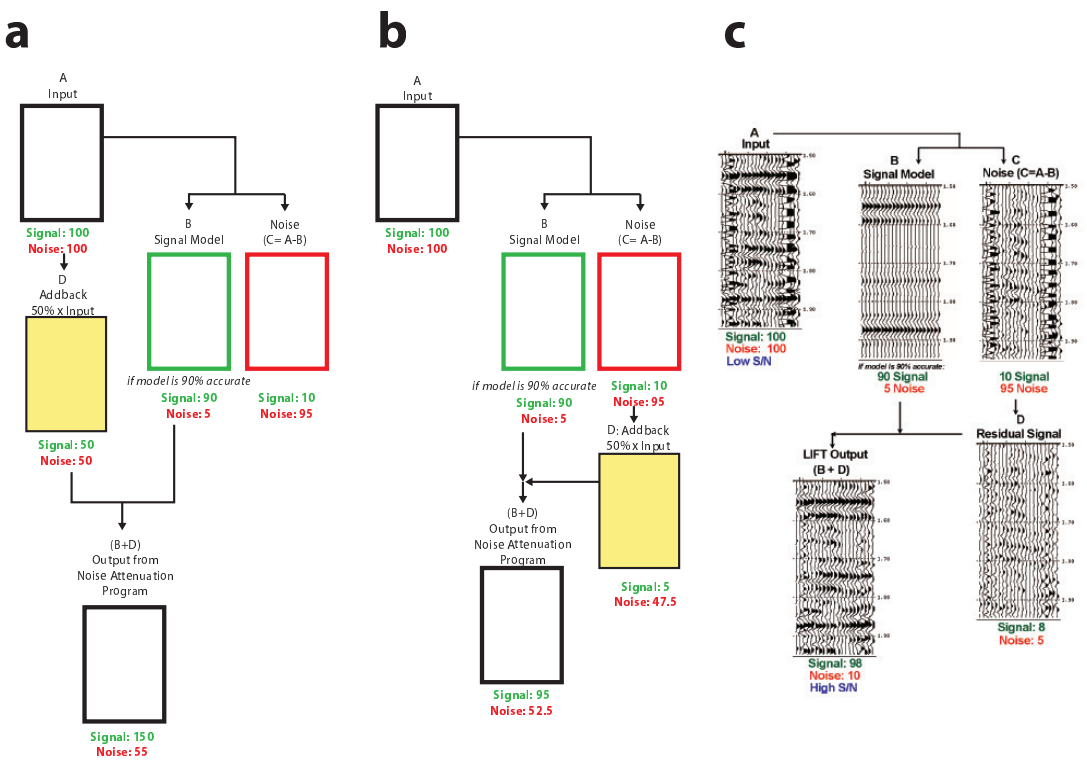

Figure 3.5: a: Diagram of noise attenuation. A: Input data; B: Signal; C: Noise; D: Percentage addback from input data (A). Adding back 50% of the original input gives a S/N of 140/55. b: Diagram of noise attenuation. A: Input data; B: Signal; C: Noise; D: Percentage addback from noise (C). Adding back 50% of extracted signal gives a S/N of 95/52.5. c: Diagram of LIFT noise attenuation. A: Input data; B: Signal; C: Noise; D: Residual Signal. By doing further processing on the noise (C) extracting as much signal from the noise as possible we get a S/N of 98/10, higher than in the two cases with a percentage add back of either input (A; S/N=140/55) or signal (B; S/N=95/52.5). Modified from *Choo et al.* (2004).

Instead of adding back a percentage, *Choo et al.* (2004) performed further processing on the noise (C) to separate out more of the signal (D; residual signal) from the noise (C; Fig. 3.5c). The extracted signal (D; residual signal) is added back to the signal (B) increasing the S/N to 98/10, significantly higher than that of the two other cases (Figs. 3.5a-3.5c). The output (LIFT) is B+D.

Exactly how we put together our workflow depends on the specific nature of the data and the noise. We still use conventional methods when separating signal and noise, e.g. FK-filter for linear noise or Radon Transform for multiples. It is often advantageous to subdivide the input data into different frequency and/or offset bands because this allows for using different noise removal algorithms on different types of

noise. In further processing of Line 85-3, I have implemented the LIFT method for both linear noise and multiple attenuation.

LIFT Noise Attenuation For linear noise attenuation, I divide the data into three frequency bands (0-3 Hz, 3-80 Hz, >80 Hz, see job in Appendix E.5.5 and Fig. 3.6). For the low band (A_L; 0-3 Hz; FILTER), I apply an FK-filter (FKFILT) followed by noise-burst attenuation (AMPSCAL). The output for low frequencies is B_L. For the middle band (A_M; 3-80 Hz; Fig. 3.6), I first apply a normal moveout (NMO) flattening the primaries and then extract the signal (B_M) from the input with the SIGNAL (local slant stack) routine. After applying reverse NMO, I subtract the signal (B_M) from input (A_M) to get the noise ($C_M = A_M$-B_M). I then apply a noise-burst attenuation routine (AMPSCAL) to the noise (C_M), resulting in the residual signal (D_M), which is added to the signal (B_M). The output for the middle frequencies is B_M+D_M. For the high band (A_H; >80 Hz), I apply only a noise-burst attenuation (AMPSCAL). Output for high frequencies is B_H. Finally, I add the three outputs together for the final output (B_L+B_M+B_H+D_M). In Fig. 3.7, a shot-gather is shown for each of the steps for the middle frequency band (A, A_M, B_M, C_M, D_M, B_M+D_M, and B_L+B_M+B_H+D_M). A shot-gather of the noise (C_M-D_M) that is removed from the input data (A_M) is also a shown. The LIFT method allows a much more aggressive approach when separating noise from signal. It is not necessary to be too careful in not eliminating any signal, since by processing the noise (C) most of the eliminated signal will be extracted and added back. Using this approach and including further noise attenuation on the separated noise (C), I am able to add back most of the "lost" signal, which results in a higher S/N.

LIFT Radon Transform Line 85-3 displays several strong water bottom multiples that overprint the signal, making it almost impossible to observe signal. For shallow water depths, the multiples arrive at early times and are numerous almost completely covering any signal in the upper crust beneath Flemish Cap. Over the slope where the water depth changes rapidly, it is very difficult to separate primaries and multiples. For multiple attenuation, several approaches (Fig. 3.8) were tested, including surface related multiple elimination (SRME; Focus modules SMACMS and SMACTRM) and the Radon Transform (PRADMUS), individually and combined. To

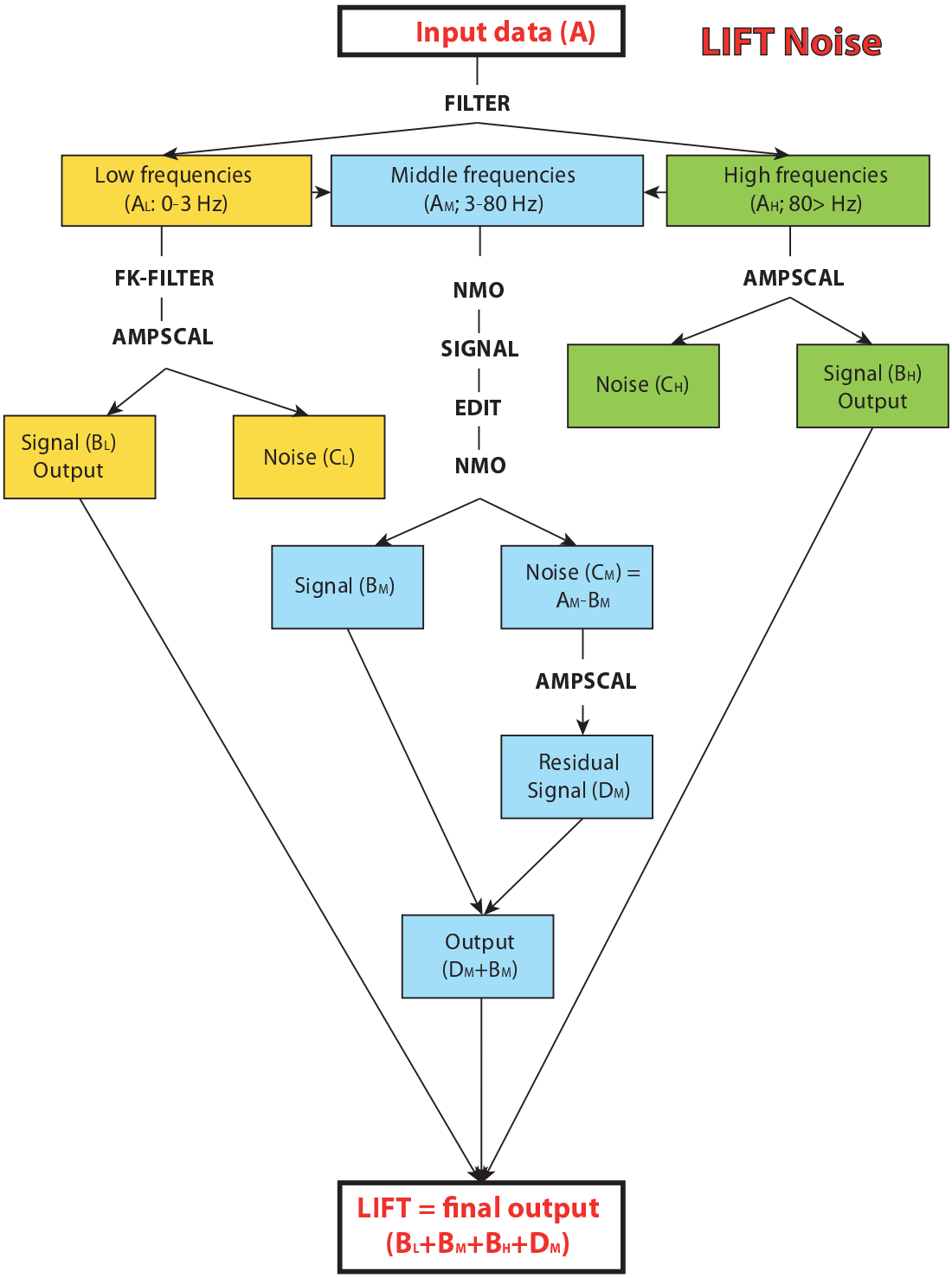

Figure 3.6: Diagram of the processing steps for LIFT noise attenuation. Capital and bold letters represent the Focus module used.

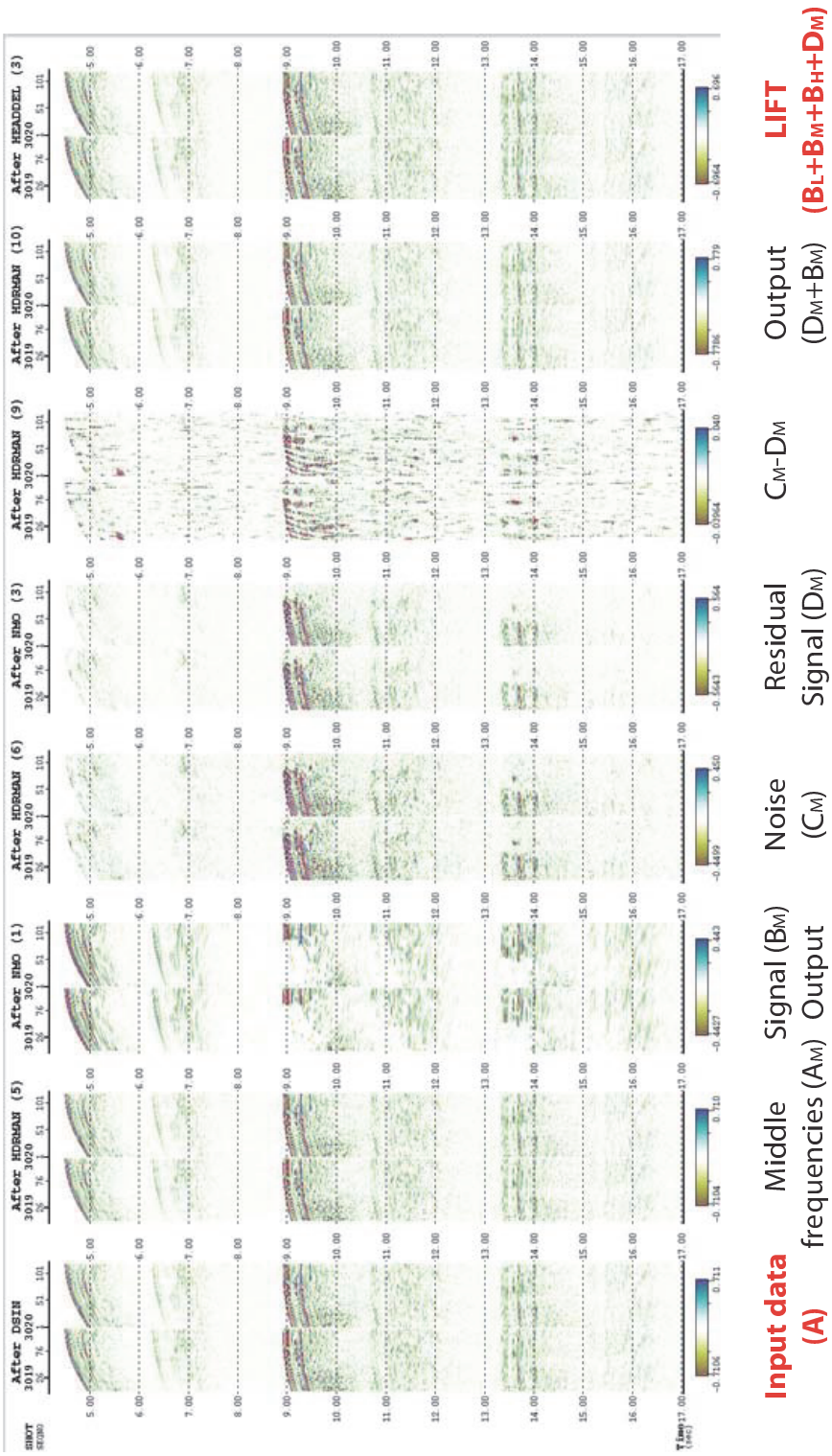

Figure 3.7: Shotgathers from LIFT noise attenuation. A: Input data; A_M: input middle frequencies (3-80 Hz); B_M: Signal of middle frequencies; C_M: Noise of middle frequencies; D_M: residual signal of middle frequencies; $LIFT_M$: Output from middle frequencies; LIFT: Total output. C_M-D_M shows the noise that has been removed from A_M, which is the same as adding D_M to B_M (LIFT=D+B).

eliminate the multiple with Radon Transform, the data are transformed into the tau-p domain, which separates the primaries and the multiples. Then either the primaries are removed before transforming back into the T-X domain and subtracting from the original input, or the multiples are removed in the tau-p domain. With SRME, the Taylor terms are predicted for the multiples, which are then subtracted from the input data. SRME and Radon Transform were tried both individually and combined with and without LIFT. The best result was SRME followed by LIFT Radon Transform (Fig. 3.8). This combination worked best on both the part of the section with shallow water depths, showing many strong multiples, as well as on the slope, which is the most challenging part of the section to demultiple. Using this combination, I am best able to preserve the primaries, while attenuating the multiples the most. For large water depths (4 s. TWT), a Radon Transform with no LIFT would have been sufficient, but SMRE and LIFT Radon Transform were applied to the entire section.

LIFT Radon Transform includes multiple steps (see Job in Appendix E.5.9 and Fig 3.9). First I apply a lowpass filter (0-10 HZ; FILTER) to the input data (A). For the low frequencies (A_L), I apply a parabolic Radon Transform (PRADMUS). Then I apply a noise-burst attenuation (AMPSCAL) on the window that includes the multiple. The result is the signal (B_L), which is subtracted from the input data (A) to give the highpass input ($A_H = AB_L$). Notice that A_H still includes the noise (C_L). I apply a Radon Transform (PRADMUS) and noise-burst attenuation (AMPSCAL) to A_H. The result is signal (B_H), which is subtracted from A_H to obtain the noise (C_H). On the noise (C_H), I apply a Radon Transform (PRADMUS) and noise-burst attenuation (AMPSCAL). The result of this step is the residual signal (D_H). For the final output, I add the residual signal (D_H) to the signal (B_H), which is then added to the output (B_L).

Processing Steps for Line 85-3: Final Poststack Kirchhoff Time Migration

In the supplementary material (see Appendix D), I give a summary of the processing steps for the poststack Kirchhoff time migration of Line 85-3, as presented in the paper (*Gerlings et al.*, 2012). I subsequently have improved and changed some of the steps (Table 3.1). From raw data to noise attenuation, I optimize some of the parameters but otherwise keep the order of the steps the same. I leave out surface

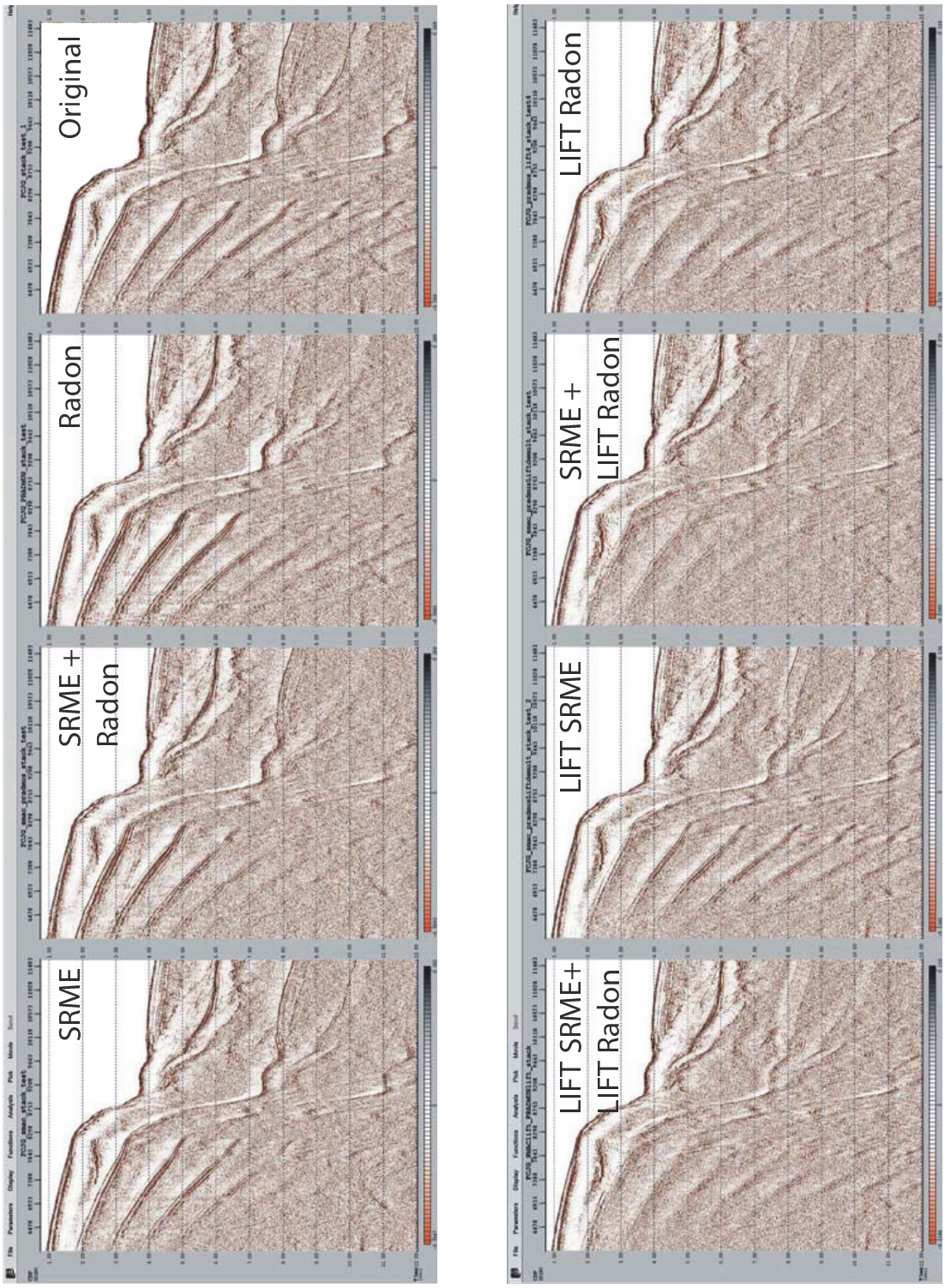

Figure 3.8: Comparison of different combinations of multiple removel with Radon Transform, Surface Related Multiple Elimination (SRME), LIFT Radon Transform and LIFT SRME. SRME followed by LIFT Radon Transform gives the best overall result.

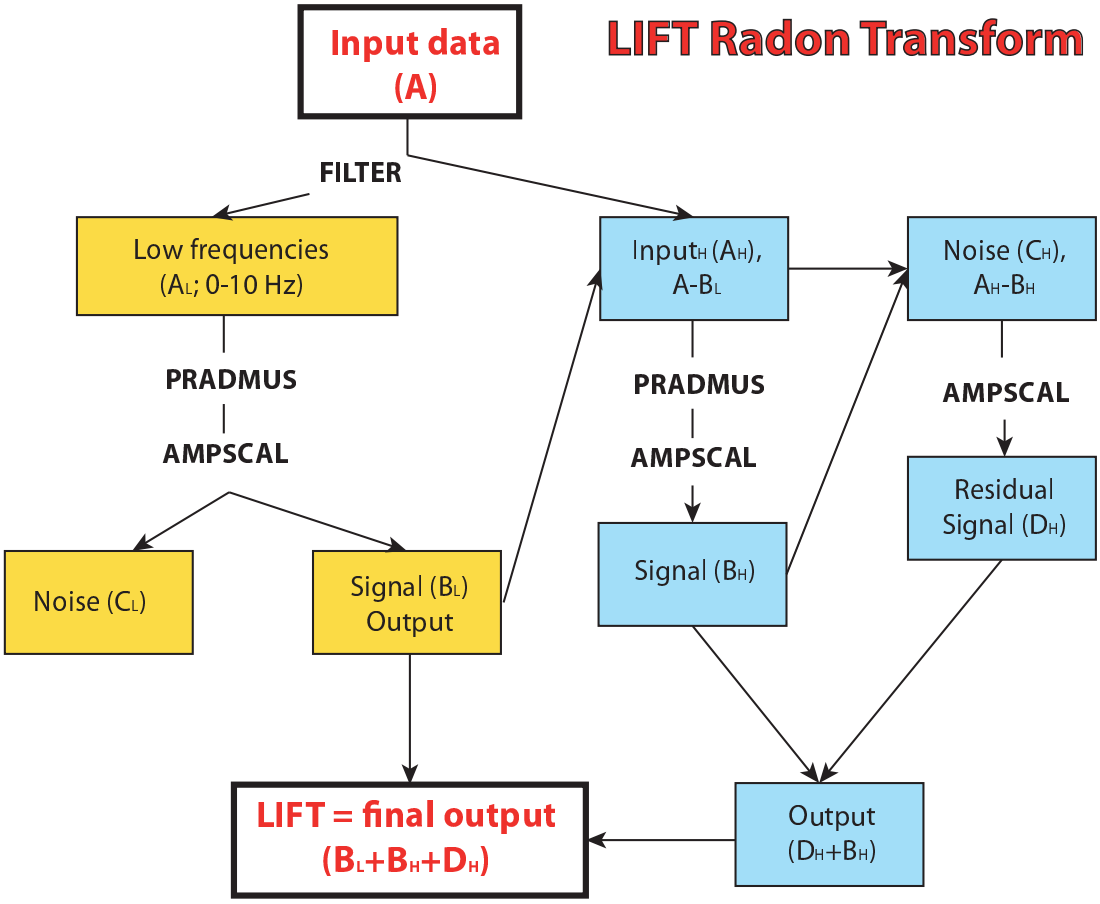

Figure 3.9: Diagram of the processing steps for LIFT Radon Transform. Capital and bold letters represent the Focus module used.

consistent deconvolution because I could not see any improvement to the signal and did not want to risk removing any signal by applying it. For noise attenuation, I use the LIFT method (see Section 3.2.1) and then add a K-filter (wave number filter), which performs a filter of the seismic traces. I double the shots by interpolating to make the shot and receiver distance the same (25 m) to reduce aliasing during LIFT demultiple, or in particular during the radon transform. Hence I need to apply new geometry. I then apply LIFT again because the shot interpolation algorithm added some noise to the new shots. The next step was multiple attenuation, which again is different from Section 3.1. I apply surface related multiple elimination (SMRE) and Radon with LIFT (see Section 3.2.1) instead of just Radon Transform. I then stack the data and apply a Kirchhoff time migration, followed by a coherency filter, bandpass filter, bottom mute and Automatic Gain Control (AGC).

3.2.2 Comparison of the Reprocessed Time Section and a Previous Processing of Line 85-3

By using the LIFT method as detailed above, I have managed to improve some of the important details in the poststack Kirchhoff time migrated seismic image of Line 85-3 (Fig. 3.10). This section will illustrate these improvements. Note, however that detailed interpretation is carried out only on the final result, which is the prestack depth migrated section (Section 3.2.3). Close-ups of the seismic sections are show in Figs. 3.11-3.14, compared with close-ups of the same sections from *Keen and de Voogd* (1988).

Overall, the new image appears to be of significantly higher resolution and S/N ratio, and reveals reflectors that were not imaged previously. A close-up of the thick continental crust landward of the continental slope shows some significant improvements (Fig. 3.11). The shallow event (T) is a strong reflection but was previously not visible. It may have been muted out in the previous processing in an attempt to get rid of the very strong seafloor multiples. Moho is also clearer both beneath the thick continental crust and where the crust begins to thin beneath the slope. Although some hints are seen in the old section, it is now obvious that Moho consists of three or perhaps four separate reflections. This could indicate that Moho may be a complex transitional boundary between the lower continental crust and mantle.

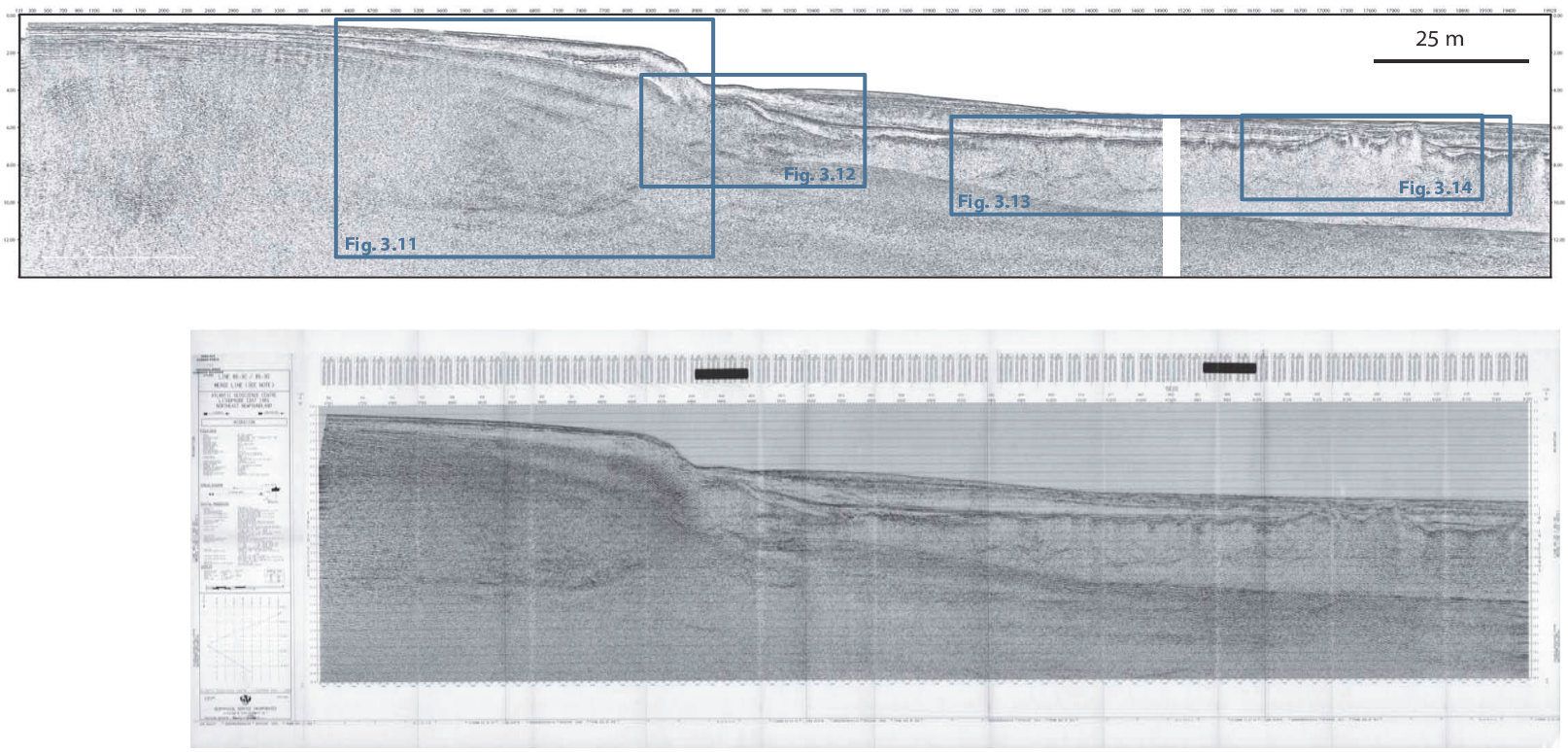

Figure 3.10: Poststack Kirchhoff time migrated section of Line 85-3 (top). High-resolution scan of the previous poststack time migrated section of Line 85-3 by *Keen and de Voogd* (1988) (bottom). Boxes indicate close-ups (Figs. 3.11-3.14).

Table 3.1: Reprocessing of Line 85-3 (time section)

Step	Process	Focus Module	Details in Appendix or Section
1	SEGD to SEGY		
2	Edit duplicated shots	EDIT HEADDEL HEADPUT	App. E.5
3	Nominal geometry, CMP binning 12.5 m	MARINE	App. E.5.1
4	Edit shot gathers	EDIT	
5	Spherical divergence	GAIN	App. E.5.2
6	Surface consistence amplitude balancing	BALAN BASOL BALAPP	App. E.5.3
7	Noise attenuation on low frequencies (0-12 Hz)	SUPPRES	App. E.5.4
8	preliminary velocity analysis combined with velocity model of wide-angle seismic data	VELDEF	
9	LIFT - Noise attenuation		Sec. 3.1 and App. E.5.5
10	K-filter	WNFILT	App. E.5
11	Shot interpolation (shot distance 25 m, before 50 m)	HXINT	App. E.5.7
12	New geometry	MARINE	
13	Noise attenuation	LIFT	Sec. 3.1
14	SRME	SMACMS SMACTRM	App. E.5.8
15	Radon LIFT	PRADMUS	Sec 3.1 and App. E.5.9
16	Velocity analysis	VELDEF	
17	Stack	STACK	
18	Kirchhoff time migration	MIGTX	
19	Coherency filter	COHERE	
20	Bandpass filter (0-5-70-80 Hz)	FILTER	
21	Water bottom mute	MUTE	
22	AGC	AGC	

A close-up of the big fault block (B; Fig. 3.12) beneath the slope now shows some deeper reflections (D) below the crustal block. I will discuss these reflections in

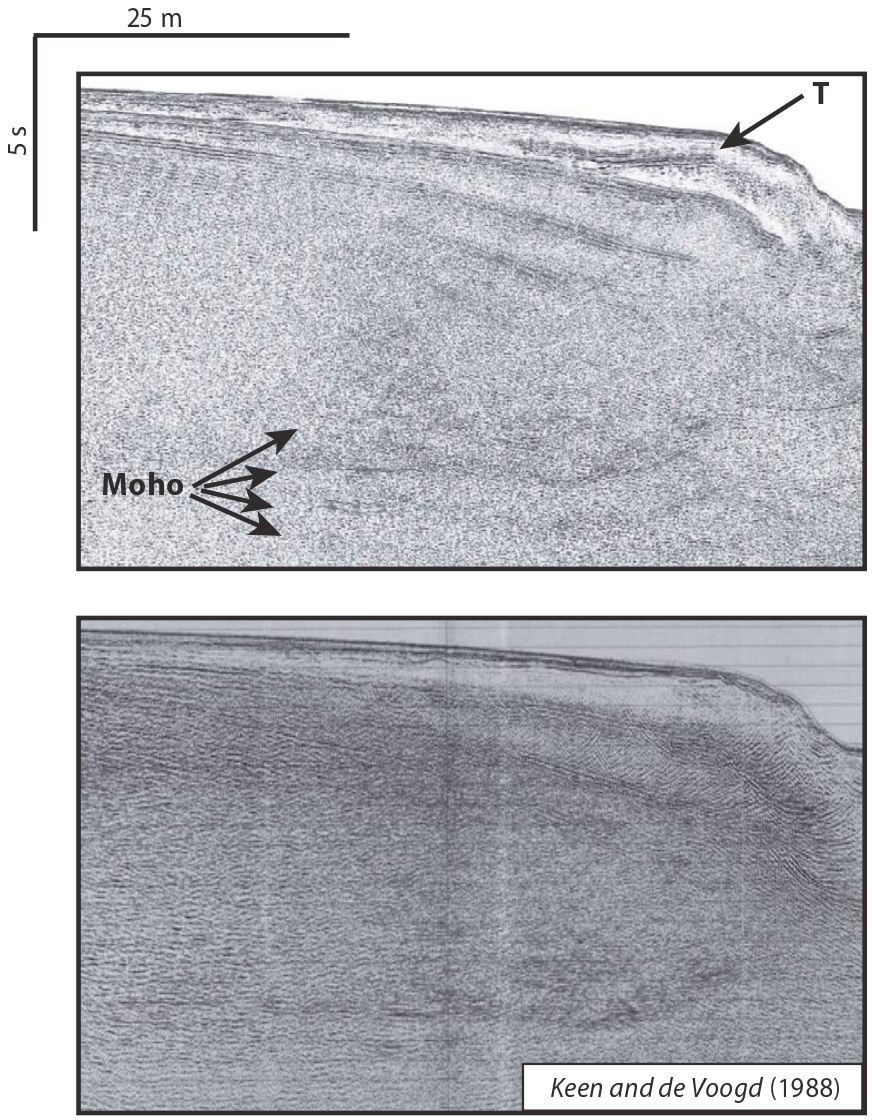

Figure 3.11: Close-up of the seaward end of the Cap. T: a reflection just below the seafloor and basement.

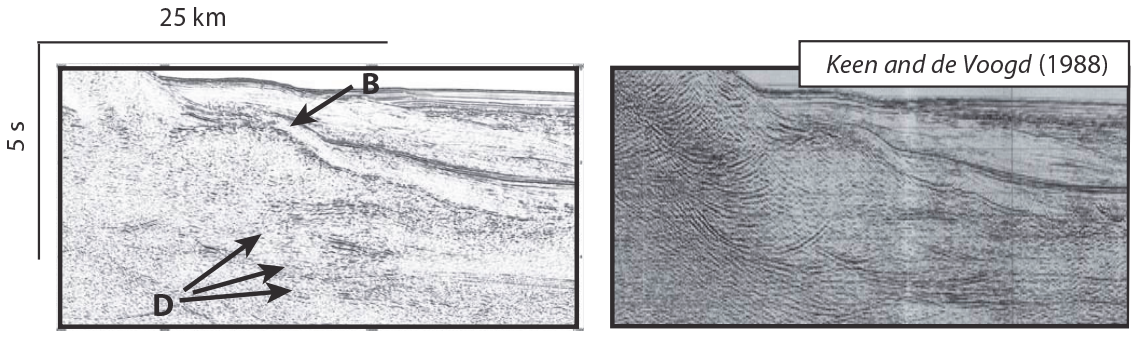

Figure 3.12: Close-up of the big fault block (B) at the foot of the slope and some strong inter-crustal reflections (D).

further detail when I present the depth migrated section, since the geometry of these reflections changes. However, the deep reflections (D) are now clearer and not overprinted by over-migrated "smiles" from the seafloor multiple as in the earlier section.

The imaging of the basement has improved significantly (Fig. 3.13). As shown in the previous chapter, it is now clear that basement in the transition zone is overlain by back-tilted sediments, and a row of rotated normal faults along the basement is obvious. The basement was previously interpreted as oceanic by *Keen and de Voogd* (1988) and later as potentially exhumed serpentinized mantle by *Louden and Chian* (1999) and *Bullock and Minshull* (2005). As discussed in Section 3.1 (*Gerlings et al.*, 2011), a normal faulted basement is consistent with the P- and S-wave velocities that suggest a continental nature. The deeper landward- and seaward-dipping reflections (X) in the transition zone (Fig. 3.13) are also both stronger and clearer, especially farther towards the ridge feature. These reflections may be related to the serpentinization of the upper mantle, perhaps serpentinization fronts.

The image of the ridge feature has improved (Fig. 3.14). From displaying an unclear basement and deeper crustal reflections (R and X) overprinted by over-migrated "smiles", which could suggest the nature of the ridge feature as anything from continental crust, to oceanic crust, to a serpentinized ridge, the new reprocessed image of the ridge feature now more clearly suggests the presence of diapiric intrusive material. We suggest that a small amount of serpentinized mantle intruded thin continental crust. The ridge was sampled by a few S-waves, which indicated a continental composition. However, these wide-angle data do not have sufficient resolution to determine if the top part of the ridge is actually intruded by mantle.

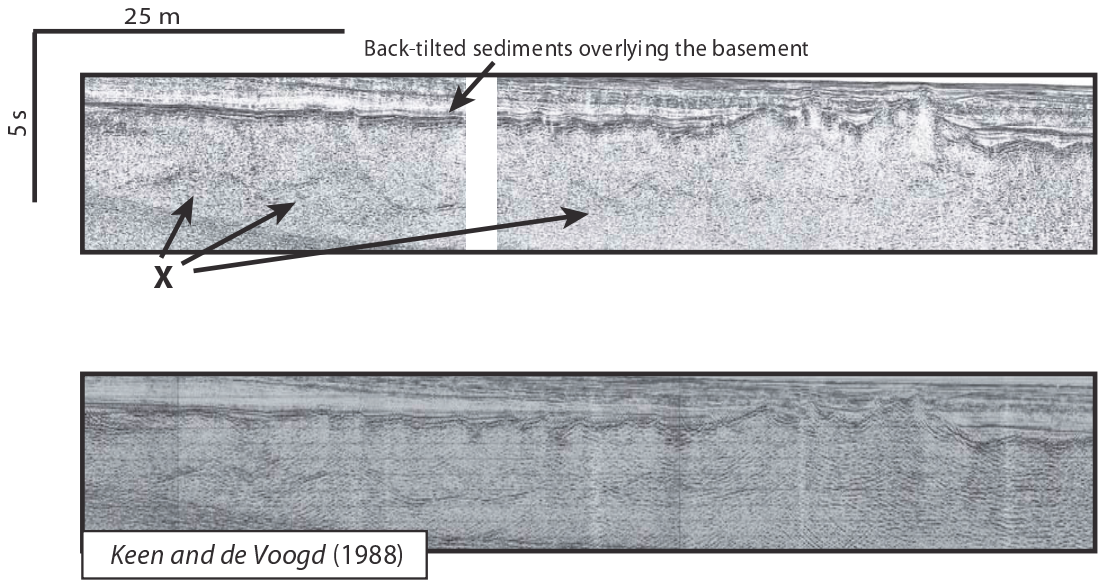

Figure 3.13: Close-up of the normal faulted basement in the transition zone of thin continental crust. Deep reflections in the crust (X) coincident with serpentinized mantle modeled by the wide-angle data.

The sediments overlying the basement beside and on top of the ridge feature display different characteristics. The landward sediment overlying the basement has a clear fan-like structure consistent with rifting, whereas on top and seaward of the ridge the sediments are more horizontal, perhaps indicating a change in nature of the tectonic setting from rifting to drifting from one side of the ridge to the other or a change in timing/style of deformation with sedimentation on either side. The ridge represents the seaward end of the transition zone. Where the ridge displays a diapiric nature, the overlying sediments look disturbed.

3.2.3 Prestack Depth Migration

For the depth migration, I focused on the slope and deep seaward part of the section. The processing steps are the same as for the poststack time migration up until the stack (Steps 1-15 in Table 3.1). Table 3.2 shows the processing steps 16-22. I refine the sedimentary section of the wide-angle data velocity model by picking the residuals on the cmp gathers in **Geodepth 8.2**. Then I apply prestack Kirchhoff depth migration. This is followed by a coherency filter, bandpass filter, water bottom mute and AGC on the migrated stack section (see details in Appendix). Fig. 3.15 shows the depth

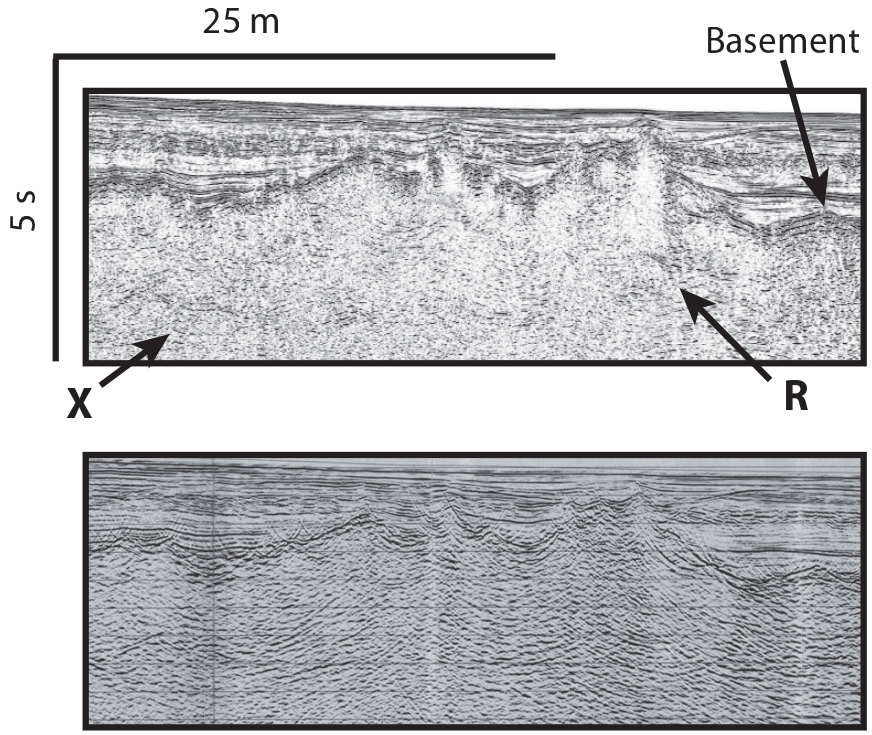

Figure 3.14: Close-up of the ridge feature. Deep reflections in the crust (X) and within the ridge feature (R).

migrated section of the seaward half of Line 85-3. Close-ups are shown in Figs. 3.16-3.22.

Table 3.2: Reprocessing of Line 85-3 (depth section)

Step	Process	
16	Residual velocity analysis	Geodepth
17	Kirchhoff depth migration	Geodepth
18	Stack	Geodepth
19	Coherency filter	Focus/COHERE
20	Bandpass filter (0-5-70-80 Hz)	Focus/FILTER
21	Water bottom mute	Focus/MUTE
22	AGC	Focus/AGC

Sedimentary Reflections

In the sedimentary package, very prominent reflections can be observed at ∼4.5-5.5 km depth (Figs. 3.15, 3.16, 3.17, 3.19 and 3.20). Two bright reflections are observed on the SCREECH 2 lines (*Shillington et al.*, 2006), the A^u and the U unconformities

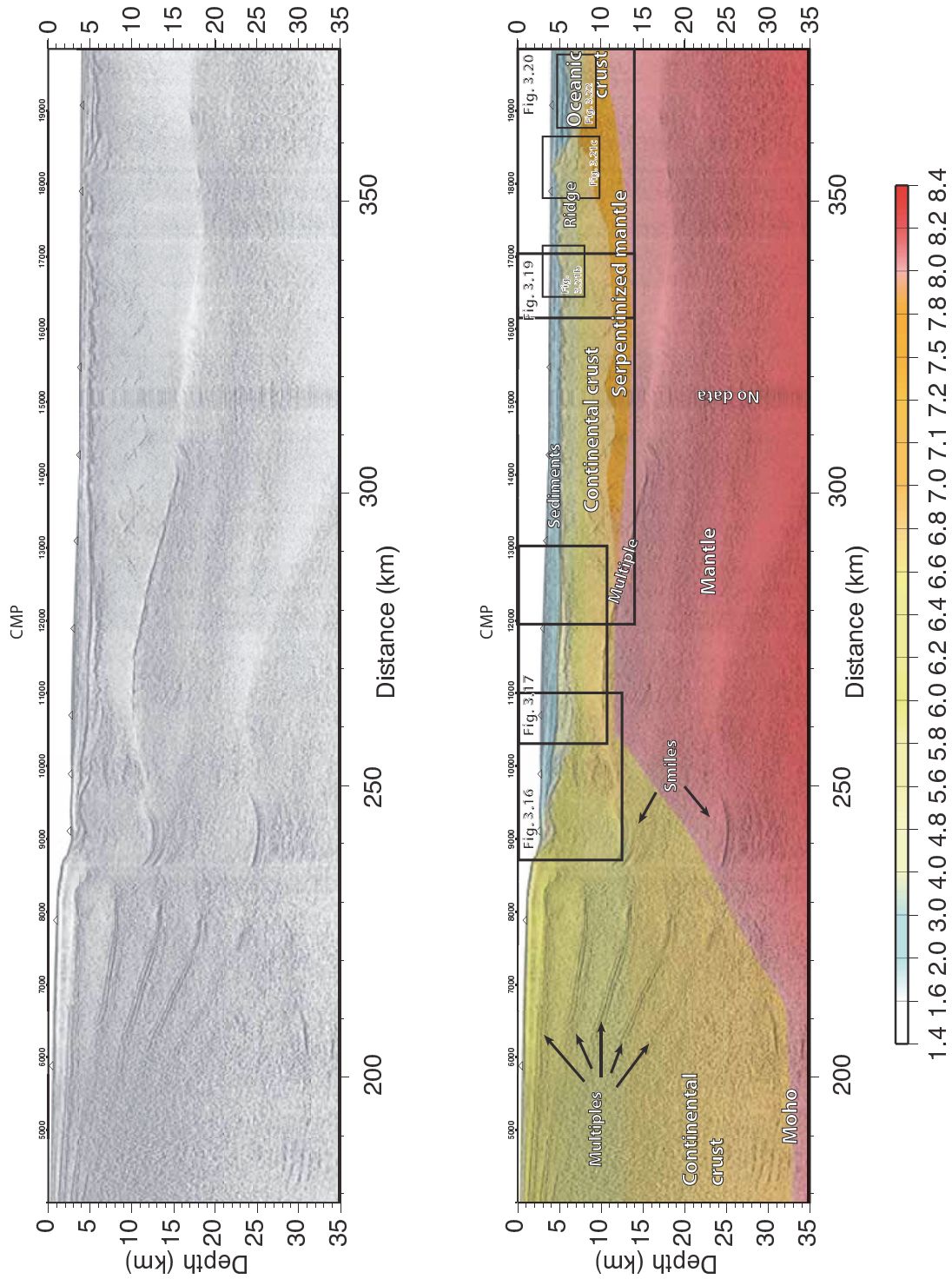

Figure 3.15: Prestack Kirchhoff depth migrated section of Line 85-3 (top). Prestack Kirchhoff depth migrated section of Line 85-3 superimposed on the P-wave velocity Model (bottom). Boxes indicate close-ups (Figs. 3.16-3.22).

(Fig. 3.18). The A^u unconformity was mapped by *Tucholke and Mountain* (1979) and drilled at Site 1276 (*Party*, 2007). The A^u reflection and underlying sediments correspond to interlayered mudstones and carbonate-cemented sandstone of an Eocene to Paleocene age (*Party*, 2004; *Shillington et al.*, 2006). The U unconformity was previously suggested to represent a breakup unconformity (*Tucholke et al.*, 1989). However, drilling (Site 1276) just penetrating this reflection encountered two diabase sills, separated by early Aptian sediments (*Party*, 2007; *Shillington et al.*, 2006). No bright reflections similar to those of the U reflection representing sills are observed in the seismic section of Line 85-3. However, a reflection that is very similar to the A^u reflection is imaged, and the sediment packages above and below display similar reflectivity to that of SCREECH Line 2.

Basement Morphology and Reflectivity within the Extended Thin Continental Crust

We can observe four different zones of reflectivity within the thin continental crust. (1) Sub-horizontal reflections are imaged in the landward-most zone showing the thinning of all of the continental crustal sections, including the disappearance of the mid crust (Fig. 3.16). (2) A reflective upper crust and non-reflective lower crust are imaged in the adjacent zone (Fig. 3.17). (3) Farther seaward a zone of both landward and seaward-dipping bright reflections in the lower crust are imaged (Fig. 3.19). (4) In the seaward-most zone, reflections are mainly seaward dipping and can be traced down from the basement (Fig. 3.19.

A close-up of the fault block (Fig. 3.16) in the depth section shows a different geometry than that of the time section (Fig. 3.12). The depth migration has tilted the block landward and the block appears more symmetric with flanks of similar dips. At the tip of the fault block, we can observe a smaller normal fault. There also appears to be another fault block just seaward of this block (Fig. 3.16). Below and slightly seaward of the fault block, we can now clearly observe several strong intercrustal reflections. These reflections are all located in the part of the continental crust where the most rapid thinning occurs and where the middle layer of continental crust pinches out. The blue dashed line in the crust represents the boundary between upper and lower crust in the P-wave velocity model. A possible interpretation is that

these bright reflections correspond to ductile deformation in the middle and lower crust related to rifting. No faults can be traced through the crust on either side of the big fault block.

Seaward of the big fault blocks, we can observe a few minor thrust faults in the basement morphology (Fig. 3.17). The minor thrust faults all seem to terminate at a horizontal reflection in the upper crust. The blue dashed line indicates the boundary between the upper and lower crust based on the P-wave velocity model (*Gerlings et al.*, 2011), which is located below this horizontal reflection. The upper first km of the crust is highly reflective (Fig. 3.17). However, there are no clear reflections in the lower crust (distances 260-285 km). Thus in this part of the thin continental crust, we observe no features in the lower crust corresponding to brittle extension, ductile deformation or serpentinization fronts. The basement morphology shows evidence of minor compression. According to *Pérez-Gussinyé and Reston* (2001), the 6-km-thin continental crust should be completely brittle and the upper mantle should be partially serpentinized. However, mantle serpentinization does not seem to have occured in part of this section. The lack of deep reflections may instead suggest that the crust is not permeable here, which is also consistent with the observations of the P-wave velocity model (*Gerlings et al.*, 2011). No layer of partially serpentinized mantle is modelled below this part of the thin continental crust (distances 255-285 km; Fig. 3.15).

Farther seaward, the basement morphology is subdued with a small number of minor offsets. Low-angle seaward dipping reflections can still be traced from basement to $\sim$1 km into the upper crust. At distance 285-340 km at 8-13 km depth, some both landward and seaward dipping bright reflections are observed within the crust (Fig. 3.19). No clear faults are observed in the basement morphology. These dipping reflections in the lower crust were interpreted in the time section to be located within the layer of partially serpentinized mantle. However, the depth migration has moved these bright reflections up so they now terminate at the top of this layer of the P-wave velocity model. If we still interpret these reflections to indicate serpentinized mantle, the boundary between lower thin continental crust and partially serpentinized mantle needs to be raised. The thick light blue line is a suggestion of where this boundary may be located. This boundary will be discussed further in Chapter 4.

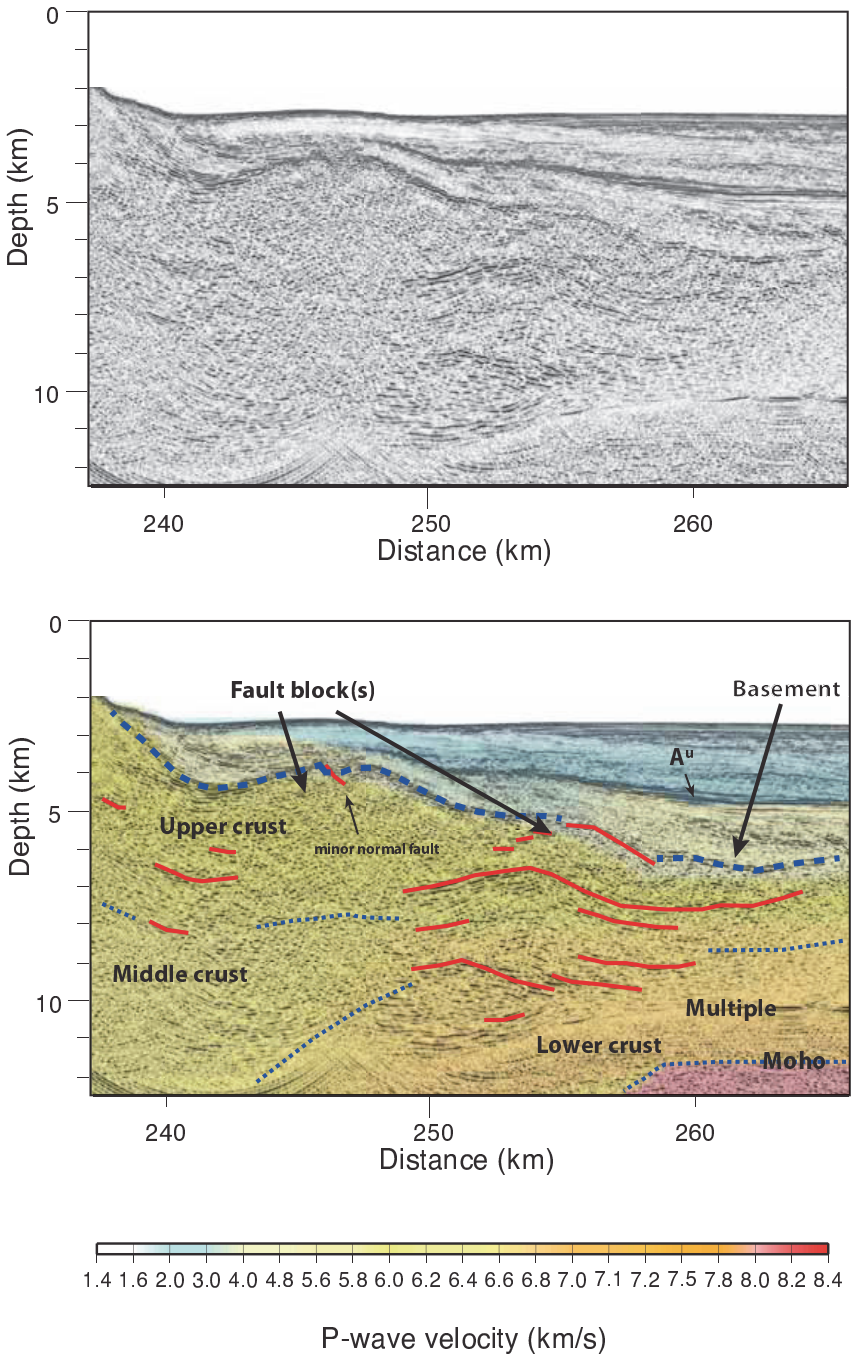

Figure 3.16: (Top) Close-up of the most landward part of the transition zone of Line 85-3 with a major fault block. (Bottom) Close-up with the P-wave velocity model superimposed (*Gerlings et al.*, 2011). Dashed blue lines indicate basement; dotted blue lines indicate the boundary between upper and lower crust in the P-wave velocity model; red lines indicate strong reflections within the crust and upper mantle.

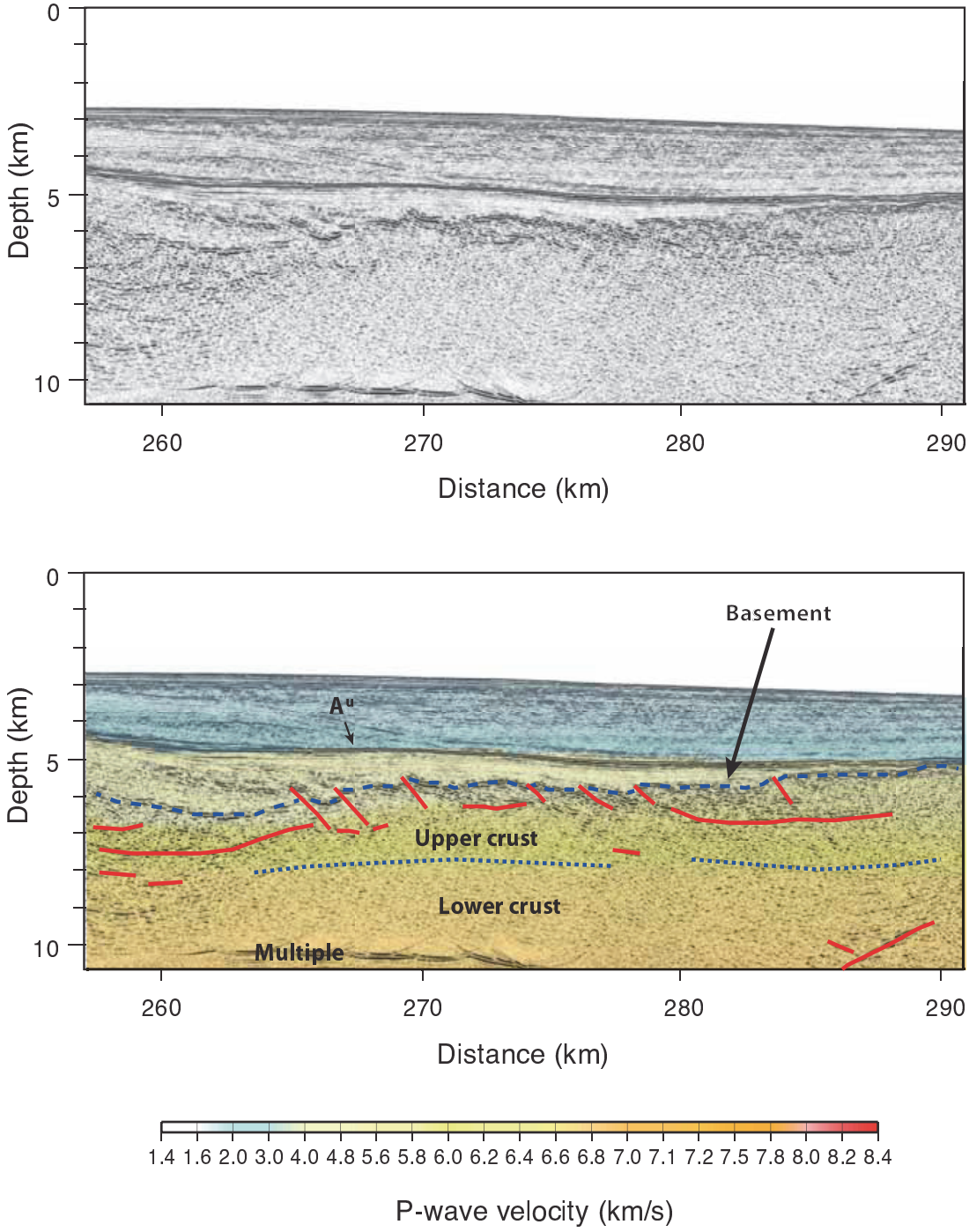

Figure 3.17: (Top) Close-up of the transition zone of Line 85-3 with a basement morphology suggeting minor thrust faults. (Bottom) Close-up with the P-wave velocity model superimposed (*Gerlings et al.*, 2011). Dashed blue lines indicate basement; dotted blue lines indicate the boundary between upper and lower crust in the P-wave velocity model; red lines indicate strong reflections within the crust and upper mantle.

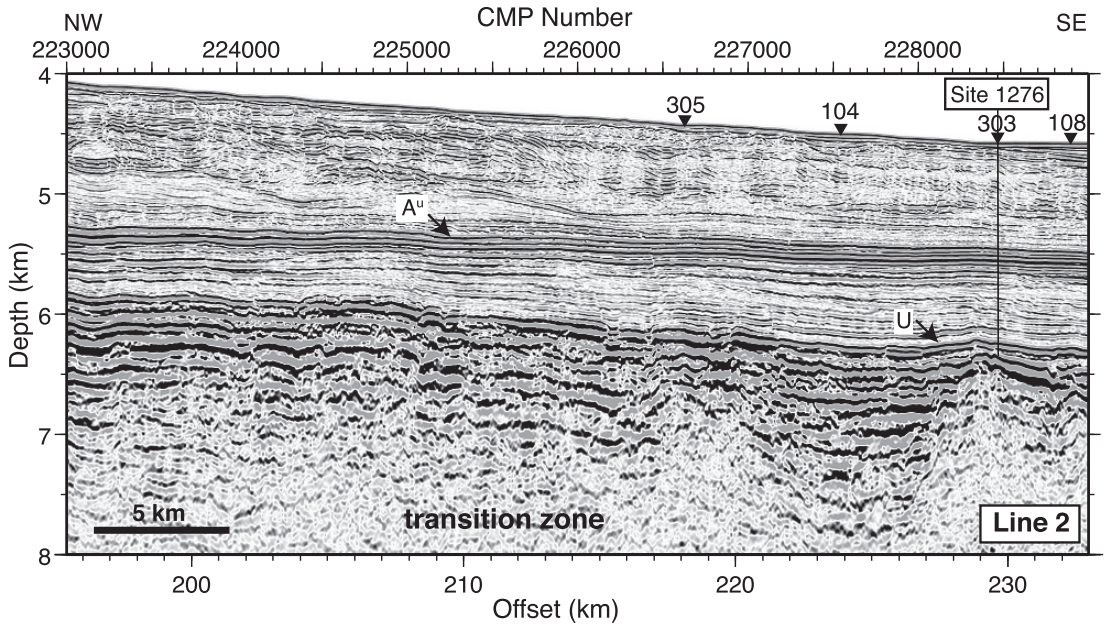

Figure 3.18: Close-up of the sediments and basement of the transition zone in SCREECH Line 2 (*Shillington et al.*, 2006). The Vertical line indicate ODP Site 1276. Two bright reflections, the A^u and the U unconformities, are imaged

The basement morphology changes farther seaward (distance ∼300 km) from minor thrust faults, then a more muted basement morphology to minor normal faults (Figs. 3.17 and 3.19). The minor normal faults are overlain by back-tilted syn-rift sediments. The deeper bright reflections seem here to be mainly seaward dipping. The normal faults are connected with these bright deep reflections in several places and may have been a conduit for the seawater down to the mantle serpentinizing the upper mantle (Fig. 3.19). These bright reflections are similar to some bright dipping reflections observed at similar depth (7-12 km) in the Central Indian Basin (*Delescluse and Chamot-Rooke*, 2008). *Delescluse and Chamot-Rooke* (2008) interpreted these bright reflections as serpentinization fronts.

Ridge Feature

Basement morphology changes character at the ridge feature (Fig. 3.20), where normal faulted basement is no longer observed. Just below basement, we can observe some short (1-2 km) semi-horizontal reflections in a few places(around distances 338, 350, 355 km) roughly parallel to the basement. Similar reflections are observed on SCREECH Line 2 at the serpentinized ridge feature at Site 1277. *Shillington et al.*

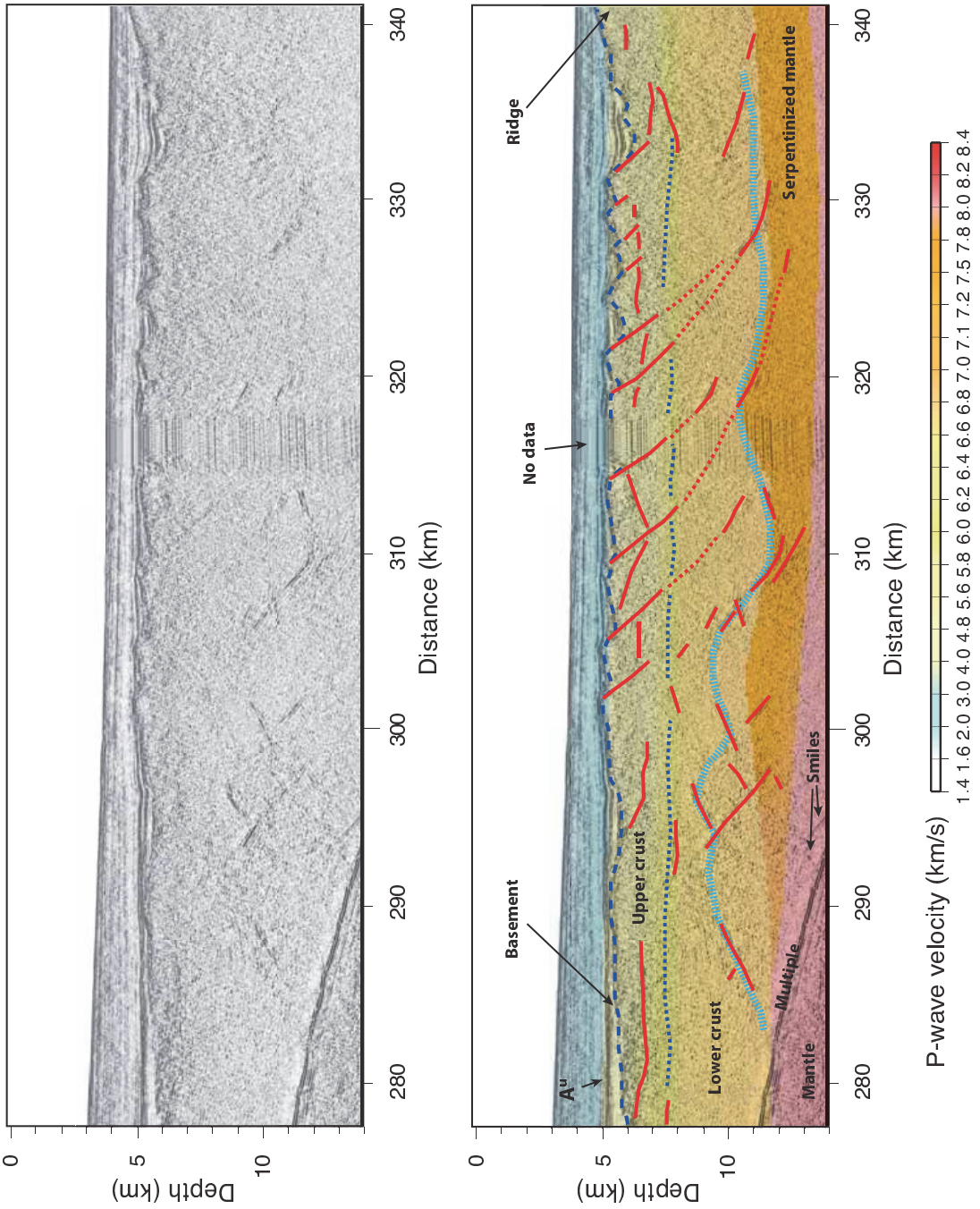

Figure 3.19: (Top) Close-up of the transition zone of Line 85-3 with a normal faulted basement. (Bottom) close-up with the P-wave velocity model superimposed (*Gerlings et al.*, 2011). Dashed blue lines (long) indicate basement; dashed blue lines (short) indicate the boundary between upper and lower crust in the P-wave velocity model; red lines indicate strong reflections within the crust and upper mantle; thick light blue dashed line is discussed in the text.

(2006) (Fig. 3.21) suggested that such a reflection could be a detachment fault. Furthermore, we can observe a couple of clear, deeper, seaward-dipping reflections at the most seaward end of the ridge (distance 355-360 km; Figs. 3.20 and 3.21). This suggests that the most seaward end of the thin continental crust may have both been faulted and intruded. It is the farthest seaward we observe these deep dipping reflections, suggesting that this is the limit of the partially serpentinized mantle, which is consistent with the P-wave velocity model. The seaward-most limit of the layer of partially serpentinized mantle terminates at distance 370 km (Fig. 3.20) just below these dipping reflections in the P-wave velocity model. Seaward of the ridge feature, formation of initial oceanic crust occurs.

Basement Morphology and Reflectivity Beneath Basement in Initial Oceanic Crust

In the oceanic part of the section (Fig. 3.20, 3.22), seaward of the ridge, reflectivity of the basement is scattered and not continuous, typical of oceanic crust. A weak horizontal reflection (distance 360-370 km) corresponds to the boundary between Layer 2 and 3 in the P-wave velocity model (blue dashed line, Fig. 3.20). No clear Moho is observed in the section in the oceanic domain. Although the velocities of the P-wave velocity model correspond to typical oceanic crust, it may be possible that at least part of the material is serpentinized mantle. This would account for the missing Moho reflections. However, the amount of serpentinized mantle is less than for the initial oceanic crust of Goban Spur (see discussion in Section 3.1).

3.2.4 Summary

LIFT and other advanced prestack data analysis techniques applied have been successful in enhancing the S/N ratio of the data relative to the previous processing of *Keen and de Voogd* (1988). SMRE followed by the LIFT Radon Transform seem to attenuate the multiples best while preserving the signal. The prestack Kirchhoff depth migration using a hybrid MCS/wide-angle data velocity model resulted in a higher resolution image that reveales several interesting features that illustrate the complexity of the transition zone of thin continental composition. We now see evidence of ductile deformation in the thin continental crust. Furthermore, we are able

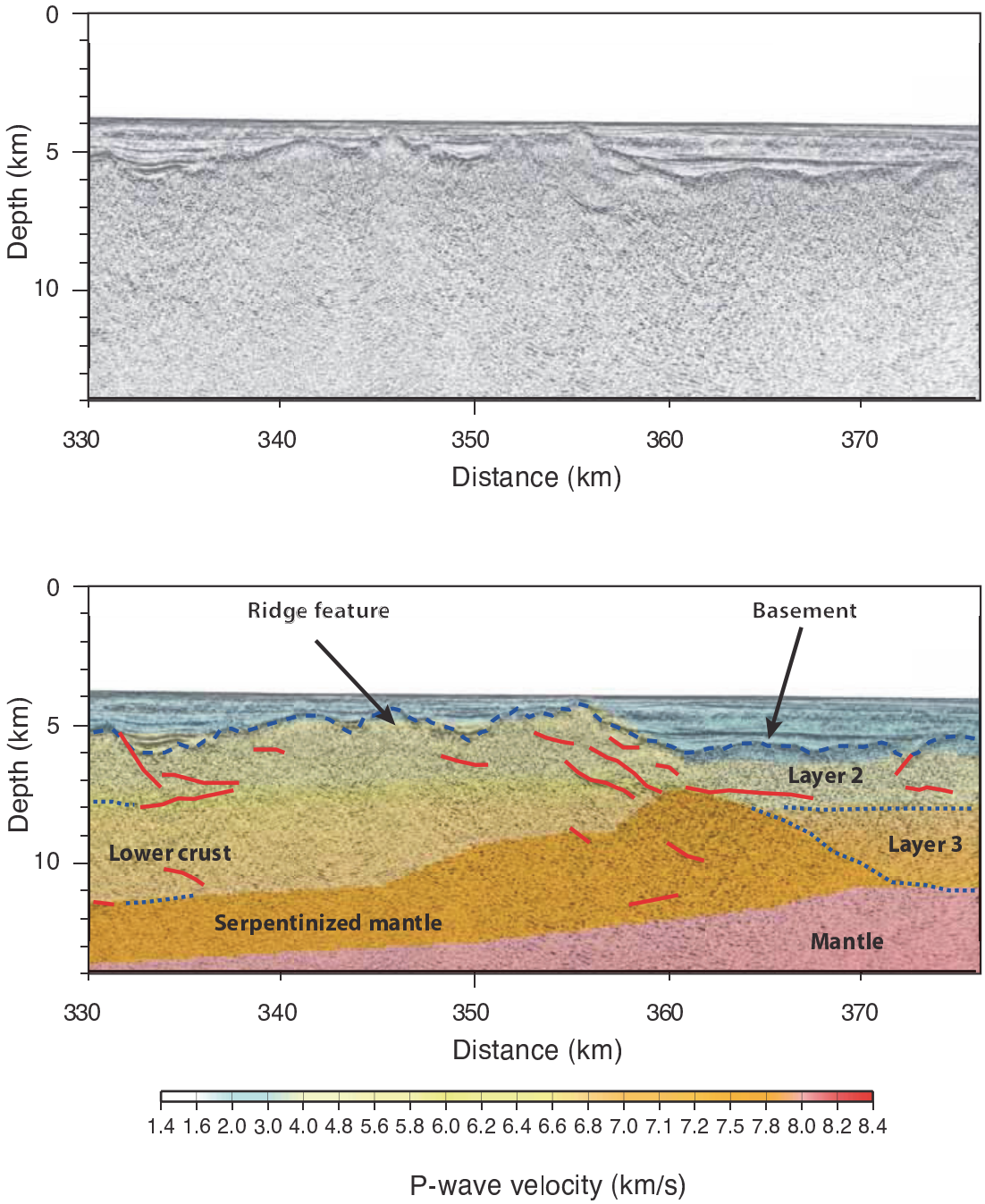

Figure 3.20: (Top) Close-up the Ridge feature. (Bottom) Close-up with the P-wave velocity model superimposed (*Gerlings et al.*, 2011). Dashed blue lines indicate basement; dotted blue lines indicate the boundary between upper and lower crust in the P-wave velocity model; red lines indicate strong reflections within the crust and upper mantle.

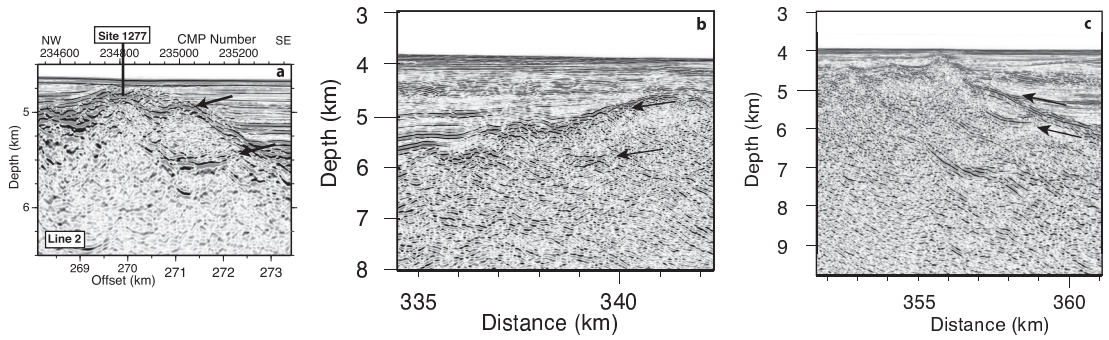

Figure 3.21: Two close-ups of the ridge feature together with a close-up of a ridge feature on SCREECH Line 2 (*Shillington et al.*, 2006). Notice the similarity in the reflections just below basement. See text for details.

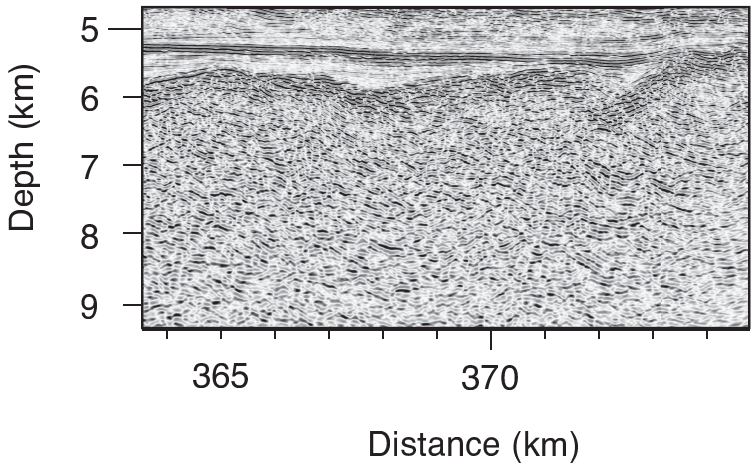

Figure 3.22: Close-up of the basement morphology of the initial oceanic crust of Line 85-3 (depth section).

to trace the small normal faults from basement down through the crust and into the mantle. The deep bright reflections may represent serpentinization fronts. The transition for ductile deformation to normal faulting is not sharp but rather a zone with a muted basement morphology and deep landward and seaward dipping reflections. These deep reflections may also be serpentinization fronts. However, the pathway for water penetration is not clear. The observations are not conclusive regarding the nature of the ridge feature. The observations best support an interpretation of continental crust possibly intruded by serpentinized mantle.

3.2.5 Acknowledgements

I would like to thank Nikola Nikic and Marjan Krpan for advice and workflows to help me understand how the LIFT method works and develop my own routines.

References

Bullock, A. D., and T. A. Minshull (2005), From continental extension to seafloor spreading: crustal structure of the Goban Spur rifted margin, southwest of the UK, *Geophysical Journal International*, *163*(2), 527–546, doi: 10.1111/j.1365-246X.2005.02726.x.

Cannat, M., D. Sauter, V. Mendel, E. Ruellan, K. Okino, J. Escartin, V. Combier, and M. Baala (2006), Modes of seafloor generation at a melt-poor ultraslow-spreading ridge, *Geology*, *34*(7), 605, doi: 10.1130/G22486.1.

Choo, J., J. Downton, and J. Dewar (2004), Lift: A new and practical approach to noise and multiple attenuation, *first break*, *22*, 39–44.

Christensen, N. I. (1996), Poisson's ratio and crustal seismology, *Journal of Geophysical Research*, *101*(B2), 3139, doi: 10.1029/95JB03446.

de Graciansky, P., C. Poag, R. Cinningham, P. Loubere, D. Masson, J. Mazzullo, L. Montadert, C. Müller, K. Otsuka, L. Reynolds, et al. (1985), The Goban Spur transect: Geologic evolution of a sediment-starved passive continental margin, *Geological Society of America Bulletin*, *96*(1), 58–76.

Dean, S., T. Minshull, R. Whitmarsh, and K. Louden (2000), Deep structure of the ocean-continent transition in the southern Iberia Abyssal Plain from seismic refraction profiles: The IAM-9 transect at 40°20'N, *Journal of Geophysical Research*, *105*(B3), 5859–5885.

Delescluse, M., and N. Chamot-Rooke (2008), Serpentinization pulse in the actively deforming Central Indian Basin, *Earth and Planetary Science Letters*, *276*(1-2), 140–151, doi: 10.1016/j.epsl.2008.09.017.

Gerlings, J., K. E. Louden, and H. R. Jackson (2011), Crustal structure of the Flemish Cap Continental Margin (eastern Canada): an analysis of a seismic refraction profile, *Geophysical Journal International*, *185*(1), 30–48, doi: 10.1111/j.1365-246X.2011.04931.x.

Gerlings, J., K. E. Louden, T. A. Minshull, and M. R. Nedimović (2012), Flemish Cap-Goban Spur conjugate margins: New evidence of asymmetry, *Geology*, *40*(12), 1107–1110, doi: 10.1130/G33263.1.

Horsefield, S., K. Whitmarsh, R. White, and J. Sibuet (1994), Crustal structure of the Goban Spur rifted continental margin, NE Atlantic, *Geophysical Journal International*, *119*(1), 1–19.

Huismans, R., and C. Beaumont (2011), Depth-dependent extension, two-stage breakup and cratonic underplating at rifted margins, *Nature*, *473*(7345), 74–8, doi: 10.1038/nature09988.

Jagoutz, O., O. Müntener, G. Manatschal, D. Rubatto, G. Péron-Pinvidic, B. D. Turrin, and I. M. Villa (2007), The rift-to-drift transition in the North Atlantic: A stuttering start of the MORB machine?, *Geology*, *35*(12), 1087, doi: 10.1130/G23613A.1.

Keen, C., and B. de Voogd (1988), The continent-ocean boundary at the rifted margin off eastern Canada: new results from deep seismic reflection studies, *Tectonics*, *7*(1), 107–124.

Keen, C., C. Peddy, B. de Voogd, and D. Matthews (1989), Conjugate margins of canada and europe: Results from deep reflection profiling, *Geology*, *17*(2), 173–176.

Leroy, S., F. Lucazeau, E. D'Acremont, L. Watremez, J. Autin, S. Rouzo, N. Bellahsen, C. Tiberi, C. Ebinger, M.-O. Beslier, J. Perrot, P. Razin, F. Rolandone, H. Sloan, G. Stuart, A. Al Lazki, K. Al-Toubi, F. Bache, A. Bonneville, B. Goutorbe, P. Huchon, P. Unternehr, and K. Khanbari (2010), Contrasted styles of rifting in the eastern Gulf of Aden: A combined wide-angle, multichannel seismic, and heat flow survey, *Geochemistry Geophysics Geosystems*, *11*(7), Q07,004, doi: 10.1029/2009GC002963.

Louden, K., and D. Chian (1999), The deep structure of non–volcanic rifted continental margins, *Philosophical Transactions A*, *357*(1753), 767.

Maillard, A., J. Malod, E. Thiébot, F. Klingelhoefer, and J.-P. Réhault (2006), Imaging a lithospheric detachment at the continentocean crustal transition off Morocco, *Earth and Planetary Science Letters*, *241*(3-4), 686–698, doi: 10.1016/j.epsl.2005.11.013.

Miller, D., and N. Christensen (1997), Seismic velocities of lower crustal and upper mantle rocks from the slow-spreading Mid-Atlantic Ridge, south of the Kane Transform Zone (MARK), in *Proceedings of the Ocean Drilling Program. Scientific results*, vol. 153, pp. 437–454, Ocean Drilling Program.

Ogg, J., and A. Smith (2004), The geomagnetic polarity time scale, in *A Geologic Time Scale 2004*, edited by O. J. Gradstein, F.M. and A. Smith, pp. 63–86, Cambridge University Press.

Party, S. S. (2004), Leg 210 summary, in *Proceedings of the Ocean Drilling Program, Initial Reports*, vol. 210, pp. 1–78.

Party, S. S. (2007), Leg 210 summary, in *Proceedings of the Ocean Drilling Program, Initial Reports*, vol. 210, pp. 1–56.

Peddy, C., B. Pinet, D. Masson, R. Scrutton, J. Sibuet, M. Warner, J. Lefort, I. Shroeder, et al. (1989), Crustal structure of the Goban Spur continental margin, Northeast Atlantic, from deep seismic reflection profiling, *Journal of the Geological Society*, *146*(3), 427–437.

Pérez-Gussinyé, M., and T. Reston (2001), Rheological evolution during extension at nonvolcanic rifted margins-onset of serpentinization and development of detachments leading to continental breakup, *Journal of Geophysical Research*, *106*(B3), 3961–3975.

Reston, T. (2009), The structure, evolution and symmetry of the magma-poor rifted margins of the North and Central Atlantic: A synthesis, *Tectonophysics*, *468*(1-4), 6–27, doi: 10.1016/j.tecto.2008.09.002.

Shillington, D. J., W. S. Holbrook, H. J. a. Van Avendonk, B. E. Tucholke, J. R. Hopper, K. E. Louden, H. C. Larsen, and G. T. Nunes (2006), Evidence for asymmetric nonvolcanic rifting and slow incipient oceanic accretion from seismic reflection data on the Newfoundland margin, *Journal of Geophysical Research*, *111*(B9), B09,402, doi: 10.1029/2005JB003981.

Srivastava, S., J. Verhoef, and R. Macnab (1988), Results from a detailed aeromagnetic survey across the northeast Newfoundland margin, Part I: spreading anomalies and relationship between magnetic anomalies and the ocean-continent boundary, *Marine and petroleum geology*, *5*(4), 306–323.

Tucholke, B., and G. Mountain (1979), Seismic stratigraphy, lithostratigraphy and paleosedimentation patterns in the North American Basin, in *Deep Drilling Results in the Atlantic Ocean: Continental Margins and Paleoenvironment, Maurice Ewing Ser., vol. 3*, edited by M. Talwani, W. Hay, and W. B. F. Ryan, pp. 58–86, American Geophysical Union. Washington, D. C.

Tucholke, B., J. Austin, and E. Uchupi (1989), Crustal structure and rift-drift evolution of the newfoundland basin, *AAPG Memoir*, *46*, 247–263.

Yilmaz, Ö., and S. M. Doherty (1987), Seismic data processing.

Chapter 4

Along-Strike Variations

The non-volcanic Iberia-Newfoundland conjugate margin pair has been the most researched passive margin pair and is often used as a reference for other magma-poor margins. Furthermore, recent geodynamical models based on this margin pair (e.g. *Huismans and Beaumont*, 2011; *Reston*, 2009; *Lavier and Manatschal*, 2006), focused on the large-scale variations across the margin, emphasise the existence of a broad zone of exposed serpentinzed mantle. Most importantly, the margins are almost exclusively evaluated two-dimensionally and often do not account for small-scale variations along a margin. Although the Flemish Cap-Goban Spur conjugate margin pair does initially appear as a simple 2-D problem, evaluation of the along-strike variations suggests otherwise. The following brief overview of the rifting phases also suggests a more complex story. Rifting between the Iberia and Newfoundland margin began in the Late Triassic-Early Jurassic (e.g. *Tucholke et al.*, 1989). Some rifting may have occurred in the Orphan Basin at this time (*Sibuet et al.*, 2007b). A second phase of rifting affected Orphan Basin in Late Jurassic-Early Cretaceous with a NW-SE rifting direction (*Lundin and Dore*, 2011; *Sibuet et al.*, 2007b). In this phase, Flemish Cap was separated from Orphan Knoll, another continental block. The final rifting phase involved a more E-W rifting direction and ended in separation of the NE Flemish Cap from Irish margins in Late Cretaceous (*de Graciansky et al.*, 1985). Flemish Cap has been suggested to be a micro-plate *Hopper et al.* (2007); *Sibuet et al.* (2007b) and *Sibuet et al.* (2007b) hypothesized that this micro-plate rotated clockwise during the formation of Orphan Basin.

The goal of this chapter is to examine the potential for identifying and describing three-dimensionality in the rifting style of the Flemish Cap-Goban Spur margin pair using the available MCS and wide-angle data. I focus on the transition zone of the NE Flemish Cap margin (Fig. 4.1), which has the greatest MCS and wide-angle data density, including improved images of profiles 85-3 and 87-4 from Chapter 3.

The new prestack migrated image of Line 87-4 displays a significantly different rifting style than that of Line 85-3. In the context providing these new images, I re-evaluate the extension and nature of the transition zone on the Erable Lines (E43, E44, E46, E48, E49, E50, E51, E52) (*Welford et al.*, 2010a), which are situated between the lines 85-3 and 87-4. The results of the wide-angle data, the reprocessed Lines 85-3 and 87-4, and as gravity data were used in this re-evaluation.

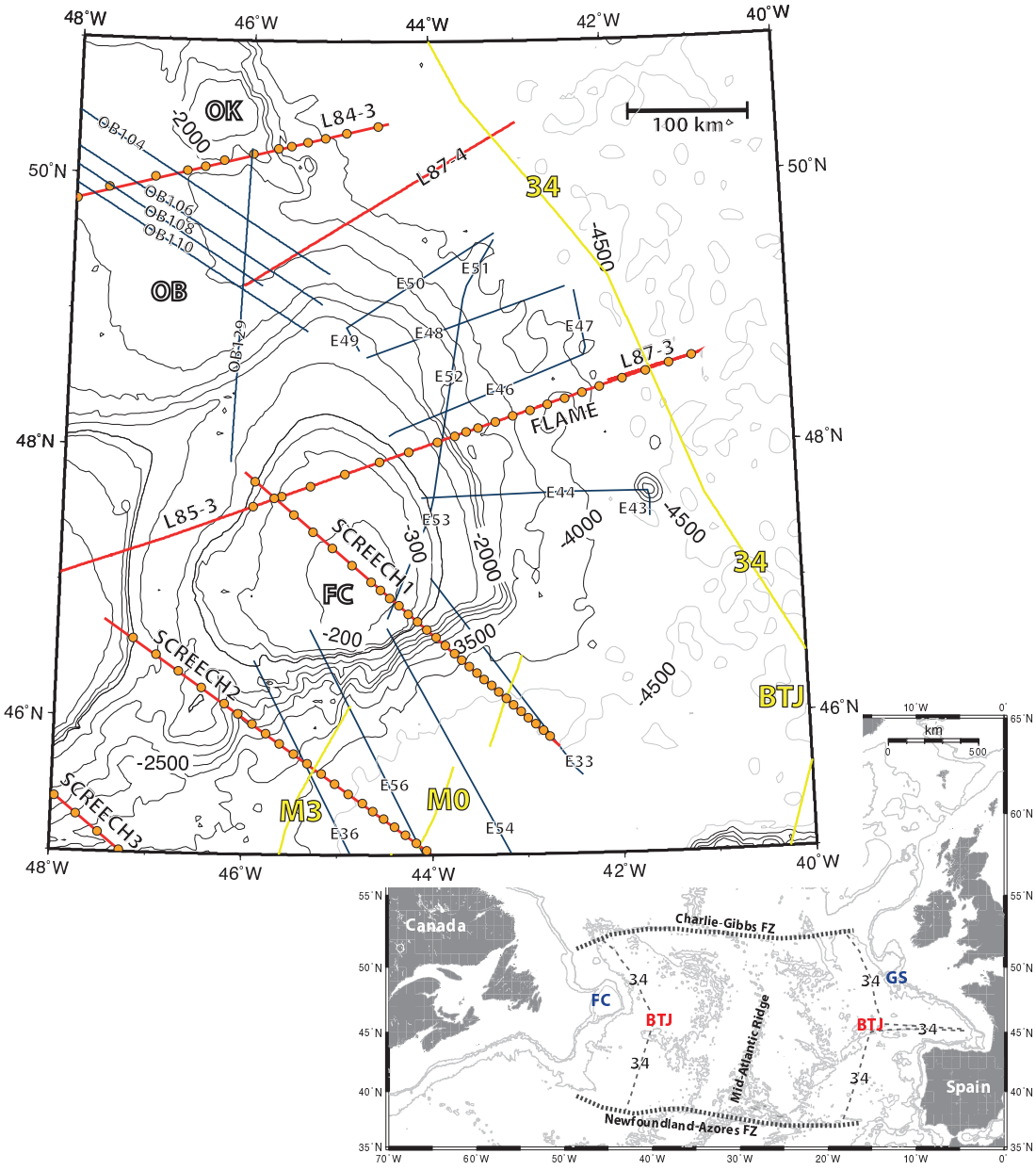

Figure 4.1: (Top) Location map of Flemish Cap with bathymetry (grey and black contours). Red lines represent seismic lines of the Lithoprobe project. Blue lines represent seismic lines from GSI (OB) and the Erable project (E). Yellow lines represent the magnetic anomalies M3, M0 and 34. Orange dots represent ocean bottom seismometers (OBS). (Bottom) Map of the North Atlantic. Thin dashed lines indicated magnetic anomaly 34. Thick dashed lines indicate the Charlie-Gibbs and Newfoundland-Azores fracture zones. The Biscay Triple Junction is indicated with red text. Abbreviations are FC: Flemish Cap; OB: Orphan Basin; OK: Orphan Knoll; GS: Goban Spur; BTJ: Biscay Triple Junction; FZ: Fracture zone.

4.1 Revised Line 85-3

In Chapter 3.2.3, I showed that in the depth migration of Line 85-3, the dipping reflections lie within the thinned continental crust at the landward end of the transition zone and not in the mantle as could be interpreted from the time migration (Fig. 3.19, distance 285-310 km; depth 8-13 km). If these reflections are located in the lower crust, it means that they could no longer represent serpentinization fronts. This part of the P-wave velocity model was not very well constrained (see Chapter 2). Hence, I have tested an alternative model where I have moved Moho up such that the dipping reflections should be located within the mantle (Fig. 4.2b; blue dashed line represent the old model). The velocities were lowered to 7.6-7.7 km s^{-1} from 7.7-7.9 km s^{-1} to keep a good fit between observed and calculated arrival times. The ocean bottom seismometers (OBS 8-14) affected by moving up the boundary, had with the previous model a traveltime residual of 77 ms and normalized χ^2 of 0.601 for 331 observations (picks) for the P-phases of PZ (layer of partially serpentinized mantle). With the alternative model the traveltime residual changed to 81 ms and normalized χ^2 of 0.665 for 331 observations.

If we include all the phases for OBS 8-14, the traveltime residual of the previous model is 98 ms and the normalized χ^2 is 0.847 for 5644 observations. For the alternative model, the traveltime residual is now 98 ms and the normalized χ^2 is 0.878 for 5007 observations.

A new gravity model was obtained as before by conversion of the P-wave velocities to densities using the empirical relationship of *Ludwig et al.* (1970). Fig. 4.2a shows the gravity fit between observed satellite gravity data along the line with both the calculated gravity of the previous P-wave velocity model of Chapter 2, as well as the re-evaluated model. The revised model shows increased gravity (up to ∼8 mGal) at distance 270-320 km. The peak of the calculated gravity high derived from the FLAME velocity model has also shifted seaward from distance 270 km to 290 km and is now displaced from the observed gravity peak. This might be explained by the presence of 3-D structure. Fig. 4.3 shows a map of the gravity anomalies at Flemish Cap. The gravity anomalies are derived from *Sandwell and Smith* (1997) (version 15.1) and filtered to remove wavelengths (λ) >80km, which allows us to observe the oceanic fabric better (*M. Delescluse*, personal communication, 2012). The gravity is

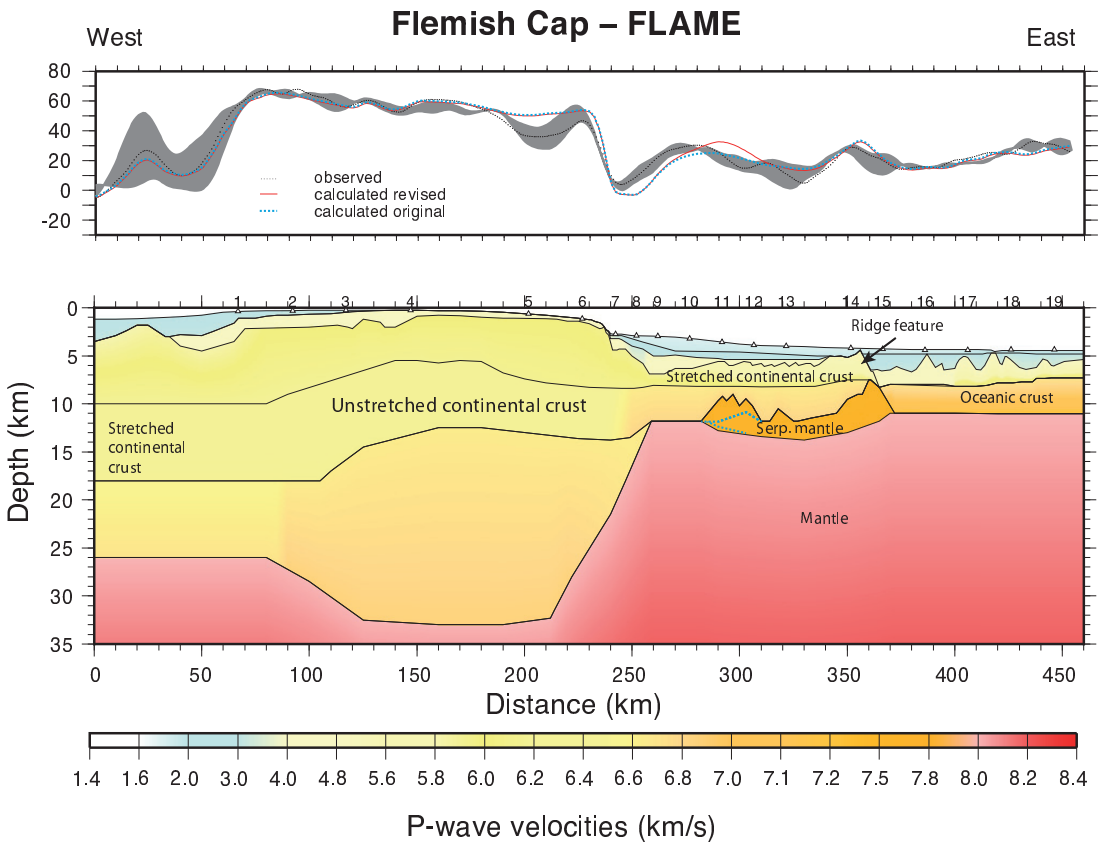

Figure 4.2: Revised P-wave velocity model (Bottom). Blue dashed line indicated the boundaries of the original model of *Gerlings et al.* (2011). Triangles represent ocean bottom seismometers. Top: Observed satellite gravity plotted together with calculated gravity from both the original velocity model (blues dashed) and the gravity of the revised velocity model (red). Grey shaded area represents the observed gravity 10 km of each side of the line.

clearly not continues aling-strike at this section of the FLAME line. The gravity high associated with the serpentinized mantle is a three-dimensional feature that shrinks north of the profile, and a small high is observed to the northeast. This might explain the seaward shift of the gravity high in the revised model. However, in order to resolve the details of this structure, we need additional crossing refraction profiles.

Another feature of the gravity map worth noticing is the gravity high associated with the ridge feature on Line 85-3 (Fig. 4.3; dashed black shape on the FLAME line). This high is followed north of the line, although the gravity anomaly is discontinuous and reduces in amplitude along-strike with the margin. The strongest gravity highs along this trend are circled (dashed lines) on the gravity map (Fig. 4.3) and may represent areas of serpentinized diapirism or become exhumed.

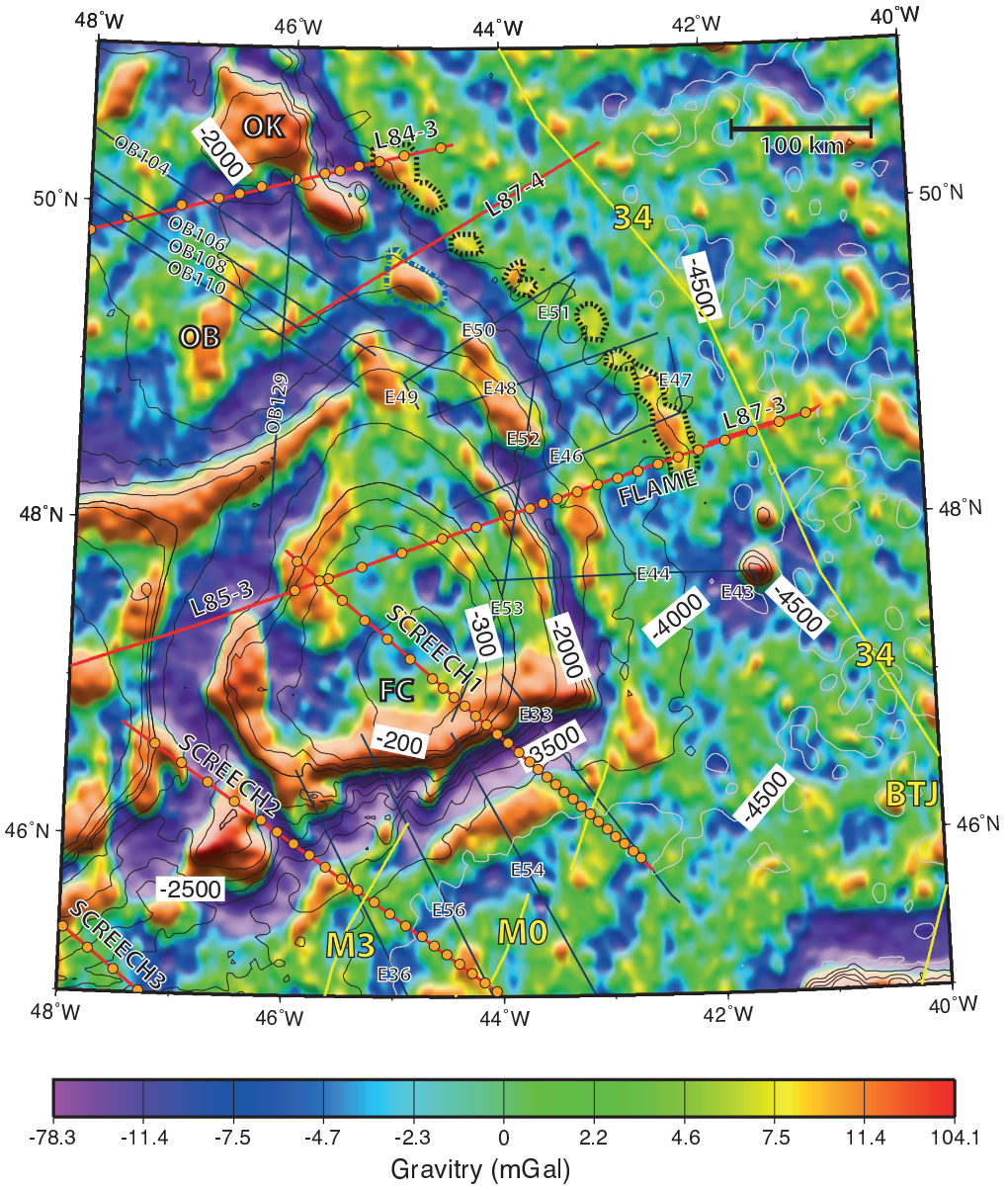

Figure 4.3: Map of gravity anomalies at Flemish Cap with bathymetry (grey and black contours). Gravity anomalies are from *Sandwell and Smith* (1997) but filtered to keep wavelengths (λ) >80 km. Red lines represent seismic lines of the Lithoprobe project. Blue lines represent seismic lines from GSI (OB) and the Erable project (E). Yellow lines represent the magnetic anomalies M3, M0 and 34. Orange dots represent ocean bottom seismometers (OBS). Possibly exposed mantle (ridge features) is encircled in black dashed lines and a 3D rifted continental block on line 87-4 is encircled in a dashed blue line (see text for discussion). Abbreviations are FC: Flemish Cap; OB: Orphan Basin; OK: Orphan Knoll; BTJ: Biscay Triple Junction.

4.2 Line 87-4

I have reprocessed the raw data of line 87-4 following the processing steps outlined for Line 85-3 in Table 3.2 with the exception of applying a prestack Kirchhoff time migration instead of a prestack Kirchhoff depth migration (see details in Appendix E). Unfortunately some of the original field data have been lost, resulting in three data gaps (Fig. 4.4a). The line is located north of Line 85-3 between Orphan Knoll and Flemish Cap (Fig. 4.1). The profile displays very different features from Line 85-3, implying that the rifting style along Line 87-4 is also different than that of Line 85-3.

The landward-most part of Line 87-4 (CDP 11500-20778) displays a muted basement morphology, with strong semi-horizontal reflections beneath basement and some landward-dipping reflections. A muted basement morphology has previously been connected with exhumed mantle (e.g. *Louden and Chian*, 1999; *Bullock and Minshull*, 2005; *Welford et al.*, 2010a). This section of the line is located in what has been proposed to be a rift basin formed in a roughly NW-SE direction and underlain by serpentinized mantle (*Lundin and Dore*, 2011). However, recent refraction models (*Watremez et al.*, 2012) suggest little or no serpentinized mantle in this region. This lack of mantle serpentinization is also consistent with the earlier model of *Chian et al.* (2001) along Line 84-3 (Fig. 4.7), which shows that Orphan Basin is underlain by thinned continental crust. Lines 87-4 and 84-3 are crossed by several Geophysical Service Incorporated (GSI) lines (OB104, OB106, OB108, OB110, OB129, OB502; Figs. 4.1, 4.5-4.6). All the lines are positioned at a small angle to the rifting direction except for OB129, which is at an angle of 45 degree clockwise to the other GSI lines. The profiles were collected in the Orphan Basin in 2000 by GSI and processed in 2001 by Veritas Geoservice Ltd. Figs. 4.5-4.6 are scans of the MCS profiles we obtained from the Canada-Newfoundland and Labrador Offshore Petroleum Board. Figs. 4.3-4.6 show a system of fault blocks and half grabens typical of a rift basin. Even OB129, which crosses the rifting direction at a different, larger angle, displays these large fault blocks (Figs. 4.3 and 4.6). The rift basin extends as far seaward as CDP 15500 on Line 87-4. The section of Line 87-4 between CDP 15500-11500 appears to be a continental block (Fig. 4.4). The semi-horizontal reflections are cut by down-going faults indicating rifting in different directions (3D rifting). A local 3D

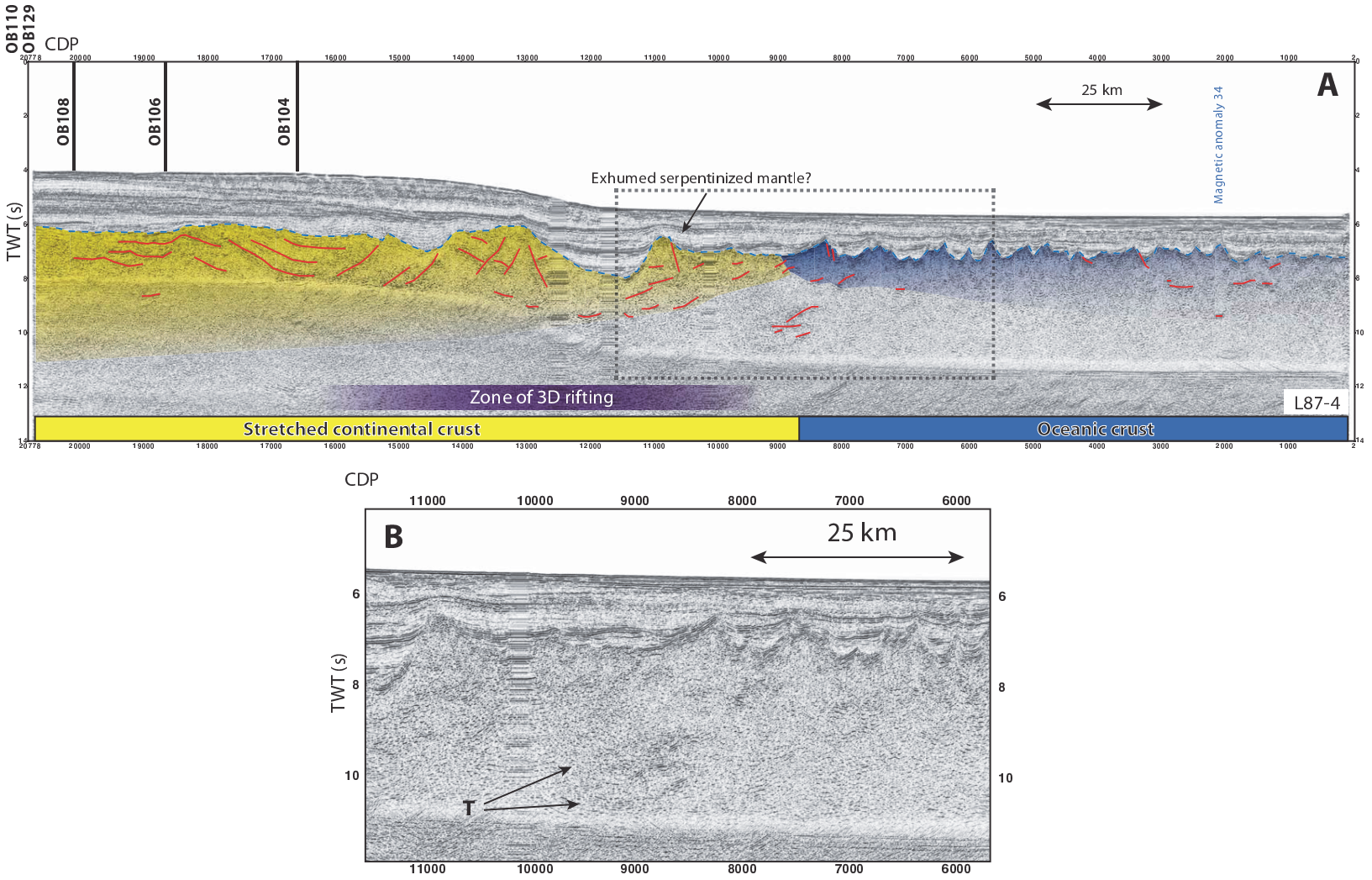

Figure 4.4: Prestack time migrated seismic profile of Line 87-4. Top: Interpretation of the crustal domains. Bar represent the interpretation and extent of crustal domains. Bottom: Close-up of strong deep reflections (T) below basement. See text for interpretations.

gravity high is created by this block (Fig. 4.3). I suggest that this block has been subjected to rifting in more than one direction and that the resulting gravity high represents a transition from the NW-SE rifting in Orphan Basin to the E-W rifting along the seaward part of Line 87-4. The gravity high appears to correlate with a series of 3D highs northward toward Orphan Knoll (Fig. 4.3).

The nature of the basement morphology between CDP 11500-8500 does not appear significantly different from the basement farther landward. Following the gravity high at the ridge feature from Line 85-3 to Line 87-4 (Fig. 4.3; dashed black lines), we can observe a gravity high on the southern edge of Line 87-4 at CDP 10500-11500 (Fig. 4.4a). The basement morphology of the seismic profile in this section (Fig. 4.4a) does not display a ridge-like feature. However, a velocity model developed along Line 84-3 (*Chian et al.*, 2001) (Fig. 4.7a) just north of Line 87-4, may display a basement morphology of serpentinized mantle. The velocity model shows stretched continental crust thinning seaward of Orphan Knoll to less 2 km. The very thin crust is underlain by partially serpentinized mantle or an alternative interpreatation is that mantle has been exhumed. In a close-up of the seismic section (Fig. 4.7b) we observe a dome-like feature similar to a one observed on SCREECH Line 3, interpreted by *Deemer et al.* (2009) as exhumed serpentinized mantle (Fig. 4.7b). This section coincides with a gravity high (Fig. 4.3; encircled by black dashed lines) to that observed for the ridge feature of Line 85-3. However, no such dome-like feature is clearly imaged on Line 87-4. Hence, I have interpreted the nature of the crust in the entire section between CDP 8500-11500 as continental.

The basement morphology has a high-relief character between CDP 2-7000, similar to oceanic crust onLine 87-3 (the extension of Line 85-3 see Fig. 3.3) (*Gerlings et al.*, 2012). Hence I interpret this section as oceanic. Beneath the basement at CDP 8000-9000 and 9-10 s depth there are strong reflections (T; Fig. 4.4b). These reflections may be an expression in the mantle of the change in rifting direction.

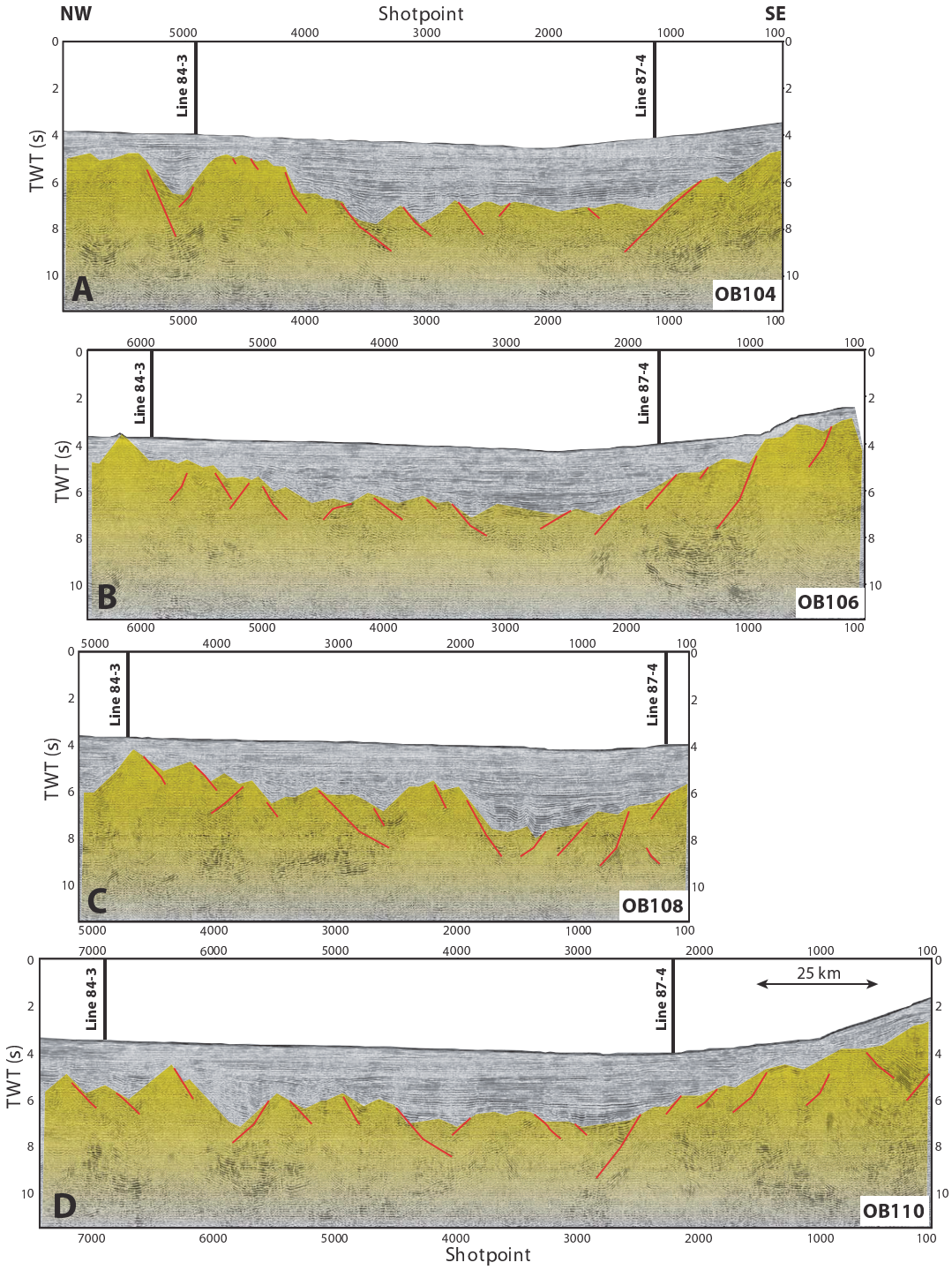

Figure 4.5: Seismic profiles of GSI Line OB104, OB106, OB108, and OB110 across a rift basin in Orphan Basin. Red lines indicate major faults and strong reflections. Black horizontal lines to basement represent the intersection with lines 87-4 and 84-3.

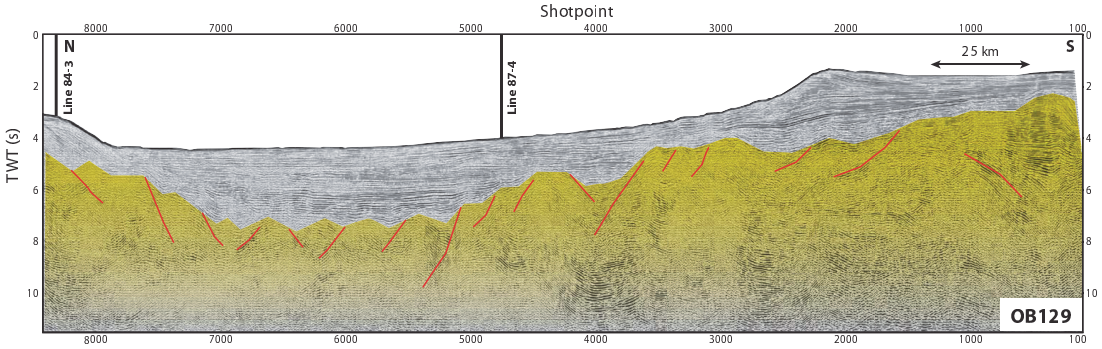

Figure 4.6: Seismic profile of GSI Line OB129 across a rift basin in Orphan Basin. Red lines indicate major faults and strong reflections. Black horizontal lines to basement represent the intersection with lines 87-4 and 84-3.

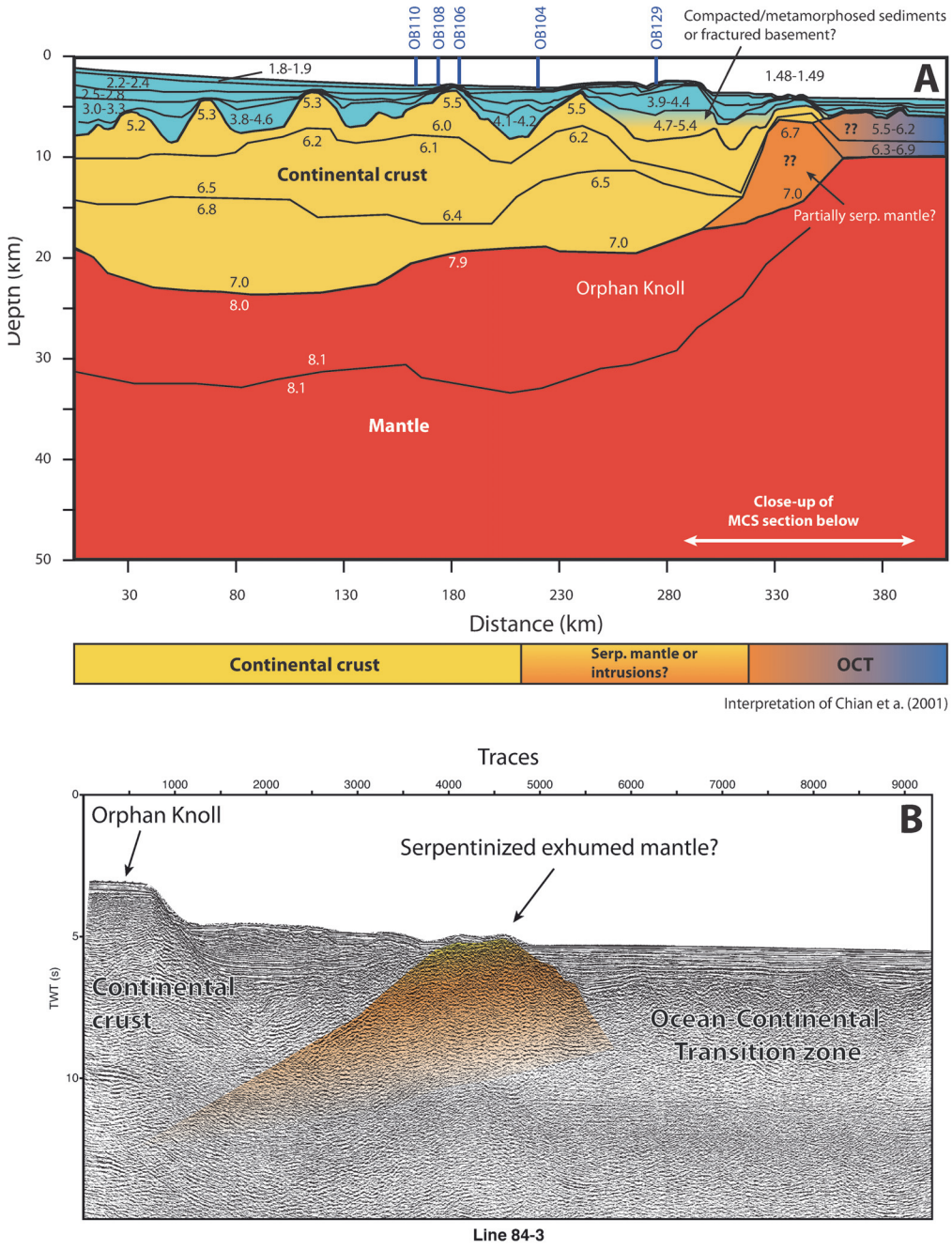

Figure 4.7: (Top) Velocity model of *Chian et al.* (2001). The profile is coincident with Line 84-3. Black horizontal lines represent layer boundaries. Black vertical lines to seafloor represent intersection with lines OB104, OB106, OB108, OB110 and OB129. Numbers represent P-wave velocities (km s^{-1}). Bar represents *Chian et al.* (2001) interpretation of the crustal domains along the profile. (Bottom) Close-up of the dome-like feature of potentially exhumed serpentinized mantle on the seaward-most end of seismic profile Line 84-3.

4.3 Crustal Domains of Erable Lines

The difference between Line 85-3 and Line 87-4 shows that the rifting style must vary along-strike to the margin. To detail such along-strike variations, I have reinterpreted the multichannel seismic reflection (MCS) profiles (Erable lines) located between Lines 85-3 and 87-4 (Fig. 4.1). The 2D MCS Erable profiles (*Welford et al.*, 2010b,a) were collected in 1992 across the Newfoundland Basin and across Flemish Cap as a joint project between the Atlantic Geoscience Centre (AGC) and the Institut Français de Recherche pour l'Exploitation de la Mer (Ifremer).

The Erable lines all cross the unstretched continental crust of Flemish Cap. Deep reflections at 9-12 s in the lower crust are imaged on all the Erable profiles (Figs. 4.8-4.10). These reflections may represent Moho. As on Line 85-3, the lines E44, E50, E52 display multiple (layered) reflections, supporting the interpretation from previous work (section 3.2.2) that Moho is a complex transitional boundary between lower continental crust and mantle in this region.

The set of lines along the margin is subdivided into a northern and southern part. The northern Erable Lines E48, E49-50 and E51-52 display similar crustal features, which are correlated northward to Line 87-4. Erable line E46, on the other hand, is strikingly similar to Line 85-3.

4.3.1 Southern Lines

Two Erable lines E44 and E46 (Fig. 4.8) are located on either side of Line 85-3. Neither E44 nore E46 have significant normal faulting landward of the shelf break. A large fault block similar to that imaged on 85-3 is not imaged on line E46 but a few horizontal intra-crustal reflections are imaged below the muted basement in the thin continental crust (CDP 4000-9000). These reflections are not as strong or as frequent as on Line 85-3 because the S/N ratio may be too low on the Erable profiles that was analyzed only to migrated stack sections. Nevertheless, the imaged crustal reflections may indicate that the area crossed by line E46 also experienced ductile deformation in the crust. The multiples make it difficult to identify potentially similar horizontal reflections on Line E44. Line E44 images one large fault block, cut by minor faults. This fault block appears different from the large fault block on Line 85-3.

On lines E44 (CDP 5000-8000) and E46 (CDP 9000-12000), normal faults imaged in the basement are similar to those on 85-3, but there are no strong deeper dipping reflections below in the crust. A ridge feature is imaged on E46 at CDP 12000-14000. As on Line 85-3, basement is shallower and the feature has distinct peaks. I suggest that this ridge feature is similar in nature to the ridge feature of Line 85-3, continental crust possibly intruded by serpentinized mantle, and that the ridge feature is the seaward limit of the thin continental crust on E46. Seaward of the ridge feature, initial oceanic crust formed. No such ridge feature is imaged on E43-44, but rather an isolated seamount is imaged on the seismic section (CDP 1000-3000). Note that as indicated by *Welford et al.* (2010a), this seamount was located close to the Biscay Triple Junction (BTJ) during its formation(see Figs. 4.2-4.3).

4.3.2 Northern Lines

Features that suggest a more complex deformation of the crust are observed on lines E48, E49-50 and E51-52. Line E48 barely crosses unstretched continental crust (Figs. 4.1, 4.9a). Although the multiples cover much of the signal in the lower crust, several weak horizontal reflections indicate that the thinning of the crust is more gradual (Fig. 4.9a). At approx. CDP 27000 on E48 the basement steps downward and increases in depth. A similar increase in basement depth is observed on E50 (CDP 8000) and E51 (CDP 7000). Another downward step of the basement is observed farther landward on E50 (CDP 4000), E51 (CDP 13000) and possibly on E48 (CDP 32500). The basement morphology of E48 between CDP 23000-32500 is also more complex than that of Line 85-3, E44 and E46. Both normal and reverse faults indicate that thin continental crust has undergone more than simple extension, probably compression and/or shearing. Similar faulting is observed on E50 (Fig. 4.9b; CDP 4000-8000) and E51 (Fig. 4.10; CDP 7000-13000). I propose that these sections of the crust were affected by both the NW-SE rifting of Orphan Basin, as well as the more E-W orientated rifting of the NE Flemish Cap margin, and that basement morphology is an expression of 3D rifting. These sections of the profiles are also coincident with the basement high correlated northward to the basement block at Line 87-4 and continuing northward to Orphan Knoll. I suggest that these gravity highs represent broken crustal blocks that have undergone poly-phase rifting, with rifting not only

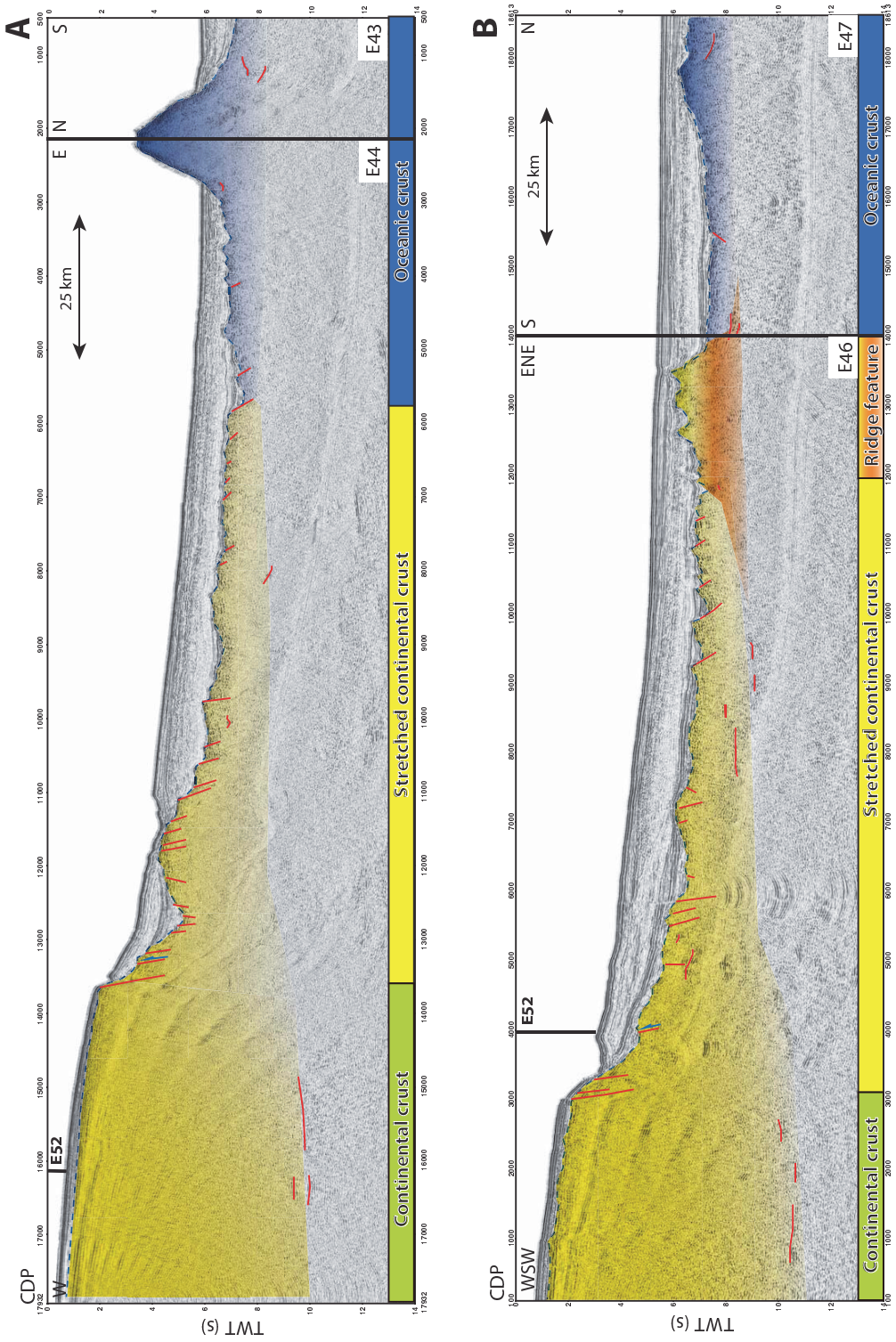

Figure 4.8: Time migrated seismic profiles of Erable Line E43-44 (Top) and E46-47 (Bottom) with interpretation of the crustal domains. Bar, below the seismic sections, represents the interpretation and extent of crustal domains. Red lines represent faults and strong reflections. Black vertical line to seafloor represents intersection with line E52.

along Line 87-4 but also at an angle to the line.

The basement morphology of E48 at CDP 18000-22000 looks strikingly similar to the basement morphology of minor normal faults in the continental domain on Line 85-3, E44 and E46. The minor normal faults seem to connect to some deeper seaward dipping reflections in a similar manner as on Line 85-3. The deeper dipping reflections may represent serpentinization fronts. These kind of minor normal faults, similar to those of Line 85-3 E44 and E46, are not imaged on E49-50 or E51-52. Line E48 displays a different character of the basement at CDP 22000-23000 relative to the same area on surrounding lines. The basement has a dome-like feature similar to that on Line 84-3. The gravity high observed at the ridge feature on Line 85-3 is correlated northward to this feature, although the gravity anomaly is not as strong (Fig. 4.3). The gravity anomaly here is also weaker than at the dome-like feature of Line 84-3. With the possibility of partially serpentinized mantle underlying the continental crust seaward of this dome feature, the dome-like feature may represent exhumed serpentinized mantle. As mentioned in previous chapters, when the crust thins to roughly less than 10 km, it becomes brittle and faults and fractures form, which channel water downward, allowing serpentinizion of the mantle (*Pérez-Gussinyé and Reston*, 2001). Although it is not possible to confirm from the Erable profiles, the thin continental crust may be underlain in places by partially serpentinized mantle. The weak positive gravity anomalies (Fig. 4.3; green to yellow shading) suggest that this is likely. However, as shown by *Gerlings et al.* (2011) and *Van Avendonk et al.* (2006), thin continental crust is not necessarily underlain by serpentinized mantle.

It is only the seaward-most part of the E48 that displays the basement morphology of a high-relief slow-spreading oceanic crust. I base this observation on only the change in basement morphology. However, none of the Erable lines extend across magnetic anomaly 34, which makes it difficult to determine the exact location of initial oceanic crust. The basement at the seaward end of line E48 could also be of continental origin, or perhaps exhumed mantle. It is even more debatable whether the nature of the crust along E49-50 (CDP 11500-14331) and E51-52 (CDP 100-3000) is continental, oceanic, or exhumed mantle. The gravity map shows no gravity high on the seaward-most end of the profiles. This section of the profiles lies on the edge of the oceanic domain. Extending the oceanic domain farther landward will require

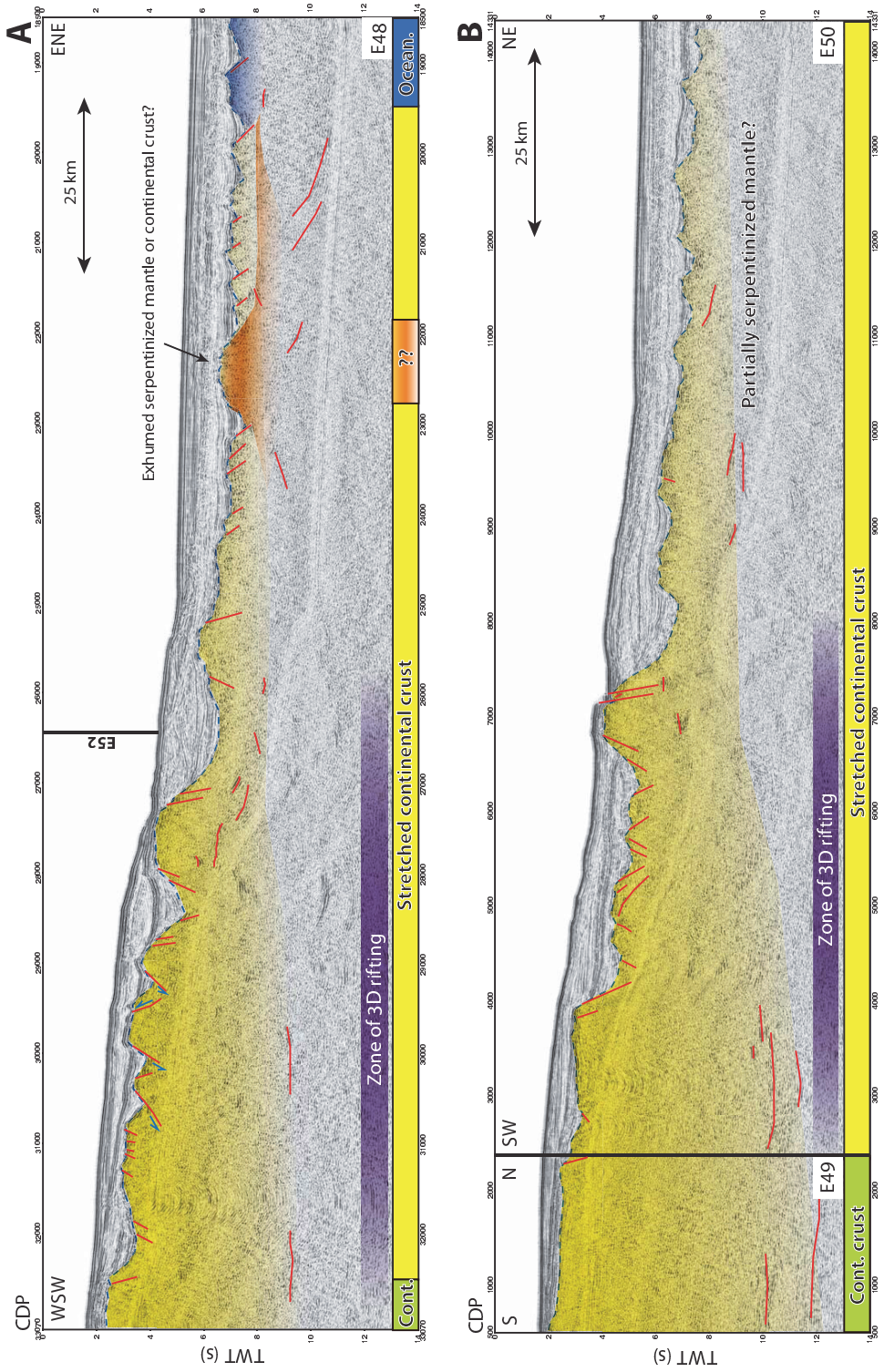

Figure 4.9: Time migrated seismic profiles of Erable Line E48 (Top) and E49-50 (Bottom) with interpretation of the crustal domains. Bar, below the seismic sections, represents the interpretation and extent of crustal domains. Purple bar represents extent of poly-phase (3D) rifting. Red lines represent faults and strong reflections. Black vertical line to seafloor represents intersection with line E52.

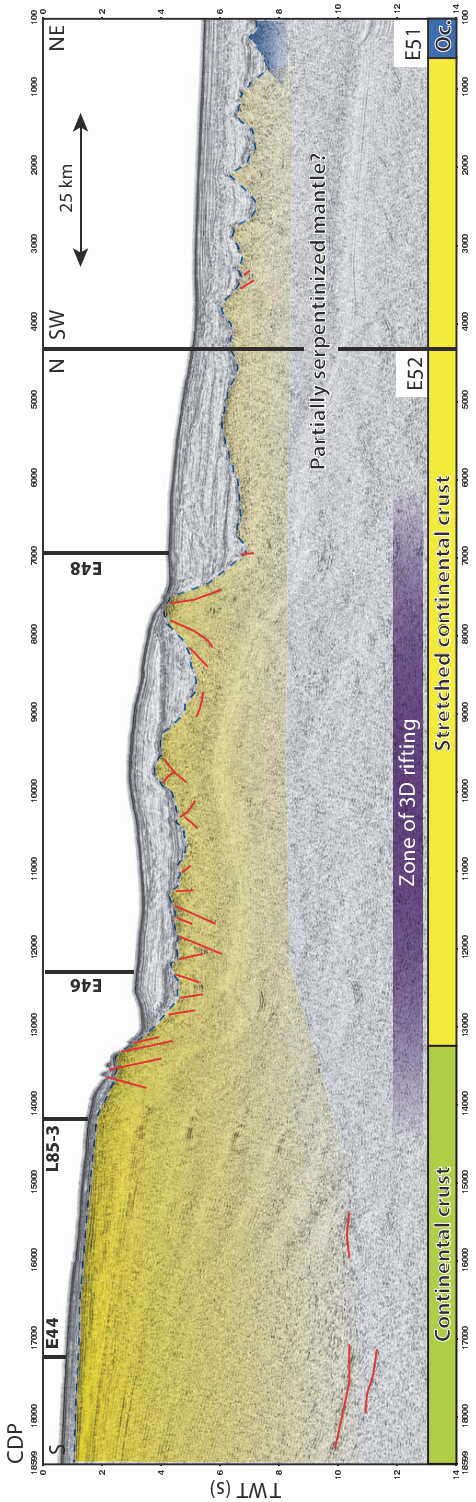

Figure 4.10: Time migrated seismic profile of Erable Line E51-52 with interpretation of the crustal domains. Bar, below the seismic sections, represents the interpretation and extent of crustal domains. Purple bar represents extent of poly-phase (3D) rifting. Red lines represent faults and strong reflections. Black vertical lines to seafloor represent intersection with lines E44, E46, E48 and 85-3.

some clearer evidence. Hence, I have left the composition of the crust as continental at the seaward end of line E50, and suggest that formation of oceanic crust initiated at the very seaward-most end of line E51.

4.4 Summary/Conclusions

A map of the crustal domains based on interpretation of the velocity models, reprocessed profiles of Line 85-3 and 87-4, and re-interpretation of the Erable lines is shown in Fig. 4.11. *Welford et al.* (2010a) have also interpreted Lines 85-3, 87-4 and the Erable lines. The main differences between the two interpretations are the extent of exhumed mantle and the zone of complex poly-phase (3D) rifting. My interpretation suggests that the margin was subjected to a small amount of mantle exhumation. *Welford et al.* (2010a) interpreted a continuous zone of exhumed mantle along the NE Flemish Cap margin, which broadens northward into a wide zone (min. 100 km) of exhumed serpentinized mantle on Line 87-4 in Orphan Basin. I have interpreted this section of the profile to be within the continental domain, with possibly a small dome-like feature of exhumed mantle at the very seaward end of the stretched continental crust. I also distinguish between a dome-like feature of exhumed mantle observed on the northern lines from a spiky peaked ridge feature of continental crust, potentially intruded by serpentinized mantle, on the southern lines. *Welford et al.* (2010a) observed features on the seismic profiles, e.g. a flower structure on the previously processed section of Line 85-3, which they used as evidence for three distinct shear zones. The flower structure is not visible in the reprocessed prestack depth migrated section. Instead, features indicating ductile deformation in the lower crust are now visible. I observe no clear evidence of shearing or major poly-phased rifting on the southern lines, whereas the northern lines display a zone of poly-phase (3D) rifting. This zone coincides with a gravity high and is correlated with the Line 87-4 structure, where a zone of poly-phase (3D) rifting is also observed. I can neither confirm nor reject the hypothesis of a clockwise rotation of Flemish Cap suggested by *Sibuet et al.* (2007b).

Some conclusion may be drawn:

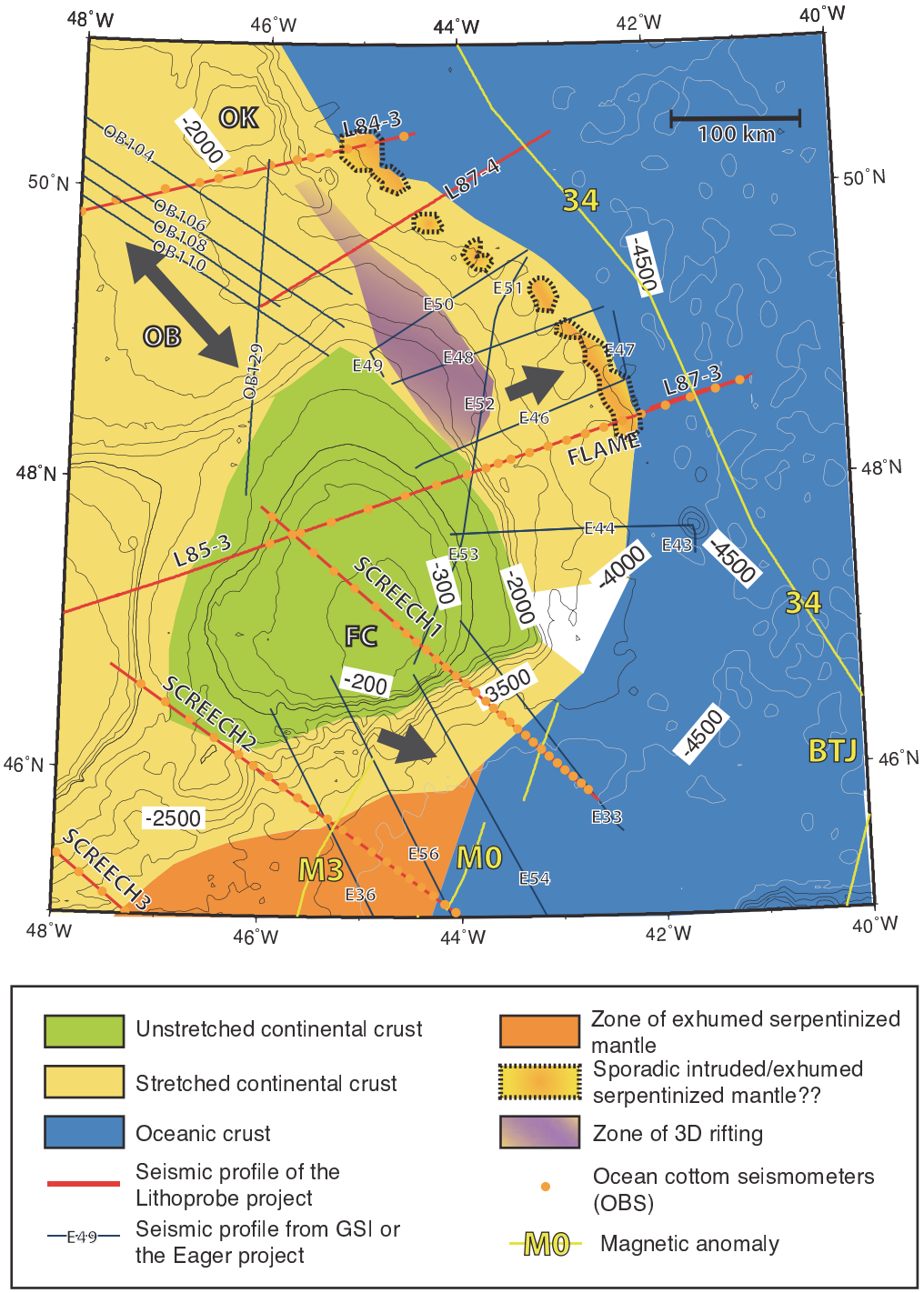

Figure 4.11: Map of the crustal domains of Flemish Cap with bathymetry (grey and black contours) based on the results of Chapter 2-4 and a re-evaluation of the Erable lines. Red lines represent seismic lines of the Lithoprobe project. Blue lines represent seismic lines from GSI (OB) and the Erable project (E). Yellow lines represent the magnetic anomalies M3, M0 and 34. Orange dots represent ocean bottom seismometers (OBS). Grey arrows indicate rifting directions. Abbreviations are FC: Flemish Cap; OB: Orphan Basin; OK: Orphan Knoll; BTJ: Biscay Triple Junction. See legend for nature of the crust.

1. Orphan Basin appears to be a rift basin and continental in nature.

2. A zone stretching from the south-eastern tip of Orphan Knoll to just southward of E48 has been subjected to poly-phase (3D) rifting. This zone coincides with a gravity high.

3. Line 85-3 and E46 only show evidence of 2D rifting. There is some evidence, strong reflections, indicating ductile deformation in the lower crust of the area crossed by lines 85-3 and E46.

4. The extent of partially serpentinized mantle underneath thin continental crust appears complex and three-dimensional.

5. Two types of features for exposed mantle are observed: i) a dome-like feature of exhumed mantle observed on the northern lines and ii) a peaked ridge feature of continental crust possibly intruded by serpentinized mantle on the southern lines.

The NE Flemish Cap margin displays lateral changes along the margin both in the style of rifting as well as mantle serpentinization. The next step in understanding the details of the processes and development of passive rifted non-volcanic margins is to focus on the 3D variations of the margins. Hence, both 3D profiles and 3D geodynamic models are needed to resolve smaller-scale features.

4.5 Acknowledgements:

Thank you to Matthias Delescluse for providing and filtering the gravity data.

References

Bullock, A. D., and T. A. Minshull (2005), From continental extension to seafloor spreading: crustal structure of the Goban Spur rifted margin, southwest of the UK, *Geophysical Journal International*, *163*(2), 527–546, doi: 10.1111/j.1365-246X.2005.02726.x.

Chian, D., I. Reid, and H. Jackson (2001), Crustal structure beneath orphan basin and implications for nonvolcanic continental rifting, *Journal of Geophysical Research*, *106*(B6), 10,923–10.

de Graciansky, P., C. Poag, R. Cinningham, P. Loubere, D. Masson, J. Mazzullo, L. Montadert, C. Müller, K. Otsuka, L. Reynolds, et al. (1985), The Goban Spur transect: Geologic evolution of a sediment-starved passive continental margin, *Geological Society of America Bulletin*, *96*(1), 58–76.

Deemer, S., J. Hall, K. Solvason, K. H. Lau, K. Louden, S. Srivastava, and J.-C. Sibuet (2009), Structure and development of the southeast Newfoundland continental passive margin: derived from SCREECH Transect 3, *Geophysical Journal International*, *178*(2), 1004–1020, doi: 10.1111/j.1365-246X.2009.04162.x.

Gerlings, J., K. E. Louden, and H. R. Jackson (2011), Crustal structure of the Flemish Cap Continental Margin (eastern Canada): an analysis of a seismic refraction profile, *Geophysical Journal International*, *185*(1), 30–48, doi: 10.1111/j.1365-246X.2011.04931.x.

Gerlings, J., K. E. Louden, T. A. Minshull, and M. R. Nedimović (2012), Flemish Cap-Goban Spur conjugate margins: New evidence of asymmetry, *Geology*, *40*(12), 1107–1110, doi: 10.1130/G33263.1.

Hopper, J. R., T. Funck, and B. E. Tucholke (2007), Structure of the Flemish Cap margin, Newfoundland: insights into mantle and crustal processes during continental breakup, *Geological Society, London, Special Publications*, *282*(1), 47–61, doi: 10.1144/SP282.3.

Huismans, R., and C. Beaumont (2011), Depth-dependent extension, two-stage breakup and cratonic underplating at rifted margins, *Nature*, *473*(7345), 74–8, doi: 10.1038/nature09988.

Lavier, L. L., and G. Manatschal (2006), A mechanism to thin the continental lithosphere at magma-poor margins., *Nature*, *440*(7082), 324–8, doi: 10.1038/nature04608.

Louden, K., and D. Chian (1999), The deep structure of non–volcanic rifted continental margins, *Philosophical Transactions A*, *357*(1753), 767.

Ludwig, W., J. Nafe, and C. Drake (1970), Seismic refraction, in *The Sea*, edited by A. Maxwell, pp. 53–84, Wiley-Interscience, New York.

Lundin, E. R., and a. G. Dore (2011), Hyperextension, serpentinization, and weakening: A new paradigm for rifted margin compressional deformation, *Geology*, *39*(4), 347–350, doi: 10.1130/G31499.1.

Pérez-Gussinyé, M., and T. Reston (2001), Rheological evolution during extension at nonvolcanic rifted margins-onset of serpentinization and development of detachments leading to continental breakup, *Journal of Geophysical Research*, *106*(B3), 3961–3975.

Reston, T. (2009), The structure, evolution and symmetry of the magma-poor rifted margins of the North and Central Atlantic: A synthesis, *Tectonophysics*, *468*(1-4), 6–27, doi: 10.1016/j.tecto.2008.09.002.

Sandwell, D. T., and W. H. F. Smith (1997), Marine gravity anomaly from Geosat and ERS 1 satellite altimetry, *Journal of Geophysical Research*, *102*(B5), 10,039, doi: 10.1029/96JB03223.

Sibuet, J.-C., S. P. Srivastava, M. Enachescu, and G. D. Karner (2007), Early Cretaceous motion of Flemish Cap with respect to North America: implications on the formation of Orphan Basin and SE Flemish Cap Galicia Bank conjugate margins, *Geological Society, London, Special Publications*, *282*(1), 63–76, doi: 10.1144/SP282.4.

Tucholke, B., J. Austin, and E. Uchupi (1989), Crustal structure and rift-drift evolution of the newfoundland basin, *AAPG Memoir*, *46*, 247–263.

Van Avendonk, H. J. A., W. S. Holbrook, G. T. Nunes, D. J. Shillington, B. E. Tucholke, K. E. Louden, H. C. Larsen, and J. R. Hopper (2006), Seismic velocity structure of the rifted margin of the eastern Grand Banks of Newfoundland, Canada, *Journal of Geophysical Research*, *111*(B11), B11,404, doi: 10.1029/2005JB004156.

Watremez, L., K. W. H. Lau, M. R. Nedimović, K. E. Louden, and G. D. Karner (2012), Orphan Basin crustal structure from tomographic inversion with dense receivers, in *3rd Conjugate Margins Conference, Dublin*.

Welford, J. K., J. Hall, J.-C. Sibuet, and S. P. Srivastava (2010a), Structure across the northeastern margin of Flemish Cap, offshore Newfoundland from Erable multichannel seismic reflection profiles: evidence for a transtensional rifting environment, *Geophysical Journal International*, *183*(2), 572–586, doi: 10.1111/j.1365-246X.2010.04779.x.

Welford, J. K., J. A. Smith, J. Hall, S. Deemer, S. P. Srivastava, and J.-C. Sibuet (2010b), Structure and rifting evolution of the northern Newfoundland Basin from Erable multichannel seismic reflection profiles across the southeastern margin of Flemish Cap, *Geophysical Journal International*, *180*(3), 976–998, doi: 10.1111/j.1365-246X.2009.04477.x.

Chapter 5

Conclusions and Suggestions for Future Work

5.1 Conclusions

In the previous chapters, I presented a P- and S-wave velocity model determined for the FLAME profile situated across the NE Flemish Cap margin (Chapter 2; (*Gerlings et al.*, 2011)). The results allowed me to determine the thickness, structure and nature of the crust and upper mantle along the FLAME Line. I also presented reprocessed and poststack Kirchhoff time migrated and prestack Kirchhoff depth migrated sections of Line 85-3 coincident with the FLAME Line. The results allowed me to address the rifting style of the Flemish Cap-Goban Spur conjugate margin pair (Chapter 3 Section 3.1; (*Gerlings et al.*, 2012)). The new information observed in the prestack depth migrated section 85-3 and the prestack time migrated image of line 87-4, both produced as part of this thesis work, have led to reinterpretation of the Erable lines and therefore a detailed look at the OCT of NE Flemish Cap (Chapter 3, Section 3.2). The combined information from all the examined profiles allowed me to address the along-strike variations of the NE Flemish Cap margin (Chapter 4). The following conclusions can be drawn:

5.1.1 Structure and Thinning of Initial Continental Crust

1. The continental crust beneath Flemish Cap is a 31-km-thick, 3-layer crust. The result is consistent with previous results of SCREECH Line 1, which is situated across the southeast segment of Flemish Cap (*Funck et al.*, 2003).

2. The thick continental crust along the FLAME profile thins rapidly in the N-E direction to 6-km-thick crust over a distance of only 40 km. In comparison, the SE Flemish Cap (*Funck et al.*, 2003) and Newfoundland (*Lau et al.*, 2006a; *Van Avendonk et al.*, 2006) margins thin from unstreched crust to about 6-km-thick

crust over a distance of ∼60 km and Goban Spur over a distance of ∼80 km (*Bullock and Minshull*, 2005; *Horsefield et al.*, 1994).

3. Strong semi-horizontal reflections are clearly imaged in the middle and lower crust of the landward part of the thin continental crust (distance 240-260 km), possibly indicating ductile deformation and depth-dependent stretching.

5.1.2 Nature of the Ocean-Continent Transition Zone

1. The nature of the crust in the OCT is predominantly of a continental composition. Poisson ratios of 0.27 in the upper crust and 0.28 lower crust were derived from P- and S-wave velocities. Together with P-wave velocities of 5.6 and 6.7 km s^{-1}, these indicate continental composition (*Christensen*, 1996). In comparison, Poisson's ratio of 0.28 and P-wave velocity of 4.5 km s^{-1} indicate basaltic composition, and Poisson's ratio of 0.36 and P-wave velocities of 5.8-7.6 km s^{-1} indicate serpentinized mantle. Before this study, it was speculated that, due to its muted basement morphology, the thin crust was instead exhumed serpentinized mantle similar to the OCT of the conjugate Goban Spur margin (e.g., *Louden and Chian*, 1999; *Bullock and Minshull*, 2005). The velocities of the FLAME Line show that to material in the transition zone is clearly not serpentinized mantle. A tongue of thin continental crust is also interpreted e.g., on the Newfoundland margin (SCREECH Line 2 and 3 *Van Avendonk et al.*, 2006; *Shillington et al.*, 2006; *Lau et al.*, 2006a,b). Although, the Poisson ratio of 0.28 could also indicate a crust of oceanic affinity, the P-wave velocities more typical of crust with a contiental affinity. However, the velocities alone cannot exclude a crust of oceanic affinity.

2. Better imaging of the MCS profile clearly shows tilted syn-rift sediment packages on the Flemish Cap margin (distances 285-340 km), which also supports the presence of thin continental crust in the OCT.

3. The results show that in order to determine the nature of the OCT, careful imaging of the basement morphology is necessary, with additional constraints from P- and S-wave velocities. Hence other margins, where subdued basement

relief has been used to infer zones of exhumed mantle, may need to be re-evaluated.

4. The OCTs of SE and NE Flemish Cap are very different. Whereas the FLAME Line on NE Flemish Cap displays a thin tongue of continental crust, thin crust of oceanic affinity is observed on SCREECH Line 1 (*Funck et al.*, 2003).

5. The thin continental crust is underlain by a layer with velocities between 7.5 to 7.9 km s^{-1}. I find it more likely that this layer represents partially serpentinized mantle, and not underplated igneous material as previously suggested by *Reid and Keen* (1990), based on: i) observations of a similar layer interpreted as partially serpentinized mantle on the Newfoundland margin just to the south, where serpentinized mantle was sampled (*Party*, 2004); ii) results from the conjugate Goban Spur margin, indicating a wide region of exhumed serpentinzed mantle; and iii) imaging of normal faults through the crust (e.g. distance 300-335 km) that likely formed pathways for water to penetrate into the mantle.

6. This partially serpentinized layer appears to terminate 30 km seaward of the thick continental crust. This is somewhat puzzling, because 6-km-thick stretched continental crust should be brittle with fractures and faults that could act as a conduit for the seawater into the mantle, which would then be serpentinized(*Pérez-Gussinyé and Reston*, 2001). We had expected to find serpentinized mantle beneath the entire thin crust, similar to observations for other eastern Canadian margins.

7. Thin crust undercrusted by serpentinized mantle seems to be the most common feature for magma-poor margins. Only SCREECH Line 2 on the Newfoundland margin has no high velocity layer modeled below the thin continental crust (*Van Avendonk et al.*, 2006).

8. The partially serpentinized layer is associated with strong landward and seaward dipping reflections imaged in the MCS data from Line 85-3 (distance 285-340 km at 8-13 km depth). The landward extension of the serpentinized mantle coincides with a strong landward dipping reflector (distance 285 km) previously interpreted as the continent-ocean boundary by *Keen et al.* (1989). The deep

bright reflections may represent serpentinization fronts. These bright reflections are similar to bright dipping reflections interpreted as serpentinization fronts at similar depth (7-12 km) in Central Indian Basin (*Delescluse and Chamot-Rooke*, 2008).

5.1.3 Ridge Feature and Mantle Exhumation

1. A ridge feature is observed at the seaward-most extension of the OCT (distance ∼340-360 km) on the FLAME line. The velocity model and the MCS profile indicate a mixed character, between continental crust and serpentinized mantle, for the ridge feature.

2. The NE Flemish Cap margin displays little evidence of exposed mantle, which only might occur over a maximum distance of 20-30 km (distance ∼340-360 km, ridge feature). Similarly, the SE Flemish Cap displays no exposed mantle, although mantle may have been exhumed and later buried by deep-marine sheet flows (*Hopper et al.*, 2004). In comparison, the Goban Spur, Iberia, and Newfoundland magma-poor margins display wider regions (∼70-100 km) of exhumed mantle.

3. Mantle on magma-poor margins appears to be exposed in different ways. Ridge features imaged on the Newfoundland margin as well as on Galicia Bank, the Iberia, and SW Greenland margins (*Boillot et al.*, 1988; *Dean et al.*, 2000; *Pickup et al.*, 1996; *Shillington et al.*, 2006; *Chian and Louden*, 1994) were interpreted as serpentinzed ridges. A more dome-like ridge feature interpreted as exhumed mantle is imaged on SCREECH Line 3 (*Deemer et al.*, 2009). A similar feature seems to be present on Line 84-3 just south of Orphan Knoll. Overall, ridge features are present in many areas where exhumed mantle is inferred.

5.1.4 Initial Formation of Oceanic Crust

1. Velocities and velocity gradients typical of oceanic crust (*White et al.*, 1992) occur seaward of the ridge feature on the FLAME line. The upper layer has a thickness that varies between 1 and 3 km with velocities of 4.8-6.0 km s^{-1}

between distance 360 and 410 km and 4.8-6.2 km s^{-1} from distance 410 km and seaward. The 3 to 4-km-thick lower layer has velocities of 6.7-7.2 km s^{-1}. These layers are interpreted as oceanic crustal layers 2 and 3. The thickness of oceanic crust (5-6.5 km) is comparable to the 3-6 km thick oceanic crust observed on the three SCREECH Lines on the Newfoundland margin (*Funck et al.*, 2003; *Van Avendonk et al.*, 2006; *Lau et al.*, 2006a).

2. Only the ridge feature separates thin continental crust from oceanic crust and hence the onset of seafloor spreading appears sharp. The transition to initial seafloor spreading appears complex and varies between the Flemish Cap-Goban Spur conjugate margins. The transition seems more gradual on Goban Spur with melt increasing seaward.

5.1.5 Rifting Style

1. The rifting style of the Flemish Cap-Goban Spur conjugate margin pair is asymmetric during all stages of formation: stretching, thinning, mantle exhumation and serpentinization, and continental breakup. This is in contrast to previous interpretations of the MCS profiles, suggesting a symmetric pure-shear rifting style of the margins (**?**). This new interpretation stresses the importance of using both wide-angle data and MCS when addressing the rifting style of a conjugate margin pair. Very little mantle (over a 20-30 km distance) exhumation occurred on the Flemish Cap margin compared to the ∼70 km wide region of mantle exhumation on Goban Spur. Thin continental crust above partially serpentinized mantle is displayed only in the velocity model of Flemish Cap. Continental breakup occurred on the Goban Spur side. This means that the interpretation of the location of continental breakup changed from the western (*Keen et al.*, 1989) to the eastern side of the margins (*Gerlings et al.*, 2012).

2. The interpretation that the continental crust thins more rapidly across Flemish Cap than Goban Spur and that a tongue of thin continental crust is left on the Flemish Cap margin contrasts conceptual and geodynamic models. The models show that thin continental crust is still attached to the margin, which thins less rapidly (e.g. *Reston*, 2009; *Huismans and Beaumont*, 2011) after the margins

have experienced asymmetric rifting. We observe that the reverse occurs for the Flemish Cap-Goban Spur margin conjugates.

5.1.6 Reprocessing of Line 85-3

1. The results from the depth migration of Line 85-3 are used to support the interpretation of P-wave velocity model as well as to get a more detailed image of the NE Flemish Cap margin. LIFT has been successful in improving the S/N ratio and preserving high frequencies of the data before migration. SRME followed by LIFT Radon Transform seem to attenuate the multiples best while preserving the signal. A comparison with the previous time migration (*Keen and de Voogd*, 1988) illustrates this and signal hidden in or covered by noise are visible.

5.1.7 Along-Strike Variation of Rifting Style and Crustal Domains

1. The interpretation of the reprocessed Line 87-4 and its crustal domains shows a different crustal structure along the profile in comparison to Line 85-3. The basement morphology is subdued in the most landward region of Line 87-4. Semi-horizontal reflections are displayed in the upper crust, possibly indicating fault blocks formed during roughly NW-SE rifting. This interpretation is supported by the GSI lines, which cross Line 87-4 in this region. Seaward, an imaged block coincident with a gravity high indicates complex poly-phased (3D) rifting. The basement morphology farther seaward indicates crust of oceanic affinity. These structures contrast with the crustal structures of Line 85-3, which show no indication of poly-phased (3D) rifting.

2. The NE Flemish Cap margin displays a wide range of along-strike variability in rifting style and crustal domains. The Erable lines situated between Lines 87-4 and 85-3 were re-interpreted. These lines, together with a velocity profile coincident with Line 84-3 (north of Line 87-4) and MCS reflection profiles (GSI) located in Orphan Basin, were used to evaluate the along-strike variation in crustal domains and rifting style. Both Line 85-3 and 87-4 cross magnetic

anomaly 34 and extend into oceanic crust. However, none of the Erable lines extend across magnetic anomaly 34, which makes it difficult to determine the exact location of initial oceanic crust on these lines. Most of the crust on the lines E48-52 appears to be thinned continental crust.

3. Mantle exposure appears limited along-strike of the NE Flemish Cap margin. The basement morphology imaged on the Erable lines and Lines 85-3, 87-4 and 84-3, combined with the velocity models along Lines 85-3 and 84-3, shows no or very narrow regions of exposed mantle. Two types of features for exposed mantle are observed: 1) a dome-like structure of exhumed mantle on the northern lines; and 2) a peaked ridge structure interpreted cas ontinental crust possibly intruded by serpentinized mantle, on the southern lines.

4. The extent of partially serpentinized mantle underneath thin continental crust appears complex and probably three-dimensional. The peak of the calculated gravity high derived from the FLAME velocity model and associated with partially serpentinized mantle is displaced from the observed gravity peak. However, the calculated gravity is based on a 2D density model along the line and does not take into account off-plane changes in density. The three-dimensionality becomes apparent when evaluating this high on the gravity map. The gravity high diminishes north of the profile, and a small high is observed to the northeast, which explains the displacement.

5. On the NE Flemish Cap, only Lines 85-3 and E46 show evidence for 2D structures. In contrast, a zone stretching from the south-eastern tip of Orphan Knoll to just south of line E48 was subjected to poly-phaed (3D) rifting.

6. I can neither confirm nor reject the hypothesis of a clockwise rotation of Flemish Cap suggested by **?**. I observe no clear evidence of shearing or major poly-phase (3D) rifting on the southern lines (Line 85-3, E46 and E44), whereas the northern lines display a zone of poly-phase (3D) rifting.

7. The Flemish Cap-Goban Spur margin pair no longer appears as simple as previously assumed. Although Line 85-3 only displays 2D rifting along the line, the

conclusions drawn above clearly illustrate the 3D variability of the NE Flemish Cap margin. Hence, treating a conjugate margin pair in 2D may limit our understanding of the rift evolution.

8. The difference between my interpretations of along-strike variations and those of *Welford et al.* (2010a) concern the extent of exhumed mantle and the zone of complex poly-phase (3D) rifting. a) In contrast to my interpretation of very limited mantle exposure, *Welford et al.* (2010a) interpreted a continuous zone of exhumed mantle along the NE Flemish Cap margin, which broadens northward into a wide zone (>100 km) of exhumed serpentinized mantle on Line 87-4 in the Orphan Basin. b) *Welford et al.* (2010a) interpreted shearing features on the seismic profiles, e.g. a flower structure on the previously processed section of Line 85-3, which they used as evidence for three distinct shear zones. The flower structure is not visible in the reprocessed prestack depth migrated section. Instead, features indicating depth-depending stretching in the lower crust are visible.

5.2 Future Work

The next step in understanding passive rifted continental margins is to focus on:

1. The transition into formation of initial oceanic crust. Not many profiles cross from contiental into unambiguous oceanic crust identified by seafloor spreading magnetic anomalies. More seismic profiles need to be collected, preferably both wide-angle and MCS data, on both sides of a conjugate margin pair. With a bigger data pool, we may observe common features and illuminate symmetry and asymmetry in the formation between the margin pair, as indicated by the results of the Flemish Cap and Goban Spur margin pair study.

2. Greater detail of structures across specific features, such as across ridge features and the OCT. To resolve such details we need denser OBS receiver sampling (3-5 km) (e.g. *Lau et al.*, 2012; *Watremez et al.*, 2012). Dense receiver-spacing also might allow for full waveform inversion (*Brenders and Pratt*, 2007), which can

provide a high-resolution velocity image of particularly complex structures in the entire crust, as well as the depth and nature of the crust-mantle transition.

3. The scale of 3D variability (gradual or sharp transition) such as crustal domains or partially serpentinized mantle undercrusting thin crust along-strike a margin. More cross-lines over features of interest and/or connecting wide-angle profiles along a margin are needed (e.g. *Watremez et al.*, submitteda).

4. The true extent of exhumed mantle on magma-poor margins. Focus has been on a wide regions (∼100 km) of exhumed mantle as observed on the Iberia margin. However, with the increased density of velocity profiles across margins it has become evident that the extent of this region is highly variable (e.g. *Funck et al.*, 2003; *Van Avendonk et al.*, 2006; *Lau et al.*, 2006a; *Funck et al.*, 2004; *Wu et al.*, 2006; *Maillard et al.*, 2006; *Chian et al.*, 1995a,b; *Chian and Louden*, 1994; *Dean et al.*, 2000; *Bullock and Minshull*, 2005).

5. Weakening of undercrusted mantle, which is partially serpentinized. Serpentinization weakens the uppermost part of mantle at a serpentine content of only 10-15% (*Escartin et al.*, 2001). This weakening of the upper mantle must affect rifting (Skelton et al. 2005). This aspect has not been much explored by geodynamic modelling, where focus has more been on a weak/strong crust vs. weak/strong mantle (e.g. *Huismans and Beaumont*, 2009).

6. 3D rifting in geodynamic models. Incorporating poly-phase (3D) rifting into geodynamic models seems to be in its infancy (e.g. *Watremez et al.*, submittedb). Further development of such geodynamic models will help illuminate many of the aspects described above.

References

Boillot, G., J. Girardeau, J. Kornprobst, et al. (1988), Rifting of the Galicia margin: crustal thinning and emplacement of mantle rocks on the seafloor, in *Proceedings of the Ocean Drilling Program, Scientific Results*, vol. 103, pp. 741–756.

Brenders, A., and R. Pratt (2007), Full waveform tomography for lithospheric imaging: Results from a blind test in a realistic crustal model, *Geophysical Journal International*, *168*(1), 133–151.

Bullock, A. D., and T. A. Minshull (2005), From continental extension to seafloor spreading: crustal structure of the Goban Spur rifted margin, southwest of the UK, *Geophysical Journal International*, *163*(2), 527–546, doi: 10.1111/j.1365-246X.2005.02726.x.

Chian, D., and K. Louden (1994), The continent-ocean crustal transition across the southwest Greenland margin, *Journal of geophysical research*, *99*(B5), 9117–9135.

Chian, D., K. Louden, and I. Reid (1995a), Crustal structure of the Labrador Sea conjugate margin and implications for the formation of nonvolcanic continental margins, *Journal of Geophysical Research*, *100*(B12), 24,239–24.

Chian, D., C. Keen, I. Reid, and K. Louden (1995b), Evolution of nonvolcanic rifted margins: New results from the conjugate margins of the Labrador Sea, *Geology*, *23*(7), 589–592.

Christensen, N. I. (1996), Poisson's ratio and crustal seismology, *Journal of Geophysical Research*, *101*(B2), 3139, doi: 10.1029/95JB03446.

Dean, S., T. Minshull, R. Whitmarsh, and K. Louden (2000), Deep structure of the ocean-continent transition in the southern Iberia Abyssal Plain from seismic refraction profiles: The IAM-9 transect at 40°20'N, *Journal of Geophysical Research*, *105*(B3), 5859–5885.

Deemer, S., J. Hall, K. Solvason, K. H. Lau, K. Louden, S. Srivastava, and J.-C. Sibuet (2009), Structure and development of the southeast Newfoundland continental passive margin: derived from SCREECH Transect 3, *Geophysical Journal International*, *178*(2), 1004–1020, doi: 10.1111/j.1365-246X.2009.04162.x.

Delescluse, M., and N. Chamot-Rooke (2008), Serpentinization pulse in the actively deforming Central Indian Basin, *Earth and Planetary Science Letters*, *276*(1-2), 140–151, doi: 10.1016/j.epsl.2008.09.017.

Escartin, J., G. Hirth, and B. Evans (2001), Strength of slightly serpentinized peridotites: Implications for the tectonics of oceanic lithosphere, *Geology*, *29*(11), 1023–1026.

Funck, T., J. Hopper, H. Larsen, K. Louden, B. Tucholke, and W. Holbrook (2003), Crustal structure of the ocean-continent transition at Flemish Cap: Seismic refraction results, *Journal of Geophysical Research*, *108*(B11), 2531.

Funck, T., H. Jackson, K. Louden, S. Dehler, and Y. Wu (2004), Crustal structure of the northern Nova Scotia rifted continental margin (eastern Canada), *Journal of Geophysical Research*, *109*(B9), B09,102.

Gerlings, J., K. E. Louden, and H. R. Jackson (2011), Crustal structure of the Flemish Cap Continental Margin (eastern Canada): an analysis of a seismic refraction profile, *Geophysical Journal International*, *185*(1), 30–48, doi: 10.1111/j.1365-246X.2011.04931.x.

Gerlings, J., K. E. Louden, T. A. Minshull, and M. R. Nedimović (2012), Flemish Cap-Goban Spur conjugate margins: New evidence of asymmetry, *Geology*, *40*(12), 1107–1110, doi: 10.1130/G33263.1.

Hopper, J. R., T. Funck, B. E. Tucholke, H. Christian Larsen, W. S. Holbrook, K. E. Louden, D. Shillington, and H. Lau (2004), Continental breakup and the onset of ultraslow seafloor spreading off Flemish Cap on the Newfoundland rifted margin, *Geology*, *32*(1), 93, doi: 10.1130/G19694.1.

Horsefield, S., K. Whitmarsh, R. White, and J. Sibuet (1994), Crustal structure of the Goban Spur rifted continental margin, NE Atlantic, *Geophysical Journal International*, *119*(1), 1–19.

Huismans, R., and C. Beaumont (2009), Structural style of formation of passive margins, insights from dynamical modelling, *Trabajos de geología*, *29*(29).

Huismans, R., and C. Beaumont (2011), Depth-dependent extension, two-stage breakup and cratonic underplating at rifted margins, *Nature*, *473*(7345), 74–8, doi: 10.1038/nature09988.

Keen, C., and B. de Voogd (1988), The continent-ocean boundary at the rifted margin off eastern Canada: new results from deep seismic reflection studies, *Tectonics*, *7*(1), 107–124.

Keen, C., C. Peddy, B. de Voogd, and D. Matthews (1989), Conjugate margins of canada and europe: Results from deep reflection profiling, *Geology*, *17*(2), 173–176.

Lau, K. W. H., K. E. Louden, T. Funck, B. E. Tucholke, W. S. Holbrook, J. R. Hopper, and H. Christian Larsen (2006a), Crustal structure across the Grand Banks-Newfoundland Basin Continental Margin - I. Results from a seismic refraction profile, *Geophysical Journal International*, *167*(1), 127–156, doi: 10.1111/j.1365-246X.2006.02988.x.

Lau, K. W. H., K. E. Louden, S. Deemer, J. Hall, J. R. Hopper, B. E. Tucholke, W. S. Holbrook, and H. Christian Larsen (2006b), Crustal structure across the Grand Banks-Newfoundland Basin Continental Margin - II. Results from a seismic reflection profile, *Geophysical Journal International*, *167*(1), 157–170, doi: 10.1111/j.1365-246X.2006.02989.x.

Lau, K. W. H., L. Watremez, K. E. Louden, M. R. Nedimović, J. K. Welford, and G. D. Karner (2012), New wide-angle seismic constraints across a magma-starved, hyperextended North Atlantic rift basin Orphan Basin, in *3rd Conjugate Margins Conference, Dublin*.

Louden, K., and D. Chian (1999), The deep structure of non–volcanic rifted continental margins, *Philosophical Transactions A*, *357*(1753), 767.

Maillard, A., J. Malod, E. Thiébot, F. Klingelhoefer, and J.-P. Réhault (2006), Imaging a lithospheric detachment at the continentocean crustal transition off Morocco, *Earth and Planetary Science Letters*, *241*(3-4), 686–698, doi: 10.1016/j.epsl.2005.11.013.

Party, S. S. (2004), Leg 210 summary, in *Proceedings of the Ocean Drilling Program, Initial Reports*, vol. 210, pp. 1–78.

Pérez-Gussinyé, M., and T. Reston (2001), Rheological evolution during extension at nonvolcanic rifted margins-onset of serpentinization and development of detachments leading to continental breakup, *Journal of Geophysical Research*, *106*(B3), 3961–3975.

Pickup, S., R. Whitmarsh, C. Fowler, and T. Reston (1996), Insight into the nature of the ocean-continent transition off West Iberia from a deep multichannel seismic reflection profile, *Geology*, *24*(12), 1079–1082.

Reid, I., and C. Keen (1990), High seismic velocities associated with reflections from within the lower oceanic crust near the continental margin of Eastern Canada, *Earth and Planetary Science Letters*, *99*(1), 118–126.

Reston, T. (2009), The structure, evolution and symmetry of the magma-poor rifted margins of the North and Central Atlantic: A synthesis, *Tectonophysics*, *468*(1-4), 6–27, doi: 10.1016/j.tecto.2008.09.002.

Shillington, D. J., W. S. Holbrook, H. J. a. Van Avendonk, B. E. Tucholke, J. R. Hopper, K. E. Louden, H. C. Larsen, and G. T. Nunes (2006), Evidence for asymmetric nonvolcanic rifting and slow incipient oceanic accretion from seismic reflection data on the Newfoundland margin, *Journal of Geophysical Research*, *111*(B9), B09,402, doi: 10.1029/2005JB003981.

Van Avendonk, H. J. A., W. S. Holbrook, G. T. Nunes, D. J. Shillington, B. E. Tucholke, K. E. Louden, H. C. Larsen, and J. R. Hopper (2006), Seismic velocity structure of the rifted margin of the eastern Grand Banks of Newfoundland, Canada, *Journal of Geophysical Research*, *111*(B11), B11,404, doi: 10.1029/2005JB004156.

Watremez, L., K. W. H. Lau, M. R. Nedimović, K. E. Louden, and G. D. Karner (2012), Orphan Basin crustal structure from tomographic inversion with dense receivers, in *3rd Conjugate Margins Conference, Dublin*.

Watremez, L., S. Rouzo, E. d'Acremont, and S. Leroy (submitteda), Crustal thinning and segmentation of the young northern-eastern Gulf of Aden rifted margin, *Tectonophysics, Special Issue: The Gulf of Aden rift*.

Watremez, L., E. Burov, E. d'Acremont, S. Leroy, B. Huet, L. L. Pourhiet, and N. Bellahsen (submittedb), Buoyancy and localising properties of cratonised mantle lithosphere: insights from thermomechanical models of the Eastern Gulf of Aden, *Earth Planet. Sci. Lett.*

Welford, J. K., J. Hall, J.-C. Sibuet, and S. P. Srivastava (2010), Structure across the northeastern margin of Flemish Cap, offshore Newfoundland from Erable multichannel seismic reflection profiles: evidence for a transtensional rifting environment, *Geophysical Journal International*, *183*(2), 572–586, doi: 10.1111/j.1365-246X.2010.04779.x.

White, R., D. McKenzie, and R. O'Nions (1992), Oceanic crustal thickness from seismic measurements and rare earth element inversions, *J. geophys. Res*, *97*(19), 683–19.

Wu, Y., K. E. Louden, T. Funck, H. R. Jackson, and S. A. Dehler (2006), Crustal structure of the central Nova Scotia margin off Eastern Canada, *Geophysical Journal International*, *166*(2), 878–906, doi: 10.1111/j.1365-246X.2006.02991.x.

References

Boillot, G., J. Girardeau, J. Kornprobst, et al. (1988), Rifting of the Galicia margin: crustal thinning and emplacement of mantle rocks on the seafloor, in *Proceedings of the Ocean Drilling Program, Scientific Results*, vol. 103, pp. 741–756.

Brenders, A., and R. Pratt (2007), Full waveform tomography for lithospheric imaging: Results from a blind test in a realistic crustal model, *Geophysical Journal International*, *168*(1), 133–151.

Bullock, A. D., and T. A. Minshull (2005), From continental extension to seafloor spreading: crustal structure of the Goban Spur rifted margin, southwest of the UK, *Geophysical Journal International*, *163*(2), 527–546, doi: 10.1111/j.1365-246X.2005.02726.x.

Cannat, M., D. Sauter, V. Mendel, E. Ruellan, K. Okino, J. Escartin, V. Combier, and M. Baala (2006), Modes of seafloor generation at a melt-poor ultraslow-spreading ridge, *Geology*, *34*(7), 605, doi: 10.1130/G22486.1.

Cannat, M., G. Manatschal, D. Sauter, and G. Péron-Pinvidic (2009), Assessing the conditions of continental breakup at magma-poor rifted margins: What can we learn from slow spreading mid-ocean ridges?, *Comptes Rendus Geoscience*, *341*(5), 406–427, doi: 10.1016/j.crte.2009.01.005.

Chian, D., and K. Louden (1994), The continent-ocean crustal transition across the southwest Greenland margin, *Journal of geophysical research*, *99*(B5), 9117–9135.

Chian, D., K. Louden, and I. Reid (1995a), Crustal structure of the Labrador Sea conjugate margin and implications for the formation of nonvolcanic continental margins, *Journal of Geophysical Research*, *100*(B12), 24,239–24.

Chian, D., C. Keen, I. Reid, and K. Louden (1995b), Evolution of nonvolcanic rifted margins: New results from the conjugate margins of the Labrador Sea, *Geology*, *23*(7), 589–592.

Chian, D., I. Reid, and H. Jackson (2001), Crustal structure beneath orphan basin and implications for nonvolcanic continental rifting, *Journal of Geophysical Research*, *106*(B6), 10,923–10.

Choo, J., J. Downton, and J. Dewar (2004), Lift: A new and practical approach to noise and multiple attenuation, *first break*, *22*, 39–44.

Christensen, N. I. (1996), Poisson's ratio and crustal seismology, *Journal of Geophysical Research*, *101*(B2), 3139, doi: 10.1029/95JB03446.

Coffin, M., and O. Eldholm (1994), Large igneous provinces: crustal structure, dimensions, and external consequences, *Reviews of Geophysics*, *32*(1), 1–36.

de Graciansky, P., C. Poag, R. Cinningham, P. Loubere, D. Masson, J. Mazzullo, L. Montadert, C. Müller, K. Otsuka, L. Reynolds, et al. (1985), The Goban Spur transect: Geologic evolution of a sediment-starved passive continental margin, *Geological Society of America Bulletin*, *96*(1), 58–76.

de Voogd, B., and C. Keen (1987), Lithoprobe east: results from reflection profiling of the continental margin: Grand banks region., *Geophysical Journal of the Royal Astronomical Society*, *89*(1), 195–200.

Dean, S., T. Minshull, R. Whitmarsh, and K. Louden (2000), Deep structure of the ocean-continent transition in the southern Iberia Abyssal Plain from seismic refraction profiles: The IAM-9 transect at 40°20'N, *Journal of Geophysical Research*, *105*(B3), 5859–5885.

Deemer, S., J. Hall, K. Solvason, K. H. Lau, K. Louden, S. Srivastava, and J.-C. Sibuet (2009), Structure and development of the southeast Newfoundland continental passive margin: derived from SCREECH Transect 3, *Geophysical Journal International*, *178*(2), 1004–1020, doi: 10.1111/j.1365-246X.2009.04162.x.

Dehler, S., C. Keen, T. Funck, H. Jackson, and K. Louden (2004), The limit of volcanic rifting: A structural model across the volcanic to non-volcanic transition off Nova Scotia, in *AGU Spring Meeting Abstracts*, vol. 1, p. 04.

Delescluse, M., and N. Chamot-Rooke (2008), Serpentinization pulse in the actively deforming Central Indian Basin, *Earth and Planetary Science Letters*, *276*(1-2), 140–151, doi: 10.1016/j.epsl.2008.09.017.

Escartin, J., G. Hirth, and B. Evans (2001), Strength of slightly serpentinized peridotites: Implications for the tectonics of oceanic lithosphere, *Geology*, *29*(11), 1023–1026.

Funck, T., J. Hopper, H. Larsen, K. Louden, B. Tucholke, and W. Holbrook (2003), Crustal structure of the ocean-continent transition at Flemish Cap: Seismic refraction results, *Journal of Geophysical Research*, *108*(B11), 2531.

Funck, T., H. Jackson, K. Louden, S. Dehler, and Y. Wu (2004), Crustal structure of the northern Nova Scotia rifted continental margin (eastern Canada), *Journal of Geophysical Research*, *109*(B9), B09,102.

Gerlings, J., K. E. Louden, and H. R. Jackson (2011), Crustal structure of the Flemish Cap Continental Margin (eastern Canada): an analysis of a seismic refraction profile, *Geophysical Journal International*, *185*(1), 30–48, doi: 10.1111/j.1365-246X.2011.04931.x.

Gerlings, J., K. E. Louden, T. A. Minshull, and M. R. Nedimović (2012), Flemish Cap-Goban Spur conjugate margins: New evidence of asymmetry, *Geology*, *40*(12), 1107–1110, doi: 10.1130/G33263.1.

Holbrook, W., W. Mooney, and N. Christensen (1992), The seismic velocity structure of the deep continental crust, in *Continental lower crust*, edited by A. R. . K. R. Fountain, D.M., pp. 1–43, Elsevier Sci, New York.

Hopper, J. R., T. Funck, B. E. Tucholke, H. Christian Larsen, W. S. Holbrook, K. E. Louden, D. Shillington, and H. Lau (2004), Continental breakup and the onset of ultraslow seafloor spreading off Flemish Cap on the Newfoundland rifted margin, *Geology*, *32*(1), 93, doi: 10.1130/G19694.1.

Hopper, J. R., T. Funck, and B. E. Tucholke (2007), Structure of the Flemish Cap margin, Newfoundland: insights into mantle and crustal processes during continental breakup, *Geological Society, London, Special Publications*, *282*(1), 47–61, doi: 10.1144/SP282.3.

Horsefield, S., K. Whitmarsh, R. White, and J. Sibuet (1994), Crustal structure of the Goban Spur rifted continental margin, NE Atlantic, *Geophysical Journal International*, *119*(1), 1–19.

Huismans, R., and C. Beaumont (2009), Structural style of formation of passive margins, insights from dynamical modelling, *Trabajos de geología*, *29*(29).

Huismans, R., and C. Beaumont (2011), Depth-dependent extension, two-stage breakup and cratonic underplating at rifted margins, *Nature*, *473*(7345), 74–8, doi: 10.1038/nature09988.

Jackson, R., K. Asprey, B. Chapman, S. Goold, P. Girouard, L. Johnston, and K. Louden (2002), Cruise report Hudson 2002011, Flemish Cap Margin Transect, *Tech. rep.*, Geological Survey of Canada, Dartmouth, Nova Scotia, Canada. Open File Rep. 1234, pp. 40.

Jagoutz, O., O. Müntener, G. Manatschal, D. Rubatto, G. Péron-Pinvidic, B. D. Turrin, and I. M. Villa (2007), The rift-to-drift transition in the North Atlantic: A stuttering start of the MORB machine?, *Geology*, *35*(12), 1087, doi: 10.1130/G23613A.1.

Keen, C., and B. de Voogd (1988), The continent-ocean boundary at the rifted margin off eastern Canada: new results from deep seismic reflection studies, *Tectonics*, *7*(1), 107–124.

Keen, C., C. Peddy, B. de Voogd, and D. Matthews (1989), Conjugate margins of canada and europe: Results from deep reflection profiling, *Geology*, *17*(2), 173–176.

Keen, C. E., and D. L. Barrett (1981), Thinned and subsided continental crust on the rifted margin of Eastern Canada: crustal structure, thermal evolution and subsidence history, *Geophysical Journal International*, *65*(2), 443–465, doi: 10.1111/j.1365-246X.1981.tb02721.x.

King, L. H., G. B. Fader, W. H. Poole, and R. K. Wanless (1985), Geological setting and age of the Flemish Cap granodiorite, east of the Grand Banks of Newfoundland, *Canadian Journal of Earth Sciences*, *22*(9), 1286–1298, doi: 10.1139/e85-133.

Lau, K. (2005), Structure of the Eastern Grand Banks/Newfoundland basin rifted margin, Ph.D. thesis, Dalhousie University, Halifax, Nova Scotia.

Lau, K. W. H., K. E. Louden, T. Funck, B. E. Tucholke, W. S. Holbrook, J. R. Hopper, and H. Christian Larsen (2006a), Crustal structure across the Grand Banks-Newfoundland Basin Continental Margin - I. Results from a seismic refraction profile, *Geophysical Journal International*, *167*(1), 127–156, doi: 10.1111/j.1365-246X.2006.02988.x.

Lau, K. W. H., K. E. Louden, S. Deemer, J. Hall, J. R. Hopper, B. E. Tucholke, W. S. Holbrook, and H. Christian Larsen (2006b), Crustal structure across the Grand Banks-Newfoundland Basin Continental Margin - II. Results from a seismic reflection profile, *Geophysical Journal International*, *167*(1), 157–170, doi: 10.1111/j.1365-246X.2006.02989.x.

Lau, K. W. H., L. Watremez, K. E. Louden, M. R. Nedimović, J. K. Welford, and G. D. Karner (2012), New wide-angle seismic constraints across a magma-starved, hyperextended North Atlantic rift basin Orphan Basin, in *3rd Conjugate Margins Conference, Dublin*.

Lavier, L. L., and G. Manatschal (2006), A mechanism to thin the continental lithosphere at magma-poor margins., *Nature*, *440*(7082), 324–8, doi: 10.1038/nature04608.

Lay, T., and C. Wallace (1995), *Modern global seismology*, Academic Press.

Leroy, S., F. Lucazeau, E. D'Acremont, L. Watremez, J. Autin, S. Rouzo, N. Bellahsen, C. Tiberi, C. Ebinger, M.-O. Beslier, J. Perrot, P. Razin, F. Rolandone, H. Sloan, G. Stuart, A. Al Lazki, K. Al-Toubi, F. Bache, A. Bonneville, B. Goutorbe, P. Huchon, P. Unternehr, and K. Khanbari (2010), Contrasted styles of rifting in the eastern Gulf of Aden: A combined wide-angle, multichannel seismic, and heat flow survey, *Geochemistry Geophysics Geosystems*, *11*(7), Q07,004, doi: 10.1029/2009GC002963.

Louden, K., and D. Chian (1999), The deep structure of non–volcanic rifted continental margins, *Philosophical Transactions A*, *357*(1753), 767.

Ludwig, W., J. Nafe, and C. Drake (1970), Seismic refraction, in *The Sea*, edited by A. Maxwell, pp. 53–84, Wiley-Interscience, New York.

Lundin, E. R., and a. G. Dore (2011), Hyperextension, serpentinization, and weakening: A new paradigm for rifted margin compressional deformation, *Geology*, *39*(4), 347–350, doi: 10.1130/G31499.1.

Lutter, W., R. Nowack, and L. Braile (1990), Inversion for crustal structure using reflections from the PASSCAL Ouachita experiment, *Journal of Geophysical Research*, *95*(B4), 4623–4646.

Maillard, A., J. Malod, E. Thiébot, F. Klingelhoefer, and J.-P. Réhault (2006), Imaging a lithospheric detachment at the continentocean crustal transition off Morocco, *Earth and Planetary Science Letters*, *241*(3-4), 686–698, doi: 10.1016/j.epsl.2005.11.013.

McKenzie, D. (1978), Some remarks on the development of sedimentary basins, *Earth and Planetary Science Letters*, *40*(1), 25–32.

Miller, D., and N. Christensen (1997), Seismic velocities of lower crustal and upper mantle rocks from the slow-spreading Mid-Atlantic Ridge, south of the Kane Transform Zone (MARK), in *Proceedings of the Ocean Drilling Program. Scientific results*, vol. 153, pp. 437–454, Ocean Drilling Program.

Ogg, J., and A. Smith (2004), The geomagnetic polarity time scale, in *A Geologic Time Scale 2004*, edited by O. J. Gradstein, F.M. and A. Smith, pp. 63–86, Cambridge University Press.

Party, S. S. (2004), Leg 210 summary, in *Proceedings of the Ocean Drilling Program, Initial Reports*, vol. 210, pp. 1–78.

Party, S. S. (2007), Leg 210 summary, in *Proceedings of the Ocean Drilling Program, Initial Reports*, vol. 210, pp. 1–56.

Peddy, C., B. Pinet, D. Masson, R. Scrutton, J. Sibuet, M. Warner, J. Lefort, I. Shroeder, et al. (1989), Crustal structure of the Goban Spur continental margin, Northeast Atlantic, from deep seismic reflection profiling, *Journal of the Geological Society*, *146*(3), 427–437.

Pérez-Gussinyé, M., and T. Reston (2001), Rheological evolution during extension at nonvolcanic rifted margins-onset of serpentinization and development of detachments leading to continental breakup, *Journal of Geophysical Research*, *106*(B3), 3961–3975.

Péron-Pinvidic, G., and G. Manatschal (2008), The final rifting evolution at deep magma-poor passive margins from Iberia-Newfoundland: anew point of view, *International Journal of Earth Sciences*, *98*(7), 1581–1597, doi: 10.1007/s00531-008-0337-9.

Péron-Pinvidic, G., G. Manatschal, T. a. Minshull, and D. S. Sawyer (2007), Tectonosedimentary evolution of the deep Iberia-Newfoundland margins: Evidence for a complex breakup history, *Tectonics*, *26*(2), 1–19, doi: 10.1029/2006TC001970.

Pickup, S., R. Whitmarsh, C. Fowler, and T. Reston (1996), Insight into the nature of the ocean-continent transition off West Iberia from a deep multichannel seismic reflection profile, *Geology*, *24*(12), 1079–1082.

Reid, I., and C. Keen (1990), High seismic velocities associated with reflections from within the lower oceanic crust near the continental margin of Eastern Canada, *Earth and Planetary Science Letters*, *99*(1), 118–126.

Reston, T. (2009), The structure, evolution and symmetry of the magma-poor rifted margins of the North and Central Atlantic: A synthesis, *Tectonophysics*, *468*(1-4), 6–27, doi: 10.1016/j.tecto.2008.09.002.

Sandwell, D., and W. Smith (2009), Global marine gravity from retracked geosat and ERS-1 altimetry: Ridge segmentation versus spreading rate, *Journal of geophysical Research*, *114*(B01411), B01,411.

Sandwell, D. T., and W. H. F. Smith (1997), Marine gravity anomaly from Geosat and ERS 1 satellite altimetry, *Journal of Geophysical Research*, *102*(B5), 10,039, doi: 10.1029/96JB03223.

Shillington, D., N. White, T. Minshull, G. Edwards, S. Jones, R. Edwards, and C. Scott (2008), Cenozoic evolution of the eastern Black Sea: A test of depth-dependent stretching models, *Earth and Planetary Science Letters*, *265*(3), 360–378.

Shillington, D. J., W. S. Holbrook, H. J. a. Van Avendonk, B. E. Tucholke, J. R. Hopper, K. E. Louden, H. C. Larsen, and G. T. Nunes (2006), Evidence for asymmetric nonvolcanic rifting and slow incipient oceanic accretion from seismic reflection data on the Newfoundland margin, *Journal of Geophysical Research*, *111*(B9), B09,402, doi: 10.1029/2005JB003981.

Sibuet, J.-C. (2004), Pyrenean orogeny and plate kinematics, *Journal of Geophysical Research*, *109*(B8), B08,104, doi: 10.1029/2003JB002514.

Sibuet, J.-C., S. Srivastava, and G. Manatschal (2007a), Exhumed mantle-forming transitional crust in the Newfoundland-Iberia rift and associated magnetic anomalies, *Journal of Geophysical Research*, *112*(B6), B06,105, doi: 10.1029/2005JB003856.

Sibuet, J.-C., S. P. Srivastava, M. Enachescu, and G. D. Karner (2007b), Early Cretaceous motion of Flemish Cap with respect to North America: implications on the formation of Orphan Basin and SE Flemish Cap Galicia Bank conjugate margins, *Geological Society, London, Special Publications*, *282*(1), 63–76, doi: 10.1144/SP282.4.

Small, C. (1994), A global analysis of mid-ocean ridge axial topography, *Geophysical Journal International*, *116*(1), 64–84.

Srivastava, S., and W. Roest (1999), Extent of oceanic crust in the Labrador Sea, *Marine and Petroleum Geology*, *16*(1), 65–84.

Srivastava, S., J. Verhoef, and R. Macnab (1988), Results from a detailed aeromagnetic survey across the northeast Newfoundland margin, Part I: spreading anomalies and relationship between magnetic anomalies and the ocean-continent boundary, *Marine and petroleum geology*, *5*(4), 306–323.

Srivastava, S., J. Sibuet, S. Cande, W. Roest, and I. Reid (2000), Magnetic evidence for slow seafloor spreading during the formation of the Newfoundland and Iberian margins, *Earth and Planetary Science Letters*, *182*(1), 61–76.

Talwani, M., J. Worzel, and M. Landisman (1959), Rapid gravity computations for two-dimensional bodies with application to the Mendocino submarine fracture zone, *Journal of Geophysical Research*, *64*(1), 49–59.

Tucholke, B., and G. Mountain (1979), Seismic stratigraphy, lithostratigraphy and paleosedimentation patterns in the North American Basin, in *Deep Drilling Results in the Atlantic Ocean: Continental Margins and Paleoenvironment, Maurice Ewing Ser., vol. 3*, edited by M. Talwani, W. Hay, and W. B. F. Ryan, pp. 58–86, American Geophysical Union. Washington, D. C.

Tucholke, B., J. Austin, and E. Uchupi (1989), Crustal structure and rift-drift evolution of the newfoundland basin, *AAPG Memoir*, *46*, 247–263.

Tucholke, B. E., D. S. Sawyer, and J.-C. Sibuet (2007), Breakup of the Newfoundland Iberia rift, *Geological Society, London, Special Publications*, *282*(1), 9–46, doi: 10.1144/SP282.2.

Van Avendonk, H. J. A., W. S. Holbrook, G. T. Nunes, D. J. Shillington, B. E. Tucholke, K. E. Louden, H. C. Larsen, and J. R. Hopper (2006), Seismic velocity structure of the rifted margin of the eastern Grand Banks of Newfoundland, Canada, *Journal of Geophysical Research*, *111*(B11), B11,404, doi: 10.1029/2005JB004156.

Watremez, L., K. W. H. Lau, M. R. Nedimović, K. E. Louden, and G. D. Karner (2012), Orphan Basin crustal structure from tomographic inversion with dense receivers, in *3rd Conjugate Margins Conference, Dublin*.

Watremez, L., S. Rouzo, E. d'Acremont, and S. Leroy (submitteda), Crustal thinning and segmentation of the young northern-eastern Gulf of Aden rifted margin, *Tectonophysics, Special Issue: The Gulf of Aden rift*.

Watremez, L., E. Burov, E. d'Acremont, S. Leroy, B. Huet, L. L. Pourhiet, and N. Bellahsen (submittedb), Buoyancy and localising properties of cratonised mantle lithosphere: insights from thermomechanical models of the Eastern Gulf of Aden, *Earth Planet. Sci. Lett.*

Welford, J. K., J. Hall, J.-C. Sibuet, and S. P. Srivastava (2010a), Structure across the northeastern margin of Flemish Cap, offshore Newfoundland from Erable multichannel seismic reflection profiles: evidence for a transtensional rifting environment, *Geophysical Journal International*, *183*(2), 572–586, doi: 10.1111/j.1365-246X.2010.04779.x.

Welford, J. K., J. A. Smith, J. Hall, S. Deemer, S. P. Srivastava, and J.-C. Sibuet (2010b), Structure and rifting evolution of the northern Newfoundland Basin from Erable multichannel seismic reflection profiles across the southeastern margin of Flemish Cap, *Geophysical Journal International*, *180*(3), 976–998, doi: 10.1111/j.1365-246X.2009.04477.x.

Wernicke, B. (1981), Low-angle normal faults in the basin and Range Province: nappe tectonics in an extending orogen, *Nature*, *291*, 645–648.

White, R., and D. McKenzie (1989), Magmatism at rift zones: the generation of volcanic continental margins and flood basalts, *Journal of Geophysical Research*, *94*(B6), 7685–7729.

White, R., G. Spence, S. Fowler, D. McKenzie, G. Westbrook, and A. Bowen (1987), Magmatism at rifted continental margins, *Nature*, *330*(6147), 439–444.

White, R., D. McKenzie, and R. O'Nions (1992), Oceanic crustal thickness from seismic measurements and rare earth element inversions, *J. geophys. Res*, *97*(19), 683–19.

Whitmarsh, R., R. White, S. Horsefield, J. Sibuet, M. Recq, and V. Louvel (1996), The ocean-continent boundary off the western continental margin of Iberia: Crustal structure west of Galicia Bank, *Journal of Geophysical Research*, *101*(B12), 28,291–28.

Whitmarsh, R. B., G. Manatschal, and T. a. Minshull (2001), Evolution of magma-poor continental margins from rifting to seafloor spreading., *Nature*, *413*(6852), 150–4, doi: 10.1038/35093085.

Wu, Y., K. E. Louden, T. Funck, H. R. Jackson, and S. A. Dehler (2006), Crustal structure of the central Nova Scotia margin off Eastern Canada, *Geophysical Journal International*, *166*(2), 878–906, doi: 10.1111/j.1365-246X.2006.02991.x.

Yilmaz, Ö., and S. M. Doherty (1987), Seismic data processing.

Zelt, C., and P. Barton (1998), Three-dimensional seismic refraction tomography: A comparison of two methods applied to data from the Faeroe Basin, *Journal of Geophysical Research*, *103*(84), 7187–7210.

Zelt, C., and D. Forsyth (1994), Modeling wide-angle seismic data for crustal structure: Southeastern Grenville Province, *Journal of Geophysical Research*, *99*(B6), 11,687–11.

Zelt, C. A. (1999), Modelling strategies and model assessment for wide-angle seismic traveltime data, *Geophys. J. Int.*, *139*, 183–204.

Zelt, C. A., and R. B. Smith (1992), Seismic traveltime inversion for 2-D crustal velocity structure, *Geophys. J. Int.*, *108*, 16–34.

Ziegler, P. (1988), Evolution of the arctic-north atlantic and the western tethys–a visual presentation of a series of paleogeographic-paleotectonic maps, *Mem.-Am. Assoc. Pet. Geol*, *43*, 164–196.

Appendix A

Wide-angle Seismic Data: Relocation of Ocean Bottom Seismometers (OBS)

OBS numbers are in this appendix as the were during the cruise. Two OBSs (5 and 15) had no information on them. For modelling purposes the remaining nineteen OBSs were renumbered from 1 to 19. This is how they are refered to in the thesis.

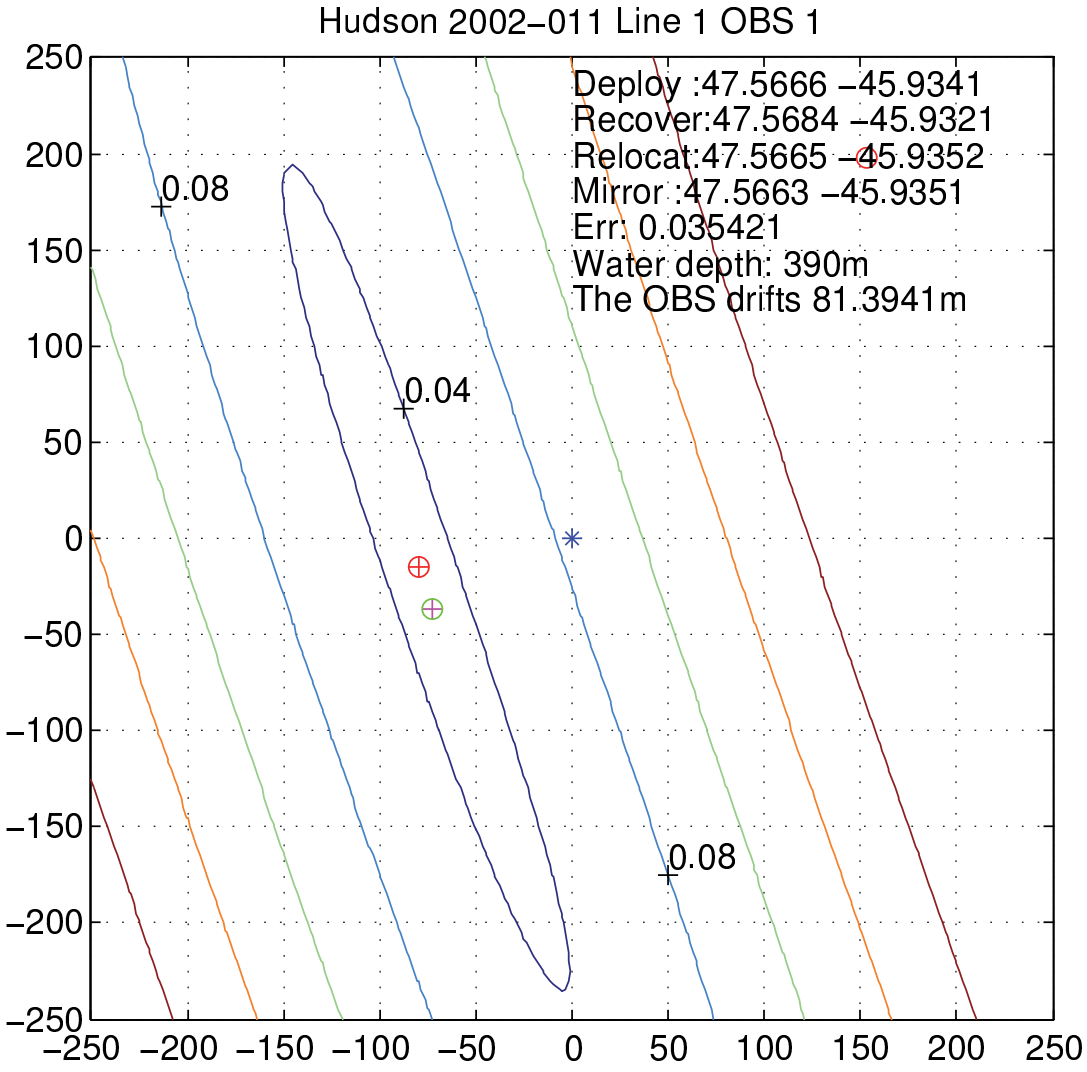

Figure A.1: Relocation of OBS 1. Blue star represents deployment position, red circle represents recovery position, red circle with red cross and green circle with red cross represent relocated positions.

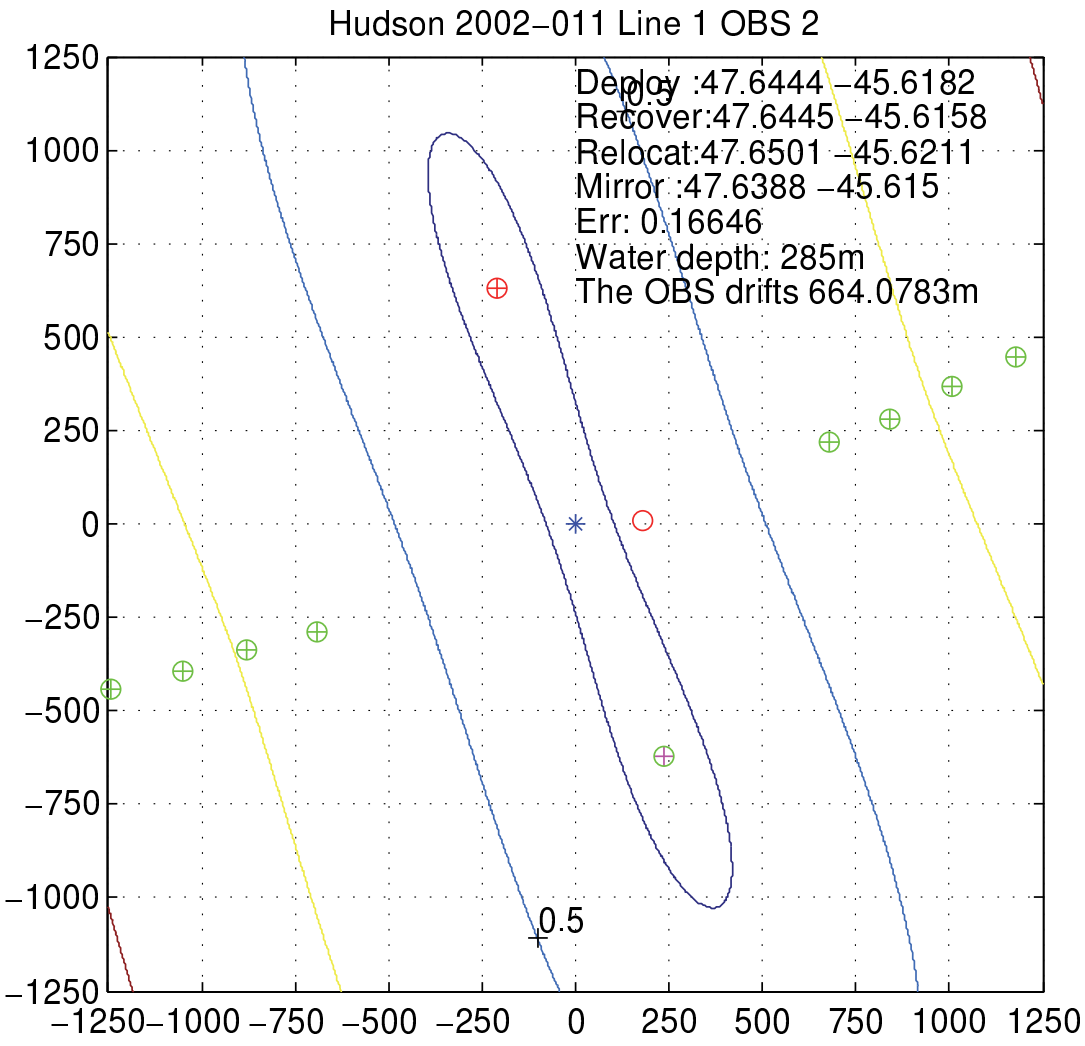

Figure A.2: Relocation of OBS 2. Blue star represents deployment position, red circle represents recovery position, red circle with red cross and green circle with red cross represent relocated positions.

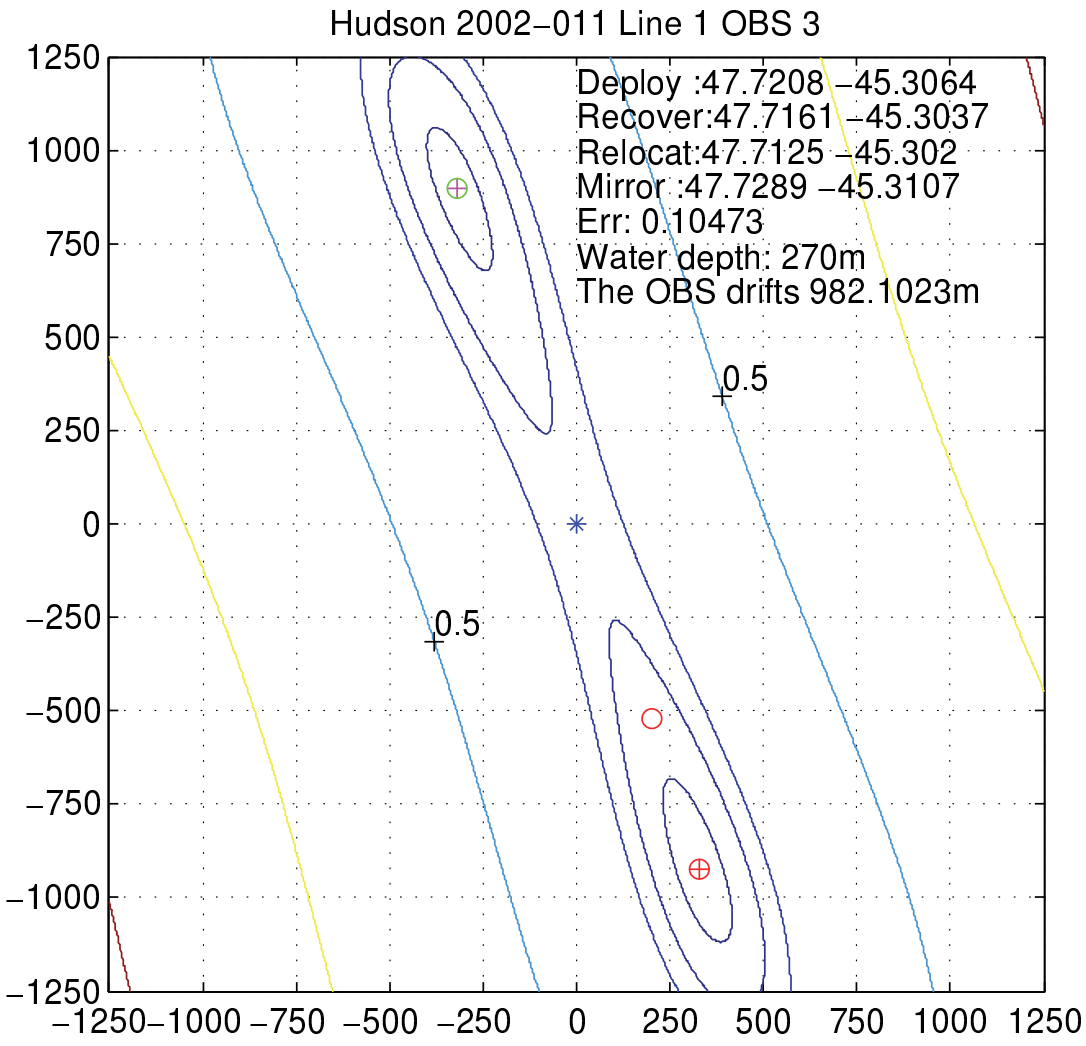

Figure A.3: Relocation of OBS 3. Blue star represents deployment position, red circle represents recovery position, red circle with red cross and green circle with red cross represent relocated positions.

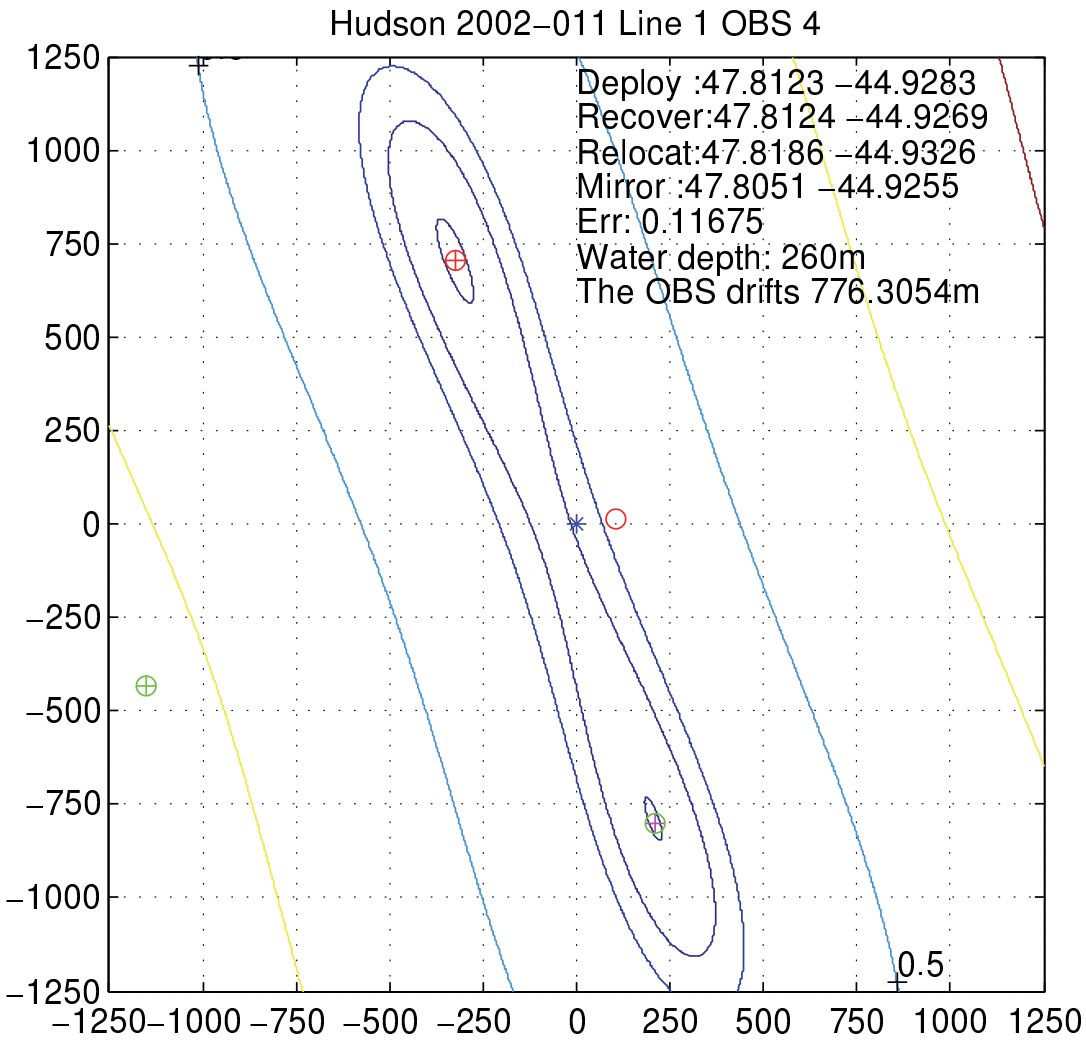

Figure A.4: Relocation of OBS 4. Blue star represents deployment position, red circle represents recovery position, red circle with red cross and green circle with red cross represent relocated positions.

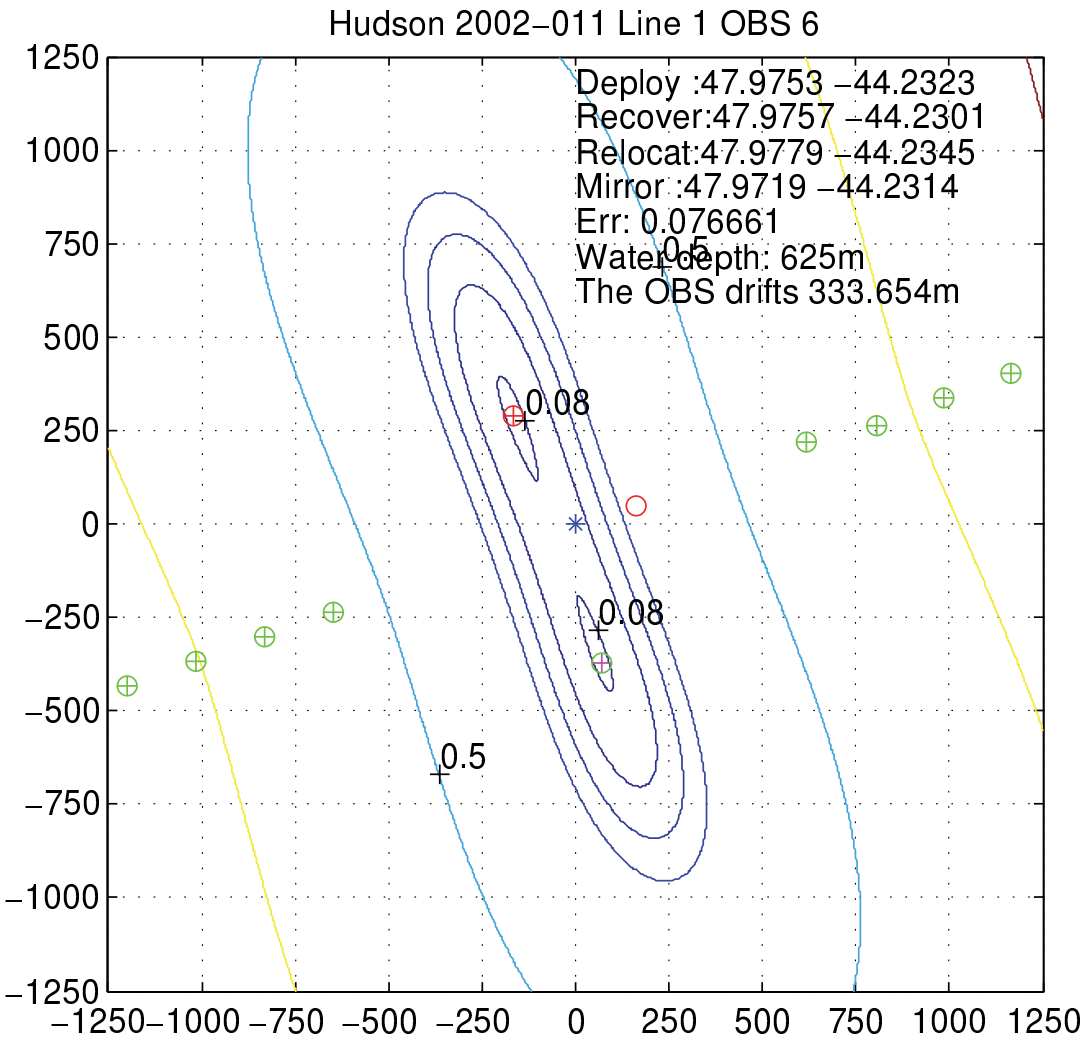

Figure A.5: Relocation of OBS 6. Blue star represents deployment position, red circle represents recovery position, red circle with red cross and green circle with red cross represent relocated positions.

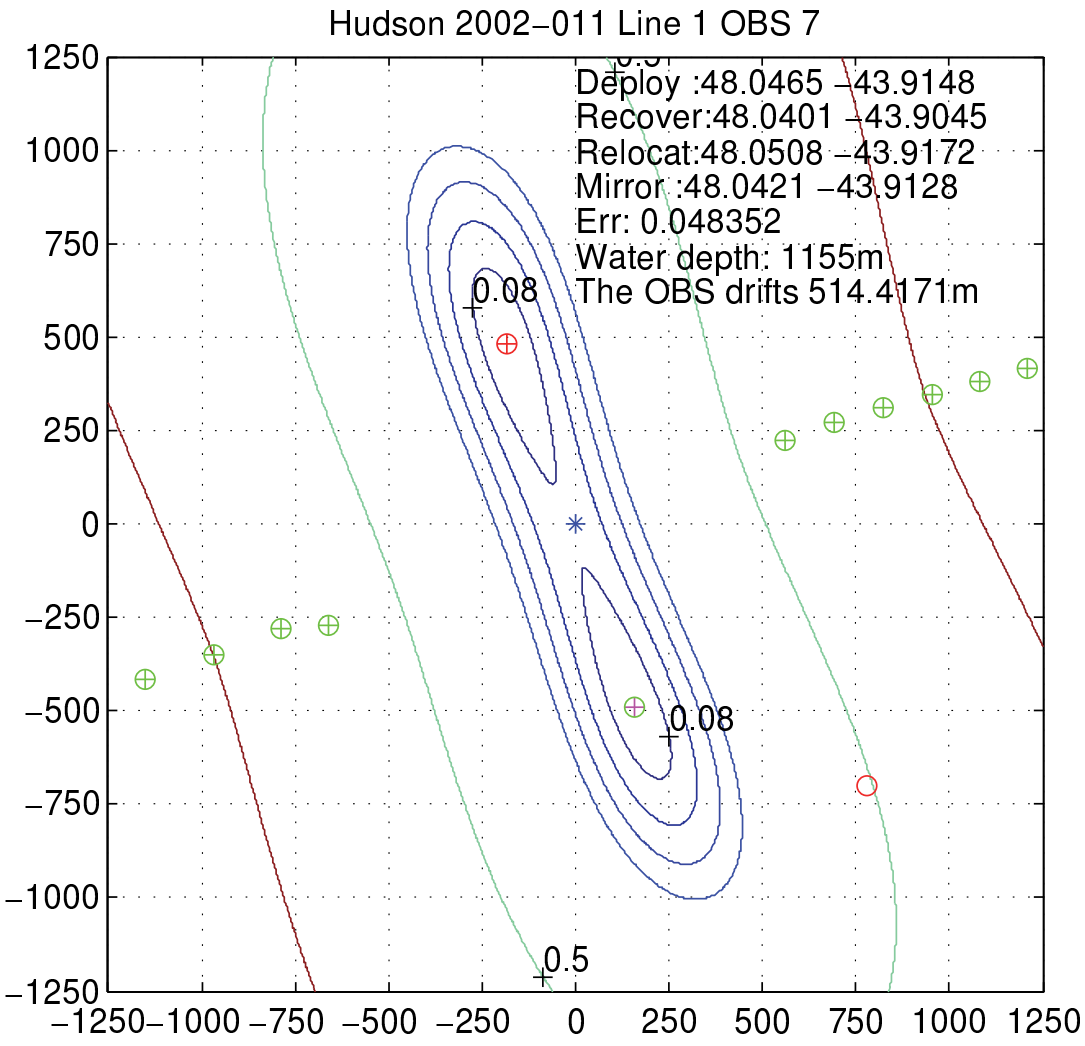

Figure A.6: Relocation of OBS 6. Blue star represents deployment position, red circle represents recovery position, red circle with red cross and green circle with red cross represent relocated positions.

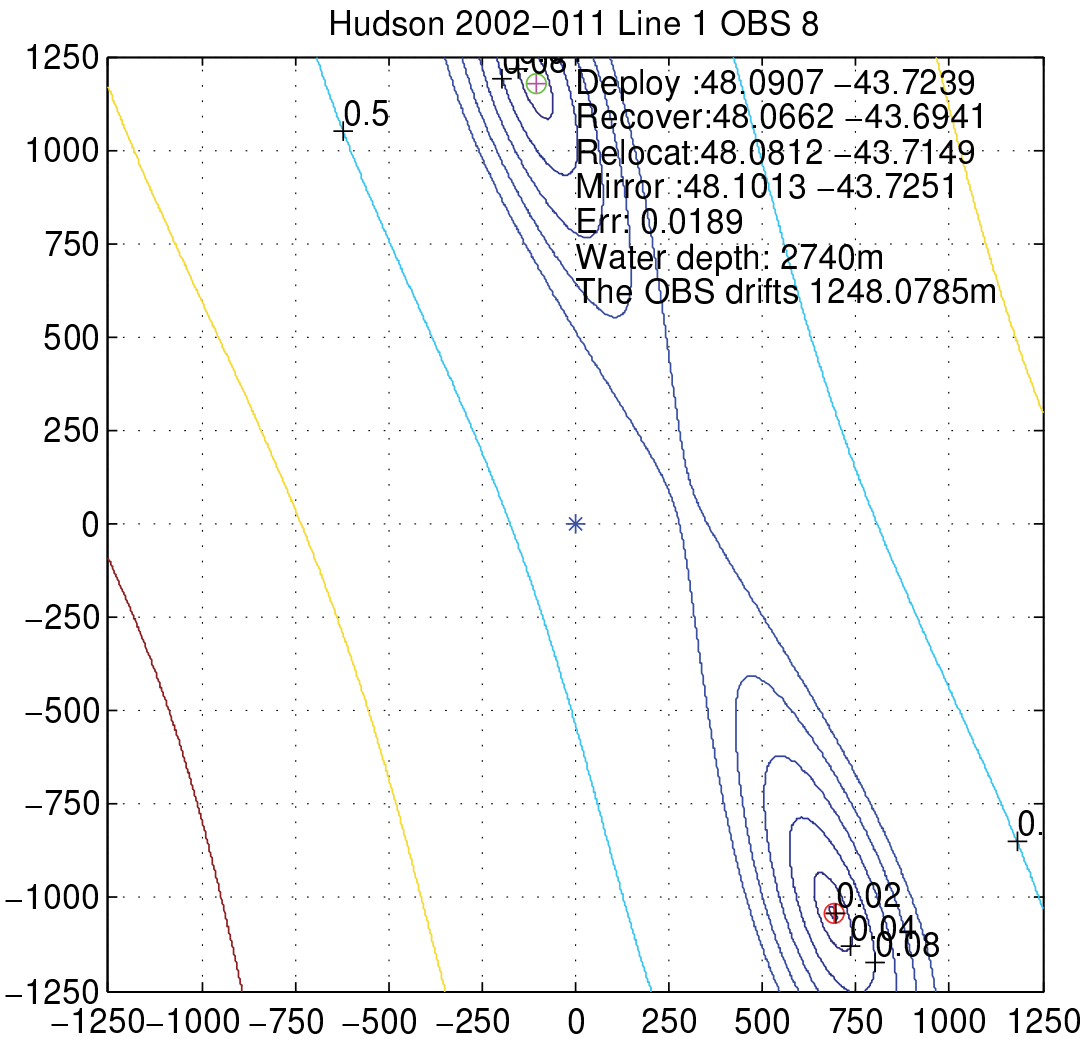

Figure A.7: Relocation of OBS 8. Blue star represents deployment position, red circle represents recovery position, red circle with red cross and green circle with red cross represent relocated positions.

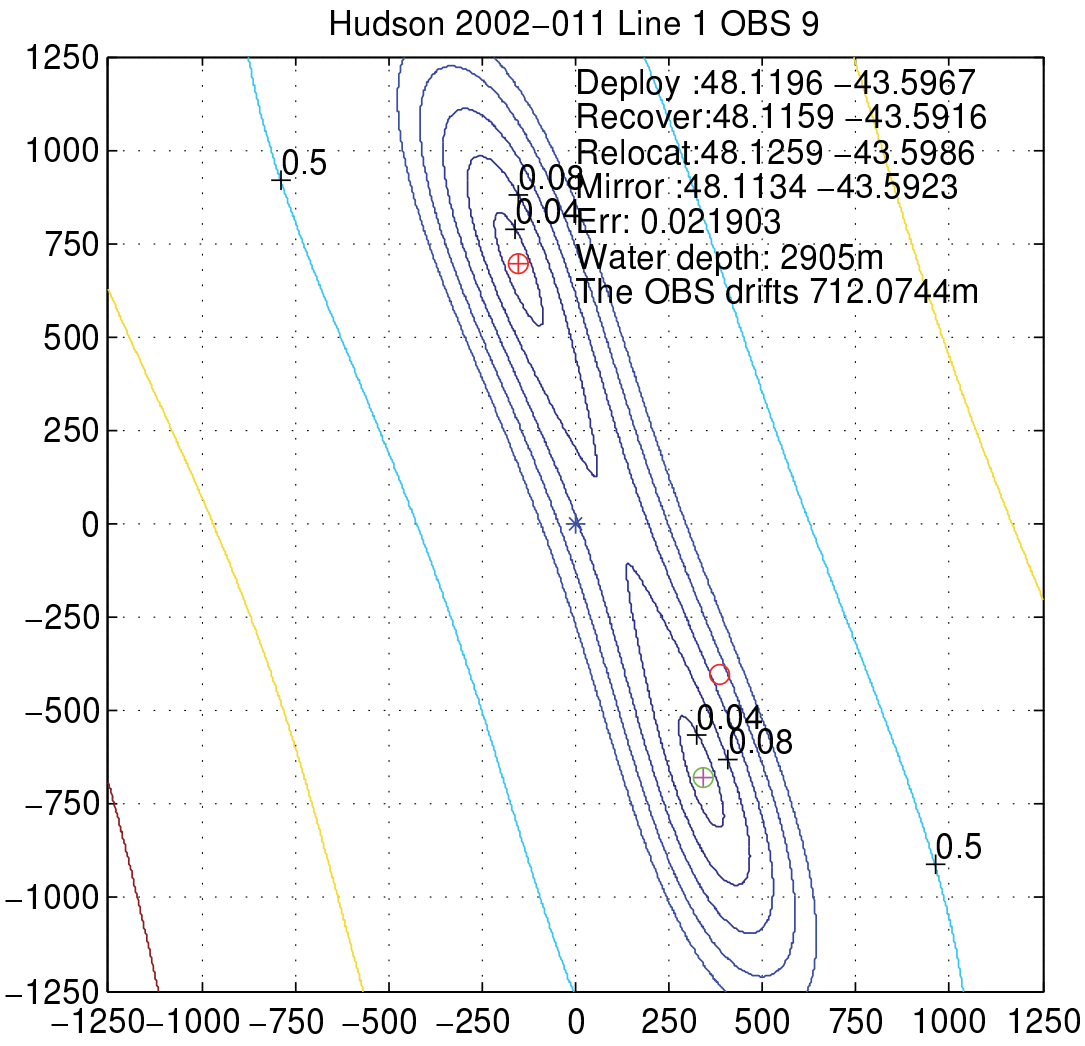

Figure A.8: Relocation of OBS 9. Blue star represents deployment position, red circle represents recovery position, red circle with red cross and green circle with red cross represent relocated positions.

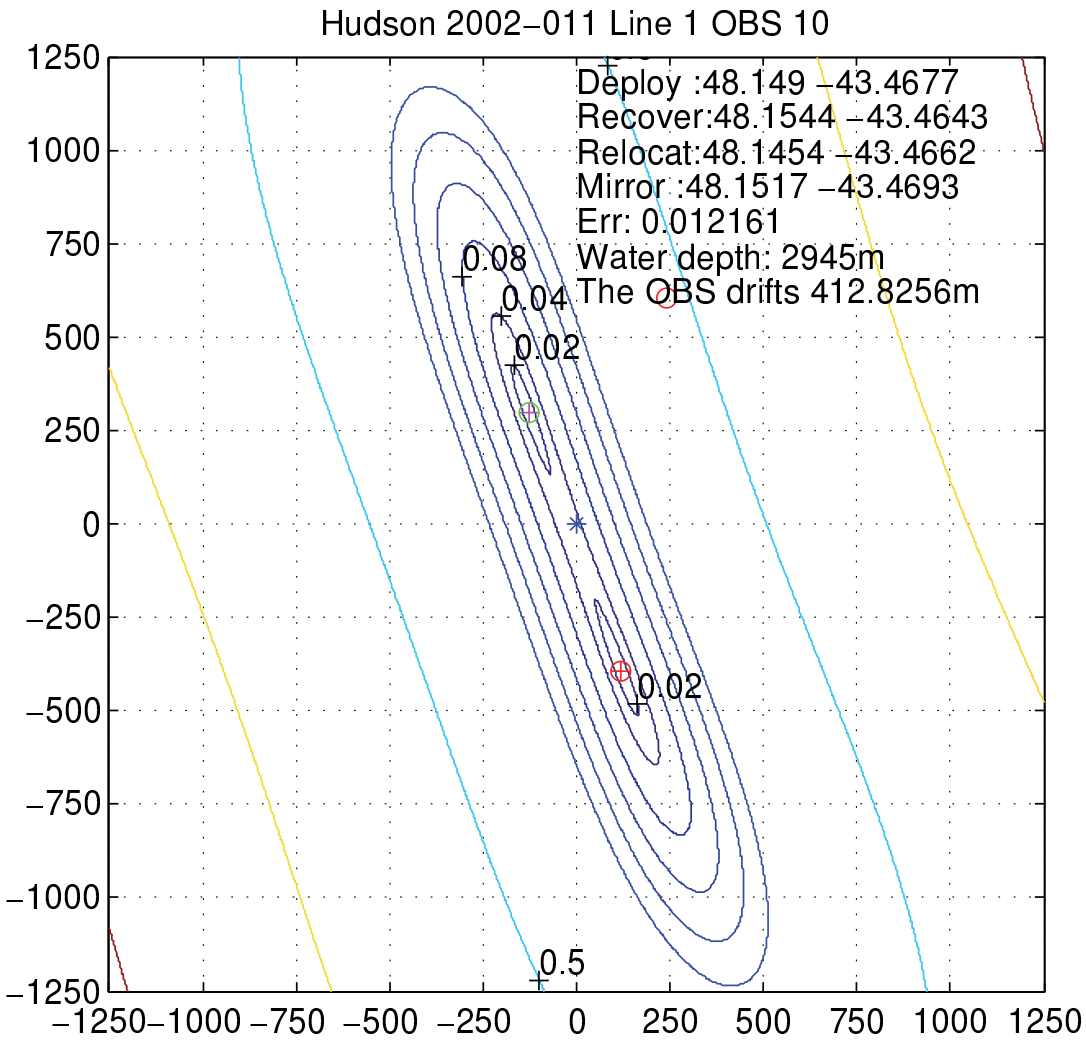

Figure A.9: Relocation of OBS 10. Blue star represents deployment position, red circle represents recovery position, red circle with red cross and green circle with red cross represent relocated positions.

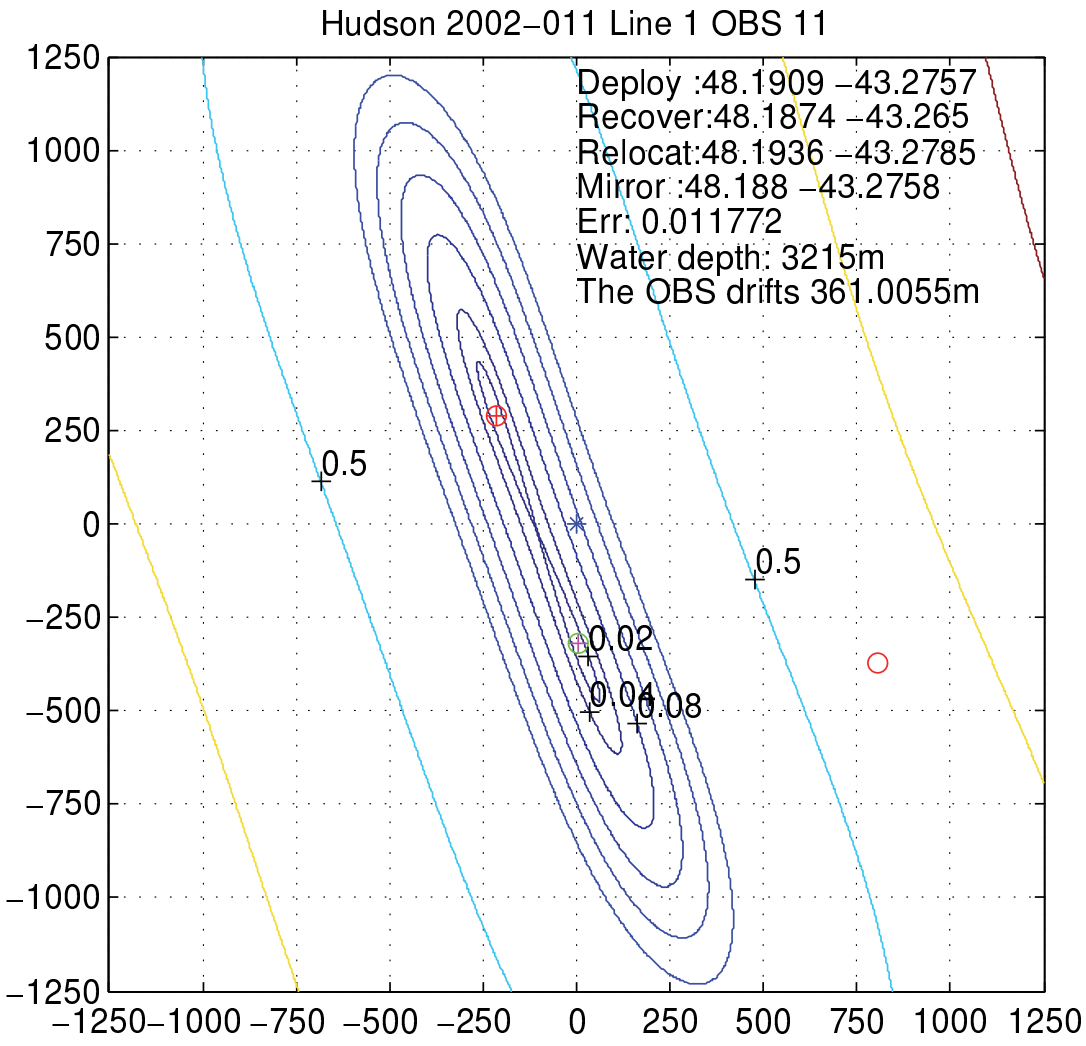

Figure A.10: Relocation of OBS 11. Blue star represents deployment position, red circle represents recovery position, red circle with red cross and green circle with red cross represent relocated positions.

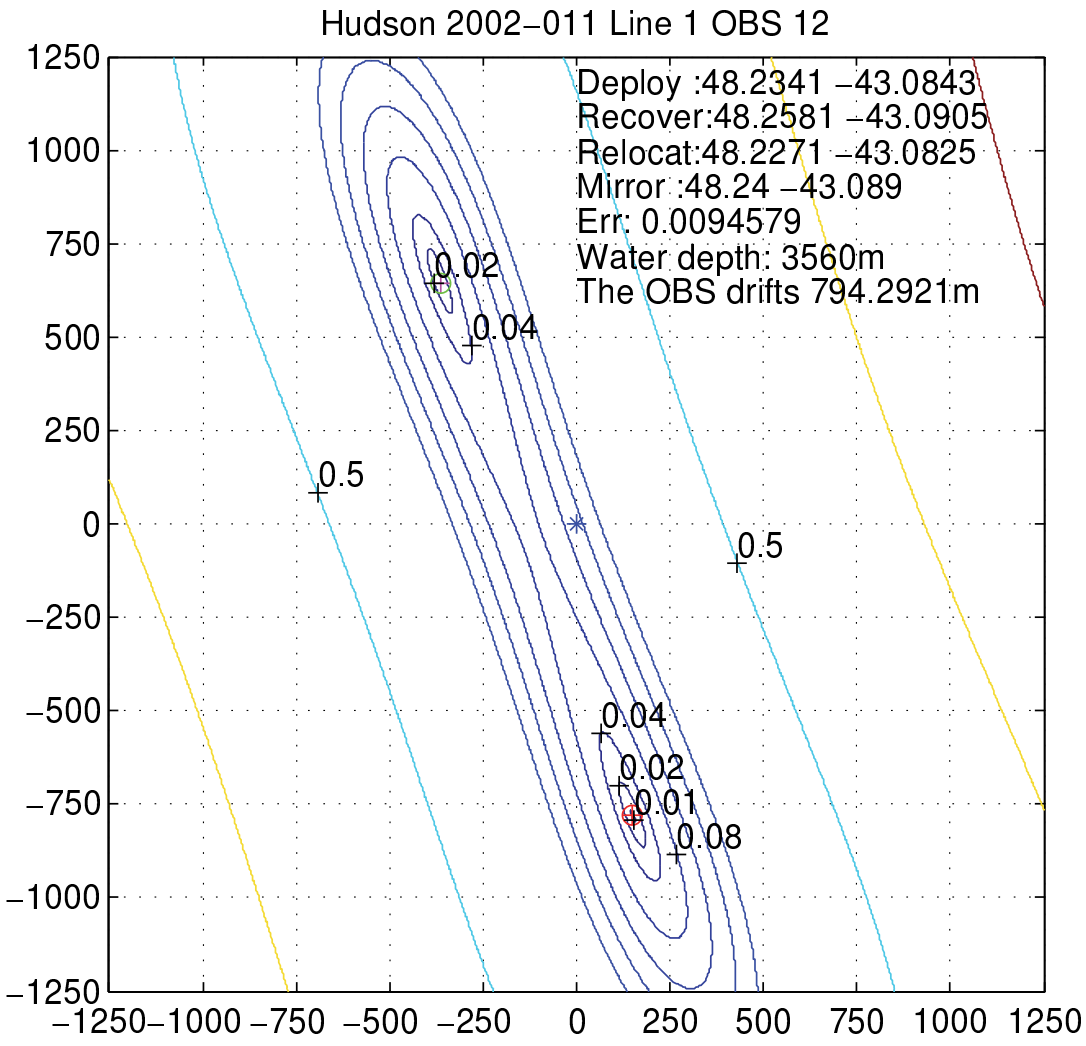

Figure A.11: Relocation of OBS 12. Blue star represents deployment position, red circle represents recovery position, red circle with red cross and green circle with red cross represent relocated positions.

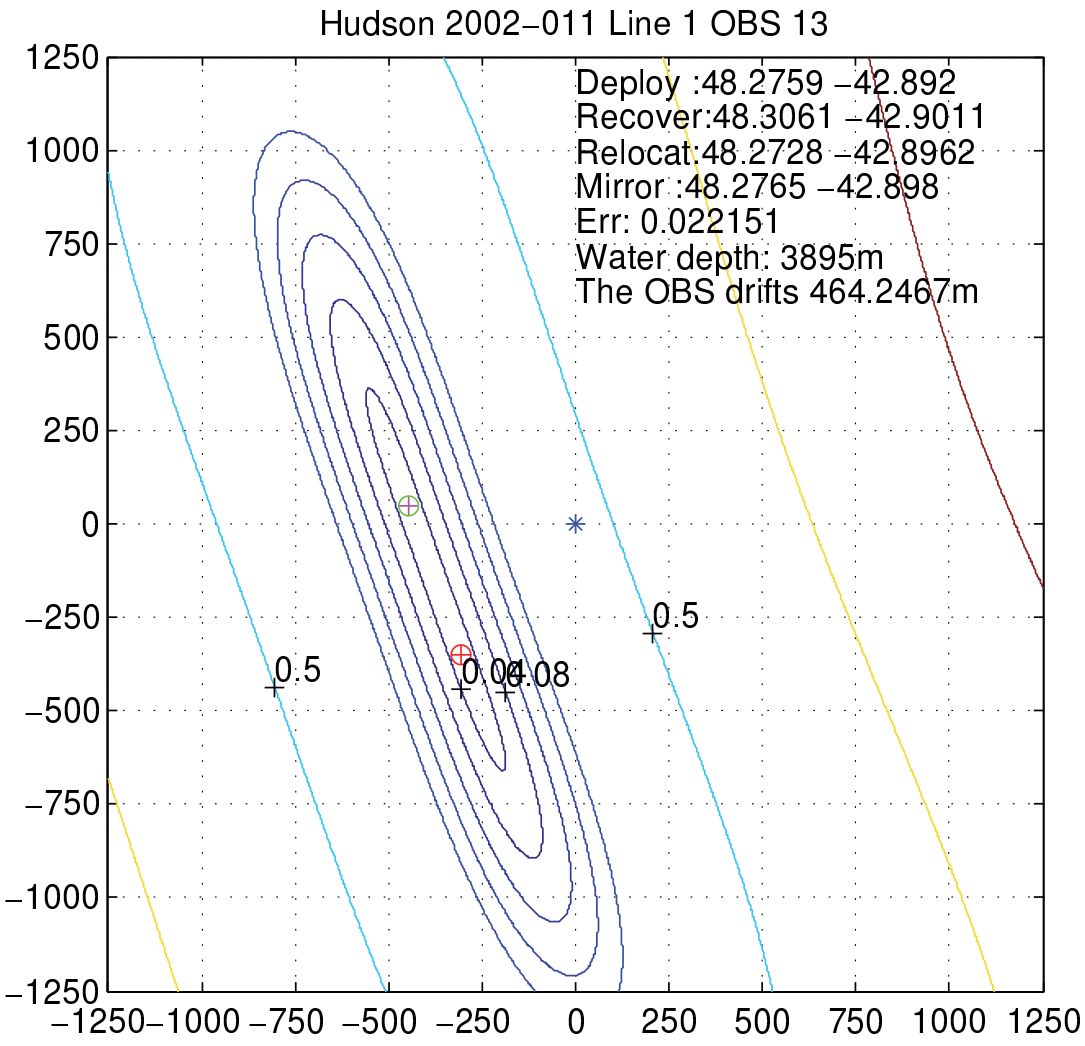

Figure A.12: Relocation of OBS 13. Blue star represents deployment position, red circle represents recovery position, red circle with red cross and green circle with red cross represent relocated positions.

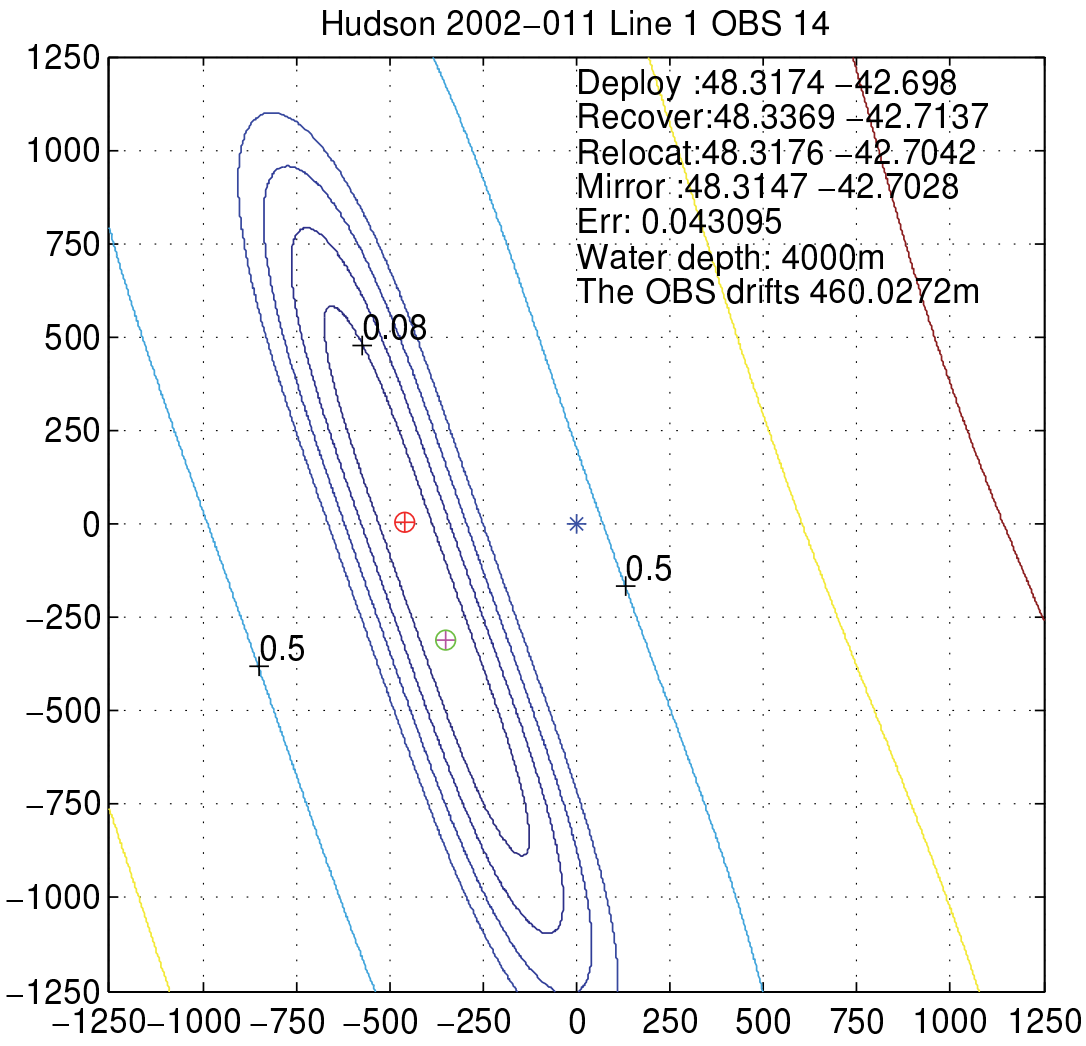

Figure A.13: Relocation of OBS 14. Blue star represents deployment position, red circle represents recovery position, red circle with red cross and green circle with red cross represent relocated positions.

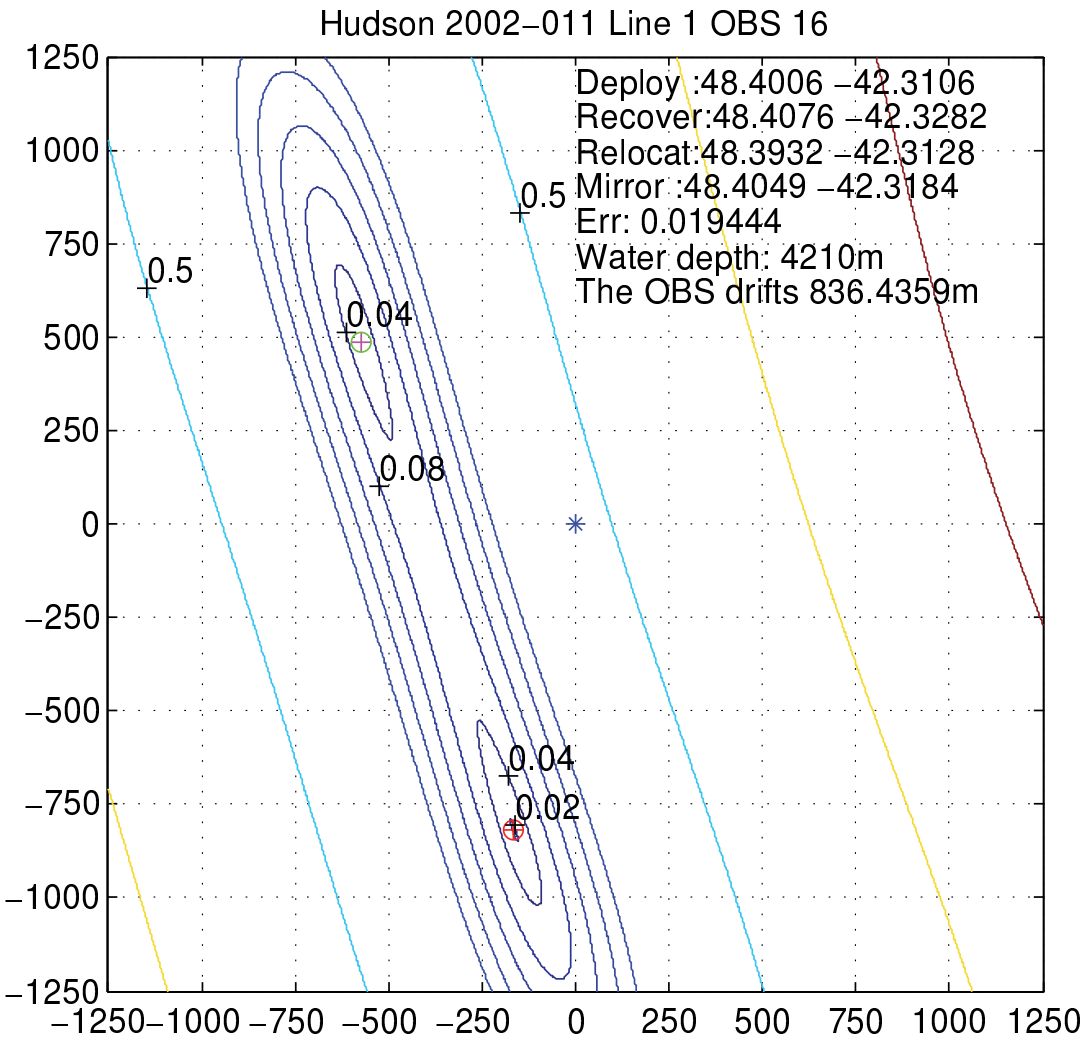

Figure A.14: Relocation of OBS 16. Blue star represents deployment position, red circle represents recovery position, red circle with red cross and green circle with red cross represent relocated positions.

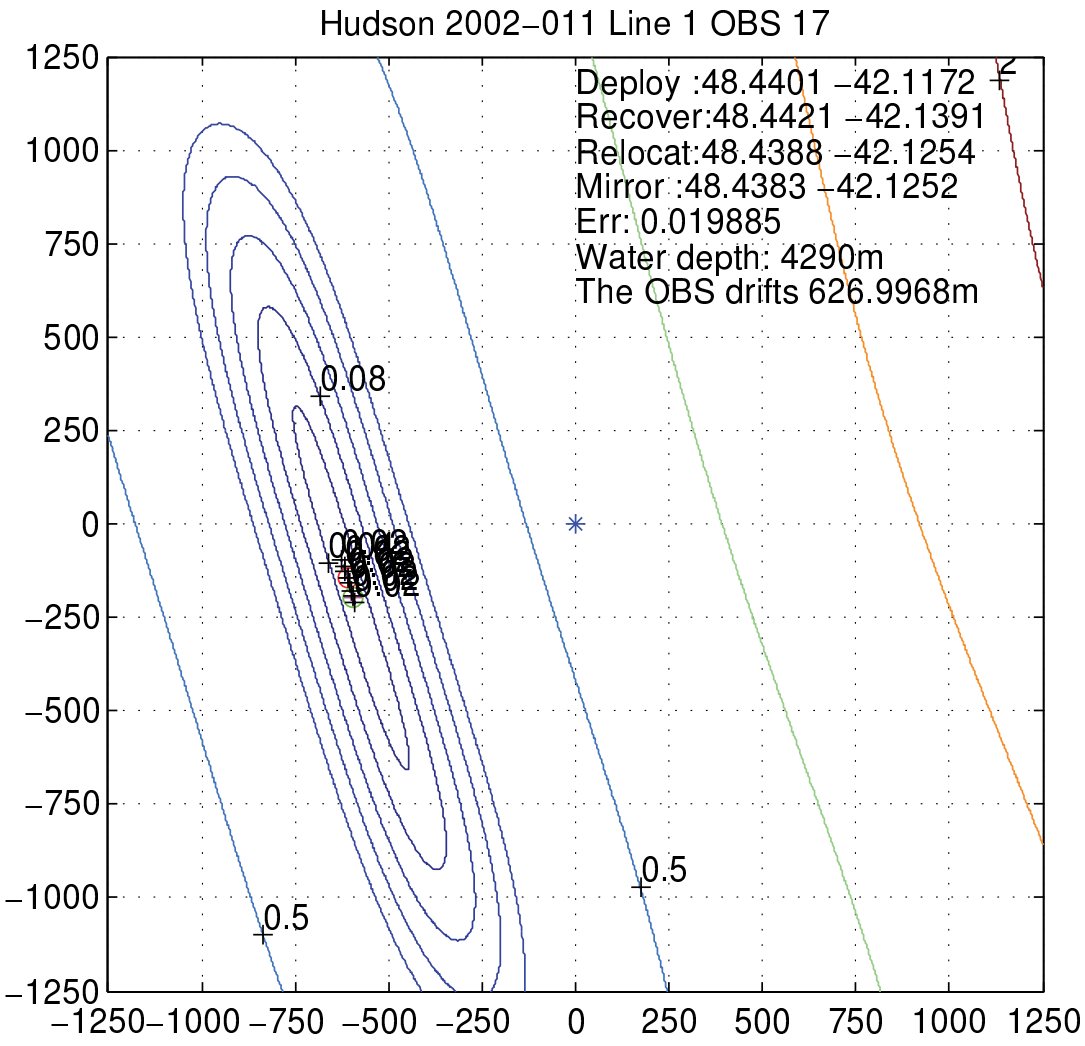

Figure A.15: Relocation of OBS 17. Blue star represents deployment position, red circle represents recovery position, red circle with red cross and green circle with red cross represent relocated positions.

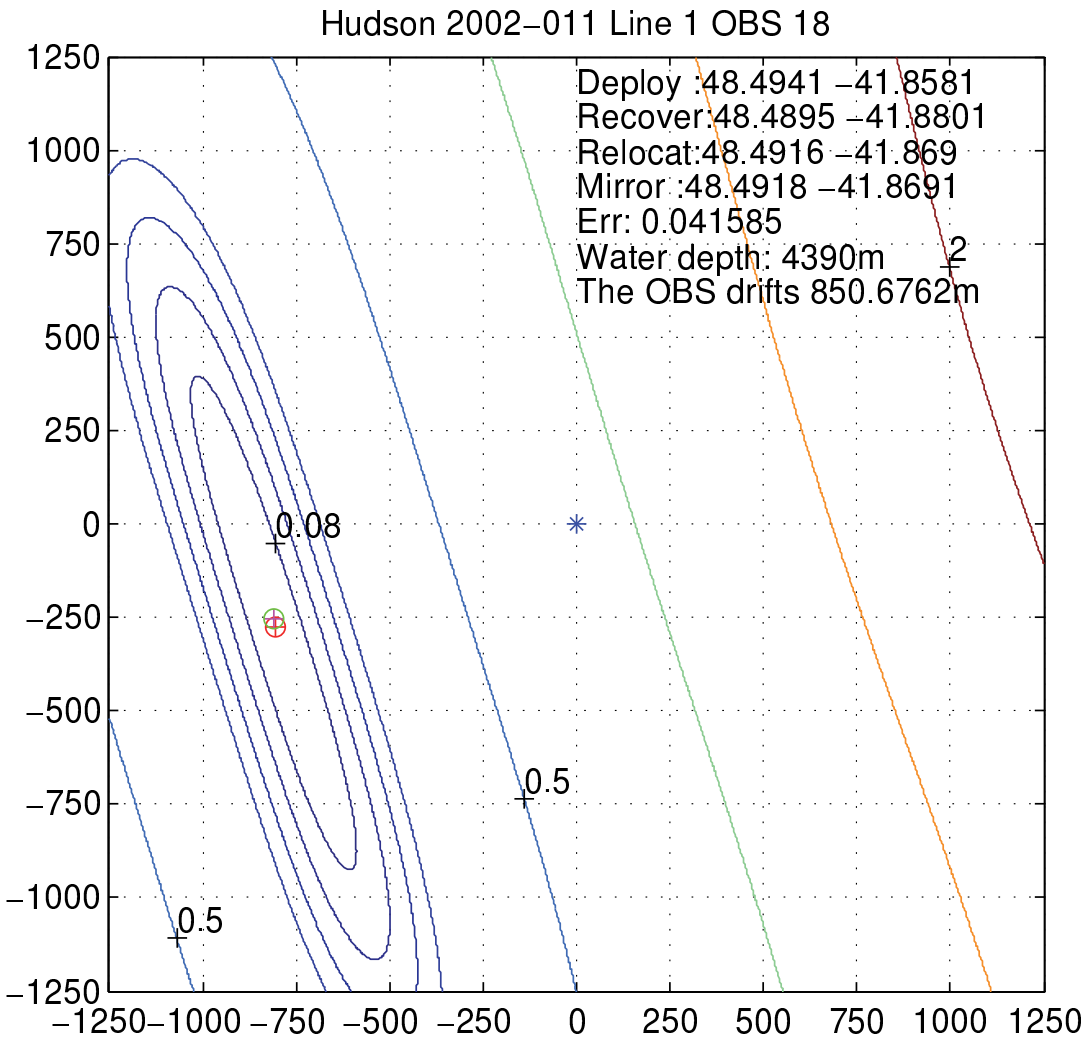

Figure A.16: Relocation of OBS 18. Blue star represents deployment position, red circle represents recovery position, red circle with red cross and green circle with red cross represent relocated positions.

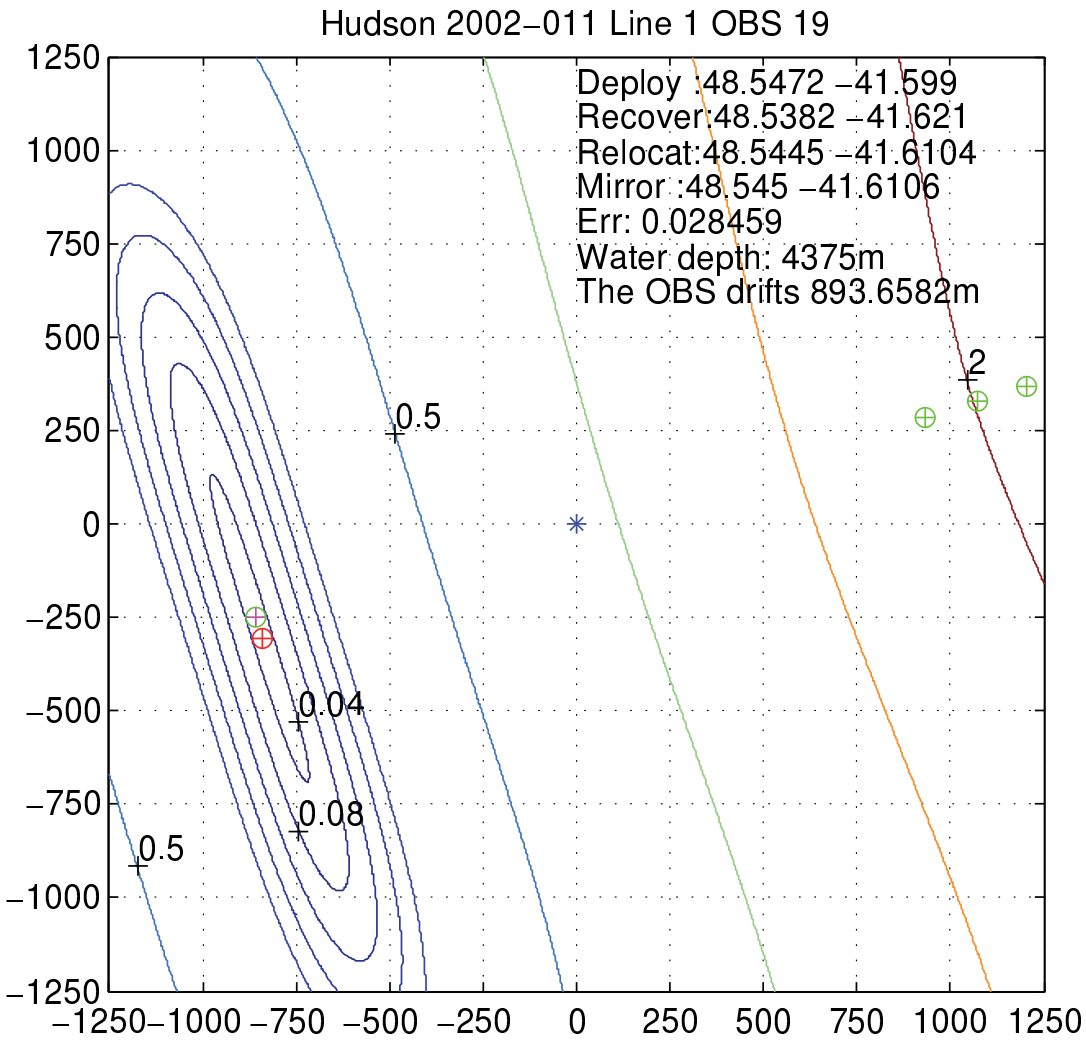

Figure A.17: Relocation of OBS 19. Blue star represents deployment position, red circle represents recovery position, red circle with red cross and green circle with red cross represent relocated positions.

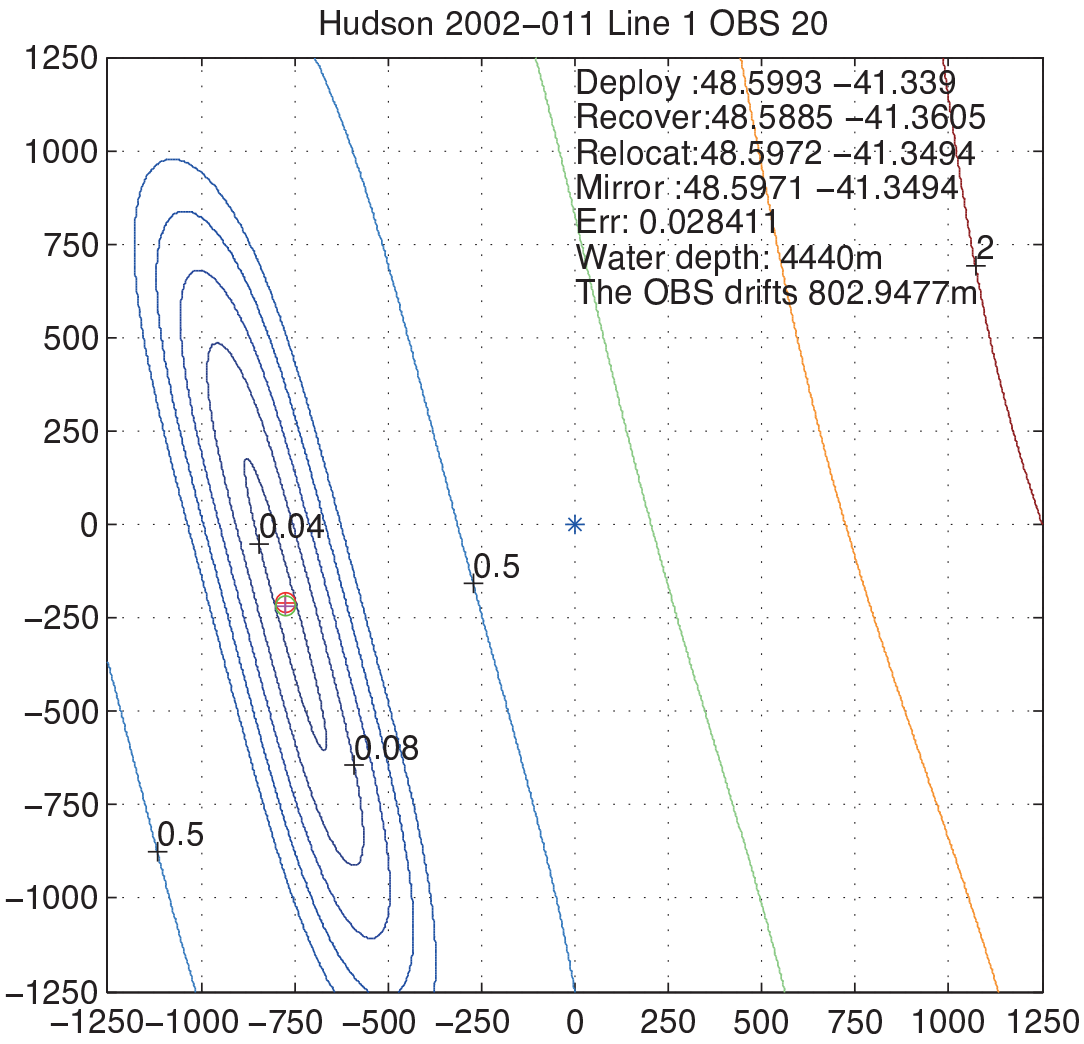

Figure A.18: Relocation of OBS 20. Blue star represents deployment position, red circle represents recovery position, red circle with red cross and green circle with red cross represent relocated positions.

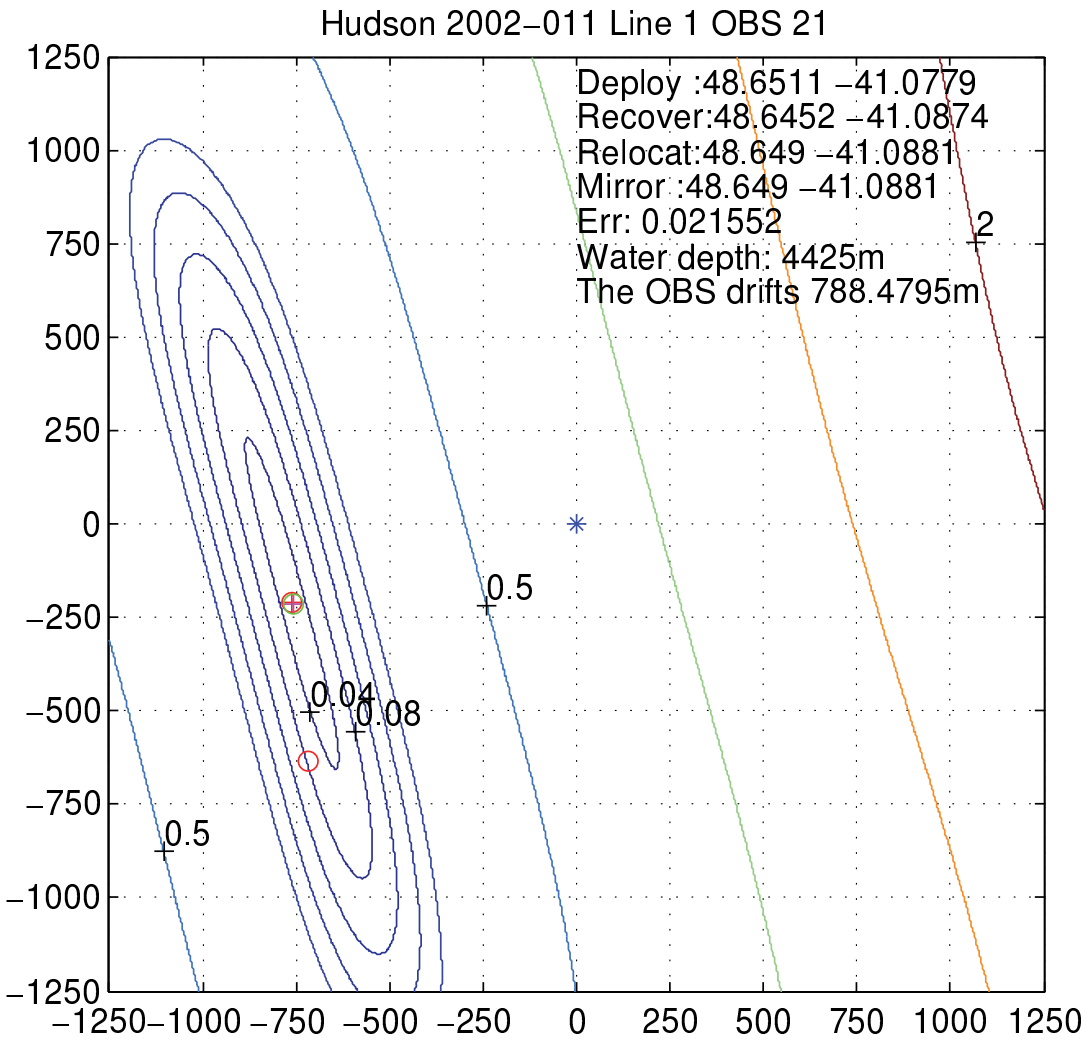

Figure A.19: Relocation of OBS 21. Blue star represents deployment position, red circle represents recovery position, red circle with red cross and green circle with red cross represent relocated positions.

Appendix B

Wide-angle Seismic Data: OBS Sections not shown in *Gerlings et al.* (2011)

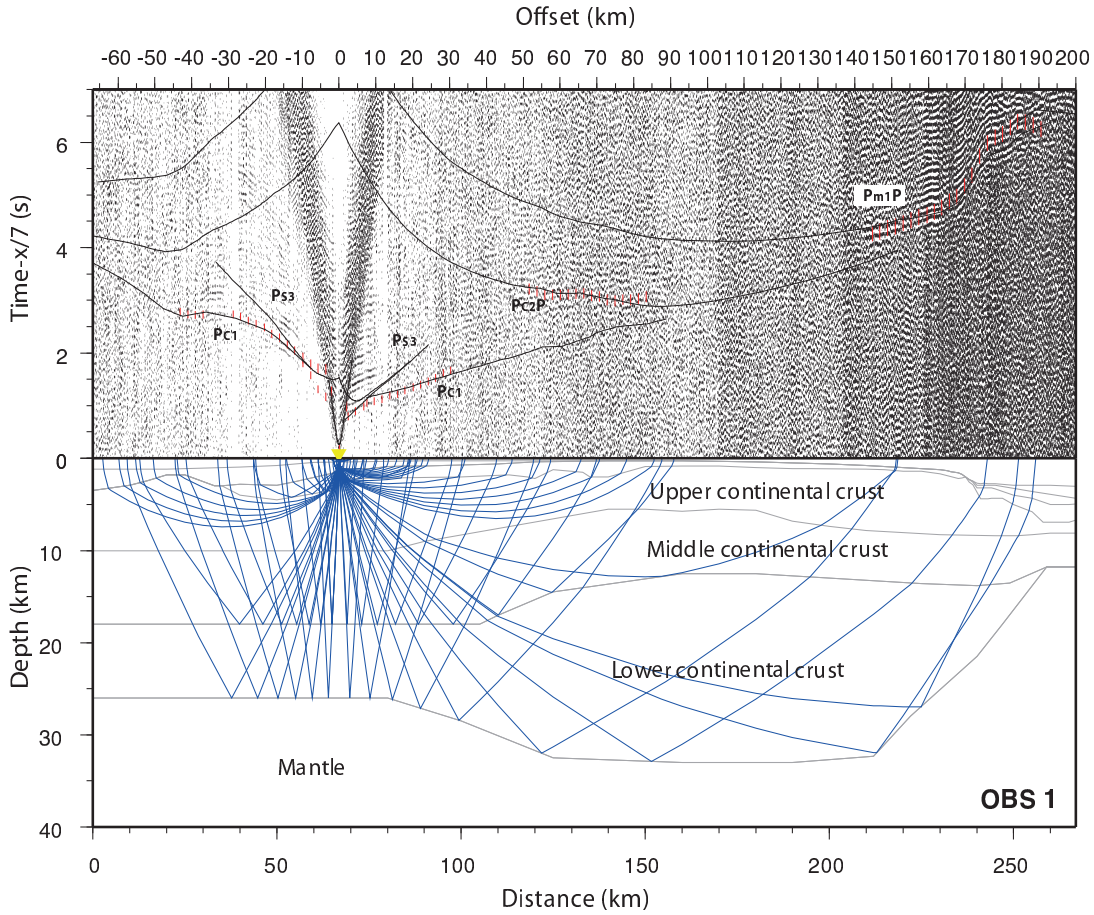

Figure B.1: Record section (top) with computed traveltimes and ray path diagram (bottom) for the vertical geophone of OBS 1. The vertical scale for the record section is traveltime (s) using a reduction velocity of 7.0 km s^{-1}, and the horizontal scale is shot-receiver distance (offset in km). The horizontal scale in the ray path diagram is distance (km) along the velocity model. Layers are labelled as interpreted in P-wave velocity model of Fig. 2.7.

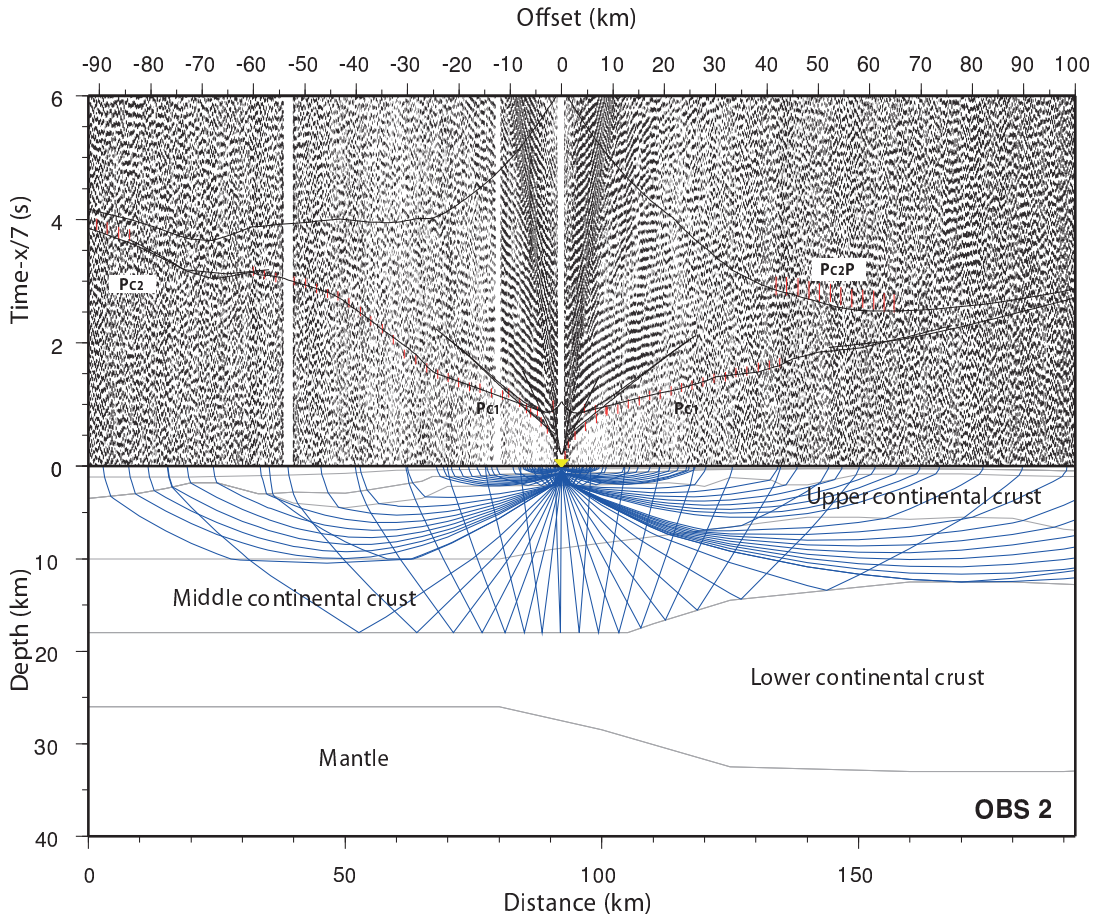

Figure B.2: Record section (top) with computed traveltimes and ray path diagram (bottom) for the vertical geophone of OBS 2. The vertical scale for the record section is traveltime (s) using a reduction velocity of 7.0 km s^{-1}, and the horizontal scale is shot-receiver distance (offset in km). The horizontal scale in the ray path diagram is distance (km) along the velocity model. Layers are labelled as interpreted in P-wave velocity model of Fig. 2.7.

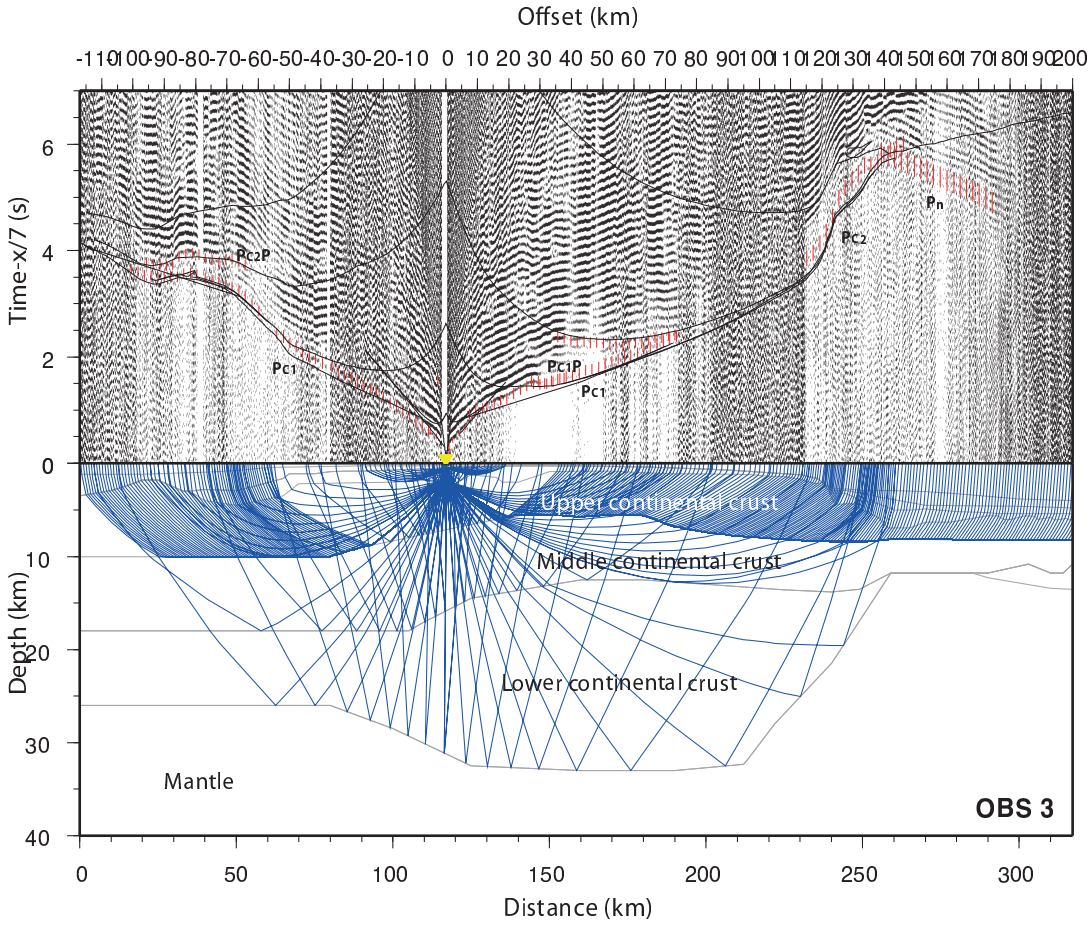

Figure B.3: Record section (top) with computed traveltimes and ray path diagram (bottom) for the vertical geophone of OBS 3. The vertical scale for the record section is traveltime (s) using a reduction velocity of 7.0 km s^{-1}, and the horizontal scale is shot-receiver distance (offset in km). The horizontal scale in the ray path diagram is distance (km) along the velocity model. Layers are labelled as interpreted in P-wave velocity model of Fig. 2.7.

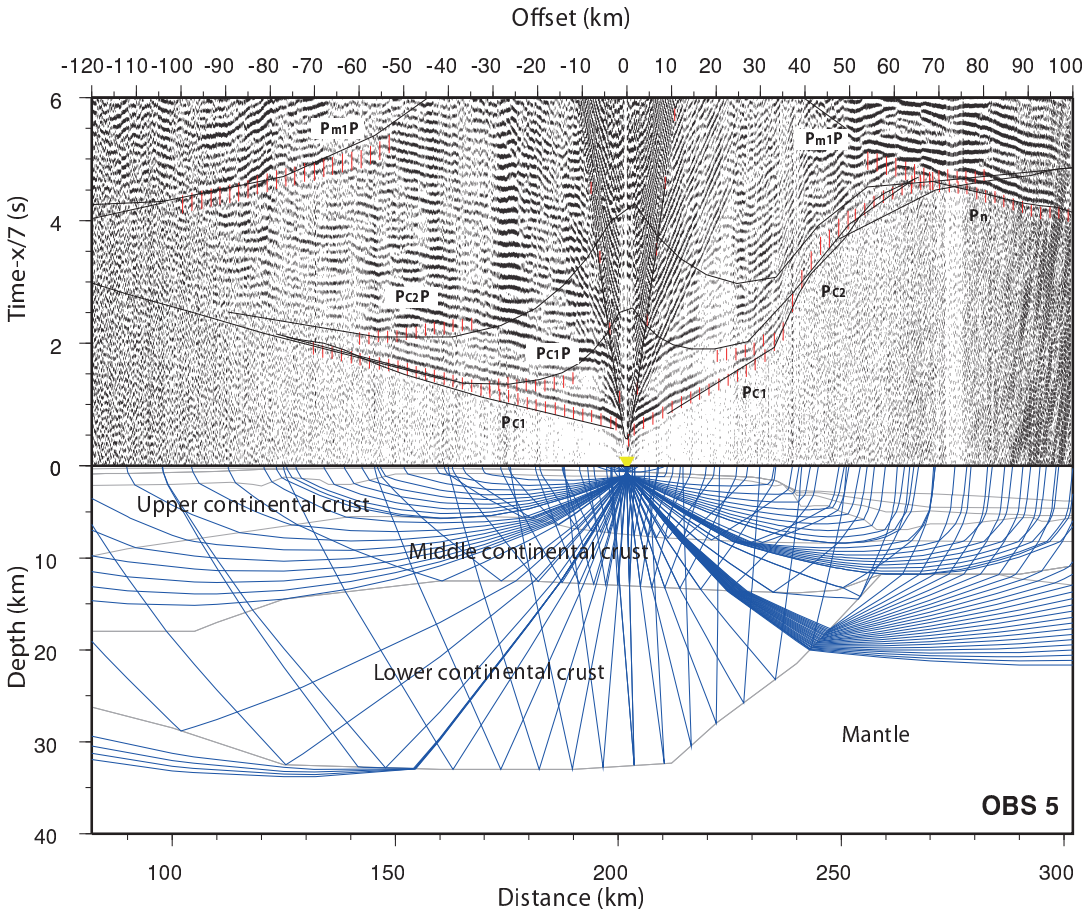

Figure B.4: Record section (top) with computed traveltimes and ray path diagram (bottom) for the vertical geophone of OBS 5. The vertical scale for the record section is traveltime (s) using a reduction velocity of 7.0 km s^{-1}, and the horizontal scale is shot-receiver distance (offset in km). The horizontal scale in the ray path diagram is distance (km) along the velocity model. Layers are labelled as interpreted in P-wave velocity model of Fig. 2.7.

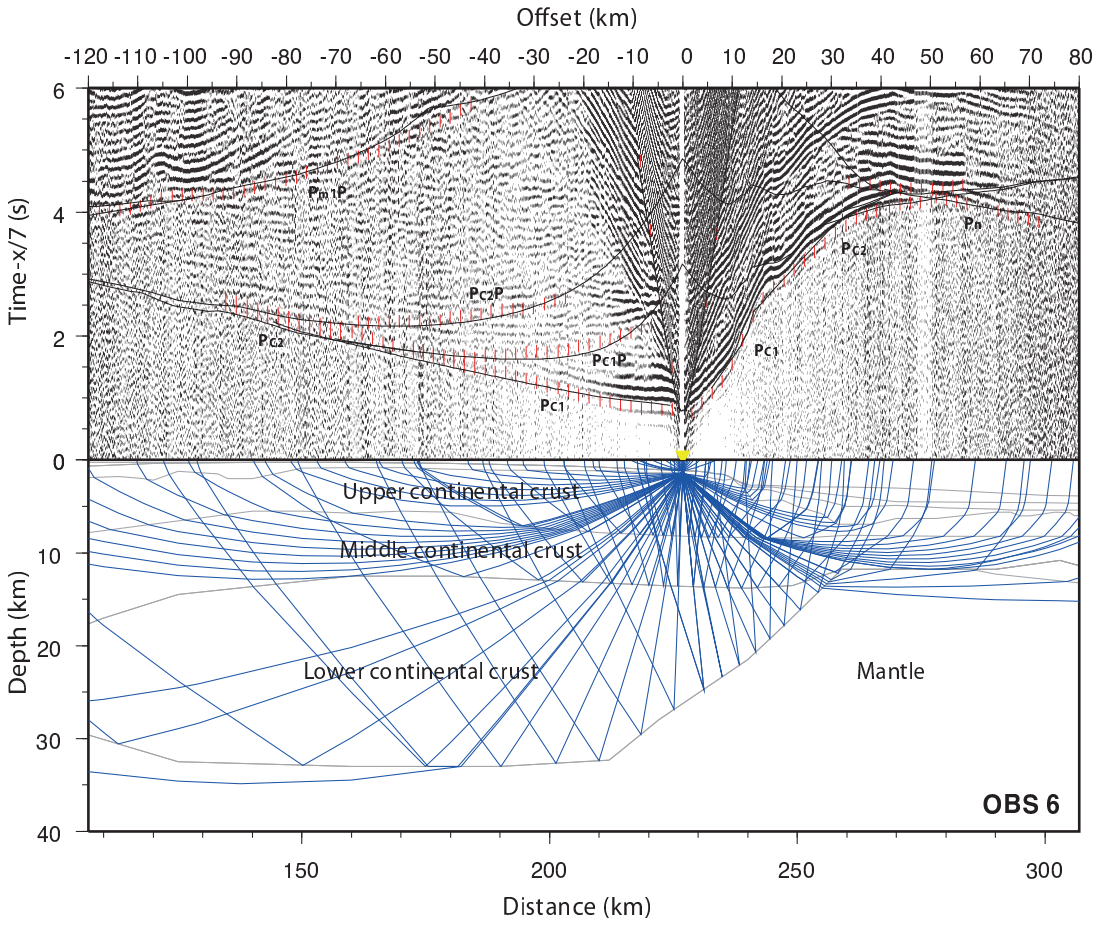

Figure B.5: Record section (top) with computed traveltimes and ray path diagram (bottom) for the vertical geophone of OBS 6. The vertical scale for the record section is traveltime (s) using a reduction velocity of 7.0 km s^{-1}, and the horizontal scale is shot-receiver distance (offset in km). The horizontal scale in the ray path diagram is distance (km) along the velocity model. Layers are labelled as interpreted in P-wave velocity model of Fig. 2.7.

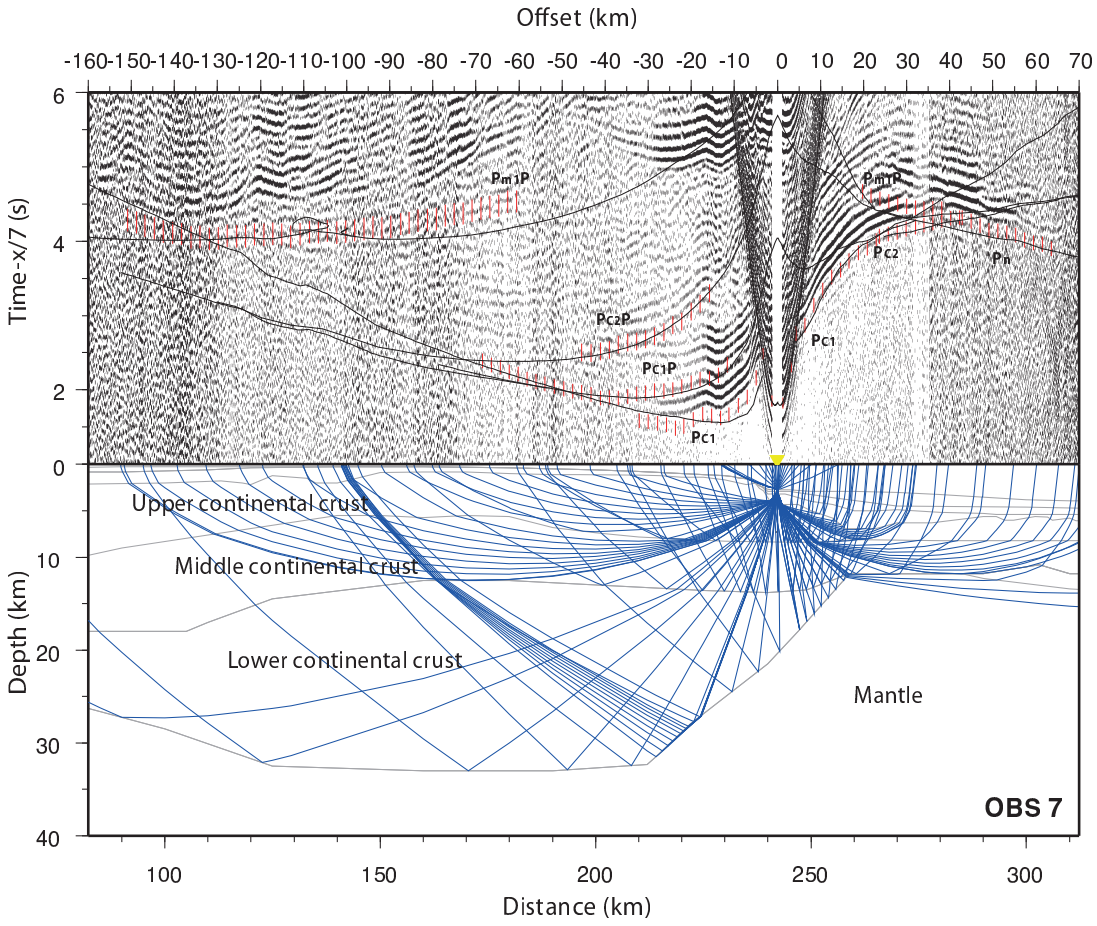

Figure B.6: Record section (top) with computed traveltimes and ray path diagram (bottom) for the vertical geophone of OBS 7. The vertical scale for the record section is traveltime (s) using a reduction velocity of 7.0 km s^{-1}, and the horizontal scale is shot-receiver distance (offset in km). The horizontal scale in the ray path diagram is distance (km) along the velocity model. Layers are labelled as interpreted in P-wave velocity model of Fig. 2.7.

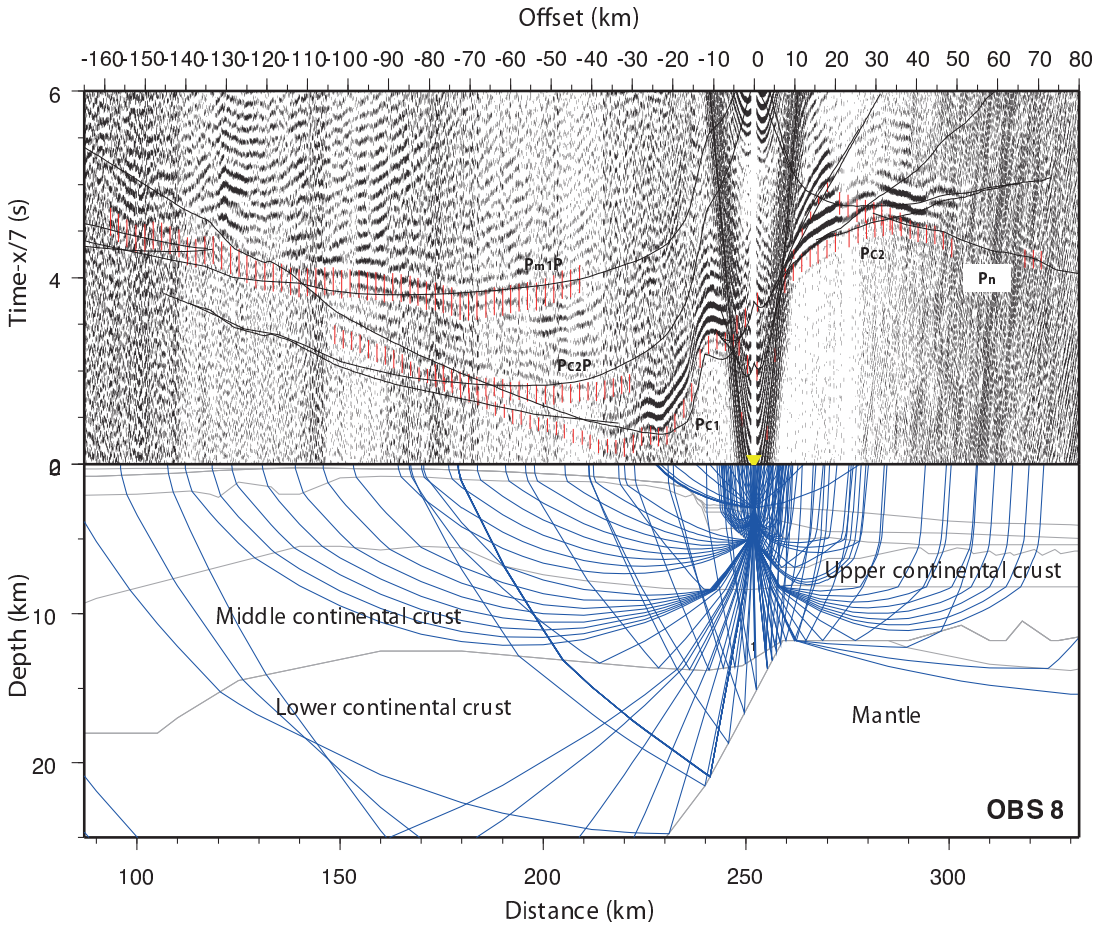

Figure B.7: Record section (top) with computed traveltimes and ray path diagram (bottom) for the vertical geophone of OBS 8. The vertical scale for the record section is traveltime (s) using a reduction velocity of 7.0 km s^{-1}, and the horizontal scale is shot-receiver distance (offset in km). The horizontal scale in the ray path diagram is distance (km) along the velocity model. Layers are labelled as interpreted in P-wave velocity model of Fig. 2.7.

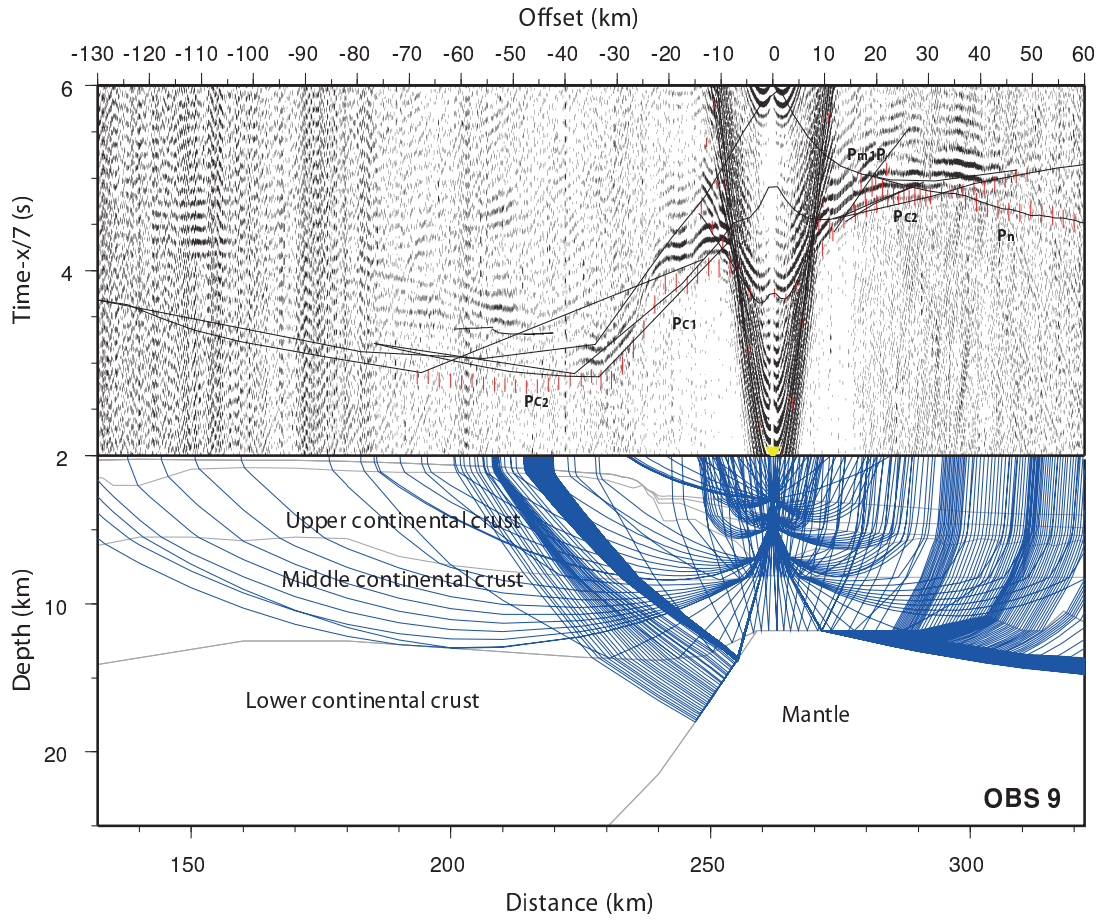

Figure B.8: Record section (top) with computed traveltimes and ray path diagram (bottom) for the vertical geophone of OBS 9. The vertical scale for the record section is traveltime (s) using a reduction velocity of 7.0 km s^{-1}, and the horizontal scale is shot-receiver distance (offset in km). The horizontal scale in the ray path diagram is distance (km) along the velocity model. Layers are labelled as interpreted in P-wave velocity model of Fig. 2.7.

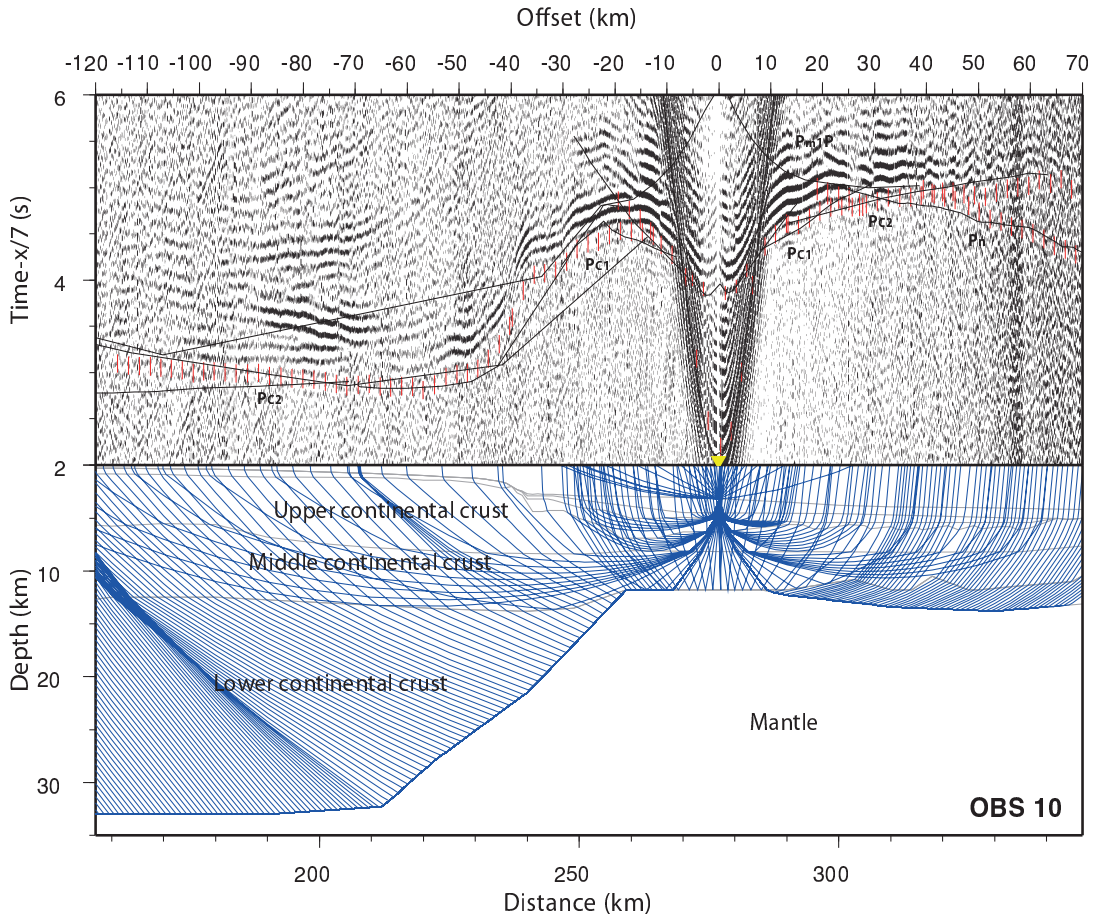

Figure B.9: Record section (top) with computed traveltimes and ray path diagram (bottom) for the vertical geophone of OBS 10. The vertical scale for the record section is traveltime (s) using a reduction velocity of 7.0 km s^{-1}, and the horizontal scale is shot-receiver distance (offset in km). The horizontal scale in the ray path diagram is distance (km) along the velocity model. Layers are labelled as interpreted in P-wave velocity model of Fig. 2.7.

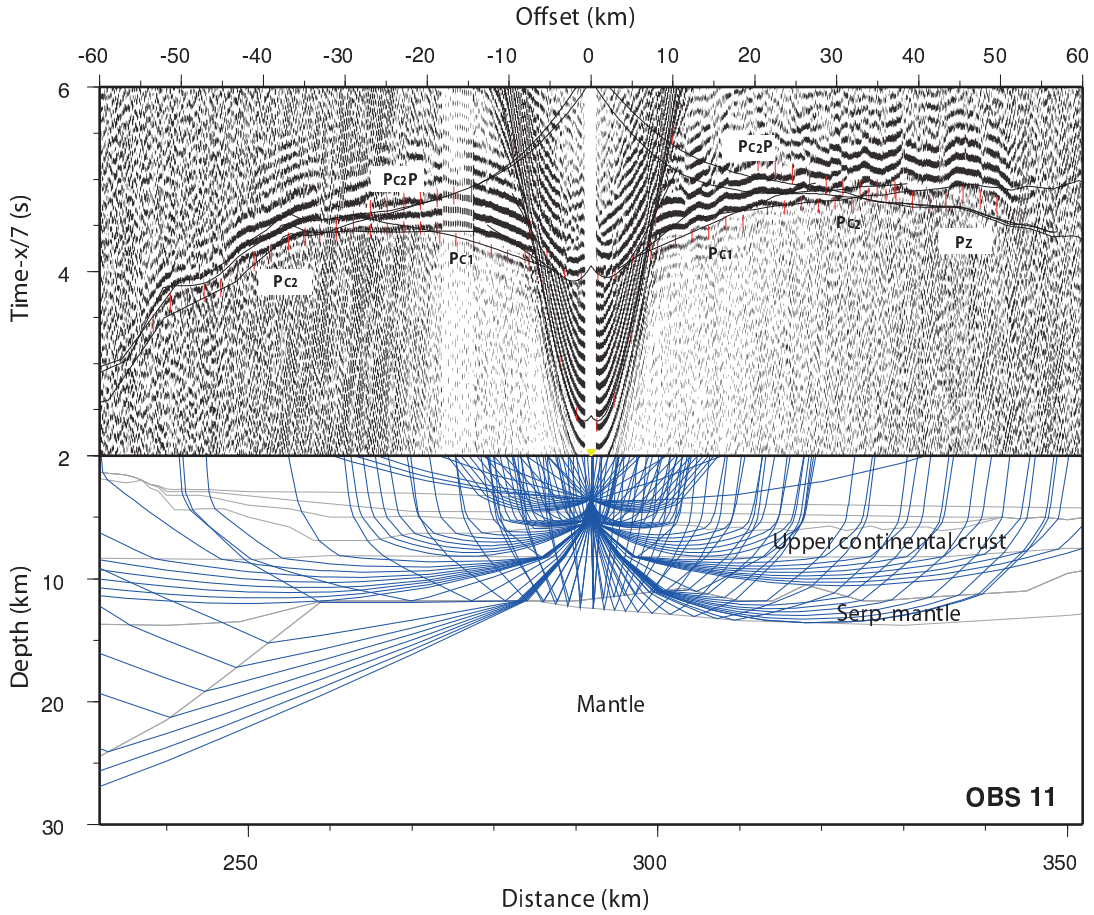

Figure B.10: Record section (top) with computed traveltimes and ray path diagram (bottom) for the vertical geophone of OBS 11. The vertical scale for the record section is traveltime (s) using a reduction velocity of 7.0 km s^{-1}, and the horizontal scale is shot-receiver distance (offset in km). The horizontal scale in the ray path diagram is distance (km) along the velocity model. Layers are labelled as interpreted in P-wave velocity model of Fig. 2.7.

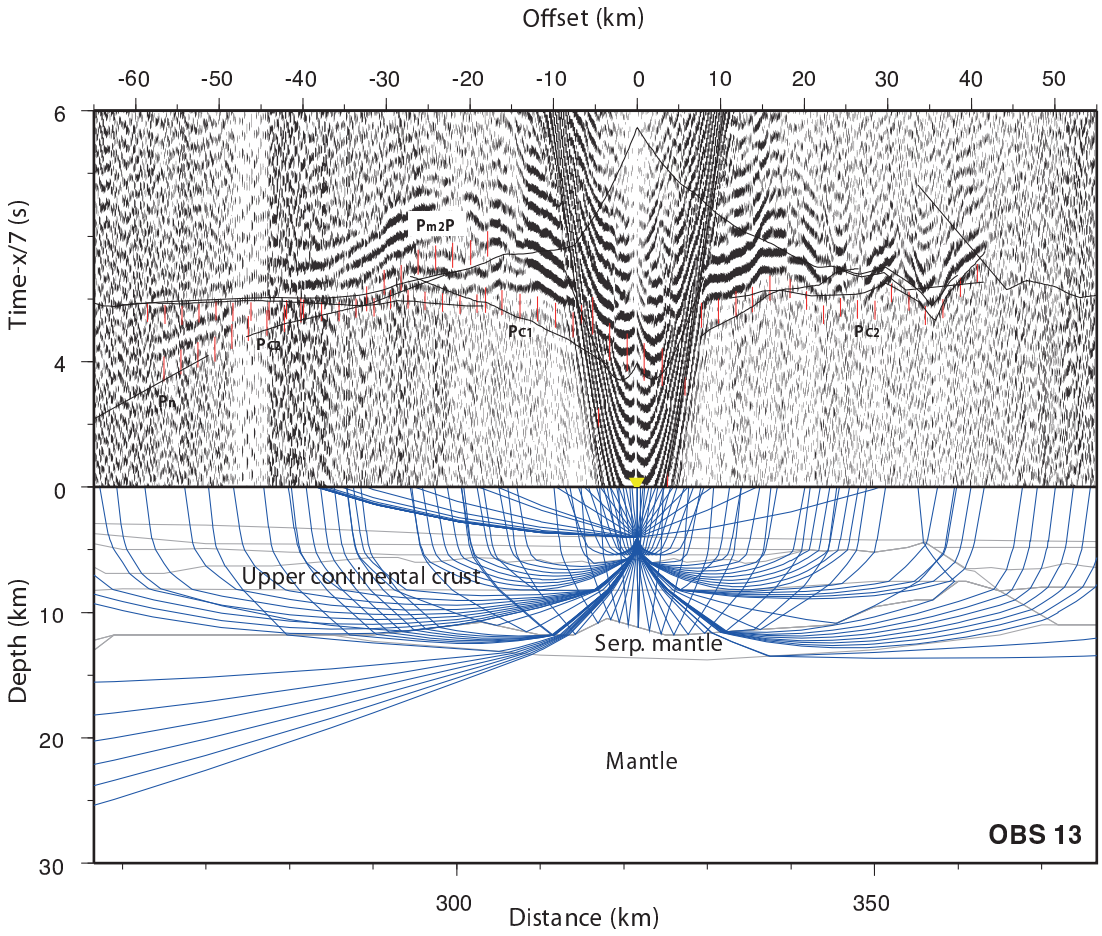

Figure B.11: Record section (top) with computed traveltimes and ray path diagram (bottom) for the vertical geophone of OBS 13. The vertical scale for the record section is traveltime (s) using a reduction velocity of 7.0 km s^{-1}, and the horizontal scale is shot-receiver distance (offset in km). The horizontal scale in the ray path diagram is distance (km) along the velocity model. Layers are labelled as interpreted in P-wave velocity model of Fig. 2.7.

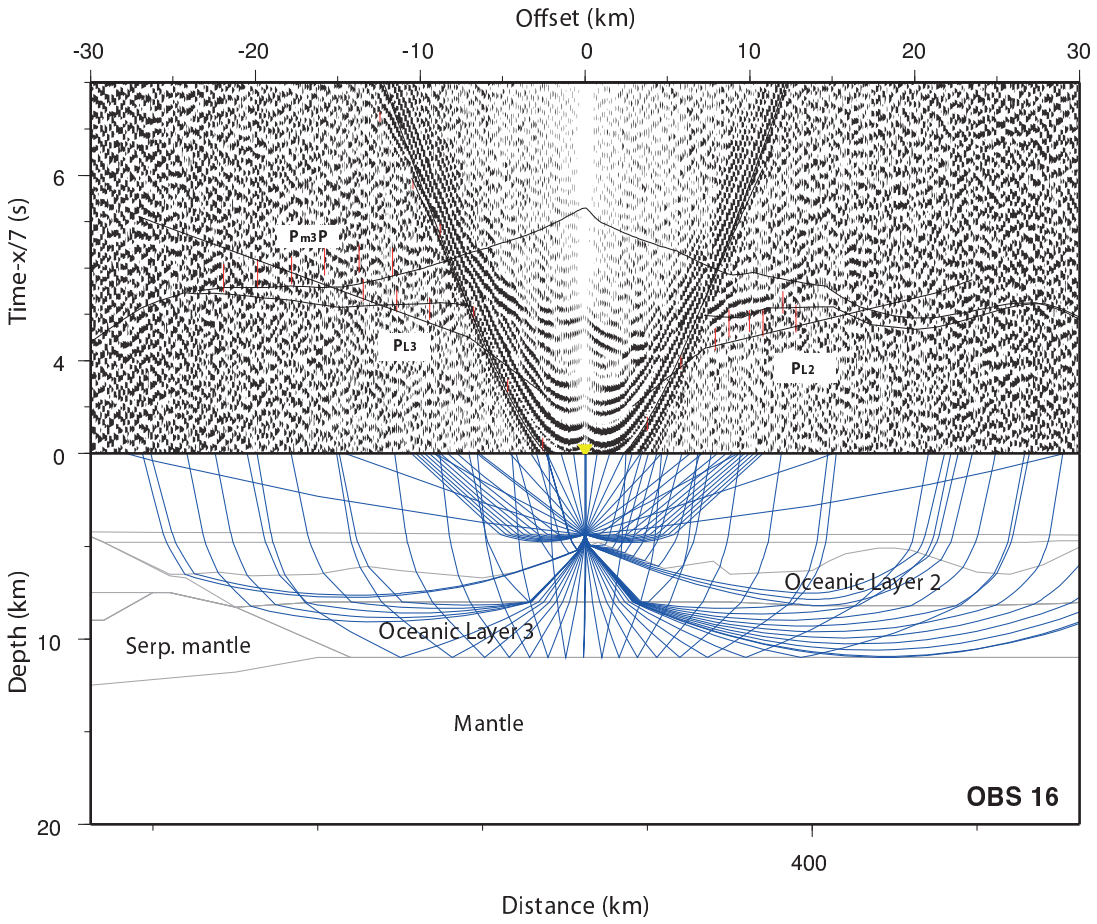

Figure B.12: Record section (top) with computed traveltimes and ray path diagram (bottom) for the vertical geophone of OBS 16. The vertical scale for the record section is traveltime (s) using a reduction velocity of 7.0 km s^{-1}, and the horizontal scale is shot-receiver distance (offset in km). The horizontal scale in the ray path diagram is distance (km) along the velocity model. Layers are labelled as interpreted in P-wave velocity model of Fig. 2.7.

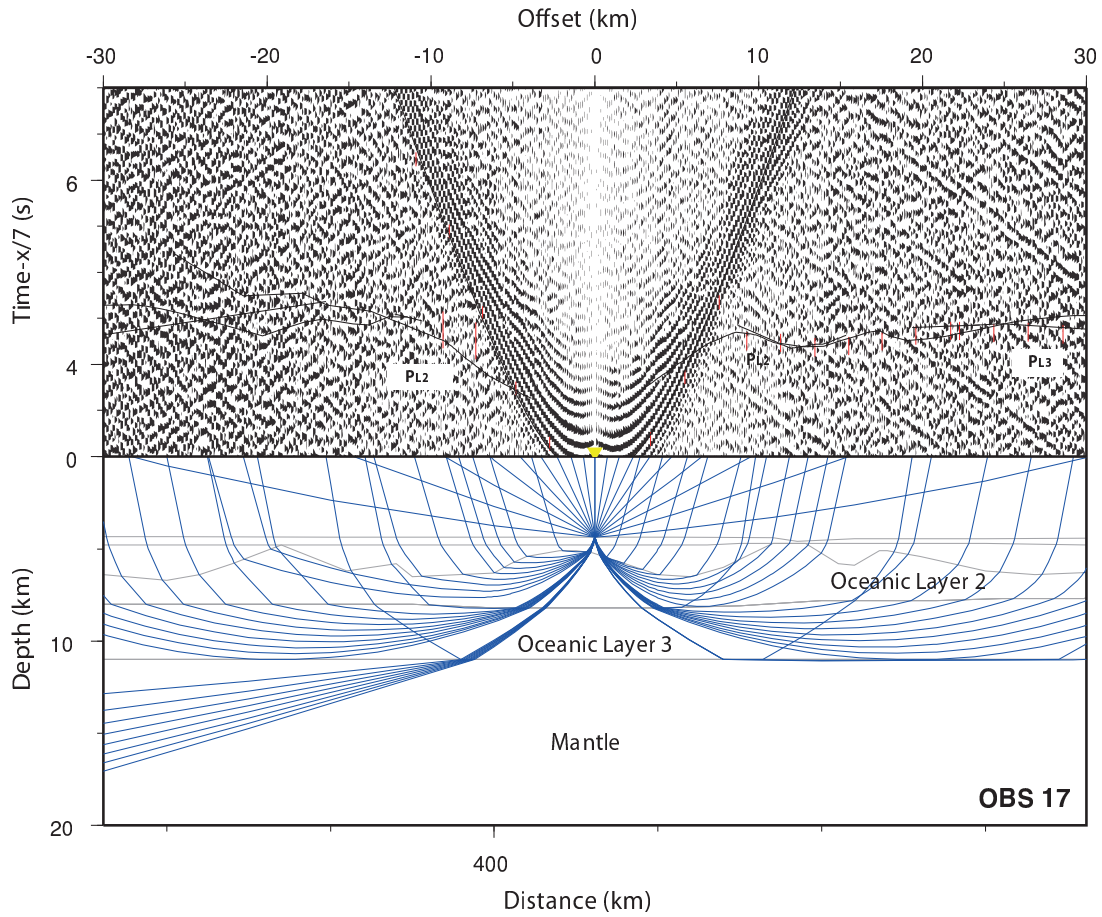

Figure B.13: Record section (top) with computed traveltimes and ray path diagram (bottom) for the vertical geophone of OBS 17. The vertical scale for the record section is traveltime (s) using a reduction velocity of 7.0 km s^{-1}, and the horizontal scale is shot-receiver distance (offset in km). The horizontal scale in the ray path diagram is distance (km) along the velocity model. Layers are labelled as interpreted in P-wave velocity model of Fig. 2.7.

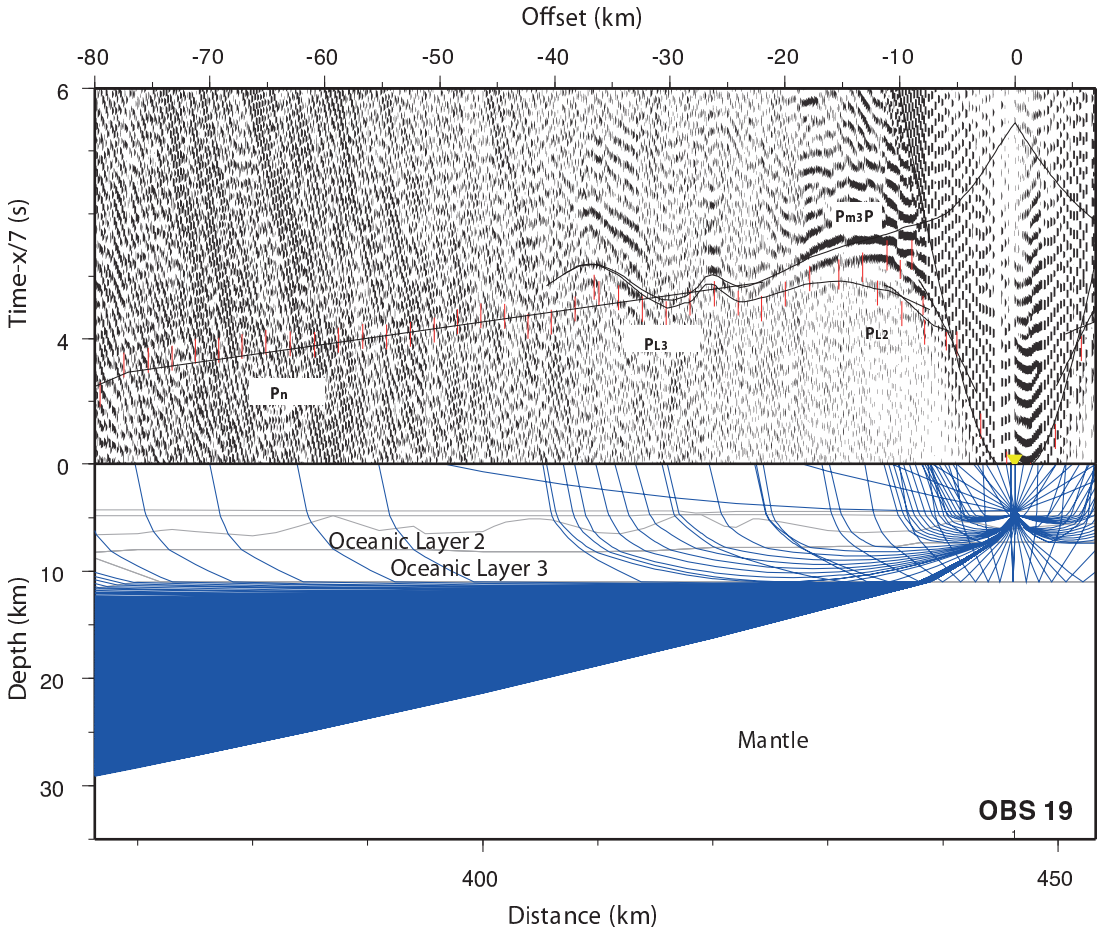

Figure B.14: Record section (top) with computed traveltimes and ray path diagram (bottom) for the vertical geophone of OBS 19. The vertical scale for the record section is traveltime (s) using a reduction velocity of 7.0 km s^{-1}, and the horizontal scale is shot-receiver distance (offset in km). The horizontal scale in the ray path diagram is distance (km) along the velocity model. Layers are labelled as interpreted in P-wave velocity model of Fig. 2.7.

Appendix C

Wide-angle Seismic Data: Full Error Analysis

C.1 P-wave phases

Table C.1: The number of observations (n), the root-mean-sqzares (rms) traveltime residzal (t_{rms}) and the normalized χ^2 for individual P-phases.

OBS	Phase	n	t_{rms}	χ^2
1	Direct	26	0.128	1.708
1	Ps3	68	0.079	1.126
1	Ps3P	29	0.091	0.854
1	Pc1	209	0.056	0.551
1	Pc2P	174	0.068	0.467
1	Pm1P	196	0.167	1.244
1		702	0.107	0.827
2	Direct	10	0.173	3.308
2	Ps1	14	0.071	0.972
2	Ps3	71	0.074	0.983
2	Ps3P	39	0.069	0.877
2	Pc1	392	0.044	0.348
2	Pc2	39	0.107	1.174
2	Pc2P	121	0.157	1.099
2		686	0.086	0.667
3	Direct	6	0.213	5.461
3	Ps3	58	0.022	0.194
3	Ps3P	19	0.020	0.041
3	Pc1	541	0.119	1.413
3	Pc1P	62	0.088	0.788
Continued on next page				

Table C.1 – *Continued from previous page*

OBS	Phase	n	t_{rms}	χ^2
3	Pc2	310	0.158	1.355
3	Pc2P	342	0.065	0.419
3	Pm1P	9	0.061	0.104
3		1347	0.115	1.049
4	Direct	6	0.150	2.698
4	Ps3	79	0.095	0.918
4	Pc1	573	0.065	0.761
4	Pc1P	113	0.047	0.393
4	Pc2	183	0.162	1.168
4	Pc2P	231	0.139	1.386
4	Pm1P	249	0.170	1.297
4	Pn	185	0.046	0.212
4		1619	0.112	0.900
5	Direct	76	0.125	1.571
5	Pc1	391	0.124	1.102
5	Pc1P	144	0.109	1.206
5	Pc2	240	0.092	0.855
5	Pc2P	136	0.124	1.538
5	Pm1P	284	0.160	1.142
5	Pn	220	0.056	0.316
5		1491	0.119	1.023
6	Direct	77	0.124	1.567
6	Pc1	450	0.100	1.010
6	Pc1P	256	0.104	1.078
6	Pc2	170	0.138	0.866
6	Pc2P	300	0.069	0.481
6	Pm1P	381	0.111	1.231

Continued on next page

Table C.1 – *Continued from previous page*

OBS	Phase	n	t_{rms}	χ^2
6	Pn	75	0.058	0.339
6		1709	0.103	0.955
7	Direct	25	0.055	0.557
7	Pc1	197	0.114	1.299
7	Pc1P	288	0.082	0.674
7	Pc2	63	0.042	0.179
7	Pc2P	148	0.038	0.149
7	Pm1P	457	0.188	1.571
7	Pm2P	70	0.149	1.003
7	Pn	75	0.097	0.948
7		1323	0.133	1.021
8	Direct	43	0.071	0.921
8	Ps2P	18	0.124	1.625
8	Ps3	42	0.044	0.795
8	Ps3P	14	0.114	1.408
8	Pc1	360	0.073	0.710
8	Pc2	45	0.069	0.493
8	Pc2P	246	0.113	1.291
8	Pm1P	581	0.122	0.659
8	Pm2P	51	0.087	0.532
8	Pn	65	0.067	0.456
8		1465	0.102	0.784
9	Direct	52	0.069	0.862
9	Ps1	25	0.054	1.214
9	Ps2	23	0.055	1.243
9	Ps2P	37	0.022	0.206
9	Ps3	62	0.081	1.198
9	Pc1	126	0.096	0.934

Continued on next page

Table C.1 – *Continued from previous page*

OBS	Phase	n	t_{rms}	χ^2
9	Pc1P	15	0.091	0.881
9	Pc2	266	0.077	1.060
9	Pm2P	48	0.139	1.961
9	Pn	192	0.034	0.117
9		846	0.076	0.835
10	Direct	49	0.111	1.268
10	Ps2P	34	0.048	0.424
10	Ps3	61	0.072	0.529
10	Pc1	121	0.105	1.119
10	Pc2	509	0.091	0.823
10	Pm2P	31	0.136	1.324
10	Pn	118	0.082	0.686
10		923	0.093	0.845
11	Direct	44	0.073	0.976
11	Ps1	47	0.100	1.028
11	Ps2P	40	0.031	0.403
11	Ps3	10	0.075	0.632
11	Pc1	81	0.058	0.612
11	Pc2	118	0.038	0.268
11	Pm2P	70	0.061	0.375
11	Pz	61	0.106	1.138
11	PzP	62	0.110	1.225
11	Pn	161	0.112	1.268
11		694	0.085	0.812
12	Direct	46	0.067	0.827
12	Ps2P	37	0.097	0.963
12	Pc1	80	0.104	1.106
12	Pc2	156	0.056	0.319

Continued on next page

Table C.1 – *Continued from previous page*

OBS	Phase	n	t_{rms}	χ^2
12	Pm2P	45	0.079	0.633
12	Pz	92	0.079	0.627
12	PzP	101	0.147	1.525
12	Pn	321	0.151	1.019
12		878	0.118	0.880
13	Direct	51	0.063	0.718
13	Ps2P	36	0.174	1.380
13	Pc1	78	0.102	1.048
13	Pc2	232	0.075	1.016
13	Pm2P	53	0.112	1.274
13	Pn	153	0.129	0.775
13		603	0.105	0.970
14	Direct	42	0.050	0.446
14	Ps1P	10	0.150	1.109
14	Pc1	56	0.102	1.052
14	Pc2	44	0.103	1.080
14	Pz	178	0.080	0.648
14	PzP	18	0.146	1.003
14	Pn	75	0.122	1.504
14		423	0.097	0.890
15	Direct	60	0.063	0.715
15	Ps1P	25	0.101	1.055
15	Ps2P	21	0.104	0.785
15	PL2	22	0.124	1.619
15	Pc1	27	0.134	1.874
15	PL3	30	0.055	0.308
15	Pz	107	0.136	0.980

Continued on next page

Table C.1 – *Continued from previous page*

OBS	Phase	n	t_{rms}	χ^2
15	Pn	79	0.136	1.297
15		371	0.117	1.027
16	Direct	59	0.052	0.496
16	Ps1	6	0.022	0.242
16	PL2	39	0.099	0.702
16	PL3	16	0.130	0.802
16	Pm3P	47	0.126	0.722
16		167	0.097	0.614
17	Direct	70	0.064	0.750
17	PL2	12	0.235	1.502
17	PL3	47	0.078	0.621
17	Pn	23	0.095	0.949
17		152	0.097	0.780
18	Direct	42	0.053	0.509
18	Ps2	21	0.122	1.553
18	PL2	37	0.109	1.217
18	PL3	109	0.109	1.207
18	Pm3P	30	0.092	0.873
18	Pn	233	0.185	1.535
18		472	0.148	1.290
19	Direct	38	0.110	1.253
19	Ps2	10	0.082	1.314
19	PL2	18	0.092	0.904
19	PL3	75	0.066	0.439
19	Pm3P	26	0.147	1.551
19	Pn	202	0.114	1.314
19		369	0.107	1.111
	Direct	822	0.090	1.011

Continued on next page

Table C.1 – *Continued from previous page*

OBS	Phase	n	t_{rms}	χ^2
	Ps3	451	0.073	0.822
	Ps3P	101	0.078	0.763
	Pc1	3682	0.093	0.928
	Pc2P	1698	0.099	0.804
	Pm1P	2157	0.151	1.139
	Ps1	92	0.082	0.992
	Pc2	2375	0.106	0.893
	Pc1P	878	0.091	0.850
	Pn	2177	0.115	0.844
	Pm2P	368	0.112	0.947
	Ps2P	223	0.097	0.736
	Ps2	54	0.091	1.325
	Pz	438	0.100	0.787
	PzP	181	0.135	1.357
	Ps1P	35	0.117	1.038
	PL2	128	0.124	1.074
	PL3	277	0.091	0.769
	Pm3P	103	0.123	0.954
Total		16240	0.109	0.921

C.2 S-wave phases

Table C.2: The number of observations (n), the root-mean-sqzares (rms) traveltime residzal (t_{rms}) and the normalized χ^2 for individual S-phases.

OBS	Phase	n	t_{rms}	χ^2
2	Sc1	123	0.117	1.380
5	Sc1	178	0.080	0.650
6	Sc1	278	0.092	0.850
8	Sc2S	54	0.052	0.270
9	Sc2	132	0.142	0.900
10	Sc2	216	0.111	1.220
10	Sc2S	83	0.043	0.180
10		299	0.097	0.930
11(west)	Sc2	59	0.105	1.110
11(west)	Sc2S	31	0.122	1.530
11(west)		90	0.111	1.239
11(east)	Sc2	57	0.092	0.860
11(east)	Sc2S	41	0.084	0.730
11(east)		98	0.089	0.798
12	Sc2	134	0.124	1.540
13(west)	Sc2	107	0.113	1.290
13(west)	Sc2S	51	0.169	1.280
13(west)		158	0.134	1.279
13(east)	Sc2	31	0.057	0.330
13(east)	Sc2S	60	0.107	0.520
13(east)		91	0.093	0.451
	Sc1	579	0.095	0.898
	Sc2S	320	0.100	0.623
	Sc2	736	0.116	1.149
Total		1635	0.106	0.956

Appendix D

Supplementary Material from Section 3.1

The material can also be found at: GSA Data Repository item 2012320, seismic reflection profiles, is available on-line at www.geosociety.org/pubs/ft2012.htm, or on request from editing@geosociety .org or Documents Secretary, GSA, P.O. Box 9140, Boulder, CO 80301, USA.

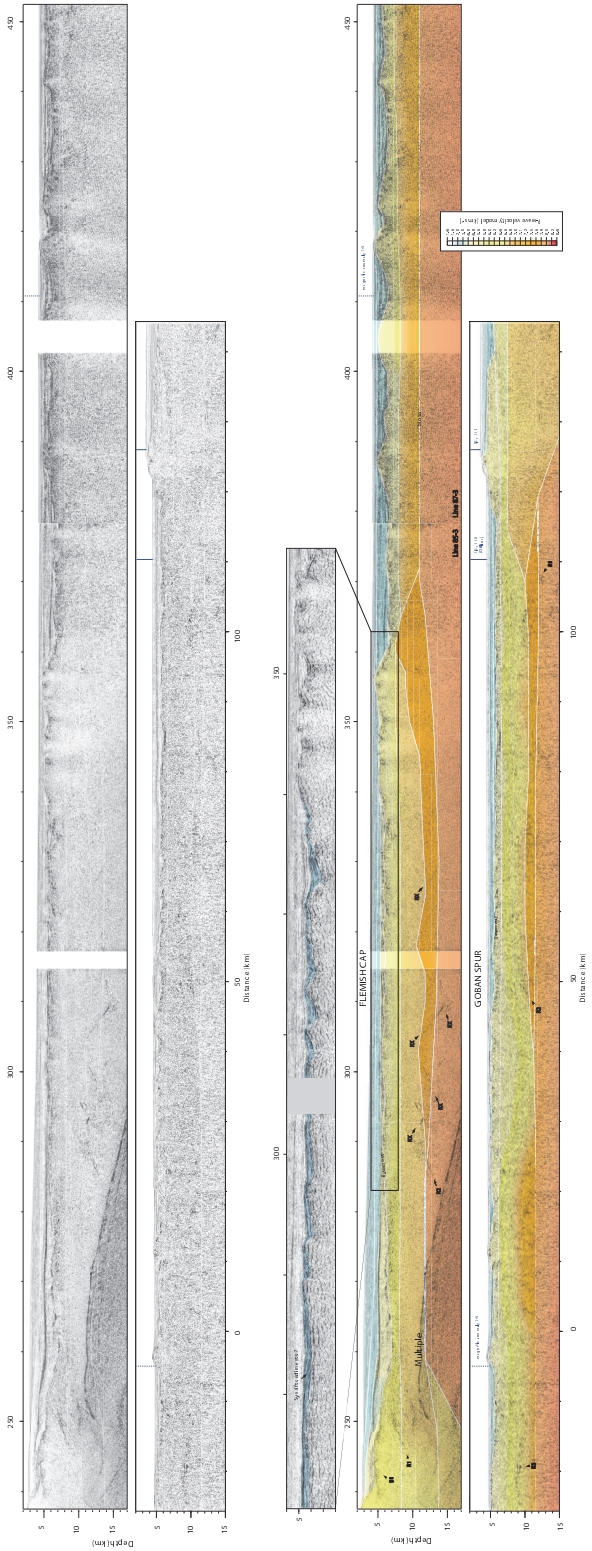
FLEMISH CAP
GORAN SPUR
Distance (km)
Depth (km)

Supplementary material:

The figure shows the multichannel seismic depth profiles of Flemish Cap (Line 85-3, Line 87-3) and Goban Spur (WAM Line). We have reprocessed Line 85-3 with **FOCUS 5.4** starting from the raw field tapes. Processing flowchart is shown in the tables 1 below. Line 87-3 was processed by Western Geophysical in 1988. Full details of processing applied are given in Western Geophysical (1988). The WAM Line was processed by Seismograph Services, Ltd (SSL). Full details are given in Klemperer (1989). Poststack time migration at 1.48 km s^{-1} was done by Bullock and Minshull (2005). We have time-to-depth converted the three time migrated profiles using **SeisWide 5.9** and the velocity models derived from the wide-angle data. The lower two sections are identical to Figure 3 in the paper, except the sections have no vertical exaggeration. The sections have the multichannel seismic data superimposed on the velocity models (Bullock and Minshull, 2005 and Gerlings et al., 2011). Layer boundaries of the velocity model are indicated by white lines. The velocity model of Bullock and Minshull (2005), which deviates by up to 8 km from the WAM profile (Figure 1), has been modified to better fit the seabed, basement and sedimentary layer boundaries. The upper two sections show the multichannel seismic profiles with no vertical exaggeration. The middle section is a close-up of the basement feature of Line 85-3 showing tilted fault blocks overlain by a (syn-rift?) sediment package (light blue).

Table 1. Reprocessing of Line 85-3:

SEGD to SEGY	Noise attenuation
Edit duplicated shots	Multiple removal, Radon
Nominal geometry, CMP binning 12.5 m	Velocity analysis
Edit shot gathers	Stack
Spherical divergence	AGC
Surface consistence amplitude balancing	Kirchhoff time migration
Noise attenuation on low frequencies (0-12 Hz)	Coherency filter
Surface consistence deconvolution	Bandpass filter (0-5-70-80 Hz)
(preliminary velocity analysis combined with velocity model of wide-angle seismic data)	Water bottom mute

References:

Bullock, A.D., and Minshull, T.A., 2005 From continental extension to seafloor spreading: crustal structure of the Goban Spur rifted margin, southwest of the UK, Geophysical Journal International, v. 163, p. 527-546.

Gerlings, J., Louden, K.E. and Jackson, J.R., 2011, Crustal structure of the Flemish Cap Continental Margin (Eastern Canada): An analysis of a seismic refraction profile, Geophysical Journal International, v. 185, p. 30-48.

Appendix E

Multi-channel Seismic Data

Here you find the tables of processing steps also shown in Section 3.2, examples of job flows from some of the processing steps and some figures of shots and stacked sections.

E.1 Processing steps

The seismic processing was done with the software package **FOCUS 5.4** and **GeoDepth 8.2** from Paradigm.

Table E.1: Reprocessing of Line 85-3 (time section)

Step	Process	Focus Module	Details in Appendix or Section
1	SEGD to SEGY		
2	Edit duplicated shots	EDIT HEADDEL HEADPUT	App. E.5
3	Nominal geometry, CMP binning 12.5 m	MARINE	App. E.5.1
4	Edit shot gathers	EDIT	
5	Spherical divergence	GAIN	App. E.5.2
6	Surface consistence amplitude balancing	BALAN BASOL BALAPP	App. E.5.3
7	Noise attenuation on low frequencies (0-12 Hz)	SUPPRES	App. E.5.4
8	preliminary velocity analysis combined with velocity model of wide-angle seismic data	VELDEF	
9	LIFT - Noise attenuation		Sec. 3.1 and App. E.5.5
10	K-filter	WNFILT	App. E.5
11	Shot interpolation (shot distance 25 m, before 50 m)	HXINT	App. E.5.7
12	New geometry	MARINE	
13	Noise attenuation	LIFT	Sec. 3.1
14	SRME	SMACMS SMACTRM	App. E.5.8
15	Radon LIFT	PRADMUS	Sec 3.1 and App. E.5.9
16	Velocity analysis	VELDEF	
17	Stack	STACK	
18	Kirchhoff time migration	MIGTX	
19	Coherency filter	COHERE	
20	Bandpass filter (0-5-70-80 Hz)	FILTER	
21	Water bottom mute	MUTE	
22	AGC	AGC	

Table E.2: Reprocessing of Line 85-3 (depth section)

Step	Process	
16	Residual velocity analysis	Geodepth
17	Kirchhoff depth migration	Geodepth
18	Stack	Geodepth
19	Coherency filter	Focus/COHERE
20	Bandpass filter (0-5-70-80 Hz)	Focus/FILTER
21	Water bottom mute	Focus/MUTE
22	AGC	Focus/AGC

E.2 Shot gathers of the important processing steps

Figure E.1-E.3 show a shot gather from the processing step: nominal geometry, spherical divergence, surface related amplitude balancing, noise attenuation on low frequencies, k-filtering, interpolation of shots, LIFT, SRME, LIFT radon transform. Notice that the shot gathers are not to same scale.

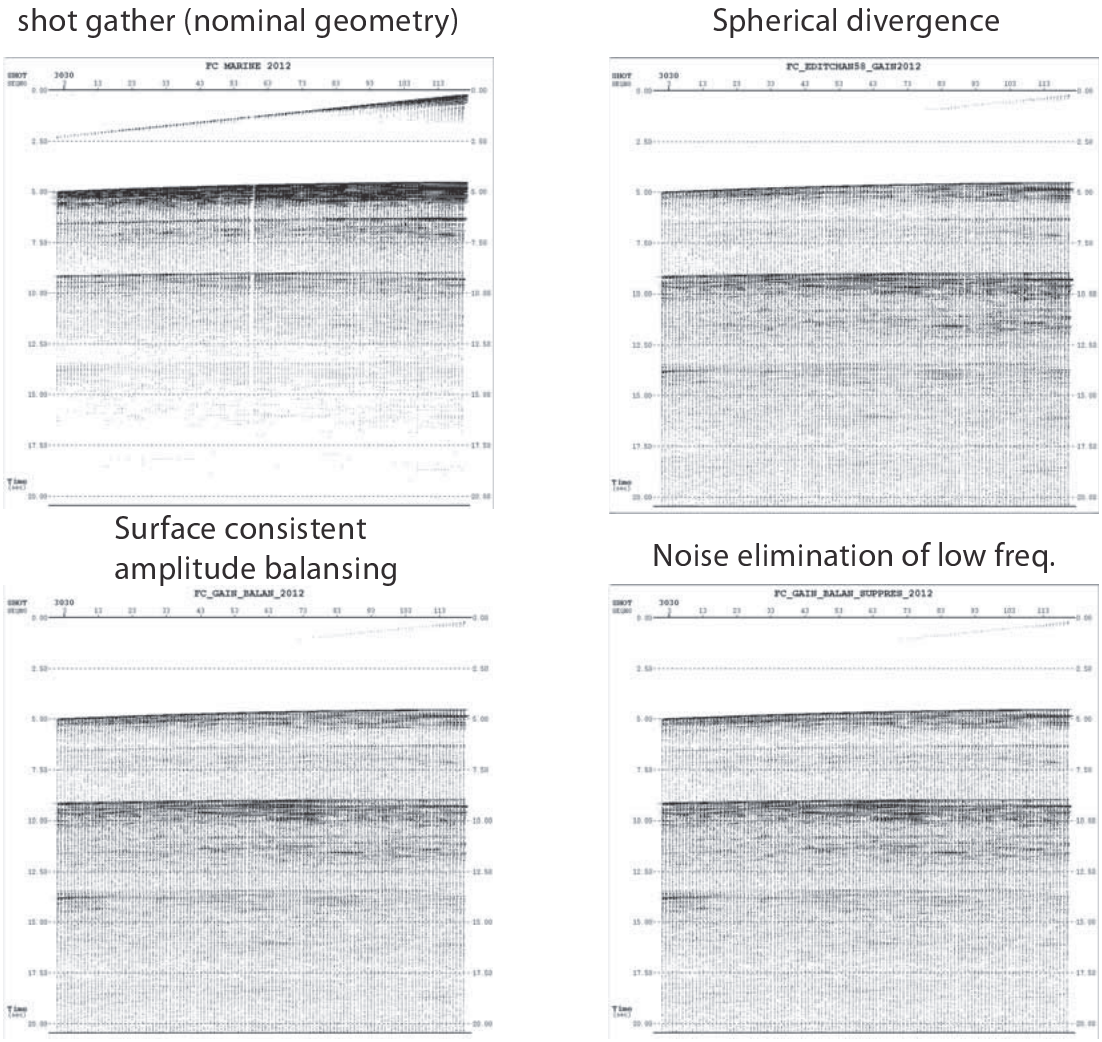

Figure E.1: Shot gather with left) nominal geometry, middle spherical divergence and right) surface related amplitude balancing applied. The shot gathers are not to the same scale.

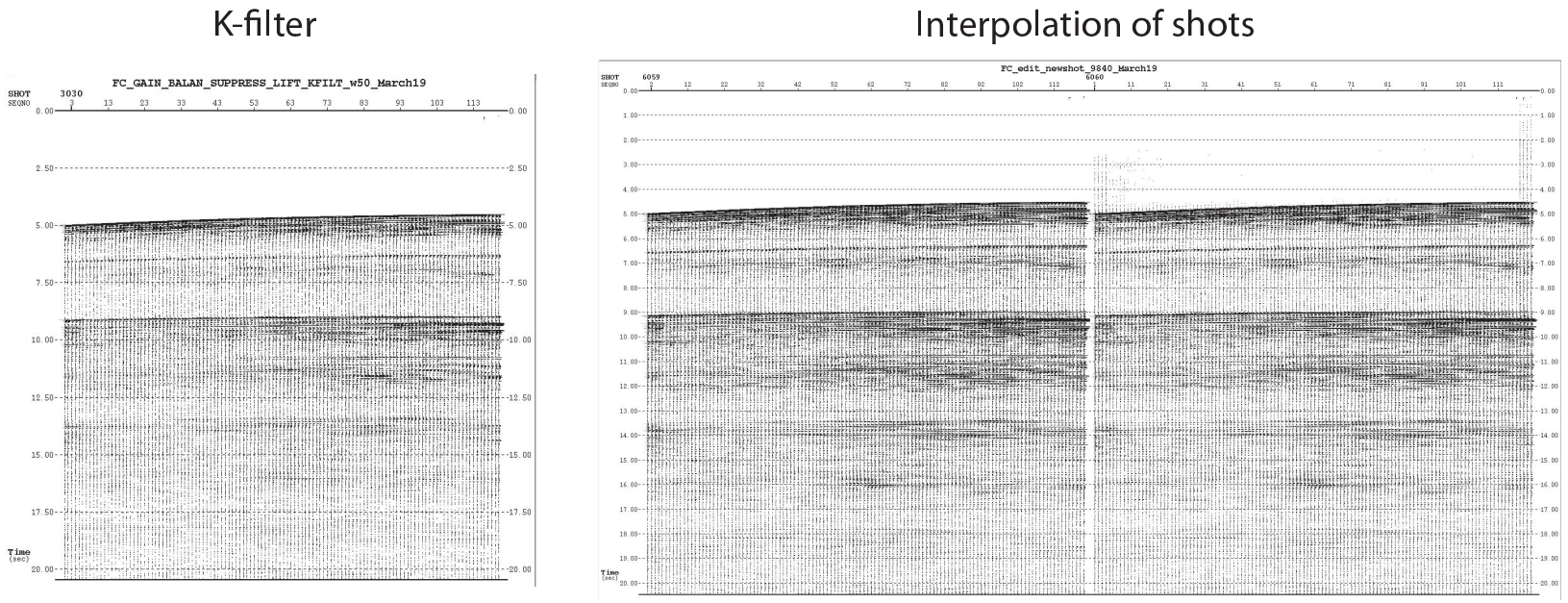

Figure E.2: Shot gather with left) k-filter and right) interpolation to double the shots applied. Notice that the interpolated 'new' shot is more noisy that the original. LIFT will reduce the noise and increase the S/N ratio. The shot gathers are not to the same scale.

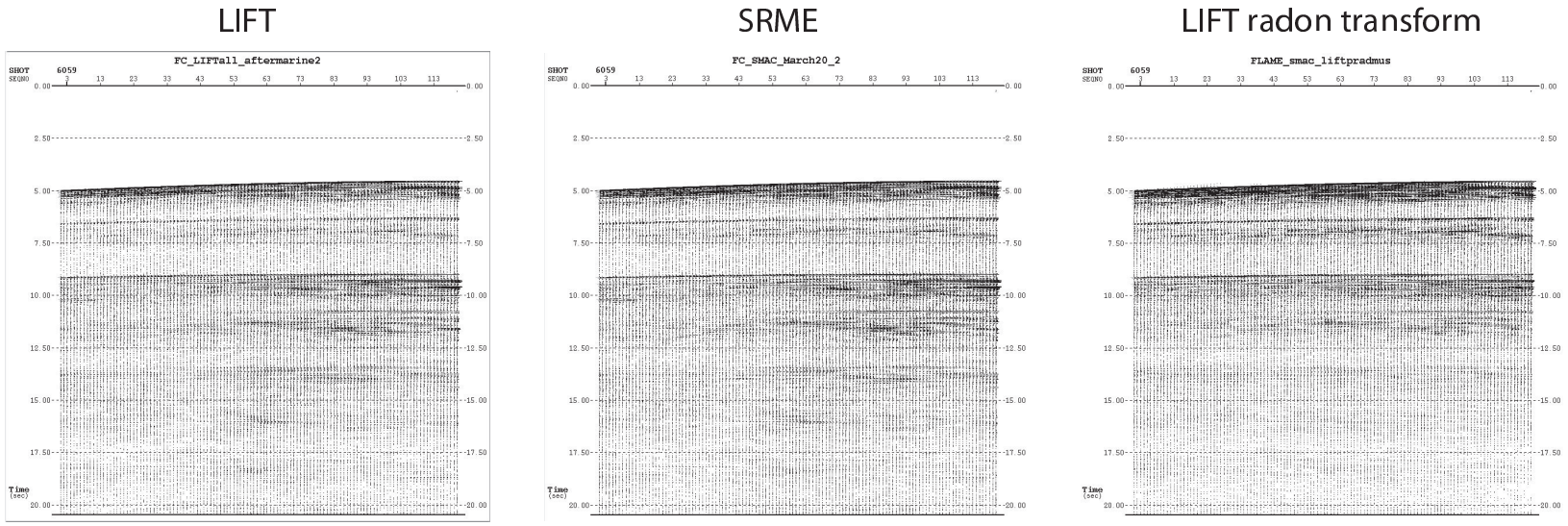

Figure E.3: Shot gather with left) LIFT, middle SRME and right) LIFT radon transform applied. The shot gathers are not to the same scale.

E.3 Examples of types of noise LIFT can attenuate

Figure E.4-E.6 show example of type of noise LIFT can eliminate.

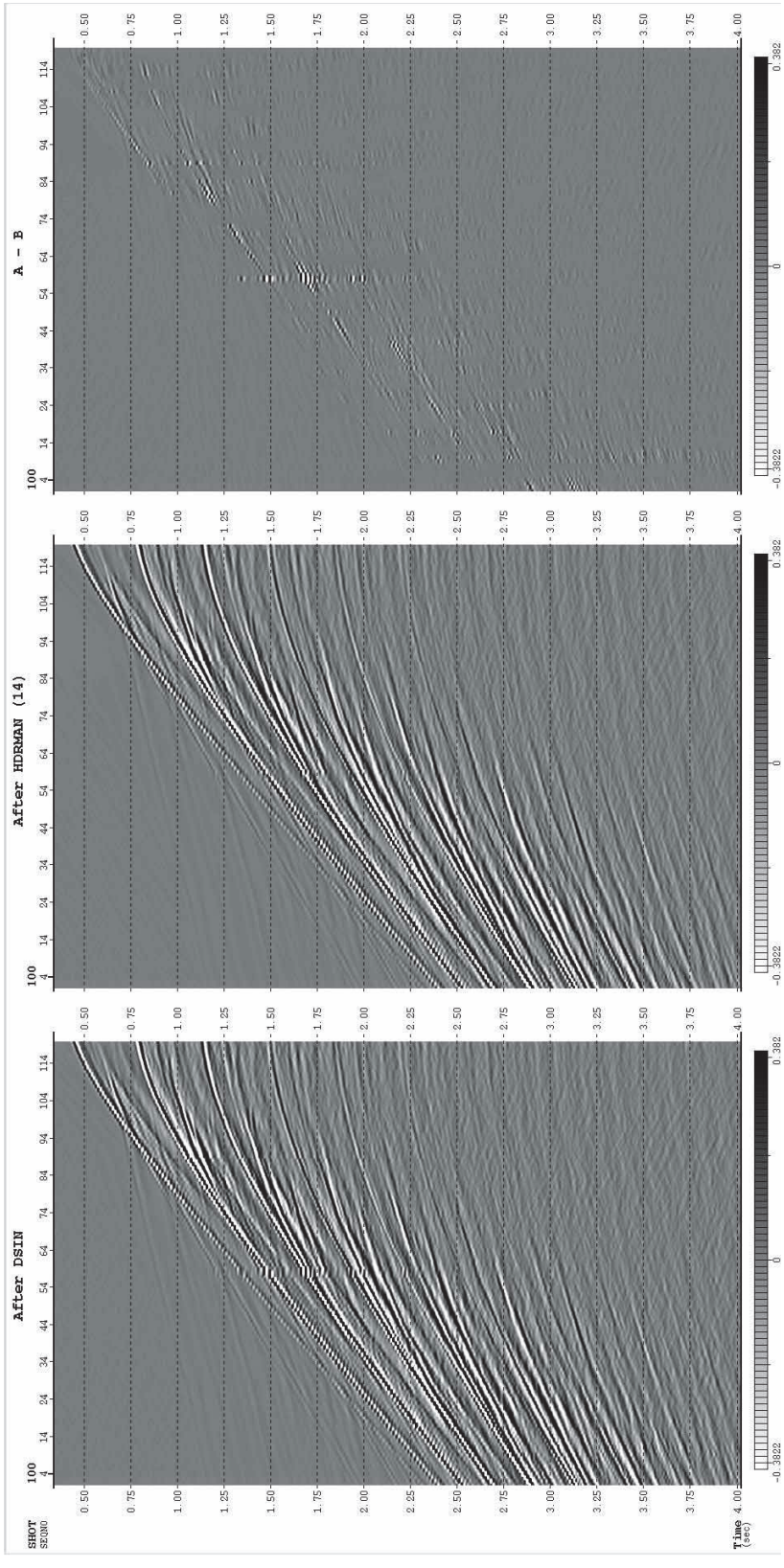

Figure E.4: Lift noise attenuation example. left) before; middle) after; right) difference

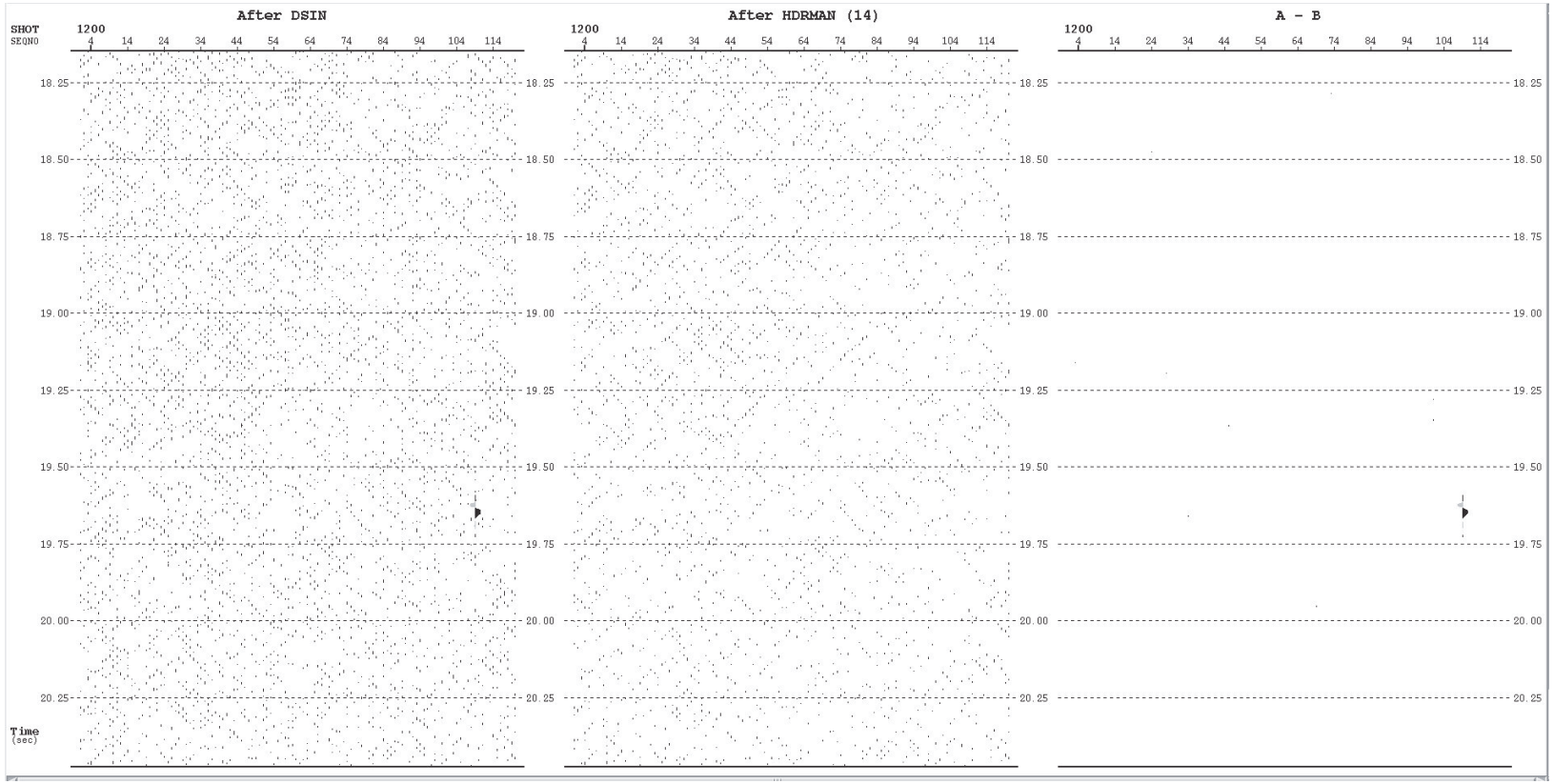

Figure E.5: Lift noise attenuation example. left) before; middle) after; right) difference

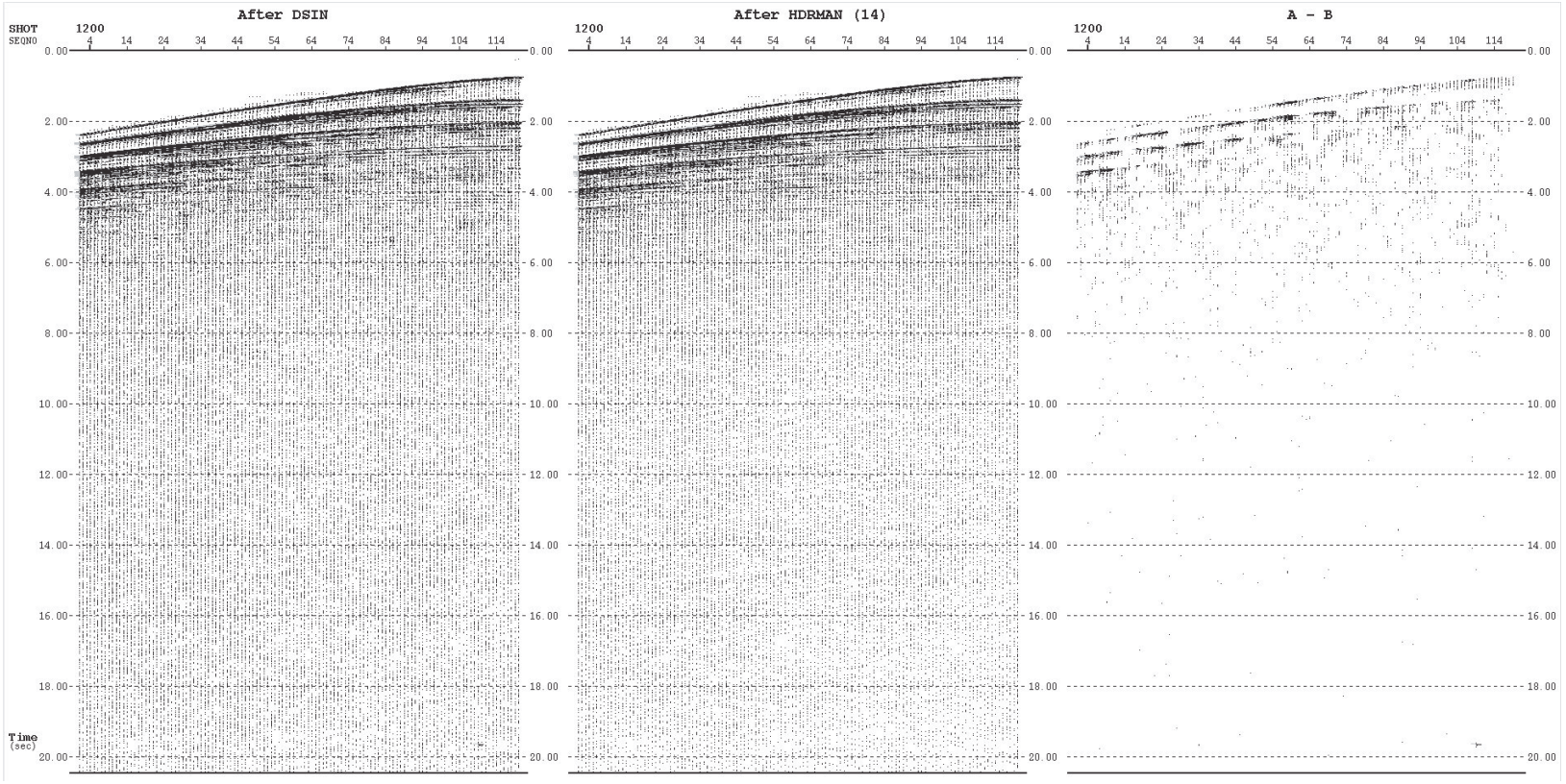

Figure E.6: Lift noise attenuation example. left) before; middle) after; right) difference

E.4 Stacked sections of the important processing steps

Figure E.7-E.15 show a stacked sections from the processing step: nominal geometry, spherical divergence, surface related amplitude balancing, noise attenuation on low frequencies, k-filtering, interpolation of shots, LIFT, SRME, LIFT radon transform. Notice that the shot gathers are not to same scale.

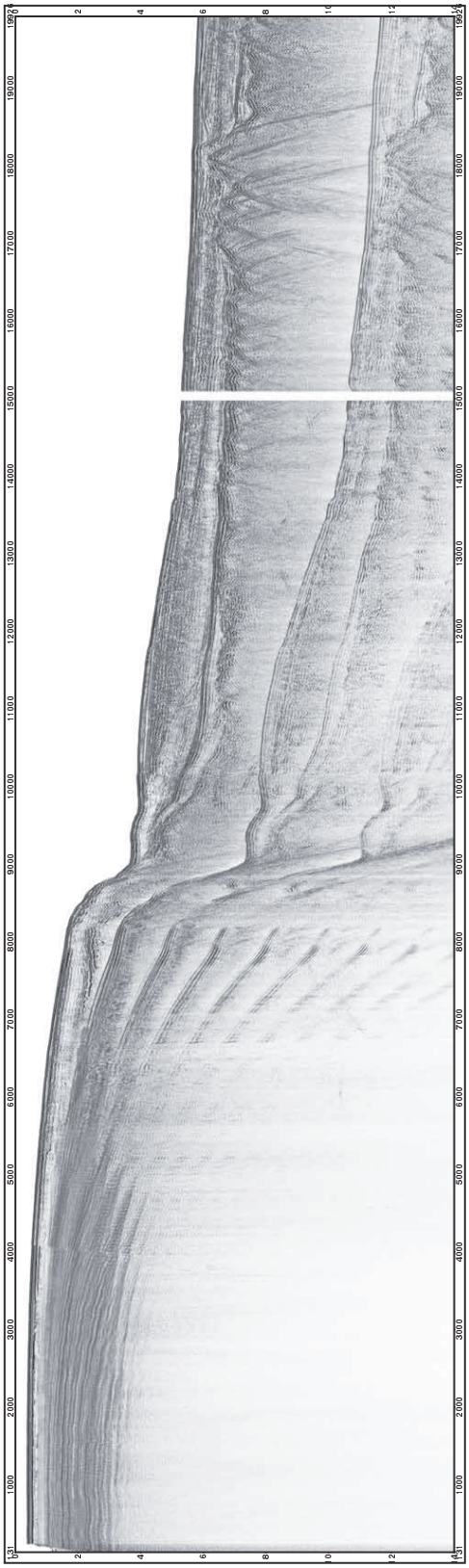

Figure E.7: Stacked section

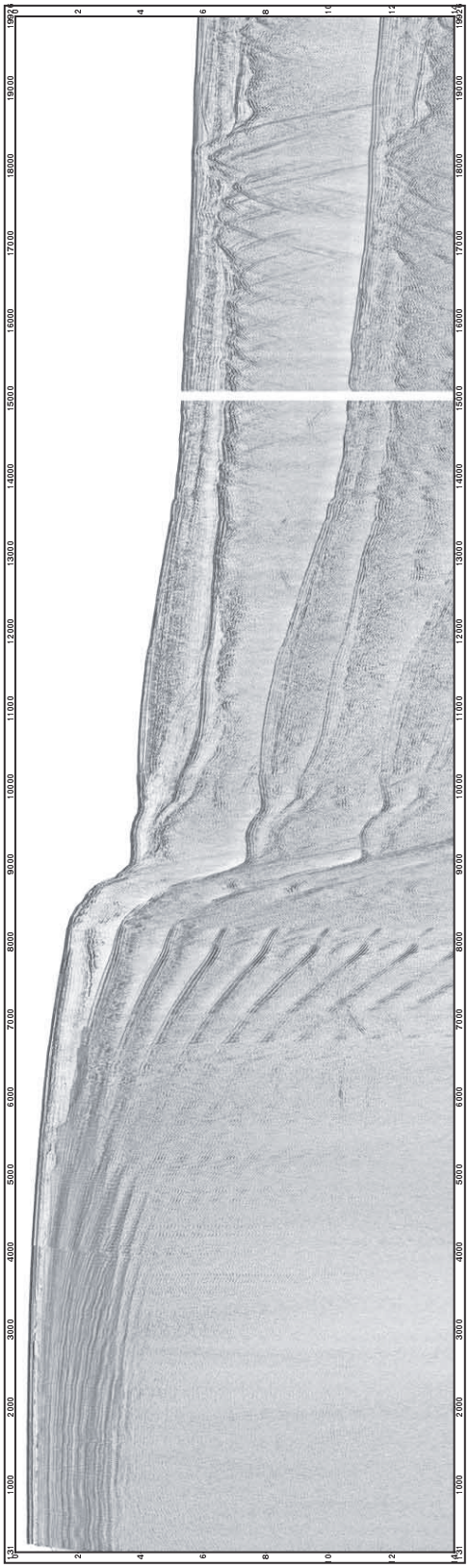

Figure E.8: Stacked section with spherical divergence applied

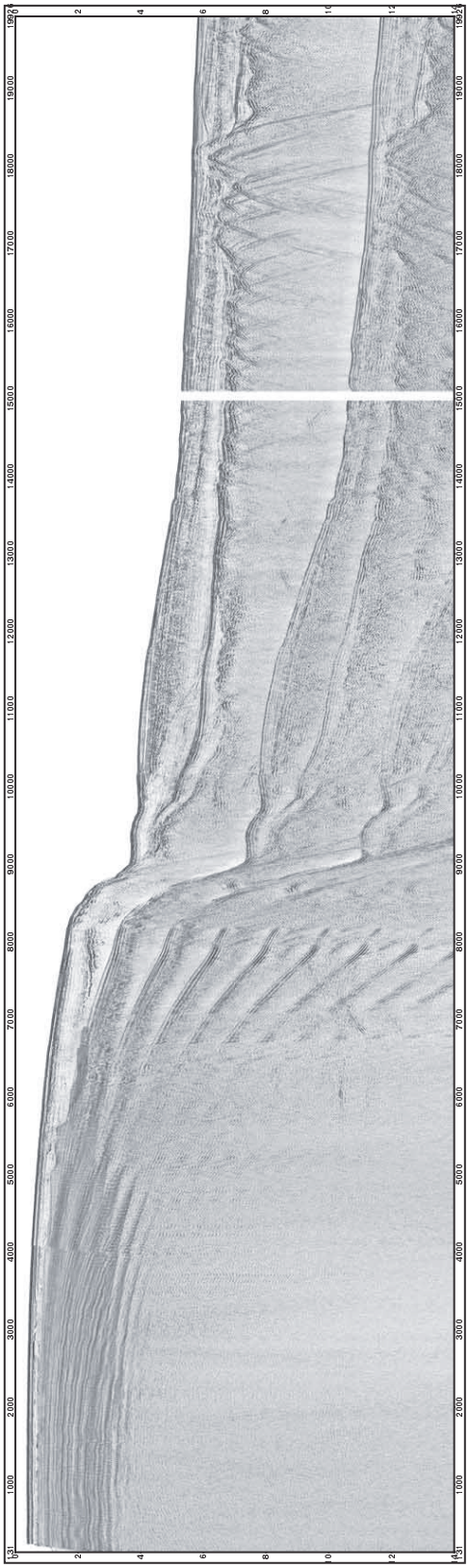

Figure E.9: Stacked section with surface related amplitude balancing applied

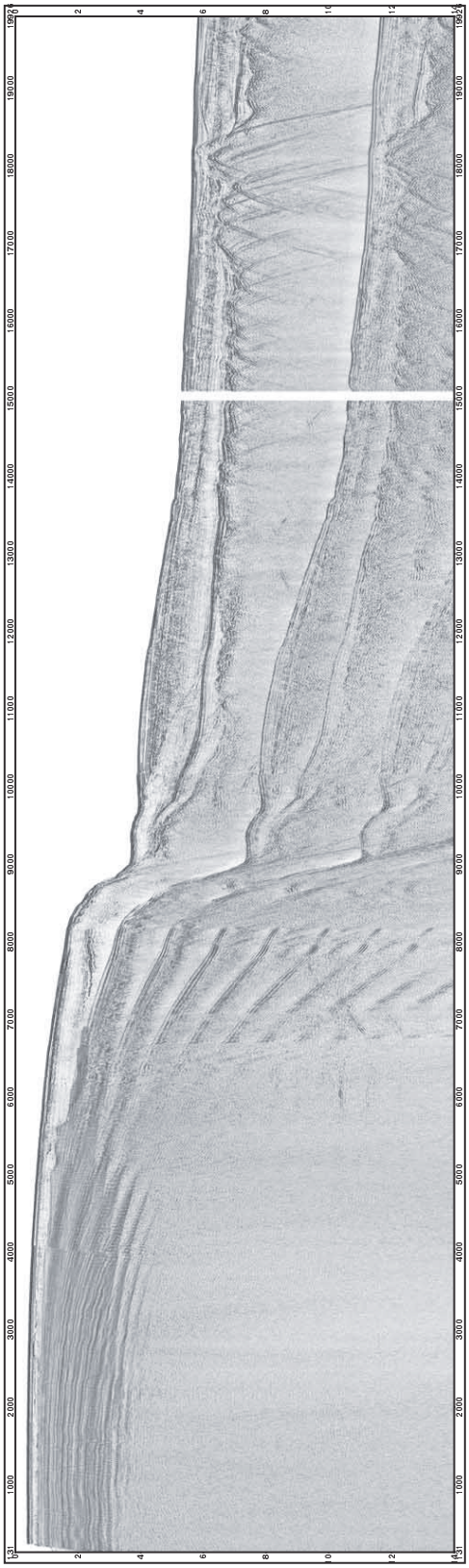

Figure E.10: Stacked section with low frequency noise attenuation applied

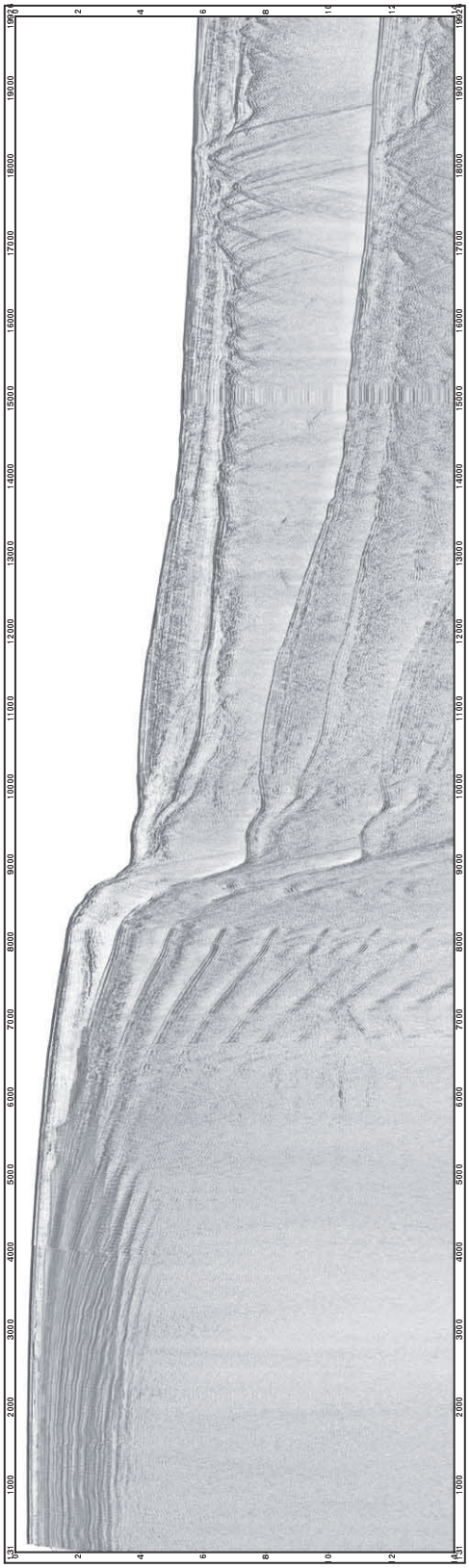

Figure E.11: Stacked section with K-filtering applied

Figure E.12: Stacked section with doubled the shots and new geometry

Figure E.13: Stacked section with LIFT applied

Figure E.14: Stacked section with surface related multiple elimination applied

Figure E.15: Stacked section with LIFT radon transform applied

E.5 Examples of jobs for adding header or patching traces.

The only header information the raw data of Lies 85-3 and 87-4 contained was the field record number (FFID). Hence, is was necessary to add shot headers to the data prior to nominal geometry.

Furthermore, there was a bad trace (channel 58) in the shot gathers and a patch was applied to this traces by combining the two surrounding traces.

```
*********************************************
EDIT SHOT NUMBERS
*********************************************

*JOB    FCAP    LINE85_3
*CALL   DSIN
LABEL   Flemish Cap line85-3
PKEYLST
1       9999
*CALL   HEADPUT SHOT            INTEGER
INPUT   FFID
DATA    1       3370
DATA    197     3566
DATA    199     3567
DATA    370     3738
DATA    715     3739
DATA    1896    4920
DATA    6449    1
DATA    7408    960
DATA    7587    961
DATA    7636    1010
DATA    7638    1011
DATA    9498    2871
DATA    9500    2872
DATA    9562    2934
```

```
DATA    9564    2935
DATA    9731    3102
DATA    9733    3103
DATA    9999    3369
*CALL   EDIT    shot    chan
SEL     1       99999
1       2       3
*CALL   DSOUT   OVERWRT
LABEL   FC_EDIT_SHOT_4920_2012
*END

*******************************************
PATCH BAD CHANNEL (58)
*******************************************

*JOB    FCAP    FCPREMIG
*CALL   DSIN
LABEL   FC_Marina_GAIN_2012
FILEID  0000400500900bc1.000000.0000000f
ORDER   SHOT    SEQNO
PKEYLST
1       4920
#*CALL   EDIT    SHOT    CHAN
SEL     1       4928
58
*CALL   PATCH           CHAN    3
TRACES  0
        20476   1       1       1       58      57      59
        20476   2       2       2       58      57      59
        20476   3       3       3       58      57      59
        20476   4       4       4       58      57      59
.......
.......
```

```
.......
.......
        20476   4914    4914    4914    58      57      59
        20476   4915    4915    4915    58      57      59
        20476   4916    4916    4916    58      57      59
        20476   4917    4917    4917    58      57      59
        20476   4918    4918    4918    58      57      59
        20476   4919    4919    4919    58      57      59
        20476   4920    4920    4920    58      57      59
        20476   4921    4921    4921    58      57      59
*CALL   PATCH                   360
BATCHES 0
5000    10000   895     894     896
BATCHES 0
5000    10000   883     882     884
BATCHES 0
5000    10000   887     886     888
*CALL   PATCH                   360
BATCHES 0
        2000    1286    1285    1287
BATCHES 0
14000   20476   1285    1284    1286
*CALL   PATCH                   3
TRACES
14000   20476   1458    1457    1459    15      15      15
*CALL   DSOUT   OVERWRT
LABEL   FC_EDITCHAN58_GAIN2012
*END
```

E.5.1 Example of a nominal geometry job

A few key values:
Number of shouts: 4290
Number of channels: 120
Offset to 1st channel: 210 m
Shot spacing: 50 m
Receiver spacing: 25 m
Streamer length: 3024 m
cdp spacing:12.5 m

```
*********************************************
NOMINAL GEOMETRY
*********************************************

*JOB    FCAP    FCPREMIG
*CALL   DSIN
LABEL   FC_EDIT_SHOT_4920_2012
FILEID  0000400500e00bc1.000000.00000008
ORDER   SHOT    SEQNO
PKEYLST
1       4920
*CALL   EDIT    SHOT    CHAN
SEL     1       4920
1       2       3
*CALL   HEADPUT CHAN
INPUT   SEQNO
DATA    1       1
DATA    120     120
*CALL   MARINE  4920    120     120     210     25      50
1
*CALL   PROFILE
*CALL   DSOUT   OVERWRT
```

```
LABEL   FC MARINE 2012
*END
```

E.5.2 Spherical divergence

Using a slightly updated version of the FLAME velocity model spherical divergences was applied to the cdp gathers.

```
*********************************************
SPHERICAL DIVERGENCE
*********************************************

*JOB    FCAP    FCPREMIG
*CALL   DSIN
LABEL   FC MARINE 2012
FILEID  0000400500a00bc1.000000.00000009
ORDER   CDP     SEQNO
PKEYLST
131     19926
*CALL   GAIN    CDP
SPHDIV  1       1       1       VR_SM20
#*CALL   GAIN    CDP
GATE    131     1
0       500     1       500     1000    1
1000    2000    1       2000    3000    1
GATE    8000
0       500     1       500     1000    1
1000    2000    1       2000    3000    1
GATE    9000
0       3000    1       3000    5000    2
5000    6000    2       6000    7000    2
SPHDIV  1       1       1       VR_SM20
*CALL   DSOUT   OVERWRT
```

```
LABEL   FC_Marina_GAIN_2012
*END
```

E.5.3 Surface consistence amplitude balancing

To apply surface related amplitude balancing three modules from Focus are necessary: BALAN, BASOL and BALAPP.

If the seismic section varies a lot laterally it may be necessary to apply BALAN several times on different cdp windows. All the analyzed output can be used all together in the following module BASOL.

```
*********************************************
SURFACE RELATED AMPLITUDE BALANCING
ANALYSING A PART OF THE MCS SECTION
WAS DONE ON CDP WINDOWS
*********************************************

*JOB    FCAP    FCPREMIG
*CALL   DSIN
LABEL   FC_EDITCHAN58_GAIN2012
FILEID  0000400500a00bc1.000000.00000010
ORDER   CDP     SEQNO
PKEYLST
5000      5249
*CALL   BALAN   ABSA    CDP     OFFSET
GATE    OFFSET
285     680     4680     1260    1100     5100
2260    1700    5700    3110    2300    6300
FNAME   FC_BALAN_5000-5249
THRSHLD 0
*END
```

```
*******************************************
SURFACE RELATED AMPLITUDE BALANCING
"SOLVING" A PART OF THE MCS SECTION
WAS DONE ON CDP WINDOWS
*******************************************

*JOB    FCAP    FCPREMIG
*CALL   DSIN
LABEL   FC_EDITCHAN58_GAIN2012
FILEID  0000400500a00bc1.000000.00000010
ORDER   CDP     SEQNO
PKEYLST
131     19926
*CALL   BALSOL  60      BSL12
KEYLIST CDP     OFFSET
FNAME   FC_BALAN_250-499
FNAME   FC_BALAN_500-749
.......
.......
.......
.......
FNAME   FC_BALAN_19000-19249
FNAME   FC_BALAN_19250-19499
FNAME   FC_BALAN_19500-19842
*END
```

```
*******************************************
SURFACE RELATED AMPLITUDE BALANCING
APPLYING
*******************************************

*JOB    FCAP    FCPREMIG
*CALL   DSIN
LABEL   FC_EDITCHAN58_GAIN2012
FILEID  0000400500a00bc1.000000.00000010
ORDER   CDP     SEQNO
PKEYLST
131     19926
*CALL   BALAPP  BSL12   CDP     OFFSET
#*CALL   NMO     RMS8RED
#*CALL   STACK   30
*CALL   DSOUT   OVERWRT
LABEL   FC_GAIN_BALAN_2012
*END
```

E.5.4 Noise attenuation on low frequencies

SUPPRES was used to try and eliminate the worst of the spikes.

```
*******************************************
TIME-VARIANT BAND-LIMETED NOISE SUPPRESSION
*******************************************

*JOB    FCAP    FCPREMIG
*CALL   DSIN
LABEL   FC_GAIN_BALAN_2012
FILEID  0000400500900bc1.000000.00000011
ORDER   SHOT    SEQNO
PKEYLST
1       4920
#*CALL   SUPPRES SHOT    SEQNO   50
FBAND   0       12
GATES   2000
1       700     20476
GATES   8000
1       3000    20476
GATES   9000
1       6700    20476
GATES   10000
1       7600    20476
GATES   14000
1       10000   20476
*CALL   SUPPRES SHOT    SEQNO   50
FBAND   0       12
*CALL   DSOUT   OVERWRT
LABEL   FC_GAIN_BALAN_SUPPRES_2012
*END
```

E.5.5 LIFT - Noise attenuation

See Section 3.2 for a description of LIFT. The Figs. E.4-E.6 show examples of types of noise LIFT can attenuate.

```
*******************************************
LIFT
*******************************************

*JOB    FCAP    FLAME
*CALL   DSIN
LABEL   FC_Marine_edit_SHOT2_9839
FILEID  0000400500a00bc1.000000.00000004
PKEYLST
4281    9840
*CALL   HDRMAN
STORE   orig
*CALL   FILTER  shot                            ZERO
KEYDEF  1
BAND    LP
                0               1       3
*CALL   HDRMAN
STORE   rawlow
MATH
rawmidhiorig    SUB     rawlow
RESTORE rawmidhi
*CALL   FILTER  shot                            ZERO
KEYDEF  1
BAND    HP
                80      90
*CALL   HDRMAN
STORE   rawhp
MATH
rawmid  rawmidhiSUB     rawhp
RESTORE rawmid
*CALL   HDRMAN
RESTORE rawlow
```

```
*CALL   HEADDEL
ENTRIES
rawmidhi
#*CALL   AMPSCAL 121
GATES
0       7000            3       1
7000    20476                   1
*CALL   TSCALE
SAVSCAL                 4
AGC
*CALL   FKBUILD klow
DESIGN
KF
500     0       500     16      200     16      20      2
-20     2       -200    16      -500    16      -500    0
500     0
*CALL   FKAPPLY klow
*CALL   DESCALE
*CALL   AMPSCAL 121
GATES
0       5500    250     1       1
5500    11200           1       1
11200   20476                   1
*CALL   HDRMAN
STORE   lowlift
*CALL   HDRMAN
RESTORE rawmid
*CALL   NMO     VR_SM20
STRETCH 65
#*CALL   AMPSCAL 121
GATES
0       20476                   1
```

```
*CALL   SIGNAL  15              60              -5      90
1       0.05
*CALL   EDIT    SHOT    SEQNO
SEL     1       9840
1       3       5       7       9       11      13      15
17      19      21      23      25      27      29      31
33      35      37      39      41      43      45      47
49      51      53      55      57      59      61      63
65      67      69      71      73      75      77      79
81      83      85      87      89      91      93      95
97      99      101     103     105     107     109     111
113     115     117     119     121     123     125     127
129     131     133     135     137     139     141     143
145     147     149     151     153     155     157     159
161     163     165     167     169     171     173     175
177     179     181     183     185     187     189     191
193     195     197     199     201     203     205     207
209     211     213     215     217     219     221     223
225     227     229     231     233     235     237     239
241     243     245
*CALL   NMO     VR_SM20         NMOREM
*CALL   HDRMAN
MATH
mtmpnois        SUB     rawmid
RESTORE mtmpnois
*CALL   NMO     VR_SM20
STRETCH 65
*CALL   GAIN    CDP
SPHDIV                          VR_SM20
*CALL   HDRMAN
MATH
scal            ABS
```

```
MATH
scal    scal    GT      0.0001
*CALL   GAIN    CDP
SPHDIV          -2      -1      VR_SM20
*CALL   HDRMAN
MATH
trace   scal    MUL
*CALL   AMPSCAL 21
GATES
0       20476           0.8
*CALL   NMO     VR_SM20         NMOREM
*CALL   HDRMAN
MATH
midnois         SUB     mtmpnois
RESTORE midnois
*CALL   HDRMAN
MATH
midlift rawmid  SUB     midnois
RESTORE midlift
*CALL   HEADDEL
ENTRIES
  midnosmtmpnoisrawmid  scal
*CALL   HDRMAN
RESTORE rawhp
*CALL   HDRMAN
MATH
scal            ABS
MATH
scal    scal    GT      .001
MATH
trace   scal    MUL
*CALL   AMPSCAL 121
```

```
GATES
0       8000    200     1
8000    20476   200
*CALL   HDRMAN
STORE   hilift
*CALL   HEADDEL
ENTRIES
rawhp
*CALL   HDRMAN
MATH
lowmid  lowlift         midlift
MATH
LIFT    lowmid          hilift
RESTORE LIFT
*CALL   HEADDEL
ENTRIES
orig    rawlow  rawhp   rawmid  lowmid  lowlift midlift hilift
rawmidhitrace   scal    LIFT
*CALL   DSOUT   OVERWRT         FLT16
LABEL   FC_LIFT_aftermarine2
*END
```

E.5.6 K-filter

K-filter or wave number filter was applied prior to other demultiple jobs. Thes module will reduces the multiple somewhat.

```
*******************************************
WAVE-NUMBER FILTER (K-FILTER)
*******************************************

*JOB    FCAP    FCPREMIG
*CALL   DSIN
LABEL   FC_GAIN_BALAN_SUPPRES_LIFT_March19
FILEID  0000400508a00bc1.000000.0000008f
ORDER   CDP     SEQNO
PKEYLST
131     19926
*IF
RANGE   CDP     8850    19926
*CALL   NMO     VR_SM20
*CALL   WNFILT  3       WITHIN
FILTER
0.5
*CALL   NMO     VR_SM20         NMOREM
#*CALL   STACK   30
*RESET
*CALL   DSOUT   OVERWRT
LABEL   FC_GAIN_BALAN_SUPPRESS_LIFT_KFILT_w50_March19
*END
```

E.5.7 Shot interpolation

Shots were interpolated (doublet) to make shot and receiver interval the same (25 m) This is an advantage when using LIFT for demultiple because it reduces aliasing. After interpolation the shot headers had to be rewritten. See below for jobs on these steps.

```
*******************************************
INTERPOLATIONS OF SHOTS
*******************************************

*JOB    FCAP    FCPREMIG
*CALL   DSIN
LABEL   FC_GAIN_BALAN_SUPPRESS_LIFT_KFILT_w50_March19
FILEID  0000400500900bc1.000000.00000090
ORDER   REC-STATSHOT
PKEYLST
2       9959
*CALL   HXINT   4       50      3       100
*CALL   DSOUT   OVERWRT
LABEL   FC_GAIN_BALAN_SUPPRES_LIFT_KFILT_March19
*END

*******************************************
EDIT SHOT AFTER SHOT SHOT INTERPOLATION
*******************************************

*JOB    FCAP    LINE85_3
*CALL   DSIN
LABEL   FC_WNFILT_HXINT_REGLO
FILEID  0000408500b00bc1.000000.00000361
ORDER   REC-STATSEQNO
PKEYLST
2       500
```

```
*CALL   HEADPUT SHOT2           INTEGER
INPUT   SHOT
DATA    1       1
DATA    1       2
DATA    4927    9855
DATA    4928    9856
*CALL   DSOUT   OVERWRT
LABEL   FC_EDTSHOT_HXINT
*END

*********************************************
MAKE NEW SHOT NUMBERS
*********************************************

*JOB    FCAP    FCPREMIG
*CALL   DSIN
LABEL   FC_GAIN_BALAN_SUPPRES_LIFT_KFILT_HXINT_March19
FILEID  0000400500b00bc1.000000.00000092
ORDER   REC-STATSEQNO
PKEYLST
2       9959
*CALL   HDRMATH
DEFINE  TYP2    FLOAT
DEFINE  SHOT2   FLOAT
DEFINE  SHOT3
DEFINE  SHOT4
HCDIV   IXTYP   2       TYP2
HHADD   TYP2    SHOT    SHOT2
HCMUL   SHOT2   2       SHOT3
HCSUB   SHOT3   1       SHOT4
*CALL   HEADDEL
ENTRIES
TYP2    SHOT2   SHOT3
```

```
*CALL   DSOUT   OVERWRT
LABEL   FC_GAIN_BALAN_SUPPRES_LIFT_KFILT_HXINT_editshot_March19
*END
```

E.5.8 SRME

the SMACTRM module extracts the Taylor terms of multiples which the SMACMS module uses to subtract from the input data.

```
*********************************************
SURFACE RELATED MULTIPLE REMOVAL
*********************************************

*JOB    FCAP    FLAME
*CALL   DSIN
LABEL   FC_LIFTall_aftermarine2
FILEID  0000400508a00bc1.000000.00000007
PKEYLST
1       9840
GATES
5000    2000
*CALL   SMACTRM 100     4       0
SPREAD  -3200   0       25              1
*CALL   SMACMS  SOFFSET 50      PONLY   4
*CALL   DSOUT   OVERWRT
LABEL   FC_SMAC_March20_1
*END
```

E.5.9 Radon LIFT

See Section 3.2 for a desciption on the multiple elimination.

```
*******************************************
LIFT RADON TRANSFORM
*******************************************

*JOB    FCAP    FLAME
*CALL   DSIN
LABEL   FC_SMAC_March20_2
FILEID  0000400500a00bc1.000000.00000009
ORDER   CDP     SEQNO
PKEYLST
135     19924
#*CALL   NMO     VR_SM20
*CALL   HDRMAN
STORE   original
*CALL   FILTER
BAND    LP
0       20476                   10      15
*CALL   PRADMUS                         21      200     3185
FORWARD 50              750     1000
INVERSE SUBTRACT
FILTER
        -400    200
BAND                    10      15
*CALL   AMPSCAL 51                      CDP
GATES
                        0.5     0.5
DSNMUTF 250
210     650     3185    1650
DSNMUTF 500
210     650     3185    1650
```

```
.......
.......
DSNMUTF 19250
210     11290   3185    11450
DSNMUTF 19500
210     11390   3185    11510
*CALL   HDRMAN
STORE   lowpass
MATH
aftfilt originalSUB     lowpass
RESTORE aftfilt
*CALL   PRADMUS                         21      300     3185
FORWARD 650             750     1000
INVERSE SUBTRACT
FILTER
        -400    200
BAND                    50      60
*CALL   AMPSCAL 51                      CDP
GATES
                        0.1
DSNMUTF 250
210     650     3185    1650
DSNMUTF 500
210     650     3185    1650
.......
.......
DSNMUTF 19250
210     11290   3185    11450
DSNMUTF 19500
210     11390   3185    11510
*CALL   HDRMAN
STORE   model
```

```
MATH
noise   aftfilt SUB     model
RESTORE noise
*CALL   PRADMUS                         21      300     3185
FORWARD 650             750     1000
INVERSE SUBTRACT
FILTER
        -400    200
BAND                    50      60
*CALL   AMPSCAL                         CDP
GATES
0       11000           0.8     0.8
12000   20476           0.5     0.5
DSNMUTF 250
210     650     3185    1650
DSNMUTF 500
210     650     3185    1650
.......
.......
DSNMUTF 19250
210     11290   3185    11450
DSNMUTF 19500
210     11390   3185    11510
#*CALL   HDRMAN
STORE   amsnoise
MATH
lift1   lowpass         amsnoise
RESTORE lift1
*CALL   HDRMAN
STORE   amsnoise
MATH
lift1   model           amsnoise
```

```
RESTORE lift1
*CALL   HDRMAN
STORE   lift1
MATH
lift2   lift1           lowpass
RESTORE lift2
*CALL   DSOUT   OVERWRT
LABEL   FLAME_smac_liftpradmus
*CALL   NMO     WATER2
*CALL   FKBUILD MultLift
DESIGN
KF
10      120     -10     120     -10     0       10      0
10      120
*CALL   FKAPPLY MultLift
MUTE    ON
*CALL   HEADDEL
ENTRIES
originallowpass aftfilt model   noise   amsnoiselift1   lift2
*CALL   NMO     WATER2          NMOREM
*CALL   DSOUT   OVERWRT
LABEL   FLAME_smac_liftpradmus_fkfilt
*CALL   NMO     VR_SM20
*CALL   STACK   60
*CALL   DSOUT   OVERWRT
LABEL   FCJG_SMAC_LIFTPRADMUS_fkfilt_stack
*END
```

Appendix F

Copyright Release for Thesis Chapters Published as Journal Articles

31 January 2013

Geology
The Geological Society of America
P.O. Box 9140
Boulder, CO 80301-9140

I am preparing my Ph.D. thesis for submission to the Faculty of Graduate Studies at Dalhousie University, Halifax, Nova Scotia, Canada. I am seeking your permission to include a manuscript version of the following paper(s) as a chapter in the thesis:

The Flemish Cap-Goban Spur conjugate margins: New evidence of asymmetry, Gerlings, J., Louden, K.E., Minshull, T.A. and Nedimovic, M.R. Geology, 40(12), 1107-1110, 2012

Canadian graduate theses are reproduced by the Library and Archives of Canada (formerly National Library of Canada) through a non-exclusive, world-wide license to reproduce, loan, distribute, or sell theses. I am also seeking your permission for the material described above to be reproduced and distributed by the LAC(NLC). Further details about the LAC(NLC) thesis program are available on the LAC(NLC) website (www.nlc-bnc.ca).

Full publication details and a copy of this permission letter will be included in the thesis.

Yours sincerely,

Permission is granted for:

a) the inclusion of the material described above in your thesis.

b) for the material described above to be included in the copy of your thesis that is sent to the Library and Archives of Canada (formerly National Library of Canada) for reproduction and distribution.

Name: ___ Title:

Signature: ___ Date:

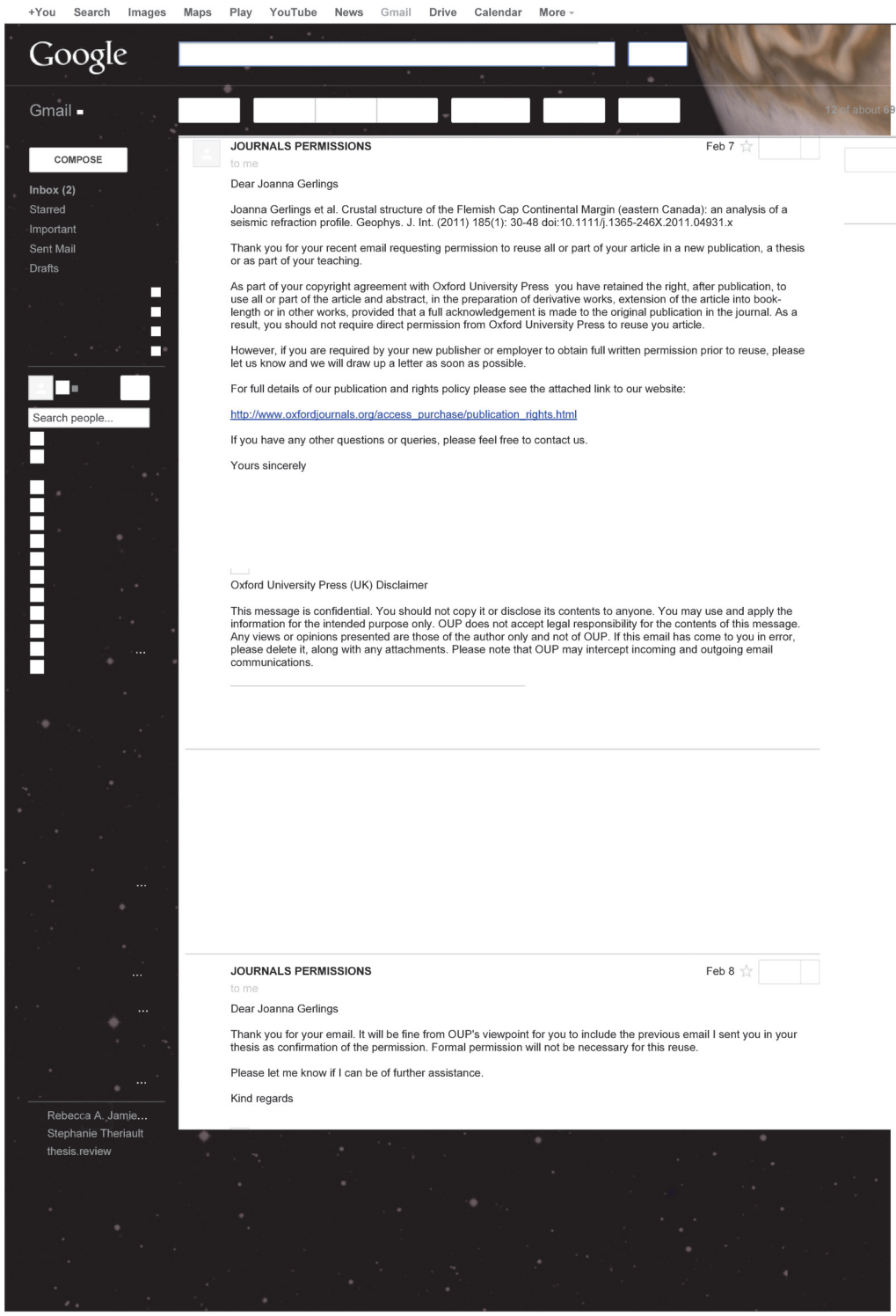

+You Search Images Maps Play YouTube News Gmail Drive Calendar More

Google

Gmail

COMPOSE

Inbox (2)
Starred
Important
Sent Mail
Drafts

Search people...

Rebecca A. Jamie...
Stephanie Theriault
thesis.review

12 of about 69

JOURNALS PERMISSIONS Feb 7

to me

Dear Joanna Gerlings

Joanna Gerlings et al. Crustal structure of the Flemish Cap Continental Margin (eastern Canada): an analysis of a seismic refraction profile. Geophys. J. Int. (2011) 185(1): 30-48 doi:10.1111/j.1365-246X.2011.04931.x

Thank you for your recent email requesting permission to reuse all or part of your article in a new publication, a thesis or as part of your teaching.

As part of your copyright agreement with Oxford University Press you have retained the right, after publication, to use all or part of the article and abstract, in the preparation of derivative works, extension of the article into book-length or in other works, provided that a full acknowledgement is made to the original publication in the journal. As a result, you should not require direct permission from Oxford University Press to reuse you article.

However, if you are required by your new publisher or employer to obtain full written permission prior to reuse, please let us know and we will draw up a letter as soon as possible.

For full details of our publication and rights policy please see the attached link to our website:

http://www.oxfordjournals.org/access_purchase/publication_rights.html

If you have any other questions or queries, please feel free to contact us.

Yours sincerely

Oxford University Press (UK) Disclaimer

This message is confidential. You should not copy it or disclose its contents to anyone. You may use and apply the information for the intended purpose only. OUP does not accept legal responsibility for the contents of this message. Any views or opinions presented are those of the author only and not of OUP. If this email has come to you in error, please delete it, along with any attachments. Please note that OUP may intercept incoming and outgoing email communications.

JOURNALS PERMISSIONS Feb 8

to me

Dear Joanna Gerlings

Thank you for your email. It will be fine from OUP's viewpoint for you to include the previous email I sent you in your thesis as confirmation of the permission. Formal permission will not be necessary for this reuse.

Please let me know if I can be of further assistance.

Kind regards